The
GEOLOGICAL BULLETIN
of the
PUNJAB UNIVERSITY

Number 35 *December 2000*

CONTENTS

Geol. Bull. Punjab, Univ. 35, 2000.

ESTIMATION OF GROUND WATER RECHARGE AND DISCHARGE FLUXES UNDER EUCALYPTUS VEGETATION

BY

JAVED AKHTER, ROBINA SHAHEEN, M. H. NAQVI
Nuclear Institute for Agriculture and Biology, Faisalabad, Pakistan.

AND

SHAFEEQ AHMAD
Institute of Geology, Punjab University, Lahore, Pakistan.

Abstract:- *Recharge or discharge fluxes and water movement in soil are important parameters for prediction of sustainability of ground water resources A field study was conducted on a high salt-affected soil planted with Eucalyptus camaldulensis. Two plots pf 5m X 20m were established one at low salinity ranging from 1-4.5 dS m^{1} (Site 1) and other on high salinity ranging from 3-g d S m^{1} (Site 2) area underlain by shallow saline aquifer. Neutron access tubes and moisture tensiometers were installed at each site to measure soil water content and hydraulic gradient at selected depths of soil profile. Soil samples collected at different times were analyzed for required physicochemical properties. Recharge or discharge fluxes were determined by physical and chemical (CI mass balance technique) methods on both the sites.*

Both Physical and chemical techniques indicated that Site 1 was a discharge area and in contrast Site 2 was a recharge area. The rate of discharge decreased from 1.86 to 2.01mm day^{1} at site 1 due to increase in ground water table depth from September 96 to March 97. In the same period the recharge rate increased from 0.48-0.68mm da^{1} at site 2 with decrease in ground water table depth due to horizontal infiltration from the drain. The tree roots penetrated to greater depth (90-180cm) at site 1 compared with 100cm depth at site 2 because of deeper water table at site 1. The recharge or discharge measured by both the methods were comparable at both the sites however, the coefficient of variation (CV) was low with chemical method. The data confirmed that both the techniques were good to estimate fluxes under eucalyptus vegetation in areas of varying salinity and water table depths. However, chemical method was economical, less time consuming and more reliable thanphysical method.

INTRODUCTION

The estimation of water recharge/discharge is essential to predict the sustainability of ground water resources and availability of water to plant roots both in irrigated and non irrigated areas. Generally it is very difficult to quantify the ground water recharge in dry climate (Daniel, 1994). Stephen and Knowlton, (1986) and Edmunds and Walton, (1980) observed that physical methods applied are problematic due to the reasons:

The small changes cannot be detected in dry areas due to low fluxes.

Several years are required to obtain mean values due to high temporal variability.

Large number of sampling locations are required to assess the recharge variability because of variation in soil texture and topography.

The environmental tracers are used to measure displacement of water or solutes directly eliminating the need of indirect calculations using quite uncertain parameters. The Cl, H^{2}, O^{18}, H^{3}, Cl^{36} and Br are used as tracers to estimate the recharge within the root zone (Edmunds and Walton, 1980; Tyler and Waker, 1994.

Fred (1994) suggested the use of conservative tracer for tracing water and Solute movement the soils and emphasized that tracer concentration should not decrease/or increase and its rate of flow should not slow down with time. Chloride is a tracer with meets this criteria. Chloride

moves in to the soil profile with infiltrating water. The volatility of Cl is negligible, so it is nearly completely retained in the soil when water is abstracted by evaporation or transpiration. Therefore, increase in Cl concentration is proportional to amount of water lost by evapotranspiration. The residual moisture flux can be estimated using piston flow model of Cl transport in soil due to its conservative behaviour (Allison and Hughes, 1978; Edmunds and Walton, 1980).

All ground waters contain solutes of varying concentration and uptake of water by plants will induce a flux of solutes into the root zone. The resultant soil salinity levels will be considerable where the upward ground water flux and/ or ground water salinity is high (Jolly et al., 1993; Wallender et al., 1979). The low osmotic potential associated with high soil salinity reduces the amount of water extracted by plants from the soil. Van Hylckma (1974) found that ground water uptake rate reduced by 50 % as the soil salinity increased due to water uptake by *Tamarix pentandra* (Saltcedar) compared with non saline control. Eucalyptus is tolerant to salinity and water logging and is commonly grown for sustainable utilization of saline wastelands. Therefore, it is important that salt fluxes from water table be considered when investigating the importance of saline ground water to plant communities and sustainability of ground water resources.

The objectives of this study were to estimate the

1). Ground water recharge and discharge fluxes on moderate and high salinity sites under eucalyptus vegetation underlain by shallow saline aquifer.

2). To compare physical method and chloride mass balance technique for measuring recharge and discharge fluxes.

MATERIALS AND METHODS

The study was conducted at Biosaline Research Station of Nuclear Institute for Agriculture and Biology (NIAB) at Pacca Anna. Two plots (20m X %m) were established at different sites vegetated with *Eucalyptus camaldulensis* (4 year old). Neutron moisture access tubes were installed in triplicate on both sites up to 200cm depth. Porous ceramic cup tensiometers were installed in duplicate at 30, 60, 90, 120 and 170cm depths.

During the study period from September 1996 to March 1997 irrigation water was not applied to the study sites. Soil samples were collected from both the sites from preselected depths after three months interval. Moisture content and matric potential along the soil profiles were recorded after every three months from preselected depths with neutron moisture meter (NMM) and tensic meter respectively. Water table depths were recorded by hydrometer from piezometers installed at each site. Bulk density at both the sites was determined by core method (Blake, 1976).

Soil samples collected were analyzed in the laboratory for gravimetric water content (0_g). Soil particle size distribution was determined using hydrometer method (Gee and Bauder 1986). Electrical conductivity (Ec_e) of the 1:1 soil suspension was measured using LF 530 EC meter. Anions CO_3, HCO_3 and Cl were determined by titrimetric method and cations Na, K, Ca and Mg were determined by flame photometer (USDA 1954) and SO_4 was determined by turbidimetric method (Helrich, 1990). The recharge was estimated both by physicial and chemical methods. IN physical method water fluxes were used to determine recharge using the following equation:

$$R = K(0)\ dp/dh$$

K(0) is unsaturated hydraulic conductivity and dp/dh is total hydraulic gradient. Recharge was also determined by chloride mass balance technique of Allison and Hughed (1978) from bulk density, Cl and 0_g data of soil profiles in September 96 and March 97.

Results

The study area is located at 73°.05 E longitude and 31°.24 N latitude. The area has an annual average temperature of 32°C. The annual average precipitation and evaporation is 320mm and 1100mm respectively. Both sites S1 and S2 underlain saline unconfined aquifer. A drain of water passes near the site 2 and water table depth remains at 100cm during whole the year. The site 1 is 500m away from site 1 with an average annual water table depth of 250cm. The area shows large variation in top soil (0-70 cm) salinity ranging from 2-72 dS m^{-1} (Shaheen et al. 1997).

The soil profiles showed large variation in salinity with electrical conductivity (EC_e) ranging from 1-4.5 dS m^{-1} and 3-9 dSm^{-1} at sites 1 and 2 respectively (Table 1). The EC increased with soil depth at site 1 but Ec_e was maximum near soil surface at site 2 and decreased with soil depth. The soil water content at saturation (0_s) at both sites increased gradually with soil depth due to increase in clay content. The 0_s was higher at site 2 compared with site 1 but at 75cm depth similar values of 0_s were observed at both the sites (Table 1). The gravimetric soil water content (0_g) at site 1decreased with time upto the depth of about 100cm and in contrast the Cl concentration increased up to similar depth (Fig. 3).

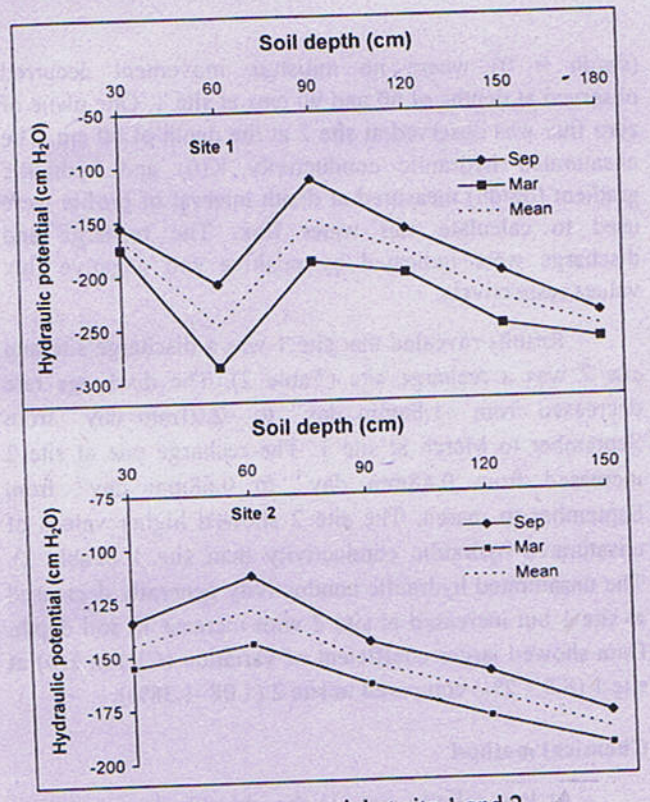

Fig. 1 Total soil water potential at site 1 and 2.

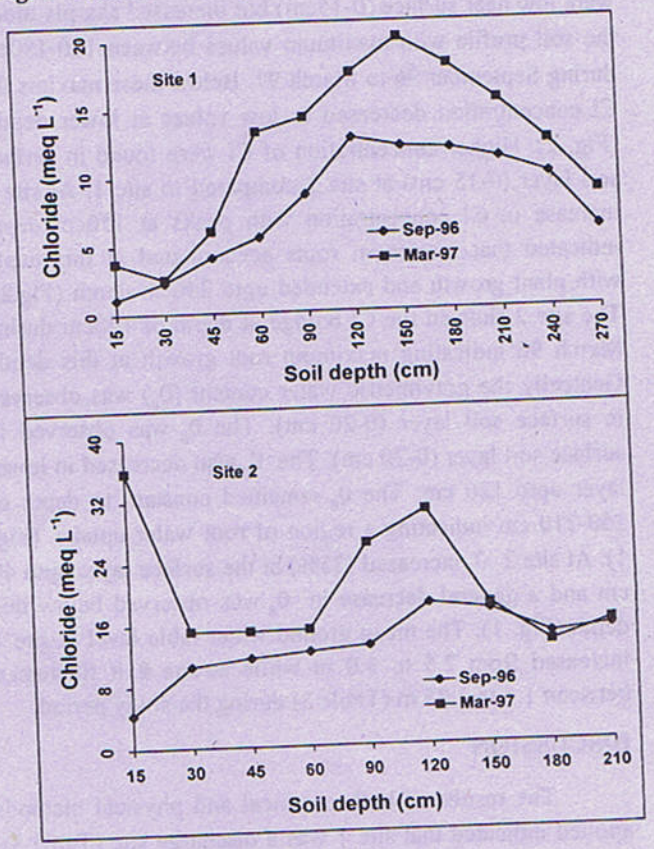

Fig. 2 Profiles of Cl Concentration in soil water at site 1 and 2.

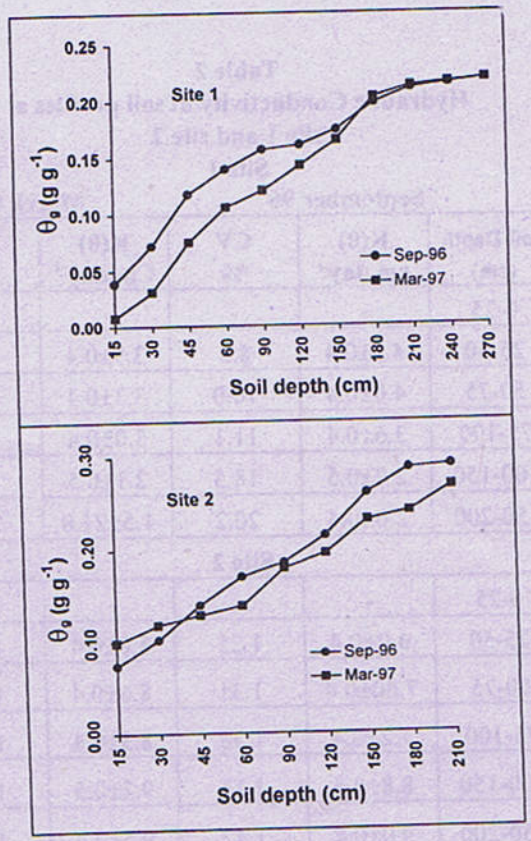

Fig. 3 Profiles of gravimetric water content (0_g) at site 1 and 2 in Sep-96 and Mar-97.

Table 1
Particle size data, Water retention at saturation (0_s) Electrical conductivity (Ece) of soil profiles at site 1 and site 2.

Site 1

Soil Depth (cm)	Sand (g Kg^{-1})	Silt (g Kg^{-1})	Clay (g Kg^{-1})	0_s (g g^{-1})	EC_e (dS M^{-1})
0-25	681	174	145	0.267	1.15
25-50	737	131	132	0.254	2.22
50-75	609	230	161	0.254	2.22
75-100	690	168	132	0.320	3.87
100-150	579	239	182	0.370	4.33
150-200	539	249	212	0.402	4.54

Site 2

0.25	629	219	152	0.309	9.19
25-50	618	223	159	0.313	6.88
50-75	609	230	161	0.332	6.08
75-100	611	229	160	0.325	6.66
100-150	588	237	175	0.341	4.89
150-200	553	238	209	0.348	2.99

Table 2
Hydraulic Conductivity of soil profiles at site 1 and site 2

Site 1

Soil Depth (cm)	September 96 K(0) cm day^{-1}	CV %	March 97 K(0) Cm day^{-1}	CV %
0-25	-	-	-	-
25-50	4.5±0.4	8.8	3.9±0.4	12.8
50-75	4.0±0.4	10.0	3.3±0.4	14.8
75-100	3.6±0.4	11.1	3.0±0.4	16.7
100-150	2.7±0.5	18.5	2.1±0.5	19.1
150-200	2.0±0.4	20.2	1.5±21.0	21.0

Site 2

0-25	-	-	-	-
25-50	6.0±0.4	1.25	8.8±0.4	1.14
50-75	7.60±0.4	1.31	8.6±0.4	1.16
75-100	7.2±0.4	1.38	8.3±0.4	1.21
100-150	8.8±0.5	1.13	9.2±0.5	1.08
150-200	9.0±0.4	1.42	9.5±0.4	1.23

K(0)=Hydraulic conductivity,CV=Coefficient of variation

Table 3
Water table depth (WTD) and Recharge or discharge or discharge (mm day^{-1}) determined by physical and chemical methods

Site & date	WTD (cm)	Physical	Chemical
Site 1 (September 96)	250±15	-1.86	-1.98
Site 1 (March 97)	311±14	-2.01	-2.87
Site 2 (September 96)	150±10	0.48	0.468
Site 2 (March 97)	174±08	0.68	0.615

Physical method

The hydraulic gradient (dp/dh) at sites 1 and 2 at two different time is shown in Fig. 1. Two planes of zero fluxes (dp/dh=0) where no moisture movement occurred were observed at depths of 60 and 90 cms at site 1. One plane of zero flux was observed at site 1 at the depth of 60 cm. The unsaturated hydraulic conductivity K(0) and hydraulic gradient (dp/dh) measured at each depth interval of soil profile were used.

The hydraulic gradient (dp/dh) at sites 1 and 2 at two different time is shown in Fig. 1. Two planes of zero fluxes (dp/dh = 0) where no moisture movement occurred observed at depths of 60 and 90 cms at site 1. One plane of zero flux was observed at site 2 at the depth of 60 cm. The unsaturated hydraulic conductivity K(0) and hydraulic gradient (dp/dh) measured at depth interval of profile were used to calculate soil water flux. The recharge and discharge were indicated by positive and negative flux values respectively.

Results revealed that site 1 was a discharge site and site 2 was a recharge site (Table 2). The discharge rate decreased from –1.86mm day^{-1} to –2.01mm day^{-1} from September to March at site 1. The recharge rate at site 2 increased from 0.48mm day^{-1} to 0.68mm day^{-1} from September to march. The site 2 showed higher values of unsaturated hydraulic conductivity than site 1 (Table 2). The unsaturated hydraulic conductivity generally decreased at site 1 but increased at site 2 with increase in soil depth. Data showed larger coefficient of variation (CV) in k(0) at site 1 (8.8 – 2%) compared to site 2 (1.08–1.38%).

Chemical method

At low salinity site (1) the chloride concentrations were low near surface (0-15cm) but increased sharply along the soil profile with maximum values between 120-180cm during September 96 to March 97. Below these maxims the Cl concentration decreased to low values at lower depths (Fig. 2). Higher concentration of Cl were found in surface soil layer (0-15 cm) at site 2 compared to site 1. At site 1 increase in Cl concentration with peaks at 150cm depth indicated that maximum roots accumulated at this depth with plant growth and extended upto 240cm depth (Fig.2). The site 2 showed the Cl buldge at depth of 120cm during March 96 indicating maximum root growth at this depth. Genteelly the gravimetric water content (0_g) was observed in surface soil layer (0-20 cm). The 0_g was observed in surface soil layer (0-20 cm). The 0_g also decreased in lower layer upto 120 cm. The 0_g remained constant to depth of 150-210 cm indicating a region of root water uptake. (Fig. 1). At site 2 0_g increased (33%) at the surface layer upto 40 cm and a general decrease in 0_g was observed below this depth (Fig. 1). The mean ground water table level at site 1 increased from 2.5 to 3.0 m while at site 2 it fluctuated between 1.5 to 1.75 m (Table 3) during the study period.

DISCUSSION

The results of both chemical and physical methods applied indicated that site 1 was a discharge site (Table 3). The Cl profiles showed that plant roots extracted required water from the depth ranging from 90-180 cm (Fig.3). The

increase in Cl concentration in the root zone may be attributed to increase in total soluble salts (TSS) concentration due to higher transpiration of eucalyptus trees. Such bulges in Cl profiles in vadose zone have commonly been found by many workers (Allison and Hughes, 1985; Peck et al., 1981).Tyler and Walker (1994) showed that in vegetation covered areas the abstraction of water from soil was almost entirely by root uptake by plants. During transpiration some cations and anions could also be taken up by roots and transferred into green parts of the plants. The Cl is not much involved in root uptake so its concentration increased with decrease in soil water content. Data confirmed that rote of discharge decreased (-1.86 to – 2.01 mm day^{-1}) at site 1 with time from (Sep-Mar). The decrease in rate of discharge with time at site 1 was certainly due to decrease in ground water table depth from September to March which may have reduced the plant available water, consequently reducing discharge. In a similar study Allison et al. (1994) used Cl concentration and suction profiles to quantify both present and past recharge rates.

Results revealed that site 2 was a recharge site with zero flux plane at 60 cm depth only (Fig. and Table 1). The Cl concentration increased in the upper soil layer (030 cm) with time (September 96- March 97). The increase in Cl in surface layer at site 2 may be attributed to higher rate of evaporation due to greater capillary rise. The data indicated that recharge rate increased from 0.48 mm day^{-1} to 0.68 mm day^{-1} from Sep to Mar. Presence of Cl bulge at 50 to 100 cm depth confirmed that roots of Eucalyptus trees penetrated upto the depth of about 100 cm at this site. The roots may have been restricted in the zone due to the presence of high ground water table at 1.5 m depth. The increase in recharge rate with time (Sep-Mar) at site 2 was because of increase in evapotranspiration as the water remained available to plant roots. The increase in recharge may be attributed to horizontal infiltration from the waste water drain passing near the site 2.

The values of ground water recharge or discharge obtained in this study, by physical and chemical methods were comparable at both the sites (Table 3).The data obtained by physical method showed high coefficient of variation (CV) at site 1 compared with site 2. Generally the CV was very low with chemical method compared with physical method under all conditions (Table 2). The smaller values of fluxes were involved at lower soil water content at site 1 with greater spread in readings which increased CV with physical method. Tyler and Walker (1994) reported that Cl mass balance provide more robust estimation of recharge in arid regions having low recharge rates. The physical method requires field equipment and labour, more time consuming and difficult to perform. The chemical method require soil sampling in the field and laboratory analysis witch is easier to perform and results are more reproducible. Results confirmed that both methods were equally good to estimate recharge or discharge under eucalyptus vegetation in areas of varying salinity and water table depths. However, the chemical method was economical, less time consuming and more reliable method than physical method.

ACKNOWLEDGEMENTS

The financial support provided by International Atomic Energy Agency (IAEA) is highly acknowledged

REFERENCES

Allison, G.B., Gee, G.W. and Tyler, S.W., 1994. Vadose-zone technique for estimating ground water recharge in arid and semi-arid regions. *Soil Sci. Soc. Amer. Jour.*, **58,** 6-14.

Allison, G.B., Hughes, M.W., 1978. The use of environmental chloride and tritium to estimate total recharge to an unconfined aquifer. *Aust. Jour. Soil Res.*, **16,** 181-195.

Allison, G.B. and Hughes, M.W., 1985. Recharge in Karast and Dune elements of a semiarid landscapes as indicated by natural isotopes and chloride. *Jour. Hydrol.*, **76,** 1-26.

Blake, G.R., 1976. Bulk density. In Black, C.A. Ed. Methods of soil analysis, Part 1, Physical and mineralogical properties, including statistics of measurement and sampling *Amer. Soc. Agron., Madison, Wisconsin, USA,* 375-395.

Daniel, B., 1994. A perspective on diffuse natural recharge mechanisms in areas of low precipitation. *Soil Sci. Soc. Amer. Jour.*, **58,** 40-48.

Edmunds, W.M. and Walton, N.R.G. 1980. A geochemical and isotopic approach to recharge evaluation in semi-arid zones-past and present. In arid zone hydrology: Investigations with isotopic techniques. IAEA, Vienna, 47-68.

Fred, M.P., 1994. Environmental tracers for water movement in desert soils of American South West *Soil Sci. Soc. Amer. Jour.*, **58,** 15-24.

Gee, G.W. and Bauder, J.W., 1986. Particle size analysis. In methods of soil analysis part 1. *Monograph No. 9 ASA. Madison, Wl. 383-411.*

Helrich, K., 1990. Sulphate in water "Turbidimetric method" In (Kenneth, H. Ed.), Official methods of analysis of association of official analytical chemists. 330.

Jolly, I.D., Walker, G.R., and Thorburn, P.J. 1993. Salt accumulation in semi-arid flood plain soils with implication for forest health. *Jour. Hydrol.*, **150,** 589-614.

Peck, A.J., Johnston, C.D. and Willamson, D.R. 1981. Analysis of solute distribution in deeply weathered soils. *Agric. Water Manage.*, **4,** 83-103.

Sheen, R., Akhter, J., and Naquvi, M.H., 1997. Evaluation of EM-technique for mapping soil salinity. *Jour Agri Res.*, **35,** 41-48.

Stephens, D.B., and Knowlton, R., 1986. Soil water movement and recharge through sand at a semi0arid site in New Mexico. *Water Resour. Res.*, **22,** 881-889.

Tyler, S.W., and Walker, G.R., 1994. Root zone effect on tracer migration in arid zones. *Amer. Jour. Soil Sci.* **58,** 25-31.

U.S. Salinity Laboratory Staff. 1954. Saline and alkali soils. USDA, Agric. Hand book No. 60. U.S. Govt. Print. Office, Washington, DC., 160.

Van Hylckma, T.E.A., 1974. Water use by saltcedar as measured by the water budget method. USGS professional paper No. 491-E. US Govt. Print. Office, Washington, USA 30.

Wallender, W.W., Grimes, D.W., Henderson, D.W., and Stromberg, L.K., 1979. Estimating the contribution of a perched water table to the seasonal evapotranspiration of cotton. *Agron. Jour.* **71,** 1056-1060.

Geol. Bull. Punjab Univ. 35, 2000.

ACID ACTIVATION AND BLEACHING CAPACITY OF ILLITE-SMECTITE RICH MUDSTONE FROM KARAK AREA, KOHAT PLATEAU, PAKISTAN.

BY

AKHTAR ALI SALEEMI, SHAFEEQ AHMED
Institute of Geology, Punjab University, Lahore 54590, Pakistan

AND

ZULFIQAR AHMED
Department of Earth Sciences, King Fahad University of Petroleum and Minerals, Dhahran 31261, Kingdom of Saudi Arabia

Abstract:-*Karak mudstone is exposed 1km north of Karak town and is sandwiched between an evaporitic sequence of Eocene age. It is predominantly composed of illite-smectite mixed layers with 30% smectite content. These clays were easily activated with HCl. Activation could be attributed to the removal of high concentration of octahedral Mg and Fe cations, uptake of OH and formation of amorphous silica gel. The activated material has been rendered suitable for decolourisation of rapeseed oil through removal of β-carotene. Optimum bleaching capacity of 93% can be attained following the treatment with 2N HCl for three hours or 3N HCl for two hours. The optimum bleaching capacity is not associated with maximum surface area.*

INTRODUCTION

Bleaching earths are mainly used for purification, decolourisation and stabilization of edible oils. They are also used for the removal of traces of metal, adsorption of phospholipides and decomposition of oxidation products such as peroxides (Siddiqui, 1968; Kheok & Lim, 1982; Griffiths, 1990). Bleaching earths are produced by acid activation of bentonite or of clays containing an appreciable amount of montmorillonite. The sorbing capacity of bentonites for dyes and other solved or diffused substances is greatly enhanced by activation treatments (Odom, 1984; Rupert et al., 1987; Srasra et al.,1989; Boyd and Jaynes, 1994; Christidis et al., 1997). The activation treatments involve the reaction of inorganic acids either, HCl or H_2SO_4, with clay. As a consequence of this reaction the surface area of the activated clay is increased along with modifications in the structure (Grim, 1962; Odom, 1984; Rupert et al., 1987; Griffths, 1990; Rhodes and Brown, 1992; Tkac et al., 1994).

A number of researchers have made investigations on the kinetics of clay minerals dissolution. Initial studies were focused on the determination of cations making up tetrahedral and octahedral sheets of layers based on the higher dissolution rate of the octahedral sheets (Brindley and Youell, 1951; Gastuche and. Fripiat, 1962). Other studies were involved in the mechanism of dissolution kinetics of pure montmorillonite (Osthaus, 1954, 1956), and polymineral montmorillonite clay in HCl (Milliken et al., 1955; Granquist and Samner, 1959; Stoch et al., 1977; Stoch et al., 1979; Grim, 1962; BrÜkman et al., 1976; Novak and Cicel, 1978; Yates, 1986).

Clay dissolution is described as pseudo first order reaction (Osthaus, 1956; Granquist and Samner, 1959; Stoch et al., 1977). During the initial contact of acid with clay impurities, such as carbonates, are dissolved resulting in a concentration of smectite fraction of the clay (Morgan et al., 1985). This is followed by replacing the interlayer cations with H^+ ion (Thomas et al., 1950; Grim, 1962; Siddiqui, 1968) and liberating some ions of Al^{+3}, Fe^{+2}, Fe^{+3} and Mg^{+2} from the octahedral layer exposed at the edges of the smectite platelets (Fijal et al., 1975; Brükman et al., 1976; Tkac et al., 1994; Kaviratna and Pinnavaia, 1994). As a result of this structural disruption, silica released from the tetrahedral layers precipitate in the form of amorphous silica (Fahn & Fenderl, 1983; Morgan et al., 1985; Yates, 1986). Some Al^{+3} from the tetrahedral sheet may also be dissolved but at much slower rate than the removal of octahedral cations (Morgan et al., 1985). Some of the liberated ions then may migrate to interlayer positions and the rest into the solution. The smectite layers take the appearance of bundle of used notes relatively unaffected in the centre but separating at the edges (Morgan et al., 1985). Prolonged reaction of acid with clay causes complete

dissolution of octahedral layer resulting in complete structural collapse (Newman, 1963), which reduces the availability of area to be attacked (Rupert et al., 1987).

Two most important physical changes in activated clays which play a vital role in bleaching are increase in surface area and pore diameter (Mills et al., 1950; Grim, 1962; Fijal et al., 1975; Morgan et al., 1985; Srasra et al., 1989; Rhodes and Brown 1992; Christidis et al., 1997). Surface area increases with increasing severity of acid treatment until a maximum is approached, beyond which surface area and bleachability decline progressively due to disruption in the structure of smectite (Mills et al., 1950; Grim, 1962; Fijal et al., 1975; Morgan et al., 1985; Clarke, 1985; Srasra et al; 1989; Griffiths, 1990; Rhodes and Brown, 1992). A positive relation is described between increase in surface area and bleachability (Novak and Gregor, 1969; Kolta et al., 1975). However the observations of Zaki et al. (1986), Morgan, et al. (1985) and this particular study found no such correlation. Micropores in clays are filled with various mineral salt constituents. Acid activation leaches out these salts, hence opening the capillaries and making the structure more open (Siddiqui, 1968). With increasing acid concentration, the progressive increase in pore volume of micropores and mesopores take place (Jovanovic and Janackovic1991).

In Pakistan investigations for the discovery of bentonites carried out so far show no evidence of natural Na-bentonite. Small to medium size pockets (2 cm to 3 feet thick) of Ca bentonite have been discovered mainly in the remote northern parts of Pakistan (O'Driscoll, 1988). However large clay deposits having illite-smectite as dominant clay mineral with low expandable component are present in the Southern and Northwestern parts of the country which need to be investigated for their bleaching suitability after acid activation. In these contribution illite-smectite rich clays from Karak, Northwest Pakistan, have been activated with HCl. The mineralogical and physiochemical properties of activated clays are measured and their performance towards bleaching the colour pigments from crude rapeseed oil have also been evaluated.

GEOLOGY OF THE KARAK MUDSTONE

Type locality for the Karak mudstone, is 1km north of Karak town (lat. 33° 7′ N; long. 71° 6′E) as shown on the geological map of Karak area given in Fig. 1. The outcrop of Karak mudstone extends for 35 km from east to west. The mudstone is 3 to 20m thick, excluding a lower gypsum bed which is 0.3 to 3m thick. Mudstone thickness increases at places due to gravity faulting or overfolded strata.

The Jatta Gypsum overlying the Karak mudstone is 6 to 30m thick. The Karak mudstone has an undulating contact with the overlying and underlying gypsum beds, possibly due to the original topography of the basin but more probably due to the mechanical behaviour of the two rock units.

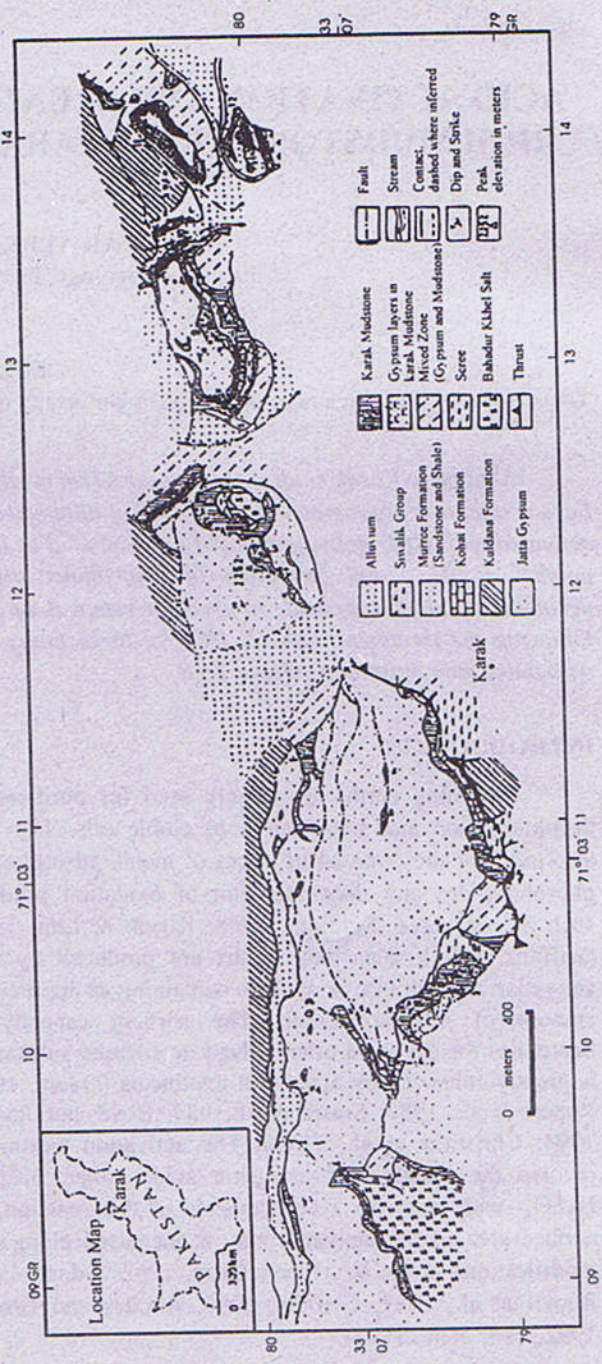

Fig.1. Geological map of Karak area modified after Chaudhry and Ashraf (1979).

The Karak mudstone is soft, sticky, plastic colloidal clay. It has a greasy and splintery appearance when fresh. Locally, it is used as a detergent for clothes-washing

purpose. When wet, it can be moulded into any shape. On drying it contracts and develops cracks. On weathered surfaces, it crumbles to small, loose pieces. The colour of mudstone varies from greenish blue to greyish and bluish grey. At some places near its contact with salt, sulphur is deposited giving a yellow colour to the contact. Some of the exposures near the base show a dark bluish grey colour due to the presence of bituminous matter. The mudstone also has thin partings of gypsiferous clay and gypsum. Saleemi and Ahmed (2000) have shown that the Karak mudstone is mainly composed of detrital clays of varied composition and concentration. The mudstone probably represents the choking of gypsum-floored bays and lagoons with fine clastics. The influx and circulation of mud-carrying fresh water would have locally halted the precipitation of gypsum and allowed the shallow water mudflats to fill the remainder of the water column. The presence of syngenetic gypsum bands and layers suggest that these clays were deposited in shallow water in a fast-sinking subevaporitic lagoon in Early Eocene age. A band of gypsum is present at the base of mudstone. Eastern half of the Karak mudstone outcrops possess a band of gypsum in the middle level; and the mudstone is folded into an anticline. The southern limb of this anticline forms an overfold which is thrust over the Siwalik shales and sandstones of Pliocene age.

The Eocene-age Bahadur Khel Salt, named by Meissner et al. (1974), underlies the Karak mudstone. The salt is massive but occasionally displays 5 to 15 cm thick salt layers. It is mostly white to cream coloured, and contains some transparent crystalline salt. The salt is diapiric, with an unexposed base. It generally fills anticlinal cores. Meissner et al. (1974) suggested a thickness of 100 m for the salt, and regarded it as a lateral facies equivalent of the Panoba Shale . At the upper contact with the Karak mudstone, a bed of gypsum is present.

MATERIALS AND METHODS

Clay sample used in this study is representative of Karak mudstone and is dominantly composed of illite-smectite with thirty % expandability. Illite-smectite is the major phase with consistent smectite content through out its exposure. However the quantities of other associated minerals slightly vary form place to place (Table 1). No other treatment was given except drying at 110 ^{o}C overnight followed by grinding. The ground material was passed through a 250 μm mesh.

Table 1

Bulk mineral composition, CEC, specific surface area and total surface area of Karak mudstone.

Mineral composition	CEC (meq/100g)	External specific surface area	Total surface area (m2/g EGME method)
illite-smectite (M), illite/muscovite (Min), kaolinite (Min), gypsum (Min), quartz (Min), dolomite (Min), feldspars (T)), pyrite (T), chlorite (T), halite (T)).	19.50	63.1	190

M is the major mineral phase, Min the minor mineral phase and T is the trace mineral phase.

The HCl used for activation was of analytical grade (FISONS) having concentration of 37% v/v. Solutions of different normalities ranging from 0.5N to 7N were prepared. For each acid strength, each sample was treated for seven different time intervals (1h, 1.5h, 2h, 3h, 4h, 5h and 6h), so 34 combinations between acid strength and time of treatment were applied. In each trial 10 gram of clay was added to 150 ml of HCl of specific strength in a double necked flask, equipped with a thermometer and condenser. The flask was placed in a water bath, thermostatically controlled at 95± 2 ^{o}C, and the slurry was subjected to continuous magnetic stirring . At the end of experiment the slurry was centrifuged and filtered through fast filter papers (Whatman No. 41). The clay residue was washed with hot water until no chloride ions could be detected. They were then dried overnight at 70 ^{o}C. The dried material was removed from the filter paper and disaggregated using pestle and mortar and was kept in sealed polythene bags to avoid any rehydration.

The structural changes of the products of activation were examined by X-ray Diffraction and Infra Red Spectrophotometery techniques. Cation Exchange Capacity of untreated and treated samples was also measured by methylene blue following the method of Inglethrope et al., (1993). Randomly oriented powder material was run for X-ray Diffraction on Philips PW 1729/1710, operating at 40 kV and 30 mA, using Ni filtered Cu Kα radiation at a scanning speed of 1°2θ per minute. Infra Red Spectroscopy was carried out on Bio-Rad, FTS-40, FTIR spectrophotometer. About 2 mg of each activated sample dried at 110 ^{o}C was dispersed in 200 mg of KBr and pressed on steel disks. External specific surface area of activated material was measured with Strohlein Area Meter II using nitrogen gas, while total surface area of untreated

clay was measured by EGME monolayer formation following the proceedure of Carter et al. (1965).

Bleaching capacity of activated clays was measured by decolourising the low euricic acid rape seed oil provided by SEATONS Ltd of Hull, UK. 20 ml oil was added to a double necked flask attached with condenser and thermometer and was heated to 90 ^{o}C. At this temperature 1 gram of activated clay was added to the flask. The mixture was heated for 20 minutes at this top temperature under constant stirring. The bleached oil was filtered under vacuum. The colour absorbence in the untreated and treated oil was measured at 450 nm with two shoulders at 480 and 430 nm in a spectrophotometer (Hewlett Packard 8452A Diode Array Spectrophotometer) by diluting 2.5 ml of oil in 10 ml of carbon tetrachloride. The amount of ß-carotene adsorbed on clay was obtained by the difference between the ß-carotene in the crude and treated oil. The following equation is used to determine the bleaching capacity.

$$BC = (C_o - C / C_o) \times 100$$

Where C_o = concentration (µg/ml) of ß-carotene in the crude oil

C = concentration (g/ml) of ß-carotene in bleached oil

The concentration of absorbed ß-carotene was converted to mole per 100 grams of clay. Similar bleaching experiments were performed on commercially available activated clay Fullmont AA for comparison.

RESULT

Structural changes

As a result of acid attack on clay minerals the structural changes in activated clay minerals involve mainly the exchange of interlayer cations and selective dissolution of the octahedral Mg, Al and Fe ions with release of silica precipitating as amorphous gel. X-ray diffraction traces of raw and activated clay for different acid strength and time intervals indicate these structural changes. After one hour activation with 1N HCl acid carbonates are dissolved. With continuous increase of acid strength and time interval there is a slight decrease in the intensities of 00l and hko reflections of I/S. A decrease in the intensities of kaolin peaks has also been noticed. A slight shift of 001/002 reflection maxima of I/S towards 10Å is also noticeable which is pronounced at 7N/6h, treatment (Fig. 2). Another important feature, which is evident from the traces and is more significant at treatment with 7N/6h is the increase in the background in the region of 16° to 28° 2θ. This is attributed to the precipitation of amorphous silica caused after the acid attack on octahedral layer.

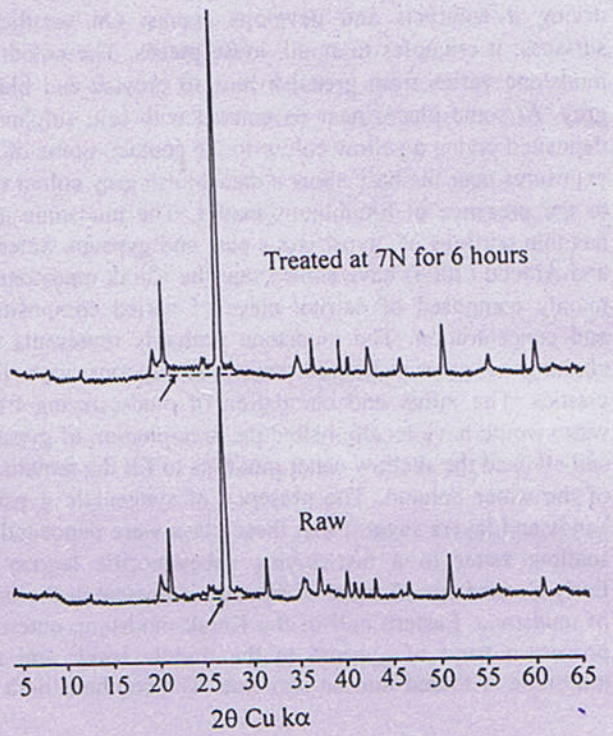

Fig. 2. XRD trace showing comparison between raw and activated clays, time and acid strength influences the structural disruption.

The analysis of infra-red spectra of acid activated clay (Fig. 3) shows a considerable difference when compared to raw material. The differences in intensities of various absorption bands characteristic of illite-montmorillonite mixed layer and other clay minerals again are pronounced only at severe treatments in terms of acid strength and time intervals. The observations noted are summarised as follow: The elimination of absorption bands present at 2527, 1443, 879 and 731 cm^{-1}; characteristic bands of dolomite, after treatment with even weak acid for short time. In the OH stretching region, the band at 3619 cm^{-1}, which arises due to the coincidence of bands of illite-montmorillonite and kaolinite and corresponds to AlAlOH and MgAlOH stretching vibrations, shows a systematic decrease in intensity with increasing severity of acid treatment. A similar change in intensity of absorption band at 3698 cm^{-1}, characteristics of kaolin is also noticeable. The band at 3425 cm^{-1}, which is due to absorption by the interlayer water diffuses with increasing severity of treatment. The intensity of Si-O out of plane stretching band at 1085 cm^{-1}, increases with the increasing severity of treatment, which is in accordance with the findings of Srasra et al. (1989) and Komadel et al. (1990), however the band at 1030 cm^{-1}, assigned to the Si-O-Si in plane vibrations does not show any change in intensity as observed by Srasra et al. (1989). The intensity of OH bending vibrations for

AlAl OH at 914 cm^{-1}, and AlMgOH at 843 cm^{-1}, decreases with increasing intensity of treatment and decreasing effect is more prominent in case of AlMgOH band intensity. The intensity of vibration bands at 796 cm^{-1} and 778 corresponding to free Si-O is also increased with increasing severity. This is because of precipitation of silica gel removed as a result of dissolution. A slight decrease in the intensity of the vibration band at 530 cm^{-1}, which corresponds to Si-O-Al and Si-O-Mg coupled with vibration band at 431 cm^{-1}, assigned to Si-O are found to be unchanged.

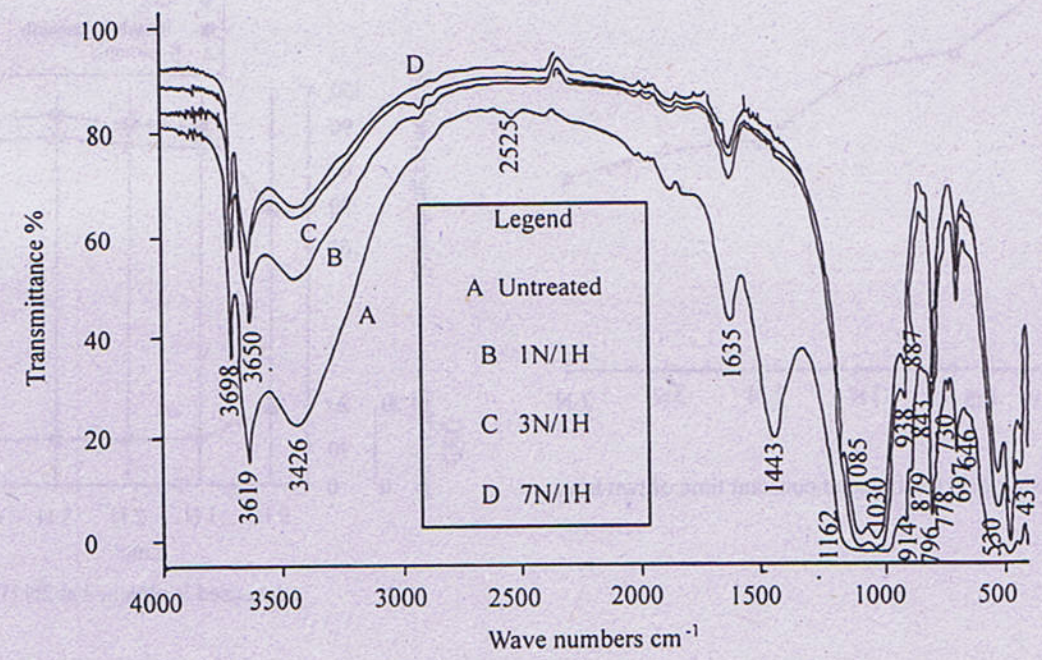

Fig. 3 Infrared spectra of untreated and acid activated clays for one hour with different acid strength.

The cation exchange capacity (CEC) of the activated material decreases with increasing acid strength and period of treatment (Figs. 4a,b, Table 2). It is evident (Fig. 4a) that the decrease in CEC occurs in steps when measured on material activated for different acid strengths, and is gradual and insignificant (Fig. 4b) for different time intervals. A comparison of variation in CEC with bleaching capacity and concentration of β-carotene absorbed shows no relation with these properties (Fig. 5).

Table. 2

Cation exchange capacity (meq. 100/g.) of activated clay treated at different acid strength and time combinations.

Acid strength→ ↓-Time	0.5N	1N	2N	3N	7N
1h	16.66	15.30	11.90	11.43	9.97
2h	16.00	15.12	11.63	11.21	9.98
3h	-------	15.10	11.62	10.81	9.83
4h	16.33	------	------	------	9.41
5h	-----	------	------	10.33	9.00
6h	16.00	11.80	11.51	10.45	8.10

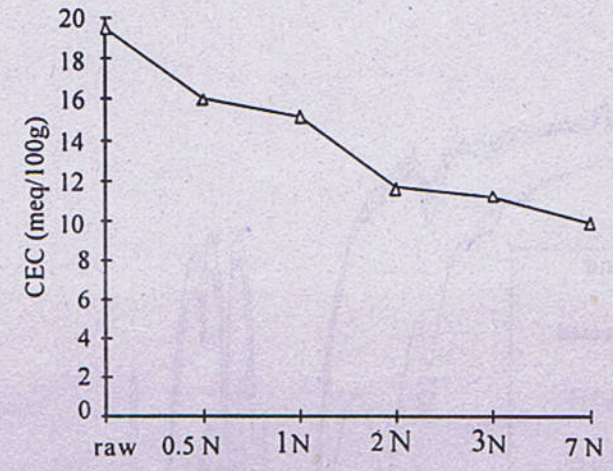

(a) Increasing acid treatment at constant time of two hours.

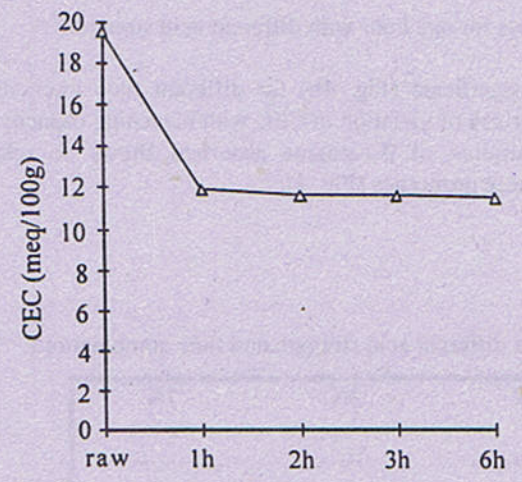

(b) increasing time at constant acid strength of 2 N.

Fig. 4 Effect of acid treatment on CEC with respect to (a) acid strength and (b) treating time.

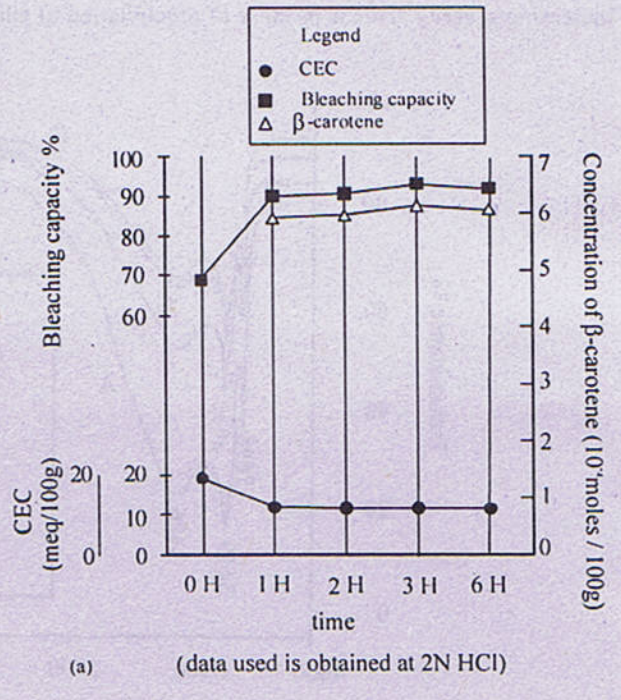

(a) (data used is obtained at 2N HCl)

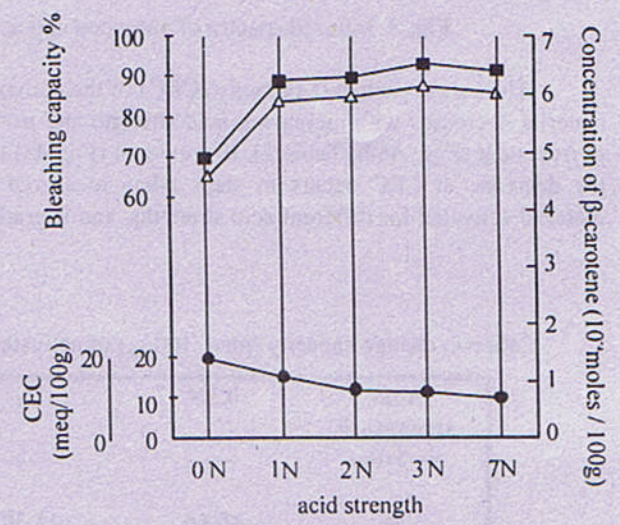

(b) (data used is obtained at 2 hours)

Fig. 5 Evaluation of CEC with increasing time (a) acid strength (b) showing no relation with bleaching capacity and ß-carotene absorbed.

Table. 3
Specific surface area (m^2/g) of activated clay at different acid strength and time combinations.

Acid Strength→ ↓Time	0.5N	1N	2N	3N	7N
1h	78.32	80.77	86.45	96.24	103.45
1.5h	78.56	-----	87.75	100.40	108.93
2h	78.72	85.54	88.50	102.25	111.34
3h	81.70	85.98	89.38	106.36	112.56
4h	85.57	86.42	93.45	110.07	113.53
5h	85.96	89.49	97.90	111.46	113.80
6h	86.39	91.70	99.46	112.08	112.30

SURFACE AREA

Surface area of activated clay increases with increasing acid strength and treatment time (Fig.6, Table 3). It is evident from the figure that the maximum surface area is attained by treating the clay for 5 hours with the acid having 7N concentration and further increase of time causes a decline in the surface area. Although activation with concentrations higher than 7N was not performed, however drop in surface area at 7N for 6 hours treatment indicates that further increase of acid concentration will cause a drop in surface area at smaller treatment time. These results are in accordance with the findings of other workers (Novak and Gregor, 1969; Kolta et al., 1975; Yates, 1986). By comparing the Figures 6a and 6b, it is found that there is a sharp increase in the surface area with the increasing acid strength for the same duration and steady increase with increasing treatment time for the same acid strength. These results show that higher surface area values are attained either by increasing the acid strength and decreasing the time of treatment or by increasing the time and decreasing the acid strength. Therefore higher values of surface area are attained with different combinations of acid strength and time treatments (Fig.7).

BLEACHING CAPACITY

Bleaching capacities of untreated and activated clay are given in Table 4 and the relation between bleaching capacity and acid concentration/treatment time is illustrated in Figure 8. The maximum bleaching capacity, which is 93%, can be attained at two combinations between acid strength and time intervals, either bleaching with clay activated with 2N acid strength for 3 hours or activated with 3N for two hours. The other combinations show smaller bleaching capacity. The treatment with weak acid like 0.5N and 1N show a progressive increase in bleaching capacity for different time intervals and remains below the maximum bleaching capacity, and the treatment with higher acid strengths i.e. 2N and 3N initially increase the bleaching capacity followed by a gradual decrease as the time of reaction increases. The bleaching capacity at the acid strength of 7N shows a continuous decrease for different time intervals.

By comparing the Figure 6 with Figure 8 it is evident that bleaching capacity does not correlate with the variations of the surface area with acid treatment. Higher values of bleaching capacity are attained at treatments with acid strengths of 2N and 3N despite the fact that surface area of the product treated with 7N acid is much higher than those treated with 2N and 3N acid strengths. These results are in accordance with the findings of Morgan et al (1985) and Zaki et al. (1986) but contradict the results of Novak & Gregor, (1969) and Kolta et al. (1975).

The absorption of ß-carotene is demonstrated in Figure 9. The pattern is similar to that of bleaching capacity as it reflects this property. It is evident from the figure that there is a progressive increase in absorption when weak 1N strength acid is used, but for the 2N and 3N acid strength initially absorption increases and reaches a maximum, beyond which prolonged treatments cause a decrease in absorption. The treatment with 7N acid strength causes a progressive decrease in absorption with increasing time intervals. The surface area measurements show higher values at 7N treatment than 2N and 3N but the absorption is less at 7N treatment indicating that maximum absorption is not associated with higher surface area values.

Absorption spectrum of ß-carotene lies between 400 and 500 nm. The degree of absorption of ß-carotene is indicated in Fig. 10. The absorption spectrum for crude oil is represented by curve (a), which is characterised by the deflection maximum at 450 nm with two subsidiary deflections at 430 and 480 nm. Curve (b) is the spectrum of oil treated with raw clay, which demonstrates a considerable decrease in absorption due to removal of ß-carotene

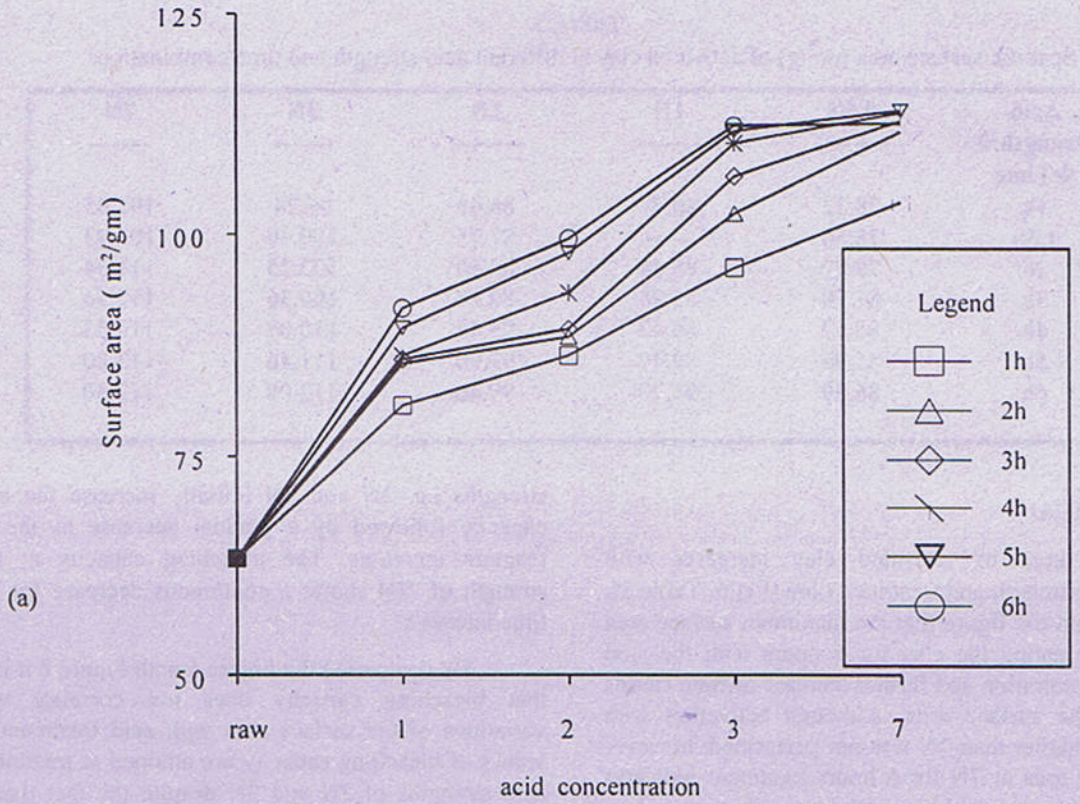

(a)

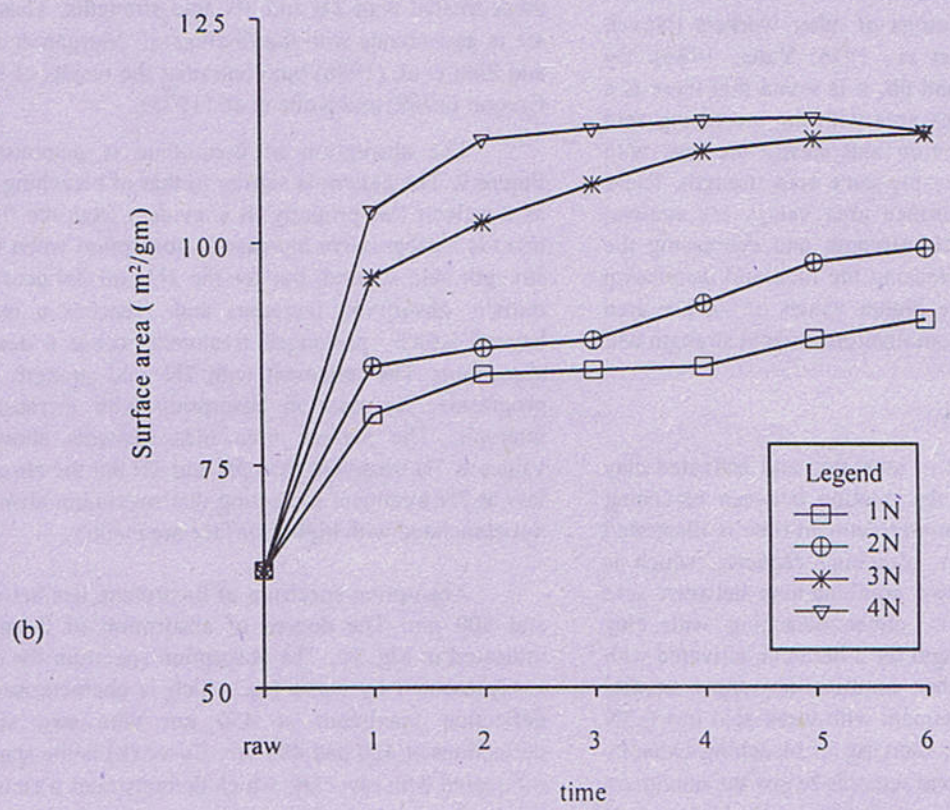

(b)

Fig. 6 Effect of the (a) increasing acid strength and (b) time on the surface area of activated clay.

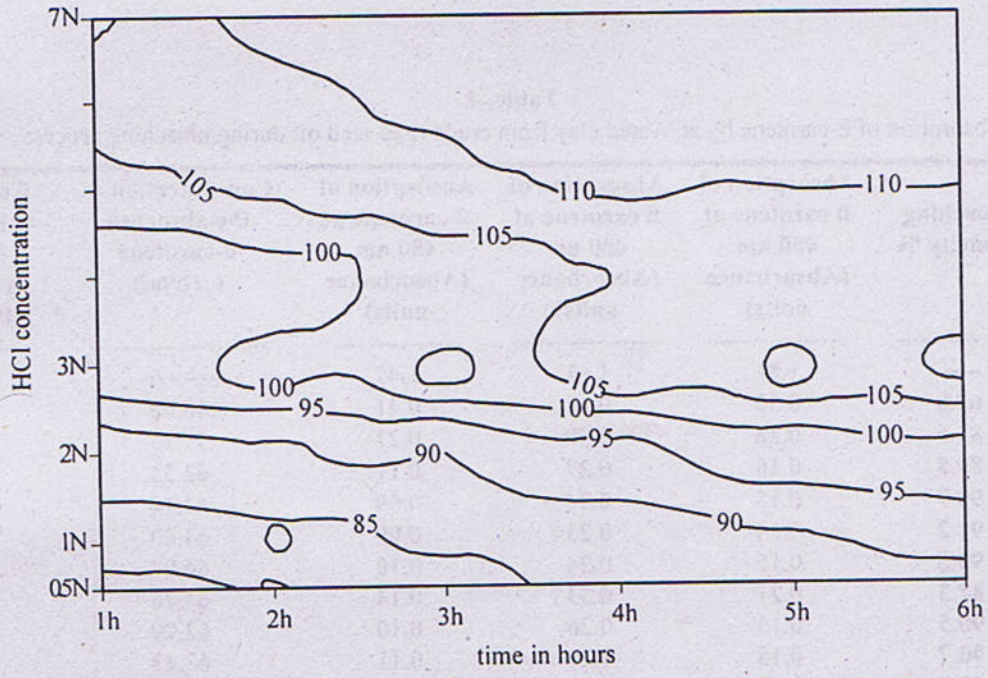

Fig. 7 Effect of acid strength and time duration on the increased surface area of activated clays.

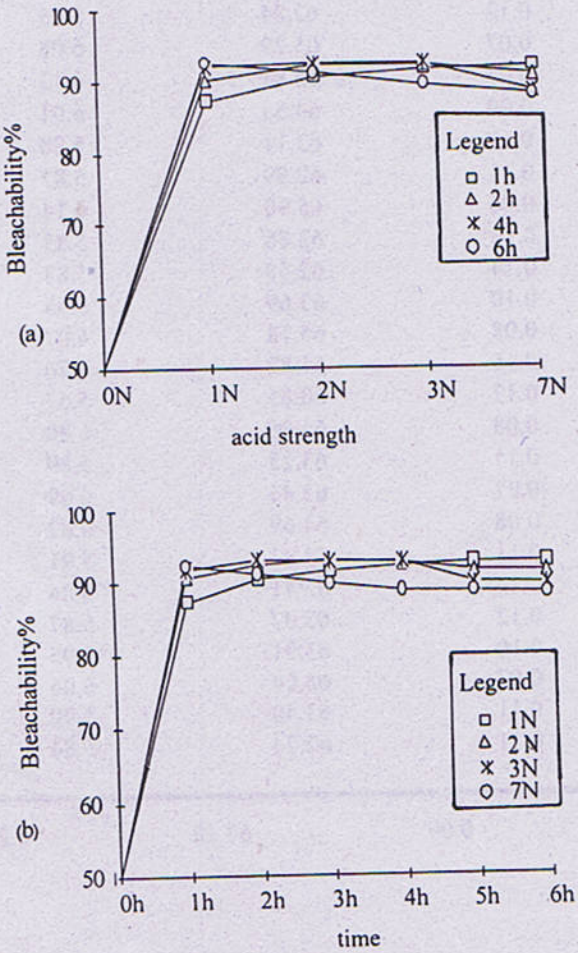

Fig. 8 Effect of increasing (a) acid strength and (b) treating time on the bleaching capacity of activated clays.

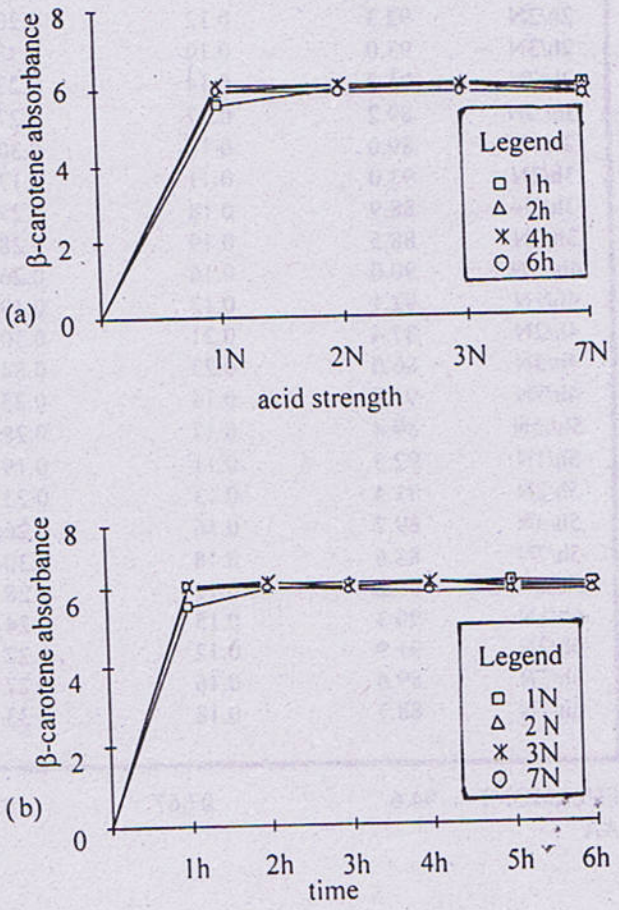

Fig. 9 Effect of (a) acid strength and (b) treating time on the absorption of ß-carotene (expressed as 10^{-4} moles/gm. of clay).

Table. 4.

Absorption of ß-carotene by activated clay from crude rape seed oil during bleaching process.

Sample Karak illite-smectite clay	Bleaching capacity %	Absorption of ß carotene at 450 nm (Absorbance units)	Absorption of ß carotene at 430 nm (Absorbance units)	Absorption of ß carotene at 480 nm (Absorbance units)	Concentration of the absorbed ß-carotene (μb/ml)	Concentration of the absorbed ß-carotene (10^{-4} moles/ 100gr. clay)
Crude oil	----	1.81	1.61	1.47	---------	------
Raw clay	68.8	0.55	0.65	0.41	48.68	4.53
1h/.5N	83.6	0.28	0.39	0.21	59.13	5.51
1h/1N	89.8	0.16	0.27	0.11	63.53	5.92
1h/2N	90.7	0.15	0.24	0.09	64.14	5.97
1h/3N	91.2	0.14	0.23	0.09	64.49	6.01
1h/7N	90.6	0.15	0.24	0.10	64.07	5.97
1.5h/.5N	87.3	0.21	0.33	0.14	61.76	5.75
1.5h/2N	90.5	0.15	0.26	0.10	63.99	5.96
1.5h/3N	90.7	0.15	0.26	0.11	63.47	5.91
1.5h/7N	92.2	0.12	0.20	0.08	65.22	6.07
2h/.5N	88.2	0.19	0.29	0.13	62.39	5.81
2h/1N	88.8	0.18	0.30	0.12	62.84	5.85
2h/2N	92.3	0.12	0.20	0.07	65.29	6.08
2h/3N	93.0	0.10	0.18	0.06	65.81	6.13
2h/7N	91.2	0.14	0.23	0.09	64.55	6.01
3h/.5N	89.2	0.17	0.27	0.12	63.11	5.88
3h/1N	89.0	0.18	0.30	0.11	62.99	5.87
3h/2N	93.0	0.11	0.17	0.06	65.90	6.14
3h/3N	88.9	0.18	0.27	0.13	62.86	5.85
3h/7N	88.5	0.19	0.28	0.14	62.58	5.83
4h/.5N	90.0	0.16	0.26	0.10	63.69	5.93
4h/1N	92.1	0.12	0.19	0.08	65.18	6.07
4h/2N	87.4	0.21	0.30	0.16	61.82	5.76
4h/3N	86.0	0.23	0.34	0.17	60.85	5.67
4h/7N	91.0	0.14	0.25	0.08	64.38	6.00
5h/.5N	89.4	0.17	0.28	0.11	63.25	5.89
5h/1N	92.5	0.11	0.19	0.07	65.44	6.09
5h/2N	91.4	0.13	0.23	0.08	64.69	6.02
5h/3N	89.7	0.16	0.26	0.11	63.43	5.91
5h/7N	88.6	0.18	0.30	0.12	62.71	5.84
6h/.5N	89.2	0.17	0.28	0.12	63.07	5.87
6h/1N	90.3	0.15	0.24	0.10	63.91	5.95
6h/2N	91.9	0.12	0.22	0.07	65.04	6.06
6h/3N	89.6	0.16	0.27	0.11	63.40	5.90
6h/7N	88.7	0.18	0.33	0.11	62.74	5.84
FULLMONT AA	94.6	0.067	0.15	0.09	67.18	6.26

alongwith decrease in intensities of deflections. Curve (c) is the spectrum of oil bleached by clay activated by 2N acid for three hours. This curve indicates a significant drop in absorption with almost complete elimination of deflections

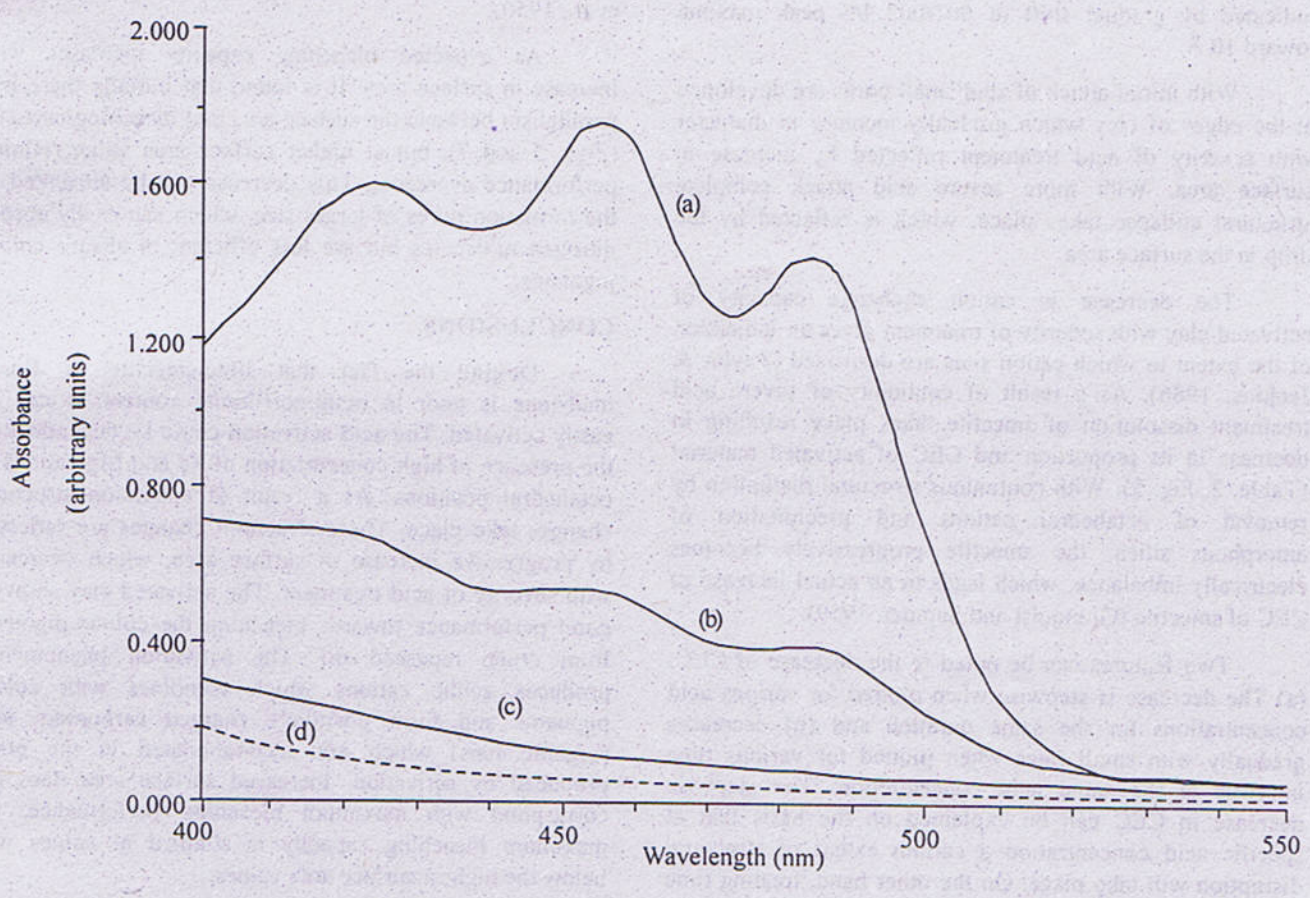

Fig. 10 Total absorption spectra for rapeseed oil (a) bleached with untreated (b) with activated karak clays (HCl 2N for 3 hours) (c) and with FULLLMONT AA (d).

DISCUSSION

Despite the fact that the concentration of the montmorillonite in I/S mixed layer is low and further diluted by the admixture of other impurities, it can be activated very easily with treatment of moderate combinations of acid strength and treatment time. The mineral chemistry (Table 1) of I/S indicates that it is rich in Fe and Mg cations, which are considered to be present in octahedral positions alongwith, Al. Initially the acid dissolves dolomite followed by attack on the octahedral sheet of montmorillonite exposed at the grain edges. As a result tetrahedral cations are released from the structure and the dissociated silica precipitates in amorphous form. The amount of released cations increases with the increase in severity of treatment. The rate of dissolution is different to different workers. Stoch et al. (1977) found higher rate of Mg release than other cations, while Osthaus (1956) proposed the same rate of dissolution for all octahedral cations. Novak and Cicel (1978) have postulated that the stability of the octahedral layer is lowered as a result of substitution of larger cations of Mg^{+2} and Fe^{+3} for Al^{+3}. This results in flattening, distortion and tension in the structure, due to which removal of Mg and Fe cations becomes easier than that of Al cations.

The infrared spectra of activated clay show a progressive decrease in intensity with severity of treatment of vibration bands (Fig.2) located at 843 cm^{-1} and 887 cm^{-1} assigned to AlMgOH and $AlFe^{+3}OH$. Comparatively higher intensity reduction of AlMgOH band may indicate higher removal of Mg^{+2} than Fe^{+3}. Further severity of treatment causes a structural collapse as evident from decrease in surface area at higher acid treatment for prolonged period (Fig.5).

The broadening of 001/002 peak of I/S, decrease in intensities of other basal and hko peaks and increase in background in (Fig.1) the region of 16° to 28° 20 due to

precipitation of amorphous silica is another piece of information indicating disruption in the clay structure. As a result of acid attack interlayer cations are replaced by H^+ ion causing a certain degree of collapse in interlayer spacing indicated by gradual shift of 001/002 I/S peak maxima toward 10 Å.

With initial attack of acid small pores are developed at the edges of clay which gradually increase in diameter with severity of acid treatment reflected by increase in surface area. With more severe acid attack complete structural collapse takes place, which is reflected by the drop in the surface area.

The decrease in cation exchange capacity of activated clay with severity of treatment gives an indication of the extent to which cation sites are destroyed (Taylor & Jenkins, 1986). As a result of continuity of severe acid treatment dissolution of smectite takes place resulting in decrease in its proportion and CEC of activated material (Table. 2, Fig. 3). With continuous structural disruption by removal of octahedral cations and precipitation of amorphous silica, the smectite progressively becomes electrically imbalance, which leads to an actual increase of CEC of smectite (Granquist and Samner, 1959).

Two features can be noted in the decrease of CEC; **(a)** The decrease is stepwise when plotted for various acid concentrations for the same duration and **(b)** decreases gradually with small rates when plotted for various time intervals at the same acid concentration. The stepwise decrease in CEC can be explained on the basis that at specific acid concentration a certain extent of structural disruption will take place. On the other hand, treating time for a specific concentration plays a limited role in decreasing CEC.

The exact modifications after activation in smectite structure are not known (Rupert et al., 1987). It is possible that octahedral Fe^{+2}, if present, may be oxidised during activation without concomitant uptake of ^-OH as in case of oxidation of Fe^{+2} in nature (Lear and Stucki, 1985). In natural samples oxidation of Fe^{+2} is accompanied by uptake of OH, therefore CEC does not decrease (Lear and Stucki, 1985). In the activated samples OH are probably removed during treatment making the situation complicated (Thomas et al., 1950).

As expected bleaching capacity increases with increase in surface area. It is found that initially there is a parallelism between the surface area and bleaching capacity (Figs. 5 and 7), but at higher surface area value refining performance decreases. This decrease can be attributed to the formation pores of larger size, which can easily absorb nitrogen molecules but are less efficient to absorb colour pigments.

CONCLUSIONS

Despite the fact that illite-smectite in Karak mudstone is poor in montmorrilonite content, it can be easily activated. The acid activation could be dependent on the presence of high concentration of Fe and Mg cations in octahedral positions. As a result of activation structural changes take place. These structural changes are reflected by progressive increase in surface area, which decreases with severity of acid treatment. The activated clay shows a good performance towards bleaching the colour pigments from crude rapeseed oil. The activation phenomenon produces acidic cations which combines with colour pigments and form positively charged carbonium ions (organic ions) which are accommodated in the pores produced by activation. Increased surface area does not correspond with maximum bleaching performance; the maximum bleaching capacity is attained at values well below the highest surface area values.

The optimum bleaching capacity, which in this study is 93%, can be attained at 2N/3h and 3N/2h acid strength and time combinations. The 3N/2h combination is the most suitable as the cost of acid is much lower as compared to energy prices in Pakistan.

REFERENCES

Boyd, S.A., and Jaynes, W.F., 1994. Role of layer charge in organic contaminant sorption by organo-clays. In Mermut, A.R. (ed.) Layer Charge Charaterstics of 2:1 silicate Clay Minerals. CMS workshop lectures, 6, 47-77.

Brindley, G.W.,and Youell, R.F., (1951). A chemical determination of "tetrahedral" and "octahedral" aluminium ions in a silicate. *Acta Crytallogr.* **4**, 495-496.

BrÜckman, K., Fijal, J., klapyta, Z., Wiltowski, T. & Zabiniski, W., (1976). Influence of different activation methods on the catalytic properties of montmorillonite. *Mineralogica Polinica.* 7, 5-14.

Carter, D.L., Heilman, M.D. & Gonzalez, F.L., (1965) Ethylene glycol monoethyl ether for determining surface area of silica minerals. Soil. Sci. **100**, 356-360.

Christidis, G.E., Scott.P.W., Dunham, A.C., (1997). Acid activation and bleaching capacity of bentonites from the islands of Milos and Chios, Aegean, Greece. Appl. Clay Sci. **12**, 329-347.

Clarke, G.M., (1985). Special Clays. Ind. Miner. **216**, 2551.

Fahn, R. & Fenderl, K., (1983). Reaction products of organic dye molecules with acid treated montmorillonite. Clay Miner. **18**, 447-458.

Fijal, J., klapyta, Z., Kwiecinska B., Zietkiewitcz, J. & Zyla, M., (1975). On the mechanism of acid activation of montmorillonite: II. changes in the morphologyand porosity in the light of electron microscopic and adsorption investigations. Mineralogica Polinica. **6**, 49-57.

Gastuche, M.C. & Friapiat, J.J.,(1962). Acid solution techniques applied to the determination of the structure of clay and controlled by physical methods. Sci. Cerm. **1**, 121-138.

Granquist, W.T. & Samner, G.G., (1959). Acid dissolution of a texas bentonite. Clays and Clay Miner. **6**, 292-308.

Griffiths, J., (1990). Acid activated bleaching clays. What's cooking in theoil industry?. Ind.Miner. **276**, 55-67.

Grim, R.E., (1962). Applied Clay Mineralogy. McGraw Hill, New York. 422pp.

Inglethorpe, S.D.J., Morgan, D. J. & Bloodworth, A. J., (1993). Industrial Mineral Laboratory Manual: bentonite. Tech. Rep. Brit. Geol. Surv. WG/93/20. pp 116.

Jovanovic, N. & Janackovic, J., (1991). Pore structure and adsorption properties of an acid-activated bentonite. Appl. Clay. Sci. **6**, 59-68.

Kheok, S.C. & Lim, E.E., (1982). mechanism of palm oil bleaching by montmorillonite clay activated at various acid concentrations. J. Am. Oil Chem. Soc. **59**, 129-131.

Kolta, D.R., Novak, I., Samir, Z. El-T. & Kamaila, A.El-B., (1975). Evaluation of bleaching capacity of acid -leached Egyptian bentonites. J. Appl. Chem. Biotechnol. **26**, 355-360.

Komadel, P., Schmidt, D., Medejova, J., Cicel, B., (1990). Alteration of smectite by treatments with hydrochloric acid and sodium carbonate solutions. Appl. Clay Sci. **5**, 113-122.

Kaviranta, H., Pinnavaia, T., (1994). Acid hydrilysis of octahedral Mg' sites in 2:1 layered silicates: An assesment of edge attack and gallery access mechanism. Clays Clay Miner. **42**, 717-723.

Lear, P. R. & Stucki, J. W., (1985). Role of structural hydrogen in the reduction and reoxidation of iron in nontronite. Clays Clay Miner. **34**, 346-352.

Meissner, C. R., Master, J. M., Rashid, M. A. and Hussain, M., 1974. Stratigraphy of the Kohat Quardrangle, Pakistan U. S. Geol. Surv. Prof. Paper, 716-D: 89pp.

Milliken, T.H., Oblad, A.G. & Mills, G.A. (1955) Use of clays as petroleum cracking catalysts. Clays Clay Miner. **1**, 314-326.

Mills, G.A., Holmes, J. & Cornelius, E.B., (1950): Acid activation of some bentonite clays. J. Phys. colloid Chem. **54**, 1170-1185.

Morgan, D.J., Shaw, D.B., Sidebottom, T.C., Soon T.C. & Taylor R.S., (1985). The function of bleaching earths in the processing of palm, palm kernal and coconut oils. J.Am. Oil Chem. Soc. **62**, 292-299.

Newman, B.S., (1963). The thermal stability of acid extracted montmorillonites. Proc. Int Clay Conf. Stockholm, Pergamon press, Oxford.

Novak, I. & Gregor, M., (1969). Surface area and decolourizing ability of some acid treated montmorillonites. Proc.Int. Clay Conf. Tokyo, 851-857.

Novak, I. & Cicel, B., (1978). Dissolution of smectites in hydrochloric acid: II. Dissolution rate as a function of crystallochemical composition. Clays Clay Miner. **26**, 341-344.

O' Driscoll, M., (1988). Bentonite; overcapacity in need of market. Ind. Miner. **250**, 43-67.

Odom, I. E., (1984). Smectite clay minerals: properties and uses. Phil. Trans. R. Soc. Lond. **A311,** 391-409.

Osthaus, B. B., (1954). Chemical determination of tetrahedral ions in nontronites and montmorillonites. Clays Clay Miner. Proc. 2nd Nat. Conf., Nat. Acad. Sci.- Nat. Research Council Publ. **327**, 407-416.

Osthaus, B., (1956). Kinetic studies on montmorillonites and nontronite by the acid dissolution technique. Clays Clay Miner. **4,** 301-321.

Rhodes, C. N., Brown, D. R., (1992). Structural characterization and optimization of acid treated montmorillonite and high porosity silica support for $ZnCl_2$ alkylation catalysts. J. Chem. Soc. **55,** 777-780.

Rupert, J.P., Granquist, W.T., & Pinnavaia, T.J., (1987). Catalytic properties of clay minerals. pp 257-318 in: Chemistry of Clays Clay Minerals (A.C.D. Newman editor). Mineralogical Society, London.

Saleemi, A.A.& Ahmed, Z.,(2000). Mineral and chemical composition of karak mudstone, Kohat Plateau, Pakistan: implications for smectite-illitization and provenance. Sed. Geol. **130,** 229-247.

Siddiqui, M.K.H., (1968). Bleaching earths. Pergamon press, Oxford, pp32-55.

Srasra, E., Bergaya, F., van Damme, H. & Arguib, N.K., (1989). Surface properties of an activated bentonite. Decolourization of rape-seed oil. Appl. Clay Sci. **4,** 411-421.

Stoch, L., Bahranowski, K., Budek, L. & Fijal, J., (1977). Bleaching properties of non-bentonitic clay material and their modifications. Stoch L., Bahranowski K., Budek L. & Fijal J.Mineralogia Polinica. **8,** 31-49.

Stoch, L., Bahranowski, K., Eilmes, J. & Fijal, J., (1979). Bleaching properties of non bentonitic clay materials and their modifications: III.. Modifications of bleaching properties of Krakowiec clays from Machow with some organic compounds. Mineralogia Polinica. **10,** 39-47.

Taylor, D.B. & Jenkins, D.B., (1986). Acid activated clay. Am. Soc.. Min. Eng. Mtng.

Tkac, I., Komadel, P., Müller, D., (1994). Acid treated montmorillonites: Astudy by ^{29}Si and ^{27}Al MAS-NMR. Clays. Clay Miner. **29,** 11-19.

Thomas, C. L., Hickey, J. & Stecker, G., (1950). Chhemistry of clay cracking catalysts. Ind. Engg. Chem. **42,** 866-871.

Yates, M.H., (1986). Acid treatment of English montmorillonite and its effect on clay structure and properties. Unpub. Paper. (Leporte inorganics, Windes, U.K).

Zaki, Abdel-Khalik, M., Habashi, G. M., (1986). Acid leaching and consequent pore structure and bleaching capacity modifications of Egyptian clays. Colloids Surf. **17,** 241-249.

Geol. Bull. Punjab Univ. 35, 2000.

DIAGENETIC ENVIRONMENTS OF THE DUNGAN FORMATION, EASTERN SULAIMAN RANGE, PAKISTAN.

BY

NAZIR AHMAD
Institute of Geology, Punjab University, Lahore-54590, Pakistan.

AND

J. D. HUDSON
Department of Geology, Leicester University, Leicester, U.K.

Abstract;-. *The Dungan Formation underwent severe diagenetic alteration which have altered its original components and texture since the time of their initial deposition until the present time. The diagenetic environments have been distinguished one from another by their own characteristic processes and the resultant features such as dissolution and cementation. The diagenetic history of Dungan Formation commenced in the early marine phreatic environment as most of the carbonate rocks started their diagenetic history there, then passed via an active fresh water phreatic environment to the last stage of shallow burial phase.*

INTRODUCTION

The Sulaiman Range is located on the north-west margin of the Indian Plate. It forms the middle part of the Indus Basin, and has been termed the Sulaiman Basin. The Dungan Formation is Palaeocene/Lower Eocene in age and comprises a 98 m thick predominantly carbonate sequence which extends about 200 km from north to south, of the Sulaiman Range.

The diagenetic environments of eight microfacies, peritidal, inner lagoon, oolitic, outer lagoon, rhodolith platform, nummulitic, larger benthonic foraminiferal and planktonic foraminiferal of the Dungan Formation (Ahmad, 1996) for which the samples are taken from three sections Raghasar, Zinda Pir and Rakhi Nala have been discussed (Fig. 1).

This paper deals with the main diagenetic environments, and their products which are recognised in the course of the petrographic studies of the stained thin section by reflected light microscopy, cathodoluminescence microscopy, electron microprobe and scanning electron microscopy in back scattered mode. It also includes the geochemical investigations.

DIAGENETIC ENVIRONMENTS

Carbonate sediments are deposited as metastable assemblage mainly of aragonite and Mg-calcite (Bathurst, 1975). The transformation of such assemblages of metastable minerals towards rocks composed of stable assemblage of calcite takes place by stages until the rocks are destroyed by weathering or metamorphism. The Dungan Formation is mainly shallow marine sediments, dominated by tests of Mg-calcite (red algae, foraminifers, echinoderms and bryozoa) and aragonite (bivalves, gastropods and corals). These sediments have undergone the following digenetic environments.

MARINE DIAGENESIS

Marine diagenesis takes place on sea-floor and just below, and on tidal flates and beaches (Fig. 2). A wide variety of cement morphologies are present in modern carbonates. They are essentially of only two mineralogies: aragonite and high-Mg calcite. The high-Mg calcite cement occurs as acicular-bladed isopachous fringes, equant crystals, micrite and peloids (Tucker and Wright, 1990).

The Dungan Formation was deposited in warm shallow (<100 m) seas, with all the pore spaces in the sediments filled with normal marine water. At this stage two principal diagenetic changes affected the sediments, which are micritization and the peloidal cement.

A. Micritization

This is one of the first stage of diagenesis seen in the sediments of Dungan Formation and it occured during deposition as most carbonates are deposited in marine

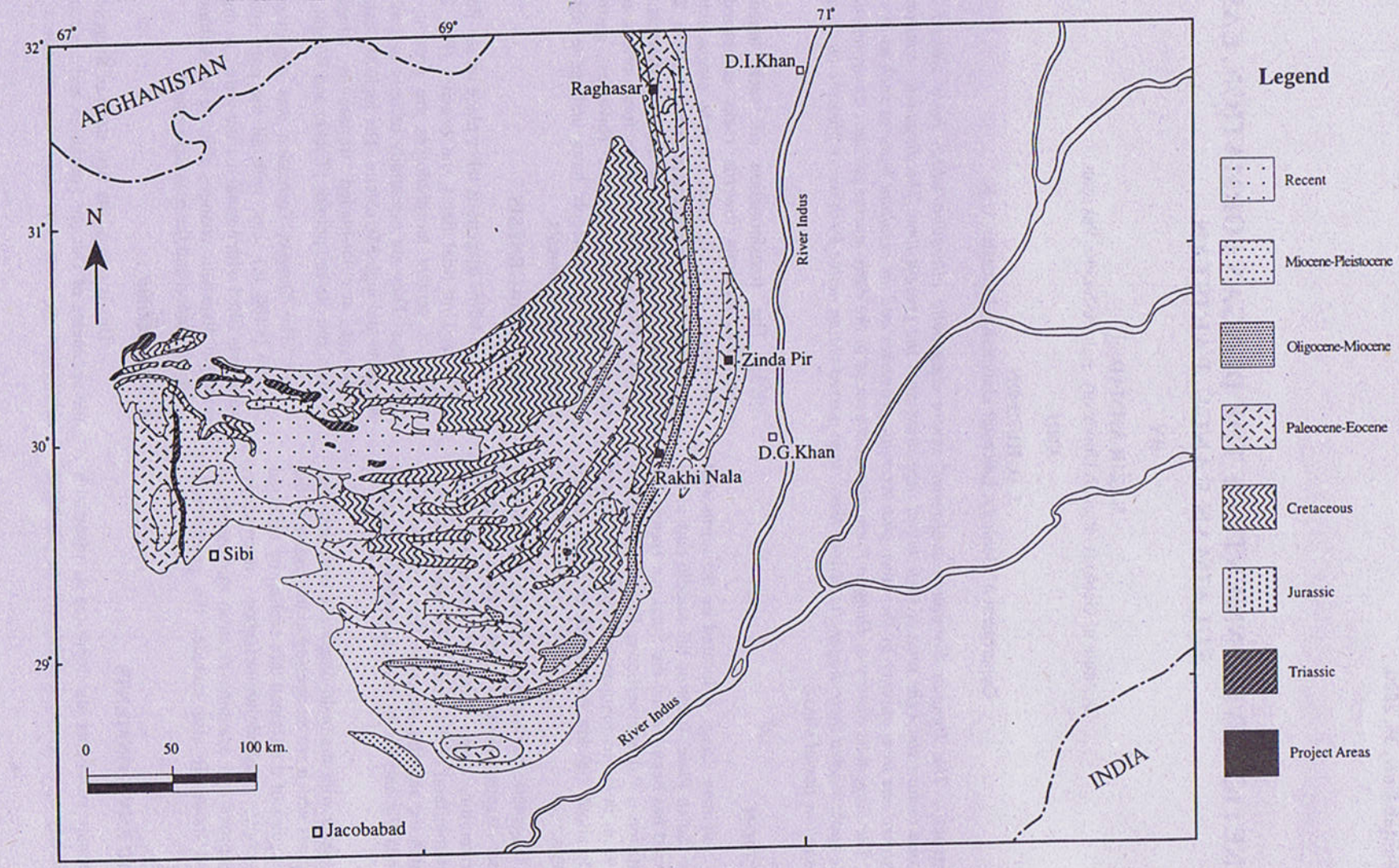

Fig.1 Generalized geological Map of the Sulaiman Basin (modified after Bakr and Jackson, 1964)

environment and thus begin their diagenetic history there. Micritic envelopes are present commonly in almost all the facies except planktonic foraminifera facies of the study area. Micritic envelopes enclose the petrographically unaltered cores of the skeletal carbonate generally high Mg-calcite (foraminifera, coralline algae) (Plate 1-A), and the totally/partially altered cores of aragonite skeletal (molluscs) (Plate 2-A). In most of the cases the micrite envelopes are regular (Plate 1-B). The encrusting algae and boring organisms are common in rhodolith platform facies (Plate 7-A). Under cathodoluminescence they do not show luminescence or very dull luminescence (Plate 1-C). Eight analysis of micrite by electron microprobe indicate the wt.% of $CaCO_3$ is 97.25 and mol% of $MgCO_3$ is 1.83 whereas in drusy cement the wt.% of $CaCO_3$ is 98.84 and mol% of $MgCO_3$ is 1.21.

Interpretation

Micritization of grains by boring algae resulted in the formation of a micritic envelope similar to those described by Bathurst (1966, 1975) and Kendall and Skipwith (1969). Many skeletal grains, such as molluscs and algae, on the present sea floor, and in ancient limestone, have been replaced partly or wholly by a fine-grained greyish mosaic of carbonate crystals, the micrite, Folk (1959). The replacement began at the exposed surface of the grain and spread irregularly inwards. An envelope of micrite was formed that simply enclosed the unaltered core of skeletal carbonate generally foraminifera, algae or molluscs . The process goes on centripetally within the grains and partially converted the grains to micrite. Absence of broken envelopes indicated that the dissolution and void-filling were completed before compaction. The encrusting algae and boring organisms that micritized the outer portions and occasionally the inner portions of the bioclastics have been observed in Recent sediments of Abu Dhabi by Kendall and Skipwith (1969) and they concluded that it was a marine phreatic process. Bathurst (1966, 1975) and Kobluk and Risk (1977) believed that these processes took place in marine phreatic zone. The mol% of $MgCO_3$ is higher as compared to that of drusy cement which suggests the same result. In summary, it is concluded that the micritization takes place in the marine phreatic environment.

B. Peloidal Cement

The peloidal cement consists of subspherical bodies of 20 to 50 μm. and are composed of micrite of less than 3 μm. The microspar cement crystal of 5 to 8 μm. are embedded in between the subspherical bodies of peloidal cement. This type of cement occurs in rhodolith platform and nummulitic facies of the Dungan formation. These facies are the main carbonate accumulating facies. In the studied sections, it is mainly present in the mid-ramp. Under cathodoluminescence microscopy, it does not show luminescence.

Interpretation

According to Scoffin (1987), peloidal cements are formed under active marine environment in reef frame. In Recent sediments, the peloidal cement is composed of high-Mg calcite and forms in marine environment (Tucker and Wright, 1990). The peloidal cements occur in interskeletal and intraskeletal cavities, but they also form surficial crust on corals (Lightly, 1985). The origin of the peloids has been extensively discussed by (Lightly, 1985; Macintyre, 1985; Chafetz, 1986;) which owes to 1) an algal origin, 2) a replacement texture, 3) detrital sediment, 4) the product of pelletizing organisms or 5) in situ precipitation.

In this study it is only present in the rhodolith platform and nummulitic facies which are considered to be the main carbonate accumulating facies. Since the peloidal cement is mainly present in the algae rich facies, and the peloids are indicative of algal origin. The cathodoluminescence studies show the lower concentration of Mn and Fe which takes place mainly in the marine water. On this basis it is considered that the peloidal cements are developed in the marine environment.

FRESH-WATER DIAGENESIS

The freshwater phreatic zone (Fig. 2) lies between the vadose and the mixed marine phreatic-freshwater zones. All pore spaces in this zone were filled with meteoric water containing variable amounts of dissolved carbonate. The top of the phreatic zone is marked by the water table. The lower boundary is gradational with marine water in areas proximal to the sea. In inland areas, the freshwater phreatic zone grades downward into a zone with subsurface fluids which might contain brines deriving from sediment compaction, clay dehydration, heating and differences in density. The geometry of the freshwater meteoric zone is controlled by topography, rainfall, and the distribution of porosity and permeability in the rocks. The saturation of water with respect to $CaCO_3$ may increase as water moves downward (Longman, 1980).

Aragonite and high Mg-calcite are more soluble than low Mg-calcite in meteoric waters. Their dissolution leads to supersaturation with respect to calcium carbonate and, in the meteoric waters with a low Mg/Ca ratio, low Mg-calcite precipitates (Tucker and Wright, 1990).

During freshwater diagenesis, both aragonite and high-Mg calcite are replaced by low Mg-calcite. As a result of these mineralogical changes, geochemical changes also occur (Gavish and Friedman, 1969) involving loss of cations present in the original marine carbonate and gains of other trace or minor elements from the meteoric fluid:

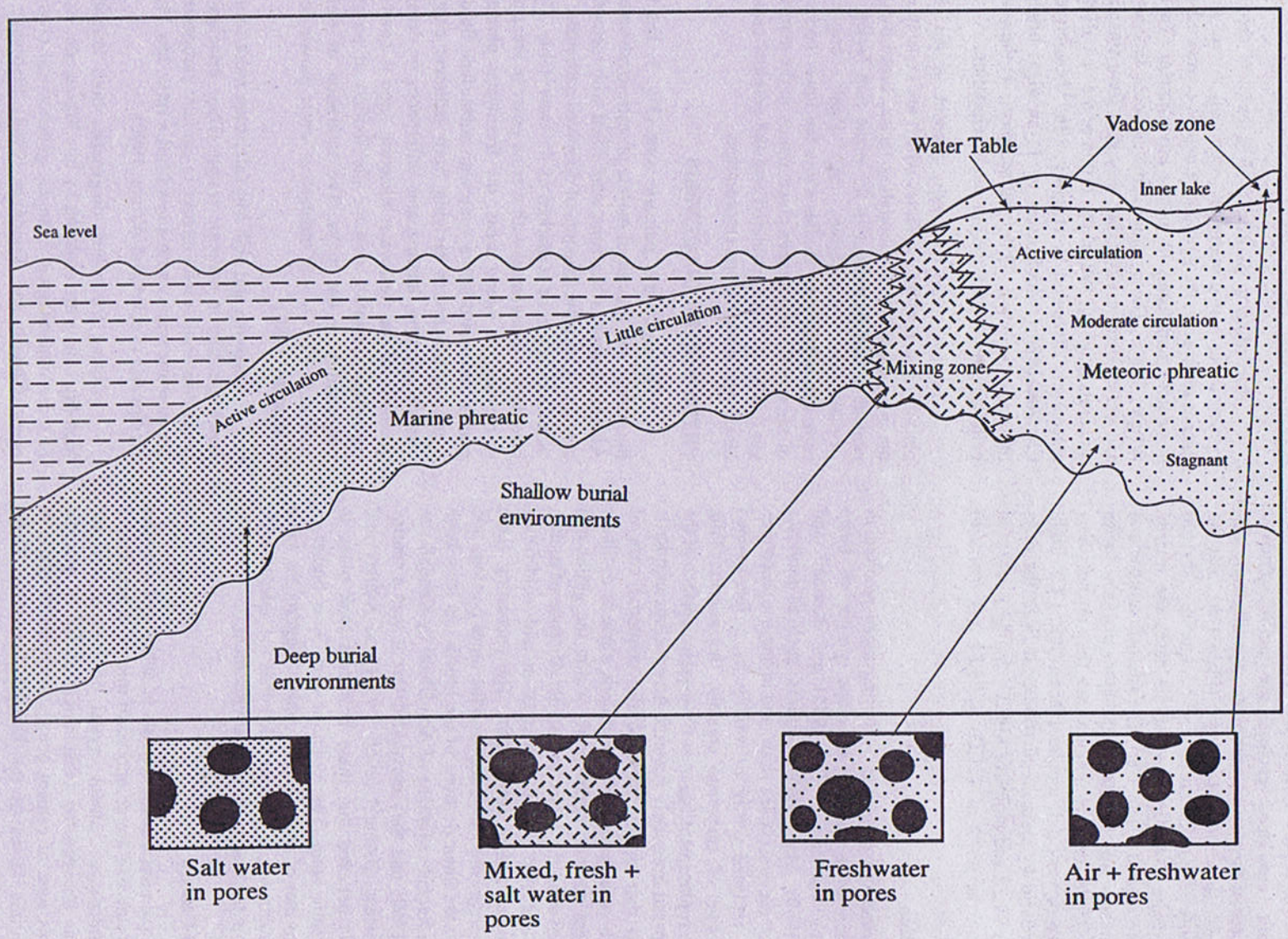

Fig. 2 Cross-section shows the distribution and relationship of major carbonate diagenetic environments, schematically drawn for a homoclinal ramp (modified after Tucker and Wright, 1990).

strontium (from aragonite) and Mg (from high Mg-calcite) are depleted (Benson, 1974), while Mn and Fe (typically present in greater amount in groundwater than sea water) may be incorporated into the diagenetic low Mg-calcite. Changes in isotopic composition of carbonate also occur (Hudson, 1977).

The first investigations of meteorically altered Pleistocene carbonate shows them to be cemented by calcite and stabilized to low-Mg calcite (Land et al., 1967; Gavish and Friedman, 1969). They believe that meteoric diagenesis is the main cause of transformation of carbonate sediments to limestones. However, many limestones in the geological record did not undergo meteoric diagenesis, while others had only the weakest of meteoric overprints (Tucker and Wright, 1990).

A. Neomorphic Spar

These are the microsparry calcite between the grains, and within the skeletal grains. The crystals are sub-equant to irregular in shape and have irregular intercrystalline boundaries (Plate 2-B). Extinction within the crystal, rarely uniform, is mainly patchy. The crystals stain pink and blue, and consequently they are non-ferroan and ferroan low magnesium calcite. There is little tendency for crystal size to increase into the pore space.

The dissolution and reprecipitation of the aragonite of shells, mainly molluscs, as a mosaic of sparry calcite is common in inner lagoonal, oolitic, outer lagoonal and rhodolith platform facies. The outer lagoonal and rhodolith platform facies are observed associated with recrystallization of some portions such as micritic matrix into microcrystalline calcite (Plate 2-B). Relics of the original grains can be faintly seen. Under cathodoluminescence microscopy the neomorphic spar crystals are mainly non luminescent but in some cases they show bright orange lines of luminescence.

Interpretation

Neomorphism is defined by Folk (1965) as transformation between one mineral and itself or a polymorph which results in the growth of new crystals that are larger or different in shape from the previous crystals. Carbonate minerals are very susceptible to such recrystallization. Neomorphism in the limestones described in this thesis was produced by micrite enlargement, a process by which crystals that measure only a few microns in diameter enlarge to a size measuring tens of microns in diameter. This micrite enlargement creates neomorphic products similar to cement in crystal size. The new crystals are known as pseudospar (Folk, 1965) or neospar (Nichols, 1967 and Flugel, 1982). Depending on water chemistry and rates of water flow, micrite may recrystallize and be neomorphosed to coarser grains in freshwater phreatic environment or in a fresh water vadose environment (Longman, 1980: Flugel, 1982). The neomorphic microspar occurs in the updip part where pore water are fresh, and it is absent downdip where formation water is saline (Longman and Mench, 1978). Aggrading neomorphism has commonly taken place in fine grained limestones to give mosaics of microspar crystals (generally in the range of 5-10 μm) and coarser pseudospar crystals (>30 μm). This neomorphism may take place during early meteoric diagenesis (Tucker and Wright, 1990).

The neomorphic microspars are observed in outer lagoonal and rhodolith platform facies of the studied area. The size distribution of the individual crystals is usually random and devoid of any regular pattern. This neosparite exists as isolated patches and thus appears to be floating in the rock. The parts of limestone which have undergone extensive micrite enlargement display relic patches of non replaced micrite. These patches reveal that the limestone originally was a micrite rather than a sparite. In summary, it is concluded that the microcrystalline calcite cement was formed due to neomorphism.

B. Dissolution

The effect of dissolution is seen in almost all the facies particularly in oolite, outer lagoonal, rhodolith platform, nummulitic, and larger benthonic foraminifera facies. The petrographic investigation indicated that the sediments had been affected by probably only one stage of dissolution. This stage probably occurred after the precititation of first calcite cement. This is indicated by the presence of moulds of large bivalve fragments (which were probably aragonite originally) and vugs which are filled by large blocky calcite crystals (Plate 2-C), interpreted as representing a second generation of calcite cementation (drusy cement).

Interpretation

Undersaturated meteoric water dissolved carbonate sediments and limestones. The meteoric waters were acidified by atmospheric and soil CO_2, as well as by soil acids. Aragonite, being more soluble than calcite, underwent more rapid dissolution. The solution chemistries are complex (Thrailkill, 1968; Plummer et. al., 1979; Bogli, 1980; Drever, 1982; Trudgill, 1985; and Lohmann, 1988).

The effect of dissolution had a broad range of intensity and generally increased the porosity. Dissolution also formed solution vugs and mouldic voids which are locally interconnected by the enlargement of the basic intergranular porosity. As a matter of fact, the dissolution process had created a vast amount of vuggy and mouldic secondary porosity.

In the freshwater environment, the content of Mg^{2+} is normally low and the precipitation of low-magnesian calcite is no longer inhibited. So, the more soluble phases, aragonite and various Mg-calcite, dissolve and the Ca^{2+} ions are reprecipitated as calcite (Bathurst, 1975, 1980). Aragonite grains dissolved totally to give a mould which filled later with calcite cement (Plate 2-C). On the basis of above discussion it is concluded that the dissolution was caused by meteoric water.

C. Cementation

i) Isopachous Bladed Cement

Isopachous balded cement is found in oolitic, outer lagoonal, rodolith platform, nummulitic and larger foraminiferal facies (Plate 3-A & B). The isopachous bladed cement is in the form of thin uniform fringe surrounding ooids in the case of oolite, and on the walls of foraminifera and grow outwards into the pore space. In general isopachous bladed calcite crystals are fine grained and they are non-ferroan. Under cathodoluminescence microscopy they show bright orange luminescence (Plate 3-C).

Interpretation

According to Scoffin (1987), isopachous bladed cements are found in the phreatic zone of permanent water where major changes in the mineralogy and texture of the original marine sediment takes place. There is an undersaturated zone near the level of water-table where solution is prevalent, and below this is the zone of active circulation of saturated water, calcite precititated as a isopachous bladed cement. Pores in the freshwater phreatic zone are always filled with water, and so crystals can grow unimpeded except by intercrystalline competition, Thus cement rind formed here, at least in the shallow lenticular phreatic, are either well developed isopachous layers of calcite crystals around pore walls (James and Choquette, 1984). The cathodoluminescence microscopic studies indicate the higher concentration of Mn and Fe which is normally in the freshwater phreatic zone as compared to sea water, consequently, it is suggested the isopachous bladed cement is formed in the freshwater phreatic environment.

ii) Drusy Cement

The drusy cement is the major cement type which found in all the facies. This type of cement occurred, as all the aragonite dissolved and low magnesian calcite precipitated, both in the primary pores and the secondary pores by the dissolution of the aragonite grains. The crystal size of the drusy cement is >10 μm and it increases from pore walls to the centre of cavity. The crystals are clear, anhedral to subhedral. The pore filling calcite is commonly an equant mosaic of ferroan and non-ferroan calcite (Plate 4-A & B). The morphology of these crystals is similar to those described by Longman (1982); that is to say, crystals of void filling cement which are optically continuous over large areas and showing almost irregular boundaries.

Under cathodoluminescence microscopy this type of cement shows dull to orange luminescence (Plate 4-C). 198 analysis by electron microprobe of ferroan drusy cement show 1.9 mol% of $MgCO_3$ and the concentration of Fe, Mn, and Sr, is 8394, 1925, and 719 ppm respectively. 207 analysis of non-ferroan drusy cement were made. On the basis of these analysis the mol% of $MgCO_3$ is 1.21, and the concentration of Fe, Mn, and Sr is 874, 281, and 646 ppm respectively.

Drusy cement was picked from two samples for the carbon and oxygen isotope analysis. On the basis of these analysis $\delta^{13}C$ values ranges from -0.38 to -0.40, mean -0.39 PDB: and $\delta^{18}O$ ranges from -9.61 to -9.78, mean -9.70 PDB.

Interpretation

In the freshwater phreatic aragonite and high Mg-calcite are more soluble than low Mg-calcite. Their dissolution makes supersaturated solutions with respect to calcium carbonate resulting in precipitation of low Mg-calcite. In the studied thin sections the bioclasts have originally high Mg-calcite (foraminifera, coralline algae, echinoderms, and bryozoa) and aragonite (corals and molluscs). The aragonite grains dissolved in slightly acidic freshwater; thus, voids originated between the grains (as long as smaller particles or cements formed earlier can be dissolved) or in the grains (as long as micrite envelopes prevent the dissolution of the whole grains). During the dissolution of a great deal of material collapse structure resulted, after which calcite precipitated as cement in the voids or between the particles. The carbonate supersaturated water precipitated calcite cement which rapidly closed the original pores. Bioclasts consisting of high Mg-calcite are an exception (e.g. coralline algae); they inverted to calcite without destroying their original structure (Richter, 1979). The cathodoluminescence studies suggest the higher concentration of Mn and Fe in the drusy cement, which is further confirmed by the electron microprobe analysis. The drusy cements are typically clear, blocky calcite, with rich in iron and Mn (Tucker and Wright, 1990). Such cements show normally dull luminescence with minor bright zones (Niemann and Read, 1988) reflecting the apparently original nature of the shallow meteoric waters. Down dip, reducing conditions develop resulting in calcite capable of luminescence. $\delta^{18}O$ values for marine limestones ranges from +1 to -1, and for freshwater limestones it ranges from -4 to -12 PDB, (Veizer and Hoefs, 1976, and Hudson, 1977). The present study indicates that the drusy cement has an average value of $\delta^{18}O$ -9.70 PDB, which is agreement with

their conclusions. In summary, on this basis it is considered that the drusy cement was formed in freshwater phreatic environment.

iii) Syntaxial Overgrowth Cement

This type of cement is present in all the facies except planktonic foraminifera facies, but it is common in outer lagoonal, rhodolith platform and nummulitic facies. The syntaxial overgrowth cement commonly forms on echinoderm fragments and it has been described by Evamy and Shearman (1965). The calcite of echinoderm fragments and of the inner parts of the overgrowths remained iron free calcite. The outer part of each overgrowth, however, showed a succession of zones of varying iron contents (Plate 5-A). The outlines of these zones represented the shape of the overgrowth at the various stages in their development. Under cathodoluminescence microscopy the syntaxial overgrowth cement shows bright zoned luminescence around the echinoderm fragments which represents the various zones of varying concentration of Mn and Fe contents (Plate 5-B).

Interpretation

According to Evamy and Shearman (1965), the syntaxial overgrowth cement served as an important clue for distinguishing the various diagenetic environments. Syntaxial overgrowths form most rapidly in the freshwater phreatic environment and generally surround the grains although they may be elongate along the c-axis. Because of the large crystal nucleus and absence of competitive crystal growth, they grow much faster than cements from adjacent non-echinoderm grains, as shown by the larger proportion of the pore they fill. According to Longman (1980), syntaxial overgrowths form most commonly in freshwater phreatic environment, they may also form in vadose (rarely) and deeper subsurface diagenetic environments.

The syntaxial overgrowth cement is very common in the studied sections. According to cathodoluminescence studies the concentration of Mn and Fe are high in the syntaxial overgrowths. On this discussion it is suggested that the syntaxial overgrowth cements are developed in the freshwater phreatic environment.

SHALLOW BURIAL DIAGENESIS

A. Compaction

The effect of compaction is seen in larger foraminiferal and planktonic foraminiferal facies. Compaction is a common diagenetic process in carbonate rocks, and compactional processes are generally divided into two catagories; mechanical and chemical processes. Mechanical compaction begins soon after deposition. Sediments of the Dungan Formation generally show only shallow burial compaction, as bioclasts are preserved without deformation or breakage in the studied thin sections. The bioclasts were probably preserved from compaction by early cementation of these sediments. The textures produced by mechanical compaction are recognised and occurred in few facies. In oolite, rhodolith platform and nummulitic facies the grains have point contacts with each others, whereas in larger foraminifera facies the grains have a concavo-convex contacts with each other (Plate 5-C).

B. Pressure Dissolution

i) Dissolution Seams

Dissolution seams are recognised in the planktonic foraminifera facies only, as this facies is more argillaceous. These are smooth, undulose seams of insoluble residue which lack the distinctive sutures of stylolites. Wanless (1979) discribed them as the non-sutured seams which pass around and between grains, rather than cutting through them. They are common in more argillaceous limestones, and develope preferentially along thin clay layers or at the junction of clay-rich and clay-poor limestones.

ii) Stylolite

The stylolites are seen only in the larger benthonic foraminifera and planktonic foraminifera facies. The seams of the stylolite usually consist of residues of dark material. The maximum amplitude observed is 1cm. although the length of the stylolite peaks is variable and ranges down to 1mm (Plate 6-A).

Dunnington (1967), suggested that undersaturated pore fluids play a role in the formation of stylolites and are necessary for solution-compaction processes. This requires increased overburden pressure or undersaturated water from an outside source (Becher and Moore, 1976). Solution results in the formation of stylolitic boundaries between clasts in response to the overburden pressure. Compaction and tight packing of clasts could be the result of this pressure solution (Longman,1980).

C. Fractures and Veins

There are two generations of calcite filled fractures/veins, early fractures which are distinguished from the later generation by being cross-cut by them. The early fractures are filled by non-ferroan calcite cement, whereas the later veins are filled by ferroan calcite cement.

i) Early Fractures

The fractures are seen in almost all the facies of the studied area. The characteristic feature of the cement fill, is pink stained non-ferroan calcite. The fracture filling calcite cystals are larger than the drusy cement, anhedral to subhedral, and have irregular boundaries. The veins are generally small ranging up to several centimeters in length

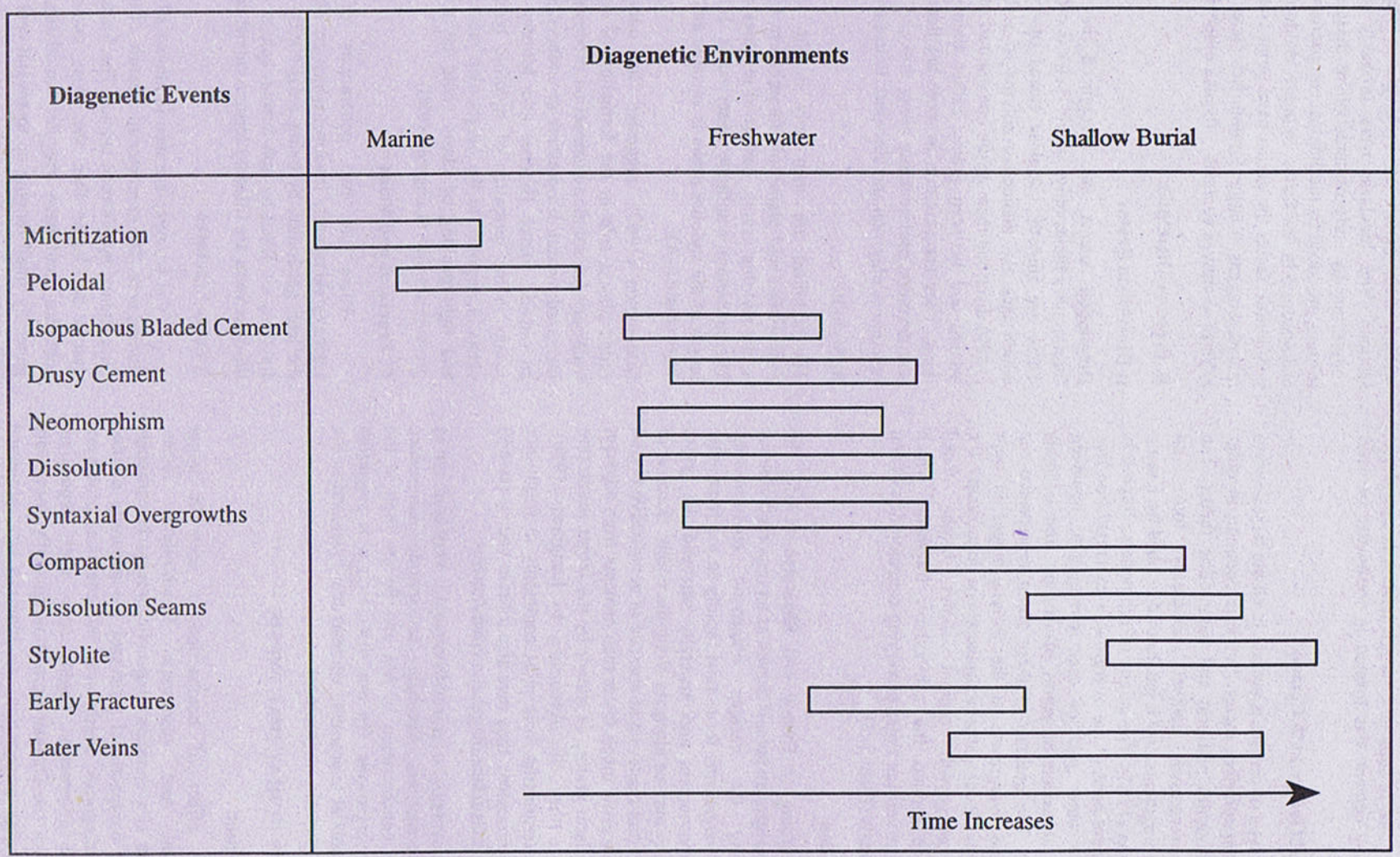

Fig. 3. Different diagentic events observed in Dungan Formation in relation to both time and Diagenetic environments.

and ranging from 0.3mm to 0.8mm in width (Plate 6-B). Most of the fractures run parallel to each other. Under cathodoluminescence microscopy they show bright zoned luminescence (Plate 6-C), which indicate the different zones of concentration of Mn and Fe contents. Three samples of cement filling the fractures were picked for carbon and oxygen isotope analysis. On the basis of these analysis δ13C values ranges from -0.03 to -2.17, mean -0.89 PDB: and $\delta^{18}O$ ranges from -10.77 to -13.42, mean -11.96 PDB.

Interpretation

These early fractures are interpreted as mechanical fractures that developed after lithification, probably during burial. These fractures are filled by sparry calcite cement under shallow burial freshwater environment, as the concentration of Fe and Mn are high in the cement (on the basis of cathodoluminescence microscopy). The concentration of Fe and Mn are high in fresh water as compared to sea water. The average $\delta^{18}O$ values of cement filling fractures is -11.96 PDB, which also indicates that the cement is formed in freshwater environment (Hudson,1977; Allan and Matthews, 1977, 1982).

ii) Later Veins

These later veins are observed in the rhodolith platform, nummulitic and larger benthonic foraminifera facies. The characteristic features of the cement filling veins is blue stained ferroan calcite. The veins are generally larger ranging up to several centimeters in length and ranging from 0.3 mm to 0.7 mm in width. They run parallel to each other but intersect the early fractures/veins. They are filled by equant anhedral to subhedral calcite crystals. Under cathodoluminescence microscopy they show bright lines of luminescence.

Five samples of cement filling the veins are picked for carbon and oxygen isotope analysis. On the basis of these analysis $\delta^{13}C$ values ranges from +1.38 to +0.91, mean +1.20 PDB: and $\delta^{18}O$ ranges from -7.08 to -10.59, mean -9.12 PDB.

Interpretation

These veins are also filled by sparry calcite cement which are mainly ferroan. They indicate the freshwater phreatic environment as the fresh water has more concentration of dissolved Mn and Fe ions as compared to sea water. The $\delta^{18}O$ values (-9.12 PDB), further strengthen the view of a fresh water diagenetic environment (Hudson,1977; Allen and Matthews, 1977, and 1982). $\delta^{18}O$ values of later veins are greater as compared to early fractures which indicates that the later veins are formed probably later under shallow burial environments by formation water. On the basis of this discussion it is suggested that the later veins were formed at later stage in shallow burial freshwater phreatic environment.

DIAGENETIC HISTORY OF THE DUNGAN FORMATION

With the marine, freshwater, and shallow burial environments and the variable array of cement texture that may be produced in each zone, interpreting diagenetic history is complex. However, sufficient evidence exists for the interpretation of these events and these are shown in Fig. 3.

The sediments of the Dungan Formation were deposited in the shallow marine environment and they are composed of red algae, foraminifera, molluscs, bryozoa, coral and echinoderm fragments. They contain both aragonite (coral and molluscs) and high Mg-calcite (red algae, foraminifera, bryozoa and echinoderm) grains. Marine water saturated the pores. The first stage of diagenesis occurred after the deposition in the relatively stagnant marine phreatic environment in the form of micritization of grains by boring algae (Plate 7-A). The micritic envelopes were formed around the grains. Minor cementation occured inside small pores of the red algae and foraminifera, perhaps because of bacterial activity (Longman, 1980). No alteration of grains nor leaching occurred.

Afterward it entered into the freshwater phreatic zone. In this zone cementation occurred and all pore spaces were filled with equant calcite cement (drusy cement). The cement coarsened towards the pore centres (Plate 7-B). Bladed isopachous cement formed on some grains if the cements nucleate on the grains and grow fastest along a preferred crystallographic axis (Longman, 1980). Syntaxial overgrowth cements formed on echinoderm fragments and grew more rapidly than the cement on adjacent grains. Because the water was saturated with respect to calcite, no leaching of the grains occurred prior to cementation. Recrystallization of unstable grains to calcite took place. Meanwhile diagenesis continued in the zone of undersaturation with aragonite. Aragonite leached from the original grains to produce mouldic porosity. The solution also attacked some Mg-calcite grains and these Mg-calcite grains neomorphosed to calcite without undergoing a solution stage. Cement so formed, in the pores of red algae, was more stable than the red algae itself. Reprecipitation of

the dissolved material as equant calcite (drusy cement) occurred almost simultaneously with solutions. Later on it changed into the shallow burial environment. In this environment, compaction of the skeletal grains, dissolution seams and stylolite and features/veins were developed. Finally the veins were formed in the freshwater phreatic zone. The early fractures were filled by the equant calcite (non-ferroan) and the veins were filled later on under shallow burial environments by the formation water, and these veins cut the original grains and early features and some of the drusy cement also became ferroan (Plate 7-C).

CONCLUSIONS

The diagenesis of the Dungan Formation starts from the marine phreatic environment, characterised by micritization and peloidal cements. These cements are of high Mg-calcite, and low in Fe and Mn. They do not show luminescence.

The active fresh water phreatic zone may involve leaching in the zone of solution, neomorphism, isopachous bladed cement around the oolites and foraminifera, syntaxial overgrowth cement on echinoderm fragments, and interlocking crystals of equant calcite that coarsen towards the pore centres (drusy cement). The neomorphic spars having irregular boundaries and are cloudy and patchy. Vug and mould porosities are developed in the fresh water vadose zone, which are filled by sparry calcite cement.

The shallow burial environment is marked by compaction of skeletal grains, stylolites and fractures. The fractures show two generations. The early fracture; filled cements are non-ferroan and show bright zoned luminescence. The later fracture filled cements are ferroan and non-luminescent.

Explanation of Plates

Plate 1

A. Photomicrograph illustrating the chambers of the foraminifera filled partially by sparry calcite cement and partially by micrite.

B. Photomicrograph illustrating the micritic envelope around the foraminifera.

C. Cl photomicrograph of the photograph (B), where the micritic envelope shows dull luminescence, the chambers and the original shell are non-luminescent.

Plate 2

A. Photomicrograph illustrating the process of dissolution and cementation. The mollusc fragments are totally dissolved leaving micritic envelopes around them and later on filled by non-ferroan sparry calcite cement.

B. Photomicrograph illustrating the neomorphic spar having irregular boundaries and patches within the crystals.

C. Photomicrograph illustrating the ghost structure, where the original structure of the skeletal allochem is totally destroyed creating a mold porosity which later on filled by sparry calcite cement.

Plate 3

A. Photomicrograph illustrating the isopachous bladed cement around the foraminifera. The isopachous bladed cement is non-ferroan and the chambers are filled partially by ferroan and partially by non-ferroan sparry calcite cement.

B. Photomicrograph showing the chambers of the foraminifera are filled by ferroan sparry calcite cement and the original structure of the foraminifera is unaltered.

C. Cl photomicrograph showing the orange luminescence of isopachous bladed cement around the oolites.

Plate 4

A. Photomicrograph showing the pores (in between the skeletal grains) are filled by drusy cement..

B. Photomicrograph illustrating the drusy cement in between the algal grains.

C. Cl photomicrograph of the photograph B, where the drusy cement showing the orange luminescence.

Plate 5

A. Photomicrograph of echinoderm fragment showing the syntaxial overgrowth cement.

B. Cl photomicrograph of the above echinoderm fragment, where the syntaxial overgrowth cement showing the bright zoned luminescence, indicating different zones of Fe and Mn concentration.

C. Photomicrograph illustrating the chambers of the foraminifera are filled by ferroan sparry calcite cement and the walls are unaltered.

Plate 6

A. Photomicrograph showing the stylolite, dark lines are solution interfaces with concentration of insoluble minerals (especially clay minerals). These lines pass around the skeletal grains.

B. Photomicrograph of the non-ferroan calcitic vein showing the irregular boundaries and anhedral to subhedral crystals of calcite.

C. Cl photomicrograph of the above vein illustrating the zoned luminescence. The zones can be differentiated on the basis of intensity of luminescence having different concentration of Fe and Mn.

Plate 7

A. Photomicrograph illustrating the micritization (may be rhodolith coralline algae) by boring algae.

B. Photomicrograph of drusy cement showing irregular boundaries and the crystal size increases towards the centre of the pore space.

C. Photomicrograph illustrating the shallow burial environment in which the drusy cement and the walls of the foraminifera became ferroan.

Plate 1

A

B

C

Plate 2

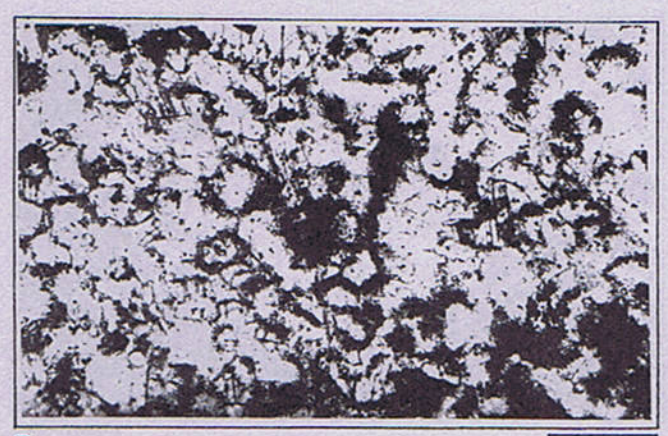

Plate 3

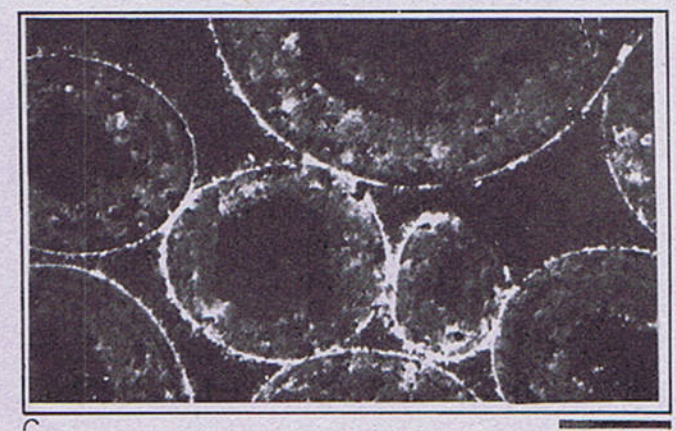

Plate 4

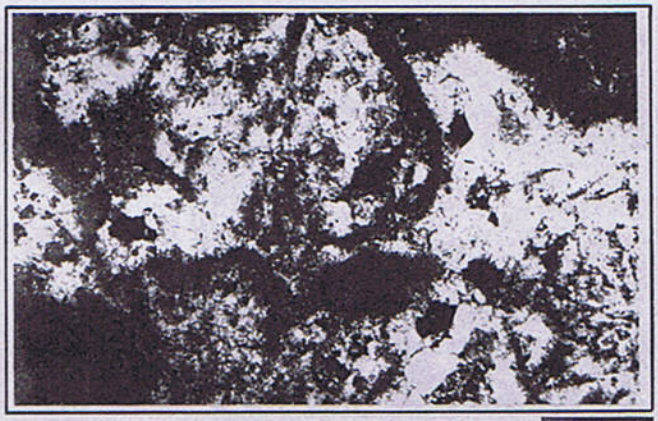

A

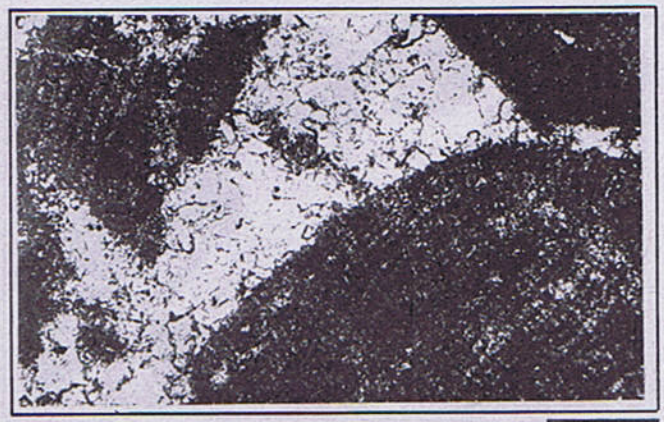

B

C

Plate 5

A

B

C

Plate 6

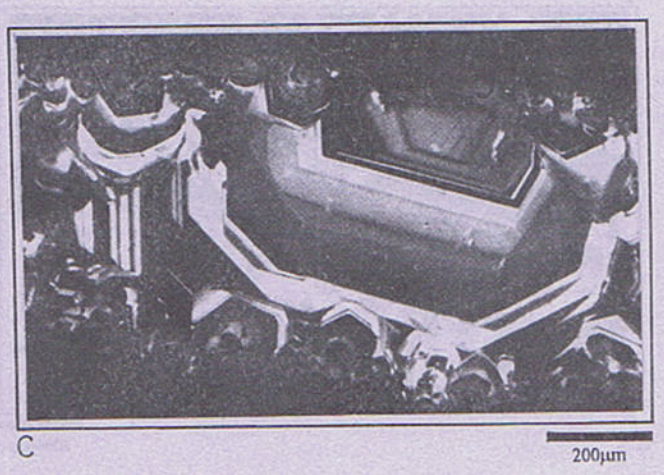

Plate 7

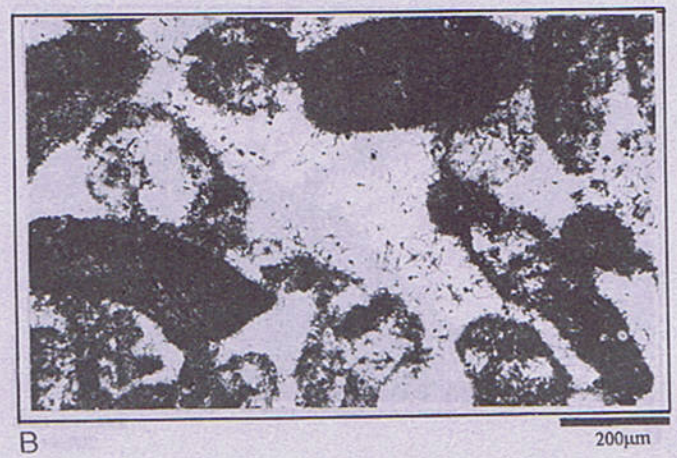

REFERENCES

Ahmad, N. 1996. Palaeoenvironments, diagenesis and geochemical studies of the Dungan Formation (Palaeocene), Eastern Sulaiman Range, Pakistan. Unpublished Ph.D. Thesis, Leicester University, U.K.

Allan, J. R. and Metthews, R. K. 1977. Carbon and oxygen isotopes as diagenetic and stratigraphic tools: surface and subsurface data, Barbados, West Indies. *Geology*, **5**, 16-20.

Allan, J. R. and Metthews, R. K. 1982. Isotope signatures associates with early meteoric diagenesis. *Sedimentology*, **29**, 797-817.

Bakr, M. A. and Jackson, R. O. 1964. Geological map of Pakistan (Scale 1:2,000,000), Pakistan Geological Survey.

Bathurst, R. G. C. 1966. Boring algae, micrite envelopes and lithification of molluscan biosparites. *Geological Journal*, **5**, 15-32.

Bathurst, R. G. C. 1975. Carbonate sediments and their diagenesis. Elsevier, Amsterdam, 1-658.

Bathurst, R. G. C. 1980. Lithification of carbonate sediments. Science Progress, **66**, 451-471.

Becher, J. W., and Moore, C. H. 1976. The Walker Creek Field: a Smackover diagenetic trap. *Trans. Gulf-Cst Assoc. Geol. Socs,* **26**, 34-56.

Benson, L. V. 1974. Transformation of a polyphase sedimentary assemblage into a single phase rock - a chemical approach. *Jour. Sed. Pet.*, **44**, 123-136.

Bogli, J. 1980. Karst Hydrology and Physical Speleology. Springer-Verlag, Berlin, 1-285.

Chafetz, H. S. 1986. Marine peloids: a product of bacterially induced precipitation of calcite. *Jour. Sed. Pet.*, **56**, 812-817.

Drever, J. L. 1982. The Geochemistry of Natural Waters. Prentice Hall, New Jersey, 1-388.

Dunnington, H. V. 1967. Aspects of diagenesis and shape change in stylolitic limestone reservoirs. *World Petrol. Congr. Proc., 7th*, Mexico, **2**, 339-352.

Evamy, B. D. and Shearman, D. J. 1965. The development of overgrowths from echinoderm fragments. *Sedimentology*, **5**, 211-233.

Evamy, B. D. and Shearman, D. J. 1969. Early stages in development of overgrowths on echinoderm fragments in limestones. *Sedimentology*, **12**, 317-322.

Flugel, E. 1982. Microfacies Analysis of Limestones. Springer-Verlag, Berlin, 1-633.

Folk, R. L. 1959. Practical petrographic classification of limestones. *Bull. Amer. Assoc. Petrol. Geol.*, **43**, 1-38.

Folk, R. L. 1965. Some aspects of recrystallization in ancient limestones. In, L. C. Pray and R. C. Murray (eds) Dolomitization and Limestone Diagenesis, Special Publication, Soc. Econ. Paleont. Miner., 14-48.

Gavish, E. and Friedman, G. M. 1969. Progressive diagenesis in Quaternary to late Tertiary carbonate sediments: sequence and time scale. *Jour. Sed. Pet.*, **39**, 980-1006.

Hudson, J. D. 1975. Carbon isotopes and limestone cement. *Geology*, **3**, 19-22.

Hudson, J. D. 1977. Stable isotopes and limestone lithification. *Jour. Geol. Soc. London,* **133**, 637-660.

James, N. P. and Choquette, P. W. 1984. Diagenesis 9. Limestones - the meteoric diagenetic environment. *Geoscience Canada,* **11**, 161-194.

Kendall, C. G. St. C. and Skipwith, S. P. A. D'E. 1969. Holocene shallow-water carbonate and evaporite sediments of Khor al Bazam, Abu Dhabi, southwest Persian Gulf. *Bull. Amer. Assoc. Petrol. Geol.*, **53**, 841-869.

Kobluk, D. R. and Risk, M. J. 1977. Micritization and carbonate-grain binding by endolithic algae. *Bull. Amer. Assoc. Petrol. Geol.*, **61**, 1069-1082.

Land, L. S., Machenzie, F. T. and Gould, S. J. 1967. Pleistocene history of Bermuda. *Bull. Geol. Soc. Amer.*, **78**, 993-1006.

Lighty, R. G. 1985. Preservation of internal reef porosity and diagenetic sealing of submerged early Holocene barrier reef, southeast Florida Shelf. In, Nahum Schneidermann and Paul M. Harris (eds) Carbonate Cements. Society of Economic Paleontologists and Mineralogists, Special Publication, 123-151.

Lohmann, K. C. 1988. Geochemical patterns of meteoric diagenetic system and their application to studies of paleokarst. In, N. P. James and P. W. Choquette (eds) Paleokarst. Springer-Verlag, New York, 58-80.

Longman, M. W. 1980. Carbonate diagenetic textures from nearsurface diagenetic environments. *Bull. Amer. Assoc. Petrol. Geol.*, **64**, 461-487.

Longman, M. W. 1982. Carbonate Diagenesis as a Control on Stratigraphic Traps. *Amer. Assoc. Petrol. Geol. Educ. Course Note Series* 21, 1-159.

Longman, M. W. and Mench, P. A. 1978. Diagenesis of Cretaceous limestones in the Edwards aquifer system of south-central Texas: a scanning electron microscopy study. *Sed. Geol.*, **21**, 241-276.

Macintyre, I. G. 1985. Submarine cements - the peloidal question. In, Nahum Schneidermann and Paul M. Harris (eds) Carbonate Cements. Society of Economic Paleontologists and Mineralogists, Special Publication, 109-116.

Nichols, R. A. H. 1967. The "...Sparite" Complex: Eosparite v. Neosparite. *J. Sed. Pet.*, **37**, 1247-1248.

Niemann, J. C., and Read, J. F. 1988. Regional cementation from unconformity-recharged aquifer and burial fluids. Mississippian Newman Limestone, Kentucky. *J. Sed. Pet.*, **58**, 688-705.

Plummer, L. N., Wigley, T. M. L. and Parkhurst, D. L. 1979. Critical review of the kinetics of calcite dissolution and precipitation. In, R. F. Gould (ed) Chemical Modelling of Aqueous Systems, Am. Chem. Soc. Symp. Series, **93**, 537-577.

Richter, D. K. 1979. Die Stufen der meteorisch-vadosen Umwandlung von Mg-Calcit in Calcit in rezenten die pliozanen Biogenen Griechen lands. *Neues Jb. Geol. Palaont. Abh.*, **158**, 277-333.

Richter, D. K. and Fuchtbauer, H. 1978. Ferroan calcite replacement indicates former magnesian calcite skeletons. *Sedimentology*, **25**, 843-860.

Scoffin, T. P. 1987. An introduction to carbonate sediments and rocks. Chapman and Hall, New York, 1-274.

Thrailkill, J. 1968. Chemical and hydrologic factors in the excavation of limestone caves. *Bull. Geol. Soc. Amer.*, **87**, 19-46.

Trudgill, S. 1985. Limestone Geomorphology. Longmans, London, 1-196.

Tucker, M. E., and Wright, V. P. 1990. Carbonate Sedimentology. Blackwell Scientific Publications, London, 1-482.

Veizer, J. and Hoefs, J. 1976. The nature of O^{18}/O^{16} and C^{13}/C^{12} secular trend in sedimentary carbonate rocks. *Geochimica et Cosmochimica Acta*, **40**, 1387-1395.

Wanless, H. R. 1979. Limestone response to stress: pressure solution and dolomitization. *J. Sed. Pet.*, **49**, 437-462.

Geol. Bull. Punjab Univ. 35, 2000.

URANIFEROUS BLACK SHALES OF PAKISTAN

BY

KHURSHID ALAM BUTT, TARIQ MAHBOOB KHAN
PAEC Hard Rock Division, P O Box No. 734, University of Peshawar.

AND

M. QASIM JAN
National Centre of Excellence in Geology, University of Peshawar.

Abstract:- *The region between the Indus Suture and Main Boundary Thrust in northern Pakistan shows a series of nappes containing Precambrian and younger rocks. These have been metamorphosed from greenschist facies in the south to amphibolite fcies in the north, The Precambrian rocks (Salkhala and Hazara Formation and Lower Swat-Buner-schistose qroup) contain uranium bearinq metamorphosed black shales.*

Black shales in Reshian (Azad Kashmir) and in Tarbela (NWFP) are highly radioactive and those in Kaghan, Thana (Malakand) and Thakot areas are less radioctive. Average chemical uranium in Reshian and Tarbela is about 50 ppm. Compared to the high radioctivity, chemical uranium is invariably low. Radioactivity is the combined product of U, Th and their dauqhter products, and K^{40}. The black shales are siliceous/argillaceous siliceous and are enriched in U,V, Ba and Pb as compared to the metal-rich black shales deposits of the world. Enrichment of elements took place during deposition by the organic matter and/or associated detrital minerals. Subsequent structural movements made the otherwise impervious rocks permeable for groundwater circulation so that the present distribution of urnanium and other elements is controlled by the topographic surface, resulting in high radioactivity and concentration of the other elements below the present surface of weatherinq.

INTRODUCTION

Beds, lenses and streaks of uraniferous black shales occur in Precambrain formations of Pakistan and Azad Kashmir in the area between the Indus Suture (Main Mantle Thrust, MMT) and the Main Boundry Thrust (MBT). These formations Include Salkhala, Hazara and the lower Swat-Buner schistose group. The salkhala Formation comprises various schistose rocks, quartzite, marble, granitic/gneissic bodies, black shales, gypsum, meta dolerite intrusions and amphibolites. The formation has been renamed as Sharda group in Kaghan Valley and confind only to the Naran gneisses, migmatites and amphibolites (Ghazanfar et al., 1985), however, regional geological correlation has not been made. The Hazara Formation is dominatly composed of shales, phyllites, black shale, limestone, and dolerite intrusions. In Tarbela area, this formation is correlated with the Manki Formation exposed in the Attock-Cherat Range. The lower Swat-Buner schistose group consists of various schistose rocks, marble, black shale and granitic bodies.

The area occupied by these formations is structurally complex and thrust southwards in the form of several nappes. The black shales in Salkhala Formation exposed at Reshian village in Azad Kashmir and in Hazara Formation exposed at Tarbela were studied in detail for radioactivity. The present study also gives a brief account of the black shale in Kaghan, Thana (Malakand) and Thakot areas. Under the microscope the rocks at Tarbela show mineral assemblages indicating greenschist facies metamorphic conditions, while those at Reshian show metamorphism in the amphibolite facies with a retrograde phase.

The black shales are invariably radioactive and display higher background radioactivity than the associated rocks. Higher radioactivity has been recorded from Reshian and Tarbela areas while it is low in Kaghan, Thana (Malakand) and Thakot areas. Chemical uranium is characteristically low compared to high radioactivity. Average chemical uranium in the black shales from Reshian and Tarbela areas is about 50ppm. This study shows that the chemical uranium and radioactivity also vary with time. Radioactivity in these areas is the combined effect of U. Th, their daughter products, and K^{40}.

Geochemical composition of the black shales indicates that these are silicous/argillaceous siliceous and high in organic carbon. They plot in the upper part of the double triangle of Stribrny et al. (1988). The corners of the triangles are represented by Q (quartz), P (phyllosilicates) and C (Carbonates plus the remaining minerals). Compared to the metal-rich black shales, these are enriched in U, V, Ba and Pb. Element concetration took place in the Stratigraphically upper part of the black shales associated with evaporites which are in contact with the upper quartzite at Reshian. These were deposited from normal sea-water at the time of the deposition of the rocks concentrated by living planktons under reducing conditions and some were associated with detrital minerals. Correlation of the elements with organic carbon is poor because of leaching of urnium in groundwater and concentration of the other elements below the present topographic surface.

GEOLOGICAL SETTING

The geology of the northern area of Pakistan is characterized by Cenozoic tectonic activity known as Himalayan orogeny. The formation of the Himalayan mountain chain has been attributed to a northwrad movement and collision of the Indian and Asian plates along the Indus suture. In northern Pakistan and Ladakh, an intra-oceanic Cretaceous island arc was trapped between the two continents. The northern contact of the island arc with the (Asian) plate has been termed as the Main Karakoram Thrust (MKT) or Shyok Suture and the sothern contact with the Indian plate as the Main Mantle Thrust (MMT) or Indus Suture (Tahirkheli, 1979). The Indian plate collided with Eurasian plate in the early Eocene about 50 miliion years ago (Partiat and Achache, 1984). Such a tectonic model requires 200 km of crustal shortening. In Pakidstan 500-700 and 550-1100 km of crustal shortening has been calculated by different methods (Coward et al., 1986; Malinconico, 1989). Consequent to the development of the Indus Suture (MMT), a great structural loop was formed around the Nanga Parbat-Haramosh massif. The Hazara-Kashmire syntxis developed during oligocent-Miocene. The Main Boundry Thrust (MBT) developed in pliocene some 13-10 Ma ago (Tahirkheli, 1979).

The leading edge of the Indian plate was extensively deformed during the Himalayan collision. While describing the deformation chronolgy for the internal zones of the northern margin of the Indian Plate, Treloar (1989) defined three major structures. As a result of collision the cover sequences were detached from the basement and were deformed by internal imbrication at different crustal levels. Such an imbricated faulting led to the formation of six nappes; the Besham nappe, Swat nappe, Hazara nappe, Upper and Lower Kaghan nappes, and Bana nappe (Fig.1)

During the Himalyayan oroogeny, the Precambrian rocks, alongwith their intrusives and cover sequences. were metamorphosed from chlorite grade in the south to sillimanite grade in the north (Calkins et al., 1975; Tahirkheli, 1979; Ghazanfar et al., 1986., Baig et al., 1989). Pre-Himalyan orogenic activities have been described from the Precambrian rocks by Ar/Ar dating, however, thier effects are largly obliterated by the younger, more instense Himalayan orogeny (Baig et al., 1988). An inverse grade of metamorphism is observed in Hazara nappe where the Mansehra Thrust places garnet-grade rocks over biotite-grade rocks, Oghi Shear places staurolite-grade rocks over garnet-grade rocks, and the shear zone south of Batagram places kyanite and sillimanite-grade rocks over the staurolite-grade rocks (Treloar, 1989). Starting from south to north in the Kaghan Valley biotite-grade, almandine-garnet-grade, staurolite-grade, and kyanite-grade metamorphism has been reported (Ghaznfar et al., 1985). The rocks of the Salkhala Formation at Reshian have been metamorphosed in the amphibolite grade and those at Tarbela are metamorphosed under the greenschist facies conditions.

Reshian Area, Azad Kashmir

The Reshian area is located at the eastern limb of the Hazara-Kashmir syntxis (Fig.2). The geology of the area can be described with reference to two major faults. Rocks of the Precambrain Salkhala Formation are thrust over the Panjal volcanics along the Panjal Fault which in turn is thrust over the younger Tertiary rocks of the Murree Formation along the Murree Thurst (Bossart et al., 1988).

The rock types comprising the Salkhala Formation in the area include quartizites, quartz-mica schist, chlorite-mica schist, garnet-mica schist, black shale, gypsum, marble bands and granite-gneiss. These are metamorphosed in the amphiblite facies, however, the cholrite-mica schist descrtibed as a transtition zone indicates a retrograde phase of metamorphism (Greco, 1986).

Several intraformational faults are proposed in the area where one corresponds to the transitional chlorite zone. While going from Panjal Fault northeast to Reshian Village, another fault has been placed at the contact of the steeply dipping lower quartizite with the gently dipping intensely sheared schistose rocks. The third fault is marked at the upper contact of the black shale (Fig. 3). All these are the minor faults associated with the Panjal and Muree thrusts. Shear zones, microfolds and two sets of cleavages indicate that area has undergone two sets of folding events first resulting in the southwestward overthrusting of the previously metamorphosed rocks, followed by the transport of overthrust units from northwest to southeast (Bossart et al., 1988).

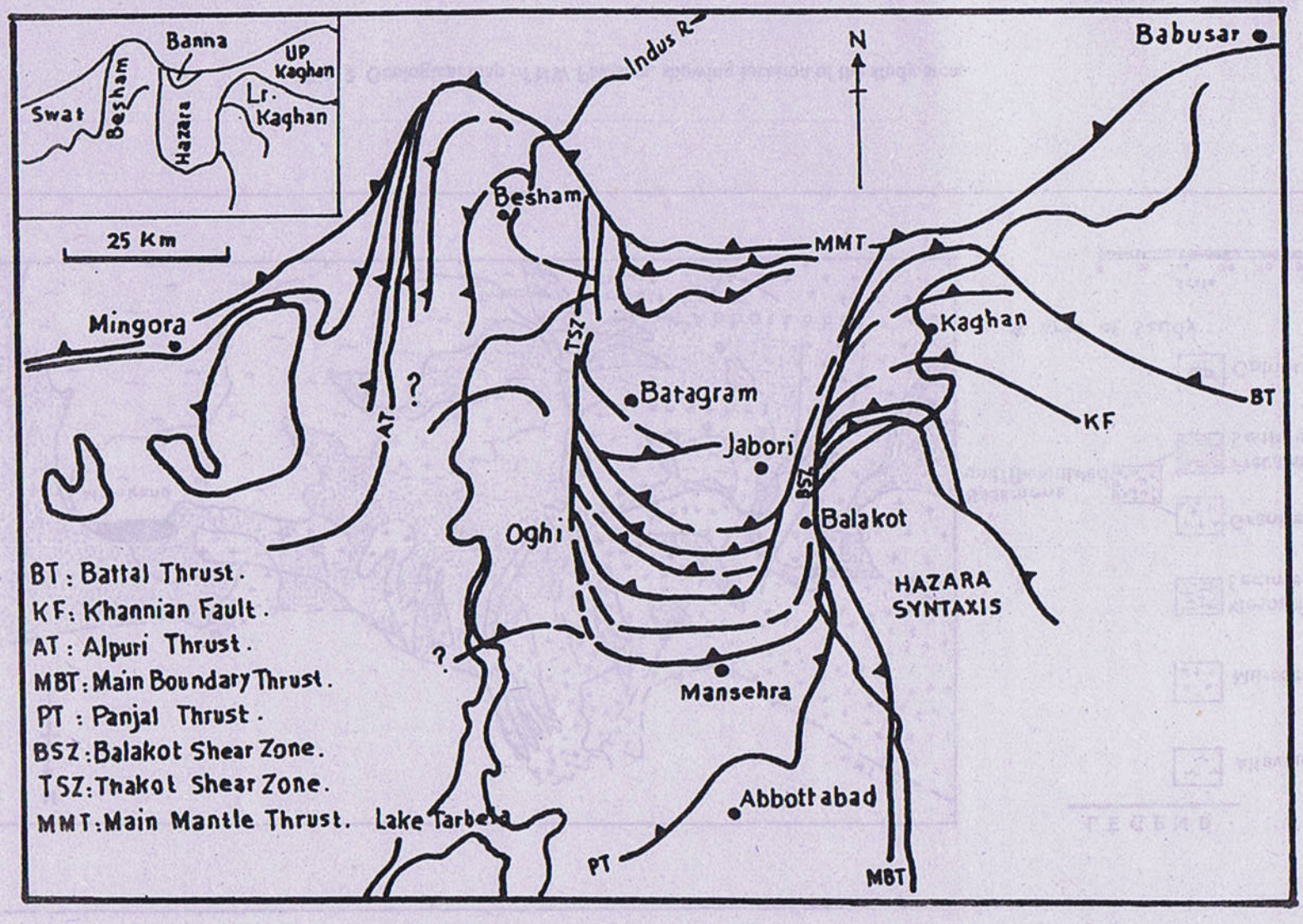

Fig. 1 Tectonic map of NW Pakistan, showing the location of the major crustal nappes (After Treloar, 1989).

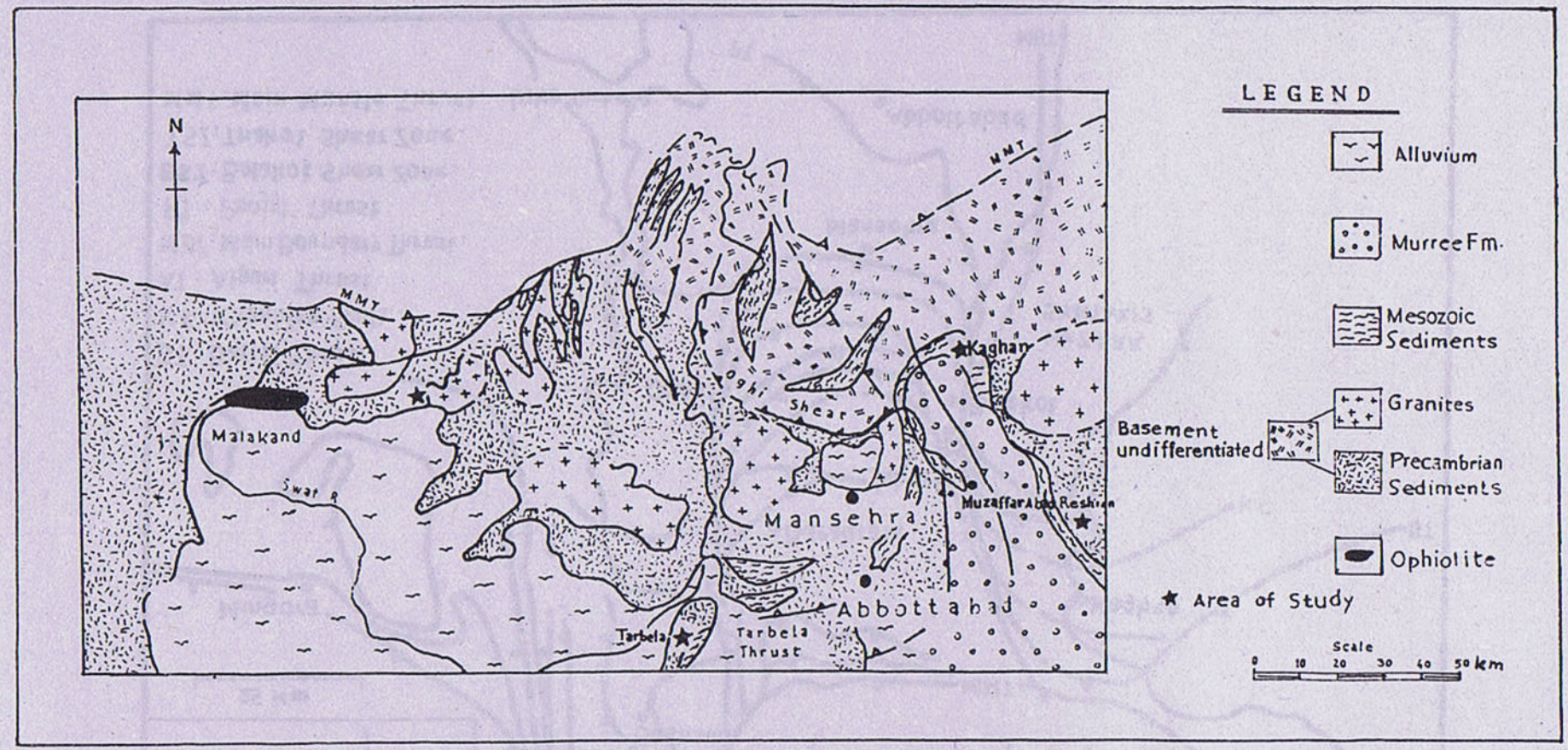

Fig. 2 Geological map of NW Pakistan, showing location of the study areas.

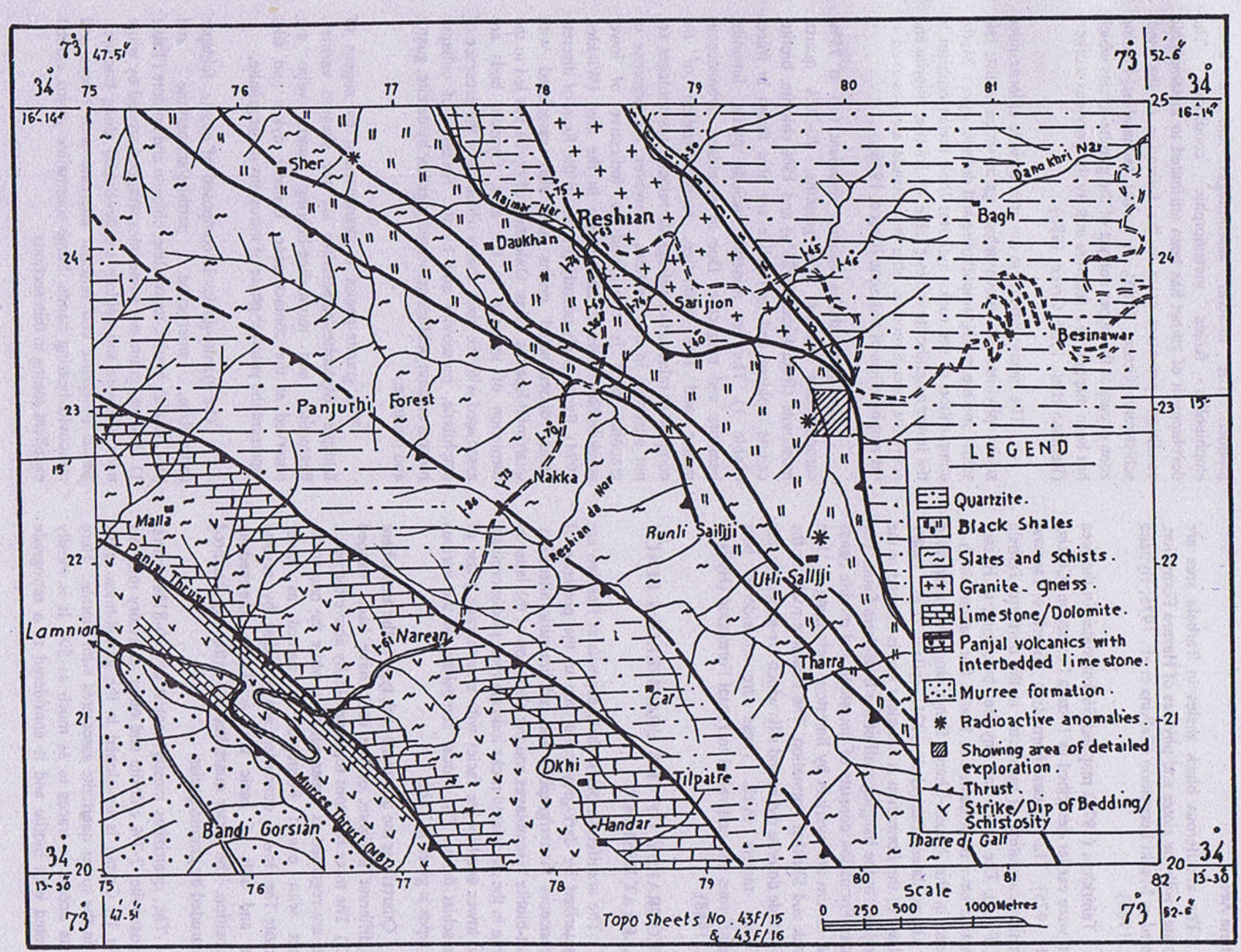

Fig. 3 Geological map of Reshian area - Azad Kashmir.

Tarbela Area

The uraniferous black shales in Tarbela area are associated with the slates and phylites of Hazara Formation, renamed as Manki Formation (Calkins et al., 1975; Hylland et al., 1988).

Tahirkheli (1971) mapped Sirikot slates in the area which were earlier described as Hazara Formation (Calkins et al. 1975). The Hazara Formation underlies Tanawal Formation consisting of quartzites in the northern Tarbela area (Fig.4). The slates and phyllites belonging to Hazara Formation have been named as Manki Formation which is exposed in the Attock-Cherat Range and also correlated with Attock slates (Tahirkheli, 1971; Hylland et al., 1988). The base of the Formation is not clear and is marked in the black shale in the hanging wall of the Baghdarra Fault. The Shahkot Formation consists of limestone and marble bands which in turn are overlain by limestone belonging to Utch Khattak and Shekhai Formation, The intursive rocks in the area include dolerite dykes and sills which are generally less than two meters thick. These are considered post Carboniferous and equivalent to Panjal Formation (Hylland et al., 1988).

PETROGRAPHY OF THE URANIFEROUS BLACK SHALES AT RESHIAN

The uraniferous black shale deposits at Reshian are characterized by dark-grey color due to the presence of carbonaceous matter/graphite and red limonitic alteration. Garnet-biotite assemblages and the alteration of the latter to chlorite in the associated rocks indicate their metamorphism in the lower amphibolite facies with a retrograde phase of green-schist facies. The modal compsition of the various rock types is given in Table 1.

Quartzite is the dominant rock type in the area where four different horizons of the rock have been mapped (Fig.3). The three horizons topographically above the black shales are regarded as upper quartzite while the one at the contact with panjal Formation is named as lower quartizite.The lower quartzites are intruded by several dykes and sills of basic and acidic to intermediate composition. The upper quartzites are extremely fractured and intruded by granite/gneiss.

The. quartizites mostly consist of 80-81% quartz, 7% muscovite, 2-7% chlorite and other accessory minerals (Table 1). Garnet is developed in the garnet-mica schist zone in the lower quartizite associated with biottite. Here chlorite occurs in traces to as much as 5%. It is mostly associated with biotite and is considered as a retrograde product. The mineral assemblages indicate lower amphibolite facies metamorphic conditions. The development of garnet has been attributed to metamorphic conditions prevalent prior to the formation of the main schistosity (Greco, 1986). A garnet (almandine)-bearing zone occurs at the upper contact of the granite-gneiss which has been mapped as a separate unit by the previous workers (Rehman et al., 1981; Greco, 1986).

The metasediments in the area include chlorite-mica schist, phyllite, calcareous schist, garnet-mica schist, talc schist, marble bands, amphibolite and dolerite dykes. Modal composition of the rocks indicates their metamorphism in the lower amphibolite facies (Table 1). Biotite, chlorite and actinolite pseudomorphs after hornblende are observed in the amphibolites of this zone (Greco, 1986).

The black shales contain abundant (up to 75%) carbonaceous mattter, 8% graphite, 20-30% quartz, muscovite (from traces to 23%) and 18% chlorite, biotite, calcite, epidote and tourmaline are also found in traces (Table 1). The ore minerals include pyrite, limonite, hematite and magnetite, Due to abundant carbonaceous matter and fine grain-size, recrystallization of the component minerals or retrograde mineral assemblages are not observed in thin sections. However, the presence of graphite itself is considered as indicative of lower amphibolite facies metamorphism in the area (Winkler, 1974). Pyrite is abundantly present in the form of discrete veins, disseminated grains and also associated with quartzofeldspathic veins. Oxidation of pyrite has led to the formation of limonite in the area, Gypsum beds are associated with the black shales which show the presence of amphibole, muscovite and biotite. Sections of collapse breccia contain pebbles cemented together by calcite, guartz and limonite.

The granite-gneiss is characterized by augens of feldspar. Mylonites/cataclasites are the sheared varities. Pegmatites and tourmaline-bearing quartz veins are observed at the contact zone. Dolerite dykes and sills represent the younger phase of intrusions in the granite,

The granite-gneiss is composed of quartz, feldspar (orthoclase, microcline, perthite/antiperthite and plagioclase), biotite, tourmaline, chlorite and epidote (Table 1). Feldspar grains are sometimes wrapped around by white mica. Chlorite and epidote are developed along fractures. Bands of quartz and feldspar alternate with biotite and muscovite-bearing bands. Some tourmaline grains exhibit excellent zoning in thin sections.

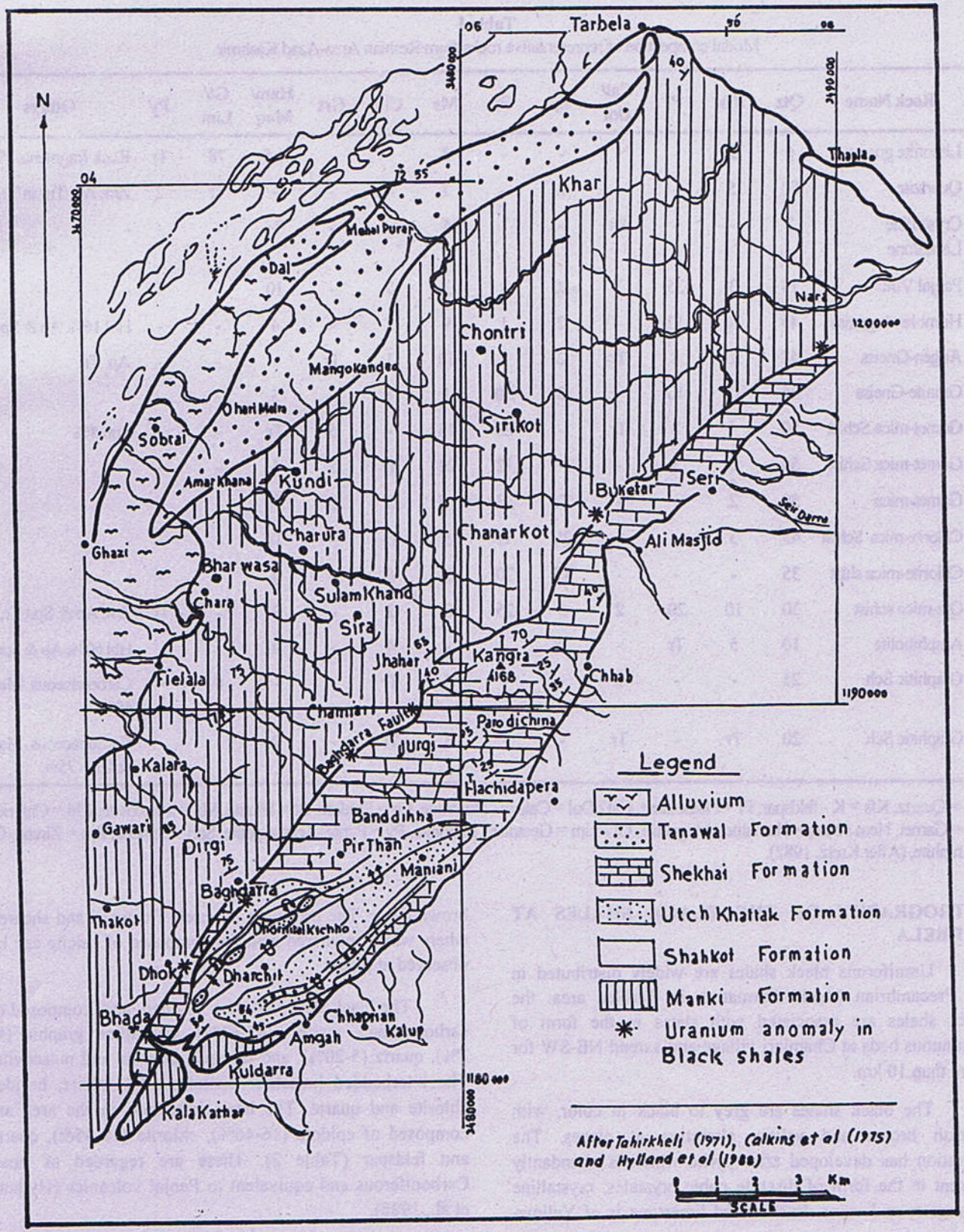

Fig. 4 Geological map of the southern Gandghar Range - Tarbela.

Table 1
Modal compostion of representative rocks from Reshian Area-Azad Kashmir.

S.No.	Rock Name	Qtz	Kfs	Pl	Cal/ Dol	Ep	Bt	Ms	Chl	Grt	Ham/ Maq	Gt/ Lim	Py	Others
1	Limonite gossan	6	2	-	-	-	-	8	-	-	1.5	78	Tr	Rock fragments 4%
2	Quartzite	80	5	-	-	2	-	7	4	-	-	Tr	2	Zrn, Ap, Tur in Tr.
3	Crystalline Limestone	7	-	-	88	-	-	5	-	-	Tr	-	-	-
4	Panjal Volc	14	3	35	3	20	-	3	7	-	10	-	5	-
5	Hornblends gneiss	43	10	12	-	2	1	9	3	-	4	-	-	Hbl 16%, Ap & Spn
6	Augen-Gneiss	48	23	8	Tr	2	8	10	1	Tr	-	-	-	Ap, Tr.
7	Granite-Gneiss	36	17	10	-	2	30	1	1	-	3	-	-	-
8	Garnet-mica Schist	50	4	2	Tr	-	20	15	-	5	Tr	-	-	Spn 4%
9	Garnet-mica Schist	50	5	3	-	-	12	24	Tr	5	1	-	-	-
10	Garnet-mica	50	2	-	-	Tr	23	15	3	5	Tr	-	-	-
11	Chlorite-mica Schist	45	5	-	-	30	Tr	5	15	-	Tr	-	-	-
12	Chlorite-mica shist	35	-	-	-	12	20	25	6	-	4	-	-	-
13	Qtz-mica schist	30	10	20	2	5	25	3	2	-	3	-	Tr	Zrn, Ap & Spn Tr.
14	Amphibolite	10	5	Tr	-	18	-	-	4	-	2	-	-	Hbl 60%, Ap & Spn Tr
15	Graphitic Sch	25	-	-	2	-	-	5	Tr	-	-	8	-	Carbonaceous Matter 60%
16	Graphitic Sch	20	Tr	-	Tr	-	-	3	Tr	-	2	-	-	Carbonaceous Matter & Gr = 75%

Qtz = Quartz, Kfs = K - feldspar, Pl = Plagioclase, Cal / Dol = Calcite / Dolomite, Ep = Epidote, Bt = Biotite, Ms = Muscovite, Chl = Chlorite, Grt = Garnet, Hem / Maq = Hematite / Magnetite, Gt / Lim = Geothite / Limonite, Py = Pyrite, Ap = Apatite, Spn = Sphene, Zrn = Zircon, Gr = Graphite, (After Kretz, 1982).

PETROGRAPHY OF THE BLACK SHALES AT TARBELA

Uraniferous black shales are widely distributed in the Precambrian Manki Formation in Tarblea area. the black shales are associated with slates in the form of continuous beds at Chamiari village and extend NE-SW for more than 10 km.

The black shales are grey to black in color, with reddish brown and yellow alteration at places. The alteration has developed after pyrite which is abundantly present in the form of discrete cubic crystales, crystalline aggregates and veins. Interbedded limestone is of Yellow-brown color. The rocks are intensely fractured and sheared where white powdered material composed of calcite can be observed at places.

The black shales are fine grained and composed of carbonaceous matter (45-62%), crystalline graphite (4-7%), quartz (5-20%), and feldspar, chlorite and muscovite. The interbedded limestone contains 69% calcite, besides chlorite and quartz. The basic intrusions in the area are composed of epidote (16-46%), chlorite (19-35&), quartz and feldspar (Table 2). These are regarded as post-Carboniferous and equivalent to Panjal volcanics (Hylland et al., 1988).

Table-2

Modal composition of representative rocks from Tarbela Area.

S.No.	Rock Name	Qtz	Kfs	Pl	Call/ Dol	Ep	Bt	Ms	Chl	Hem/ Maq	Lim	Others
1	Panjal Volcanics	15	7	-	4	16	-	2	26	1	4	Pyroxene 15%. Fine granined groundmass 10%
2	Panjal Volcanics	14	5	8	1	25	-	7	35	2	-	Clay 3%
3	Graphitic/carbonaceous phyllite	5	-	-	-	Tr	-	2	10	2	1	Carbonaceous matter and Gr = 62%
4	Graphitic / carbo naceous phyllite	20	5	15	-	Tr	-	2	10	2	1	Carbonaceous matter and Gr = 45%
5	Slate	37	11	12	-	-	-	2	Tr	-	10	Clay 26%, carbonaceous matter 2%
6	Limestone	2	-	-	96	-	-	-	-	-	-	Clay 1%, coarse grained along veins
7	Black Limestone	5	-	-	82	Tr	Tr	7	Tr	-	3	Carbonaceous matter 3%, coarse along veins
8	Altered Pegmatite	12	7	-	-	Tr	-	2	Tr	-	2	Fine grained ground-masss of Qtz + Kfs =75%, Clay 2%
9	Altered Pegmatite	36	12	-	-	-	-	4	-	2	6	Clay 40%
10	Soapstone	25	2	-	1	-	-	Tr	Tr	Tr	Tr	Carbonaceous matter 1%

RADIOACTIVITY

The studied black shales display higher background gamma counts with SPP2-NF scintillation counter compared to the associated rocks. The highest radioactivity (more than 15000 counts per second gamm) was recorded from the black shales at Reshian. The black shales at Tarbela yielded 5000 CPS gammas while those at Kaghan, Thakot and Thana (Malakand), are comparatively less radioactive.

In Reshian area, the upper horizon of the black shales, at the contact with the upper quartizite (Fig.3) gives higher radioactivity compared to its lower contact. The redioactivity is associated with shear and brecciated zones, joints/fractures and the limonite gossan, Shear zones are quite common in Rehian area and yield high radioactivity in the upper horizon in the black shales. These show crushing of the material resulting in the absence of any recongnizable laminations and planes of schistosity. These are composed of uncemented, friable and powdered black shales. These zones were probably develped as a result of the tectonic activity which led to the formation of the Hazara-Kashmir syntaxis.

Several sets of joints/fractures are observed in Reshian area. Radioactivity is found concentrated in the fractures, characterized by strong iron oxidation. The black shales in Tarbela area are also highly fractured where radioactivity is found in the alteration zones in the form of small lenses and pockets on the surface of the black shales.

In Reshian area, higher radioactivity also occurs in the brecciated rocks located near the upper contact of the black shales associated with evaporites and marble. These are composed of well-cemented fragments of the black shales, developed with the collapse of the side walls. Such a weak zone provided channed wavs for circulation of the groundwater which leached uranium and left behind its daughter products. The limoniite gossan at Reshian host higher radioactivity due to the accumulation of the daughter products of U, Th and K^{40} trapped in limonite (Jones, 1986).

The studied black shales are highly radioactive and yield low chemical uranium. Samples collected at different times from a spot with more than 15000 CPS gammas give only 16, 41, 130, 19, 515 and 177 ppm $U_2 O_8$ (Table 3) which is very low compared to the radioactivity. Tables 3 and 4 also shows that samples from highly radioactive spots yield low chemical uranium compared to the others with low radioactivity. The highest chemical uranium (0.629%) in the studied black shales analvsed from a less radioactive zone in Reshian area (Table 3), where secondary uranium mineralization has been observed along fractures. The radioactive mineral (not indentified yet) occurs as encrustation.

The negaitve disequlibriumin in the black shales is due to the presence of the daughter products of U, Th, and K_{40} (Table 5). Uranium was deposited at the time of the formation of the black shales. The black shales were made permeable with the development of fractures related to tectonic activities. These fractures provided channel wavs for groundwater circulation which leached uranium from the surface leaving behind its daughter products. Some of the uranium was redeposited along fractures which can be seen as encrustation at places.

Table-3

Radioactivity and chemical uranium at Reshian.

S.No.	Sample No.	Background Radioactivity (Cps)	Maximum Spot Rad-ioactivi-ty (Cps)	U_3O_8 ppm
1	T-6(1)/88	-	600	26
2	Cm-2/87	200	750	10
3	S-3	-	750	120
4	S-2	-	1000	33
5	R-T (17) / 87	800	1000	43
6	Cm-6 / 87	200	1000	14
7	R-T (6) / 87	800	1000	428
8	Cm-6 / 87	200	1400	14
9	T - 5 (2) / 88	-	1400	47
10	T-5 (3) / 88	-	1400	55
11	Cm-3 / 87	200	1500	10
12	Rn - 4 / 88	-	1500	23
13	R - T (7) / 87	800	2000	58
14	R-T (5) / 87	800	2500	67
15	S-4	-	2500	110
16	RN-8 / 88	-	2500	28
17	R-T (2) / 87	800	3500	100
18	R-T (13) / 87	800	4000	68
19	RN-3 / 88	-	4000	880
20	T-4 (1) / 88	-	4000	200
21	R-C (2) / 87	200	5000	23
22	R-T(16) / 87	800	5000	81
23	RN-2 / 88	-	6000	6290
24	R-C (6) / 87	250	7000	47
25	R-T (4) / 87	800	7000	170
26	R-(12) / 87	800	7000	69
27	R-C (3) / 87	250	7500	120
28	R-4	-	7500	49
29	R-T (8) / 87	800	8000	400
30	R-C (14) / 87	200	9000	65
31	R-C (3) / 87	800	10000	310
32	R-T (9) / 87	800	10000	85
33	R-T (15) / 87	800	10000	137
34	RN-1 / 88	-	11000	31
35	R-3	-	14000	85
36	RN-5 / 88	-	15000	25
37	R-C (4) / 87	250	15000	16
38	R-C (5) / 87	250	15000	41
39	R-T (11) / 87	800	15000	130
40	RN-6 / 88	-	15000	9
41	R-1	-	15000	515
42	R-2	-	15000	171

Note : - Samples were collected from three localities, i.e. Reshian, Cham and Sher Gali, Symbolized by R and Rn, C and S, RT = Trench samples.

Table-4

Radioactivity and chemical uranium at Reshian.

S.No	Sample No.	Maximum Spot Rad-ioactivity (Cps)	U_3O_8 ppm
1	TT2-36	150	12
2	Tt2-38	150	15
3	Tt2-35	200	8
3	TT4-46	200	56
5	TT3-18	300	10
6	TT5-48	300	38
7	TT5-54	350	35
8	TT6-87	350	15
9	TT1-7	400	10
10	Gn-3/90	400	63
11	TT6-64	450	45
12	TG-2/88	500	3
13	TT5-47	500	269
14	TG-3/88	600	4
15	TG-19/88	600	39
16	TG-1/88	700	8
17	TC-2-3	750	42
18	TT3-19	750	8
19	TT4-45	750	269
20	TT5-55	750	224
21	TC2-4	800	134
22	TT1-5	800	112
23	TT2-33	800	36
24	TT4-40	800	28
25	TT7-85	800	49
26	TT3-25	850	10
27	TT6-58	880	113
28	TT1-13	900	127
29	TT3-23	900	17
30	DK-4	1000	2
31	TT2-26	1000	35
32	TT1-3	100	84
33	TT3-16	1100	59
34	TT3-20	1100	77
35	T-C(1)/88	1200	66
36	TT1-2	1200	127
37	T-C(17)/88	2000	12
38	TC2-2	2000	92
39	T-C (2) /88	2200	73
40	T-C (4) /88	2500	22
41	T-C (3) /88	2500	84
42	T-C (7) /88	3000	40
43	T-C (9) /88	3000	51
44	T-C (16)	3000	25
45	/88	3500	247
46	TT1-12	4000	31
47	DK-2	5000	170
48	T-c(6)/88	5000	12
	DK-1		

TT-2: - Trench 2 in Tarbela, Gn- = Gandaf, Tq- = Graphitic - matapelite in Tarbela, TC = Chamiari Area

Table-5

Estimation of uranium and thorium of representative rock samples from Reshian, Kaghan and Thana areas.

S. No.	Rock Name	U_3O_8 ppm chemical	Radiometric Assay.
1.	RN-18+ 40	3	Traces of radioactivity mainly due to Th- DTRS plus K^{40} and U-Dtrs.
2.	RN-22	4	-do-
3.	RN-37 40	64	Traces of radioactivity mainly due to U-DTRS, plus K^{40} and Th-DTRS.
4.	RN-38	91	-do-
5.	RN-48	0.245%	-do-
6.	KN-1+	448	-do-
7.	KN-3 40	52	Traces of radioactivity mainly due to Th-DTRS, plus K and U-DTRS.
8.	KN-5	85	-do-
9.	T-1+	9	do-
10.	T-3	24	do-
11.	Ly-3(3)	137	do-
12.	Ly-3(4)	39	do-
13.	Ly-3(5) 40	44	Traces of radioactivity mainly due to U-DTRS, TH - DTRS and K^{40}
14	Ly-3(6)	29	-do-
15.	Ly-3(11) 40	19	Traces of radioactivity mainly due to Th-DTRS, plus K^{40} and Th-DTRS.
16.	Ly-3(15)	20	-do-
17.	Ly-3(17)	22	-do-
18.	Ly-3(21) 40	32	Traces of radioactivity mainly due to U-DTRS, plus K and Th-DTRS.
19.	Ly-3(24)		-do-

*DTRS = Daughters, + RN- = Surface samples from Reshian, +KN- = Surface samples from Kaghan, +T- = Surface Samples from Thana (Malakand) & +LY-3 = Core samples from Reshian.

CLASSIFICATIONS OF THE BLACK SHALES

Based on chemical analyses and petrographic studies, the uraniferous black shales at Reshian, Kaghan and Thana areas are classified, following the double triangle classification scheme of Stribrny et al. (1988). The classification scheme has been modified in the studied black shale deposits because of the presence of chlorite, biotite and kyanite, In the present work, some K_2O_3 is attributed to biotite, muscovite and the balance Al_2O_3 (after allocation to chlorite, muscovite and biotite) is assigned to sillimanite/kyanite.

The normative minerals in the black shales are plotted on a double triangle with corners represented by Q, P and C for quartz, phylllosilicates, and carbonates plus the remaining minerals respectively. Black shales with organice carbon more than 1% are plotted in the upper part of the

double triangle. The lower part of the triangle shows shales with less than 1% organic carbon (Figs. 5 & 6).

Fig. 5 shows that most of the samples plot below 60% quartz line in the upper triangle in the black shales and argillaceous-siliceous black shales from Reshian area. Four samples plot in the siliceous and only a few in the carbonatic-siliceous fields. Sampes from Trablea area mostly plot in the siliceous black shale field (Fig.6) Two samples from the area plot in the argillaceous siliceous black shale field and two polt at the boundary.

A few samples from Kaghan plot in the lower triangle indicating normal shale compsoition. Black shales from Thana (Malakand) are siliceous and argillaceous (Fig.6).

Table 6

Major and minor elements (in percent) in black shales compared to average black shale composition.

ELEMENT	AVERAGE* BLACK SHALE	RESHIAN AREA AREA	TARBELA AREA	KAGHAN AREA	THANA (MALAKAND)
Al	7	8.22	4.84	9.42	7.66
Fe	2	4.75	2.57	3.30	1.67
Mg	0.7	0.16	0.45	0.15	0.10
Ca	1.5	0.50	2.68	0.05	0.05
Na	0.7	1.38	0.38	0.80	0.73
K	2.0	5.58	1.53	3.47	2.66
Orqanic C	3.2	7.4	12.85	1.84	3.53
Ti	0.2	0.45	0.39	0.53	0.45
Mn	0.015	0.012	0.05	0.045	0.008
Ba	0.03	0.065	0.069	0.04	0.09
Co	0.001	0.00540.	0023	0.002	0.0017
Cr	0.01	0.019	0.0138	0.011	0.013
Cu	0.007	0.025	0.0080	0.065	0.014
Mo	0.001	0.008	0.005	0.005	0.0057
Ni	0.005	0.012	0.01470.	0063	0.0059
Pb	0.002	0.0068	0.0043	0.0081	0.0055
V0.	0.015	0.0387	0.0828	0.0168	0.0138
Zn	0.03	0.0031	0.020	0.009	0.007

* *After Vine and Tourtelot, 1970*

DISCUSSION

Elements Enrichment and Deposition

Chemical composition of the black shales from Reshian and Tarblea areas indicate higher organic carbon, Fe, Ti and low Mg and Ca as compared to the average black shales (Tables 6, Fig.7). Black shales are deposited in the deep to shallow marine environment over the continental slope under euxinic conditions. Deep sea conditions would not accumulate abundant organic matter and the black shales deposited there would contain low organic carbon (Convey et al., 1989). Conversely higher organic carbon in the studied black shales point to their deposition in shallow water. Higher Ti indicate the detrital minerals contribution during sedimentation perhaps in a shallow sea. The geological position of the black shales at Reshian, bounded by metamorphosed continental sediments on the one side and deep-sea metasediments on the other, also indicates

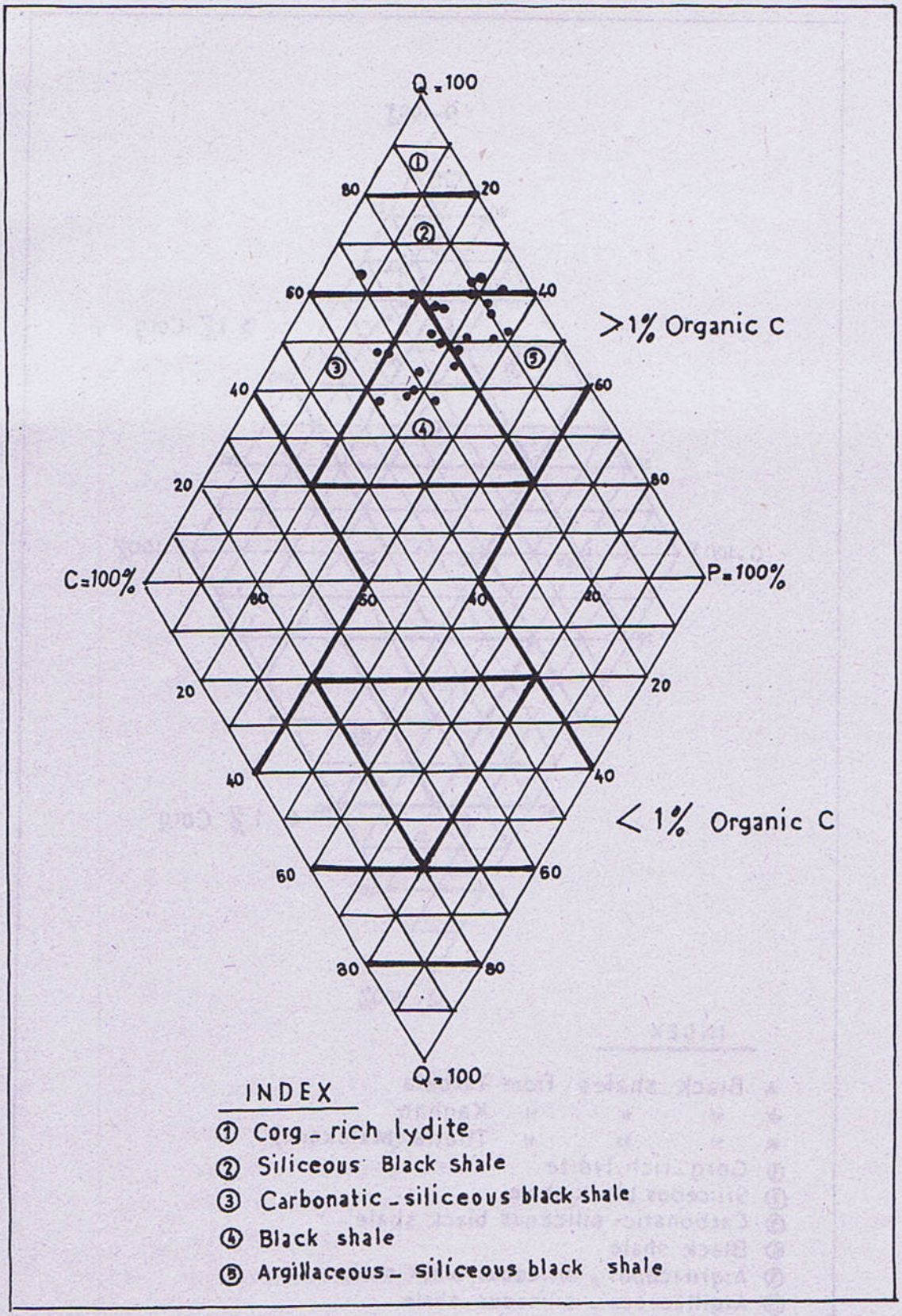

Fig. 5 Classification of black shales, Reshian area (Azad Kashmir).

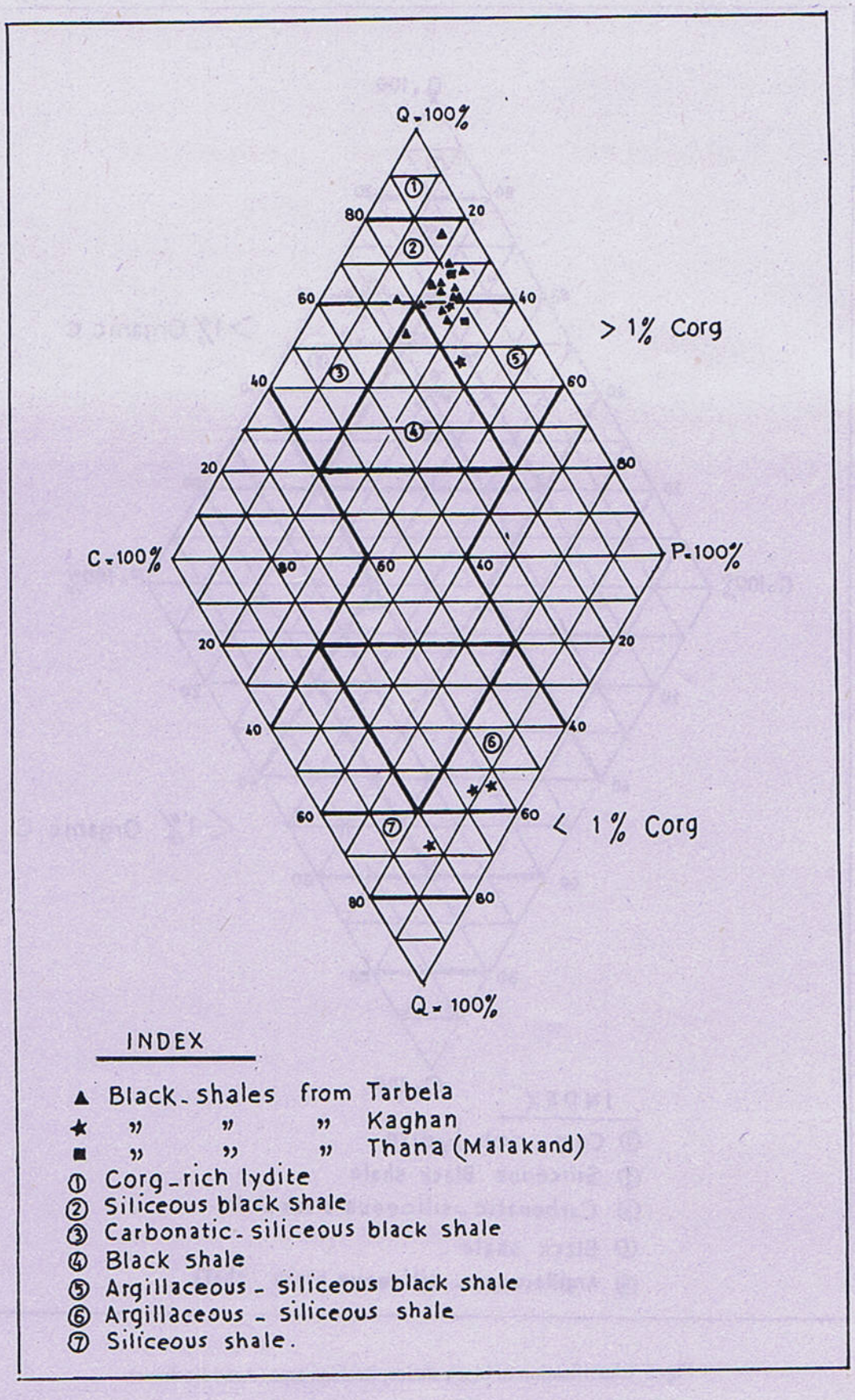

Fig. 6 Classification of black shales, Thana (Malakand), Kaghan and Tarbela areas.

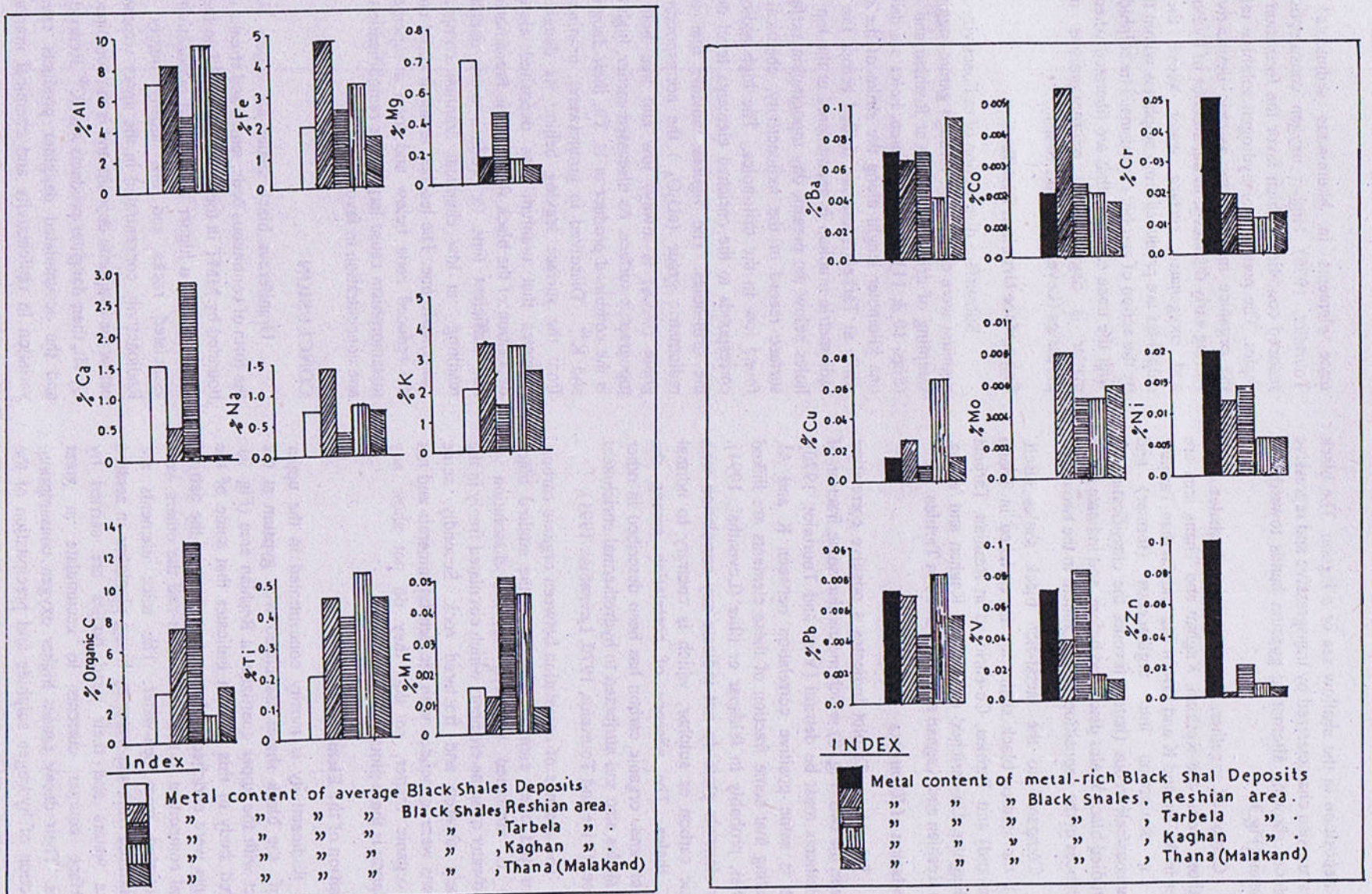

Fig. 7 Major and minor elements composition, compared to the average black shales.

their deposition in the shallow sea or a lagoon. The black shales are also characterized by transgressive and regressive sequences showing alternating gypsum bands towards the continent (Fig.3).

Compared together, the studied black shales show that those from the Reshian, Kaghan and Thana area are higher in Al, Na and K and low in Mg and Ca than Tarblea. Such a distinction into argillaceous (former) and arenaceous/calcareous (latter) favours the classification of the studied black shales discussed before, and indicate slight differences in the depositional environment in the two areas.

Compared to the metal-rich black shales (Bell, 1978), the studied black shales are Ba-enriched in Thana (Malakand) and Tarblea, Co-enriched in Reshian, Tarbela and Kaghan, Cu-enriched in Reshian, Kaghan and Thana, Pb in Reshian and Kaghan and V-enriched in Tarblea.

Correlation of Elements

The Al vs. Ti plot indicates a positive correlation between the two (Fig. 8) which means that some fraction of the elements must be detrital (Vine and Tourtelot, 1970). There is some positive correlation between K and Al, indicating that some fraction of these elements are linked together, probably in feldspar or illite (Leventhal, 1991). Other slements plots do not indicate any correlation with organic carbon or sulphur, which is contrary to normal black shales. The absence of correlation among the elements and organic carbon has been described in other black shales also and attributed to hydrothermal enrichment in places (Vine and Tourtelot, 1970, Leventhal, 1991).

The absence of correlation between organic carbon, sulphur and other elements (Fig.9) in the studied black shales is attributed primarily to the dissolution in groundwater of some elements which circulated freely in the intensely sheared and fractured rock. Secondly, some elements were associated with the detrital minerals and not with organic matter, so that they do not show any correlation is these plots.

Deposition of the Elements

Radioactivity is moslty concentrated in the upper part of the black shales associated with gypsum at the contact with the upper quartizite in Reshian area (Fig. 3). Detailed study of this horizon indicates that some of the elements were enriched with the deposition of the detrital mineral component in the black shale and the others were concentrated from sea-water. The trace elements are concentrated from sea-water by living planktons in aerated surface waters and their dead bodies are carried by subsurface counter currents to accumulate in great masses.``Their decay causes higher oxygen consumption, production of hydrogen sulphide and precipitation of the trace elements in bituminous sediments" (Vine and Tourtelot, 1970). Higher oxygen consumption results in reduced conditions which favor the formation of the black shales. The presence of hydrogen sulphide might preserve the organice matter from aerobic destructive processes. During early digenesis, in the absence of hydrogen sulphide and oxygenated surface water above the sediments, sulphides are produced from sulphates within the sediments by the action of aerobic organisms. The sulphides may react with the trace elements that are liberated when the organic matter is degraded by microorganisms or inorganic processes (Leventhal et al., 1982).

Subsurface Uranium Distribution

Subsurface distribution of radioactivity and chemical uranium were determined through gamm-logging and core-sampling of drill-holes made at Reshian and Tarblea area (Figs. 10 & 11). In Reshian area, holes are drilled in about one kilometer lenght along the strike of the black shales, while at Tarbela these are drilled across the strike. High radiometric uranium is encountered at the top levels in the holes below the present day topographic surface. Like the surface record of the radioactivity, chemical uranium is found low in the drill-holes., The high radiometric level corresponds to the enriched elements level determined in the drill-holes. The figures indicate that compared to radiometric grade (eU_3O_8) the corresponding chemical grade (U_3O_8) is always low and that both follow the topographic surface. As discussed earlier, high radioactivity is the combined product of U, Th, their daughter products and K^{40} . Dissolved in groundwater, uranium is leached from the surface leaving behind its daughters. It also indicates that uranium was deposited along with the deposition of the black shales in the Precambrian, so that it had sufficient time to produce more daughter product resulting in low chemical uranium compared to high radiometric one. The leached uranium could concentrate in the reduced zone below and form a supergene deposit; metamorphism cause large scale remobilization of uranium and concentration in favorable zones.

CONCLUSION

Uraniferous black shales are widely distributed in the form of continuous beds, lenses and streaks in the region bounded by MMT in the north and MBT in the south. The shales display a higher background radioactivity than their associated rocks and are locally highly radioactive. Radioactivity concentrated in the upper weathered surface below the evaporite deposits and is the combined product of U, Th, their daughter products and K^{40} .Remval of uranium and the accumulated daughter products cause seasonal variation in radioactivity and chemical uranium in these

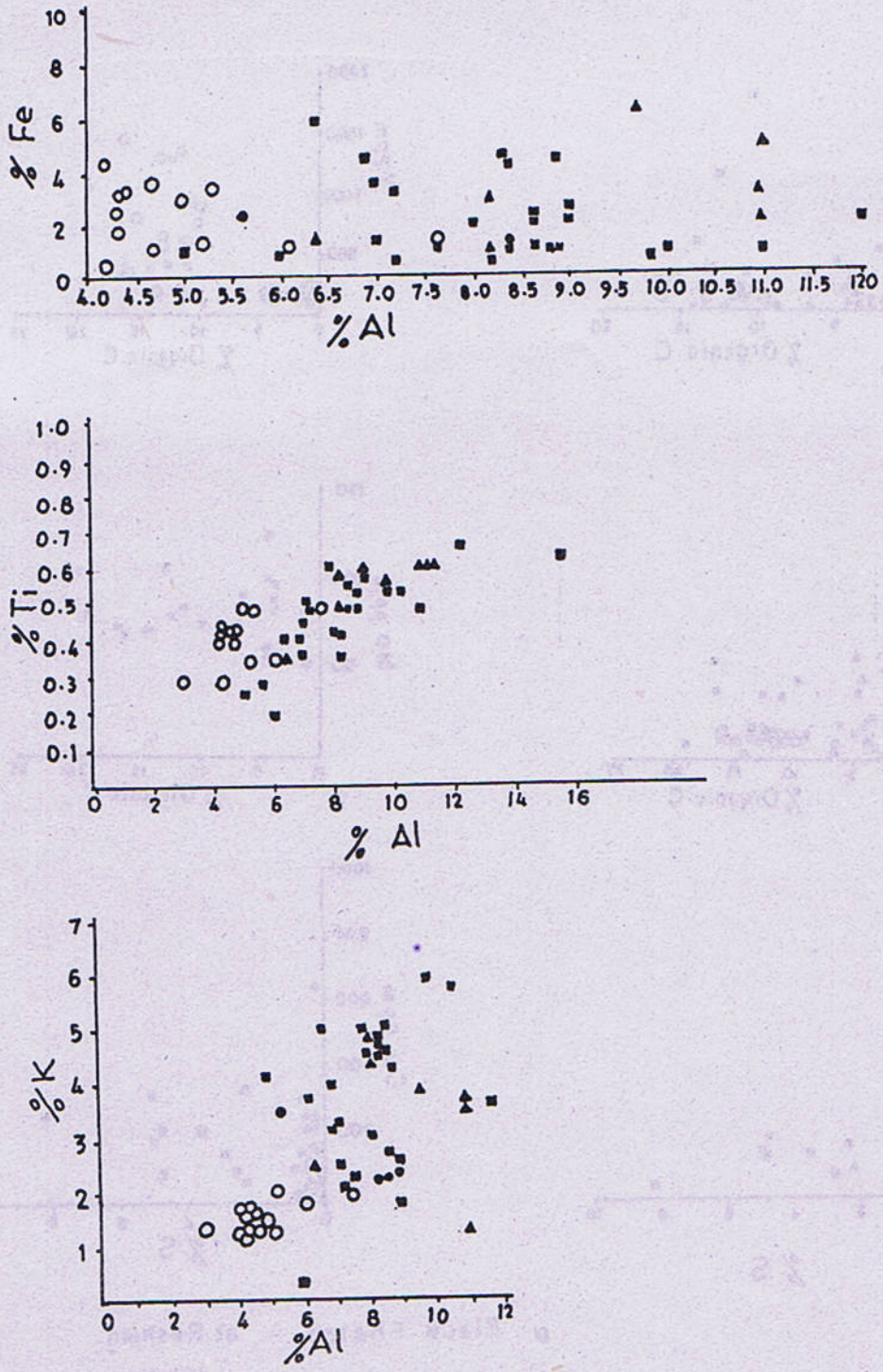

Fig. 8 Plot of Fe, Ti, and K vs. Al.

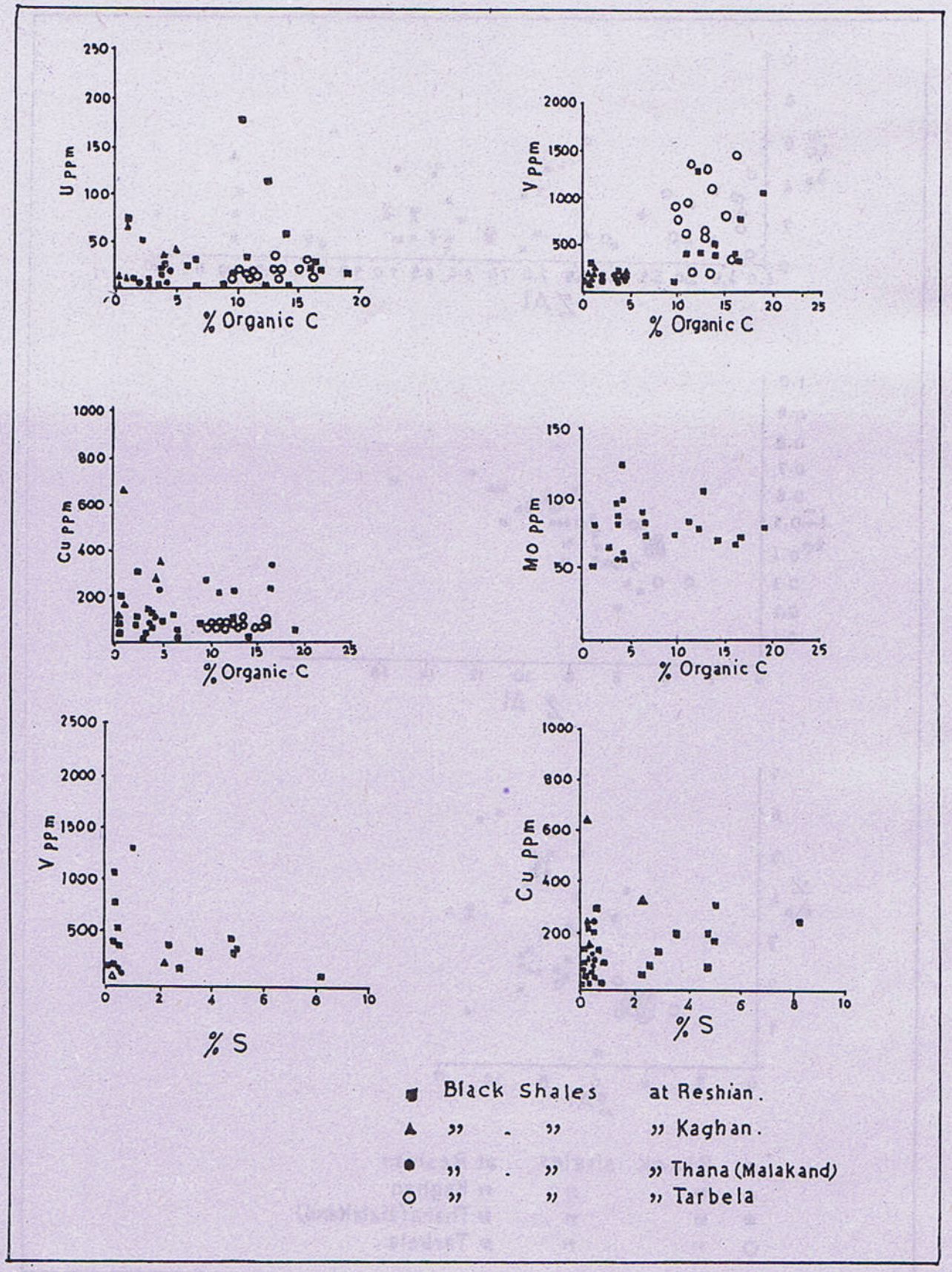

Fig. 9 Plot of U, V, Cu and Mo VS. Organic C and S.

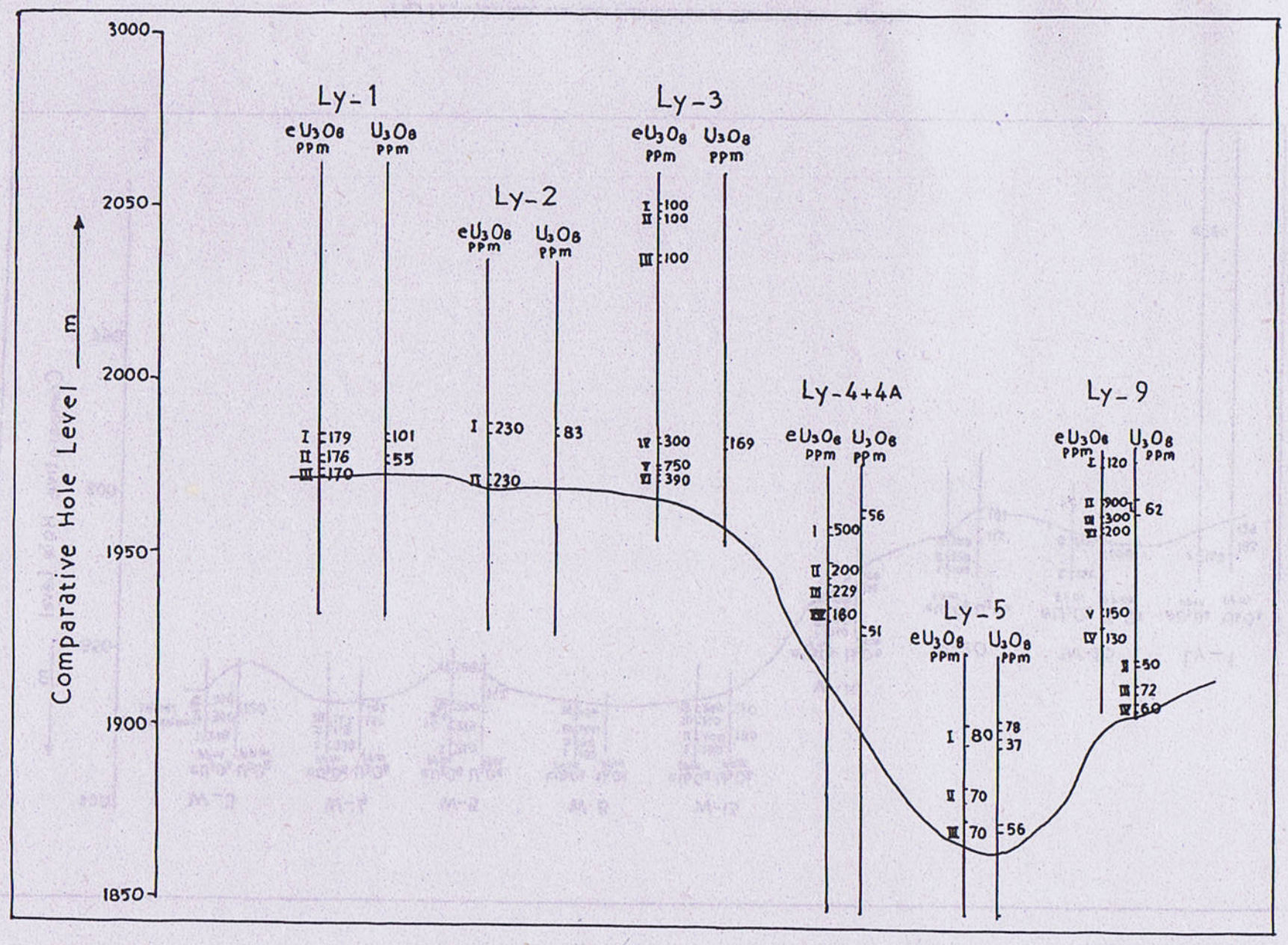

Fig. 10 Subsurface Uranium distribution at Reshain Azad Kashmir.

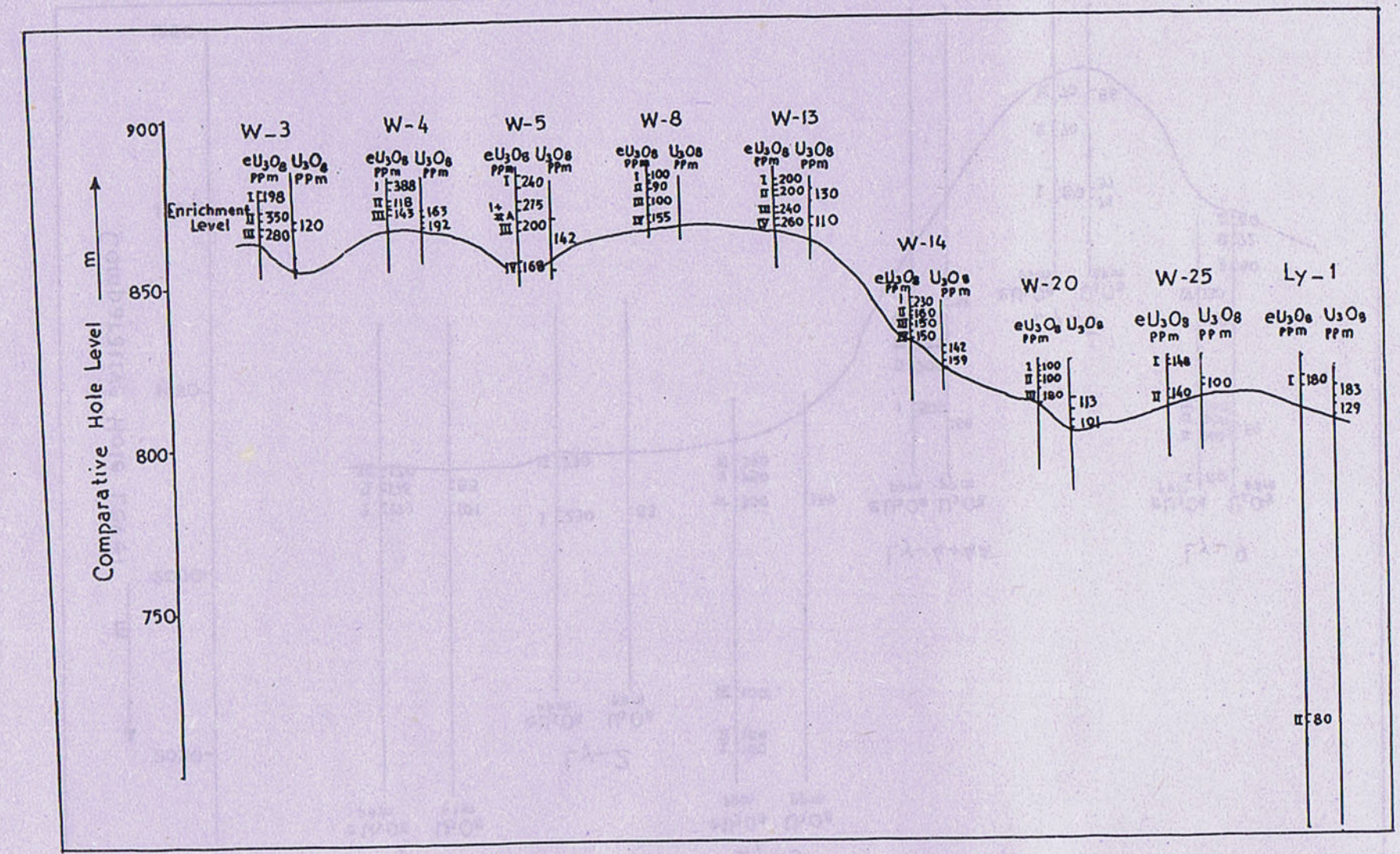

Fig. 11 Subsurface uranium distribution at Chamiari area Tarbela.

rocks. The black shales are classified as argillaceous-siliceous. These are associated with quartzites of continental origin, marine argillaceous-siliceous metaseduments and evaporite deposits, which suggest their depostion in a transitional environment close to shore-line. Unlike most black shale deposit the trace elements and uranium do not show any correlation with organice carbon, however, it is not an uncommon phenomenon. The absence of relationship is due to the association of some of the elements with the detrital mineral fraction of the rocks while others were liberated by the degrading organic matter during diagenesis.

Deposition of the elements took place from normal seawater and concentrated by living planktns in a near-shore marine environment. The conditions were reducing in the sediments where the presence of H_2 S layer might preserve the degrading orgainic matter from the aeroboic destructive processes. The black shales are a potential source of uranium. however, no large scale remboilization of the element has taken place to favour an economice grade uranium deposit in the rocks.

ANKNOWLEDGMENTS

Many scientists of PAEC, Lahore, extended their support in carrying out chemical analyses, and preparation and study of thin sections. We would particularly like to thank Dr. Fazlur Rehman and Mr. Naseemuddin. Dr. M. Asif Khan of NCE in Geology. University of Peshawar, made useful comments on some portions of an earlier draft.

REFERENCES

Baig, M.S., Snee, L.W., Lafortune, R.J., Lawrence, R.D., 1989. Timing of Pre-Himalayan Oregon events in the Northwest Himalaya Ar^{40}/Ar^{3} Contraints *Kashmir Jour. of Geol.* **6 & 7**, 29-40.

Bell, R.T., 1978. Uranium in black shales-A review. In Uranium Deposits, Their Mineralogy and Origin (M.M. Kimberley, ed.). Univ. Toronto, Press, Toronto, Canada.

Bossart, P., Dietrich, D., Greco, A., ottiger, R., and Ramsay, J.G., 1988. The tectonic structure of the Hazara-Kashmir syntaxis southern Himalyas, Pakistan *Tectonics*, 7,273-297.

Calkins, J.A., offiel.d, T.W., Abdullah, S.K.M., and Ali, S.T., 1975. Geology of the southern Himalaya in Hazara, Pakistan and adjzcent areas, *U.S.G.S. Prof. Paper,* **716-C**, 29p.

Ghazanfar. M. and Chaudhry, M.N., 1985. Geology of Bhunja-Bakhundi area, Kaghan Valley District Mansehra, Pakistan. *Geol. Bull. Univ. Punjab*, **21**, 10-18.

Ghazanfar, M. and Chaudhry, M.N., 1986. Reporting MCT in NW Himalyas, Pakistan *Geol. Bull. Univ. Punjab*, **21**, 10-18.

Greco, A., 1986. Geoilogical investigations in the Reshian area (Jhlum Valley, State of Azad Jammu and Kashmir). *Kashmier Jour. Geol.*, **4**, 51-65.

Hylland, M.D., Riaz, M. and Ahmad, S., 1998. S., 1988. Stratigraphy and structure of the southern Gandhar range. Pakistan. *Geol. Bull. Univ Peshawar*, **21**, 1-14.

Jones, C.A., 1978. Uranium occurrences in sedimetary rocks exclusive of sandstone. In; Geological Investigations of Environments Favourable for Uranium Deposits (G. Mickle and G.W. Mathews, eds.). *U.S. Deptt. Energy.*

Leventhal, J.S., 1991. Comparison of organic Geochemistry and metal enrichment in two black shales. Cambrian alum Shale of Wseden and Devonian Chattanooqa shale of United States *Mineral. Deposit*, **26**, 1-10.

Leventhal, J.S. and Hosterman, J.W., 1982. Chemical and mineralogical analysis of Devonian black shale samples from Martin Country kentucky., Caroll and Washington Counties, ohio., Wise Country, Verginia and overton Country Tennessee, U.S.A. *Chem. Geol.*, **37**, 239-264.

Malinconico, L.L. Jr., 1989. Crustal shortening in the West Himalya. *Geol. Bull. Univ. Peshwar*, **22**, 55-64.

Patriat, P., and Achache, J., 1984. India-Eurasia collsion chronology has implications for crustal shortening and driveing mechanism of plates. *Nature*, **311**, 615-621.

Rehman, M. A. and Chaudhry, M.N., 1981. Geology and Petrography of metamorphic rocks in Mauji and Reshian area District Muzaffarabad, Azad Kashmir, Pakistan. *Geol. Bull. Univ. Peshwar*, **14**, 123-139.

Stribrny, B., Urban, H. and Weeber, H., 1988. The lower carboniferous black shales formation, a possible source of nobel and base metal deposits in the NE Rhenish massif, Federal Republic of Germony. *Min. Pet.*, **39**, 129-143.

Tahirkheli, R.A.K., 1971. The geology of the Gandghar range, District Hazara, NWFP. *Geol. Bull. Univ. Peshwar*, **6**, 33-42.

Tahirkheli, R.A.K., 1979. Geotectonic evelution of Khostan. *Geol. Bull. Univ. Peshawar*, *11*, 1-30.

Treloar, P.J., 1989. Imbrication and unroofing of the Himalyayan Thrust stack of the North Indian Plate, North Pakistan. *Geol. Bull. Univ. Peshawar*, **22**, 25-44.

Venie, J.D. and Tourtelot, E.B., 1970. Geochemistry of black shale deposits- a summary report. *Econ. Geol.*, **65**, 253-272.

Winkler,. H.G.P., 1974. Petrogenesis of Metamorphic Rocks (3rd ed.). Springer Verloq, New York.

Geol. Bull. Punjab Univ. 35, 2000.

GEOLOGY AND GEOCHEMISTRY OF NEOPROTEROZOIC KIRANA VOLCANICS, SARGODHA DISTRICT, PUNJAB, PAKISTAN

BY

SYED ALIM AHMAD
Institute of Geology, University of the Punjab, Quaid-e-Azam Campus, Lahore, Pakistan.

ABDUL MATEEN
Pakistan Institute of Engineering and Applied Sciences, P.O. Nilore, Islamabad, Pakistan.

ZAHID KARIM KHAN AND MUHAMMAD NAWAZ CHAUDHRY
Institute of Geology, University of the Punjab, Quaid-e-Azam Campus, Lahore, Pakistan.

Abstract:- *In the Punjab plains, the Neoproterozoic Kirana Volcanics are exposed as isolated hills scattered around Sargodha district. These volcanics represented the oldest remnants of widespread igneous activity within the so-called Kirana-Malani basin and mark important Precambrian tectono-magmatic events in Pakistan. Kirana Volcanics are comprised of bimodal mafic and felsic rocks belonging to subalkaline tholeiitic affinity. The mafic suites consist of predominantly tholeiitic basalts, basaltic andesites and minor andesites, while the felsic rocks are predominantly rhyolites and minor dacites. Petrographic features and geochemical characteristics of mafic lavas exhibit comparable major and trace element chemistry with enriched MORB or back-arc basin tholeiites. Fractionation of olivine, pyroxene and titanomagnetite played an important role in the generation of the range of mafic compositions. The associated rhyolites are volumetrically more abundant and interpreted to be genetically unrelated to mafic rocks. Rhyolites and dacites are metaaluminous to prealuminous and medium-K high-K subaslkaline rocks, possibly originated from partial anatectic melting of continental crust in an extensional A-type environment.*

The Kirana Volcanics are interbedded with interclations of volcanogenic sediments and tuffasceous material. The volcanics and associated sedimentary rocks constitute a distinct cratonic rift assemblage and do not represent Indian Shield elements. The Kirana mafic lavas are interpreted to represent the oldest pulses of plume-related oceanic mantle-source tholeiitic magmatism in the early extensional rift in the Late Proterozoic within the Gondwana configuration of Greater India. Contemporaneously widespread anatectic rhyolite volcanism occurred during the break-up of Rodinia supercontinent as a consequent of tectonic events with Kirana-Malani basin.

INTRODUCTION

The Neoproterozoic Kirana Volcanics are represented by several isolated hills rising above the Punjab alluvium plain, mostly scattered around southeastern part of Sargodha district (Fig. 1). The Kirana Volcanics constitute the oldest remnants of widespread volcanoplutonic suites which mark important tectono-magmatic events in the Late Proterozoic period in Pakistan.

The volcanic suites belong to tholeiitic basalt-andesite-rhyolite magma association. The volcanics are interbedded with intercalations of volcanogenic sediments and tuffs. The overlying metasedimentary units are Tuguwali phyllites and Asianwala quartzites respectively (Alam, 1987).

The volcanics and associated sedimentary rocks constitute a distinct cratonic rift assemblage and do not represent Indian shield elements (Chaudhry et al., 1999) as previously believed by many workers (Heron, 1953, Davies and Crawford, 1971; Kochhar, 1973, 1974, 1984, Alam, 1987; Alam et al., 1992). The Kirana volcanics and volcanoplutonic rocks of Nagarparkar in Sindh were interpreted to have been emplaced in the extensional basins formed as a result of mantle plume activity linked with the break-up of Rodinia supercontinent. The extensional basin developed within the Late Proterozoic NE Gondwana part

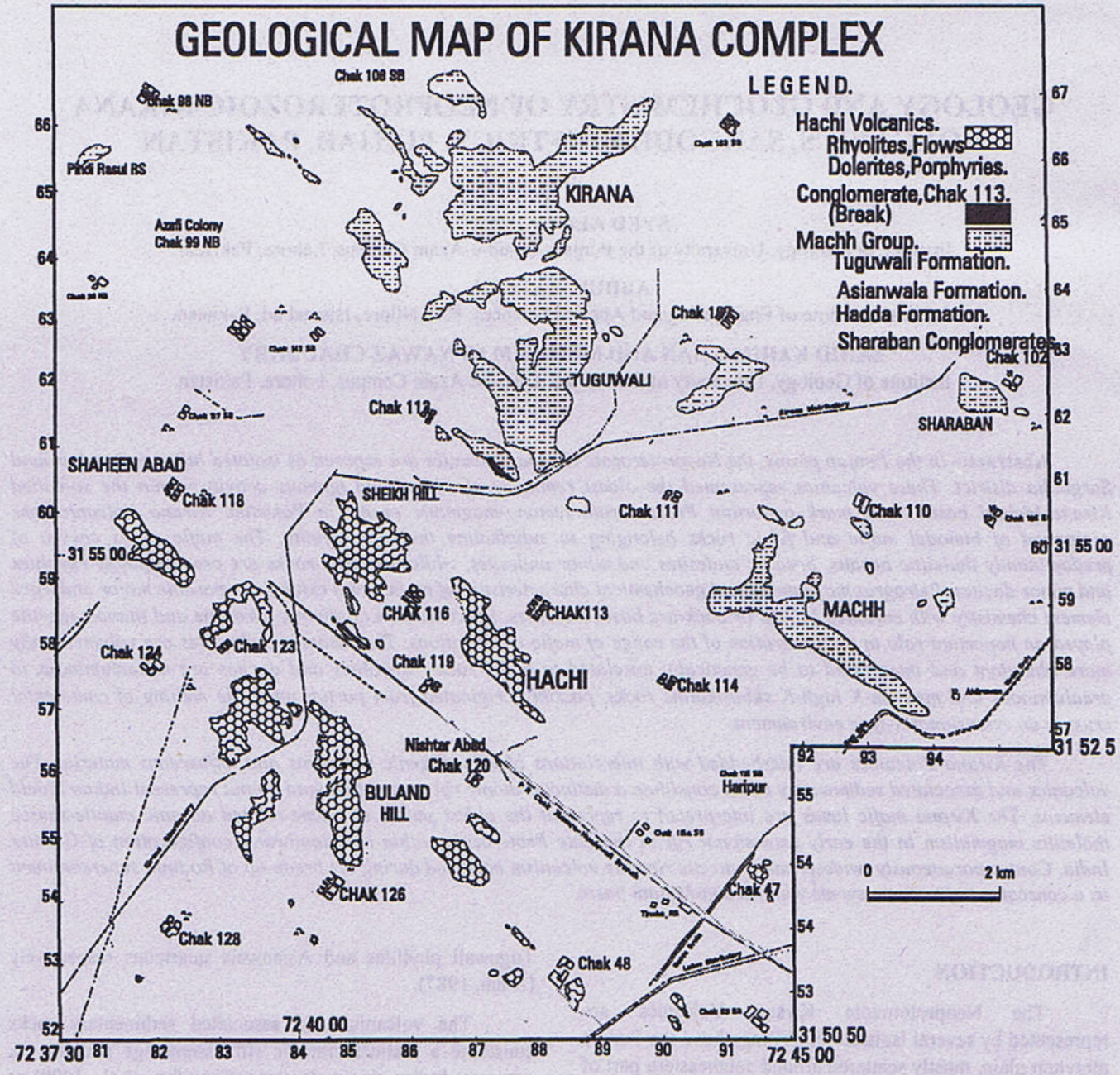

(Amended after Khan Z.K. unpublished)

Fig. 1 Map showing Geological Units of Kirna Volcanics

of Greater India is named as Malani-Kirana Basin (Chaudhry et al., 1999).

The Kirana Volcanics are an integral part of the world largest felsic volcanic field known as 'Malani Volcanics' occupying tracks along the northwestern flank of the great Aravalli mountain ranges with scattered outcrops extending from Tosham in Haryana and other places in northern districts of Rajasthan. Thus, Kirana Malani may be described as volcanoplutonic province and defined by the widespread Late – Proterozoic tectono-magmatic activity (spanning over 950 Ma to 550 Ma) with distinct rhyolitic flows and associated granites. In this paper, a detailed account of geology and geochemistry of the Kirana Volcanics is presented in an attempt the delineate tectonostratigraphy and petrogenetic attributes.

GEOLOGICAL SETTING

The Kirana Volcanics are the integral part of Precambrian igneous and metasedimentary rocks occur as isolated hills scattered around Sargodha district, Chiriot, Shahkot and Sangla areas. The Kirana Hill (31° 58′, 72° 45′) is the largest with general northwest strike. The igneous rocks are mainly comprised of volcanics and volcaniclastics (lava flows, tuff and pyroclastic), while the metasedimentary rocks are represented by quartzite, slates and phyllites.

The oldest unit cropping out in Kirana area is comprised of mafic and felsic volcanics and volcaniclastics. These are composed predominantly of rhyolite flows and rhyolitic tuffs, whereas andesites and dacites are subordinate. The volcanic sequence contains interbeds of slates, which have been considered in the past as metasediments but are at least in part volcanogenic in origin (Khan and Chaudhry, 1991). The second important group of rocks, exposed in the area is the doleritic sills, which postdate the acid volcanics. The volcanics are unconformable overlain by a sequence of phyllites, which in turn, are overlain by quartzites and quartz wackes. This unconformity is represented by polymictic conglomerates (Khan unpublished work). The clasts are well rounded and are composed of dolerites, acid volcanics and volcaniclastics. Here this unit has been designated as Chak 112 conglomerate.

The overlying phyllites have been named as Tuguwali phyllites (Alam, 1987). This unit is 1190 m thick and is composed of phyllites and quartzites. Many of the horizons described by Alam as quartzites are in fact quartz wackes. This sequence appears to be turbiditic in nature. Asianwala Quartzite overlies Tuguwali phyllites. The top of the Asianwala Quartzite is not exposed. It is comprised of quartzites, gritty quartzites and metawackes. It is often cross-bedded and ripple marked. In Sharaban and Chandar hills, are exposed Hadda quartzites and conglomerates. Hadda quartzite is composed of calcareous quartzites with minor conglomerate horizons.

Sharaban conglomerates are 119m thick. The top is however not preserved. This unit is composed of dull rusty brown conglomerates with intercalations of slate. The contact between Tuguwali phyllites and Hadda quartzites is not exposed anywhere.

The preliminary geological observations were presented by Heron (1913, 1953) who considered the Kirana Volcanics as the extension of Indian shield representing Vindhyan basin and correlated the rock units as part of the Aravalli mountain system of India. Davies and Crawford (1971) described the rock suite from Bulland hill area and delineated felsic volcanics, intercalated with thin bands of sedimentary orign as well as minor basic lava flows and tuff; intruded into this pile a number of concordant and semi – concordant sheets of sills of doleritic composition.

Stratigraphic summary

Shah (1973) presented the stratigraphic scheme of Kirana area and defined a number of formations which include; Sharaban Formation, Hadda Formation, Asianwala Formation, Tuguwali Formation and Haachi Formation. Alam (1987) modified the stratigraphy of the area and defined two distinct groups as Kirana group and Sharaban group. The Kirana group is considered older and have been divided into three units as: (a)Asianwala quartzites (b)Tuguwali phyllites (c) Hachi Volcanics. The Sharaban group has also been divided into lower and upper units as Hadda quartzites and Sharaban conglomerate respectively (Alam, 1987).

This stratigraphic division needs revision because of the following reasons: -

1. The Hachi Volcanics constitute a very distinct lithostratigraphic unit. Its base is not exposed and the top is unconformable. A polymict conglomerate designed here as Chak 112 conglomerate marks the unconformity.

2. It is a separate and distinct entity comprised predominantly of volcanics. It is correlatable with Tosham-Malani volcanics.

3. The overlying sedimentary package has a distinct history and represents a coarsening upward sequence. No significant volcanic activity is seen in this sedimentary package. There is hardly any doleritic sill or dyke in the sequence.

4. There appears to be a distinct time gap between the Hachi Volcanics and the overlying metasediments.

The two packages i.e. the lower predominantly volcanic package and the upper sedimentary sequence were formed in two distinct petrotectonic environments and represent two distinct petrotectonic assemblages. Neither the base of Sharaban Group is exposed nor its top preserved anywhere. Since there are only two small exposures of this unit in Sharaban and Chandar hills, therefore giving it the status of a distinct group, is not justified. In view of the above reasons, a modified stratigraphic framework is delineated as follows (Chaudhry et al., 1999):

Machh Super Group	a. Sharban Formation (conglomerates with slate intercalations). b. Hadda Formation (calcareous quartzites) c. Asianwala Formation (mainly quartzite with subordinate quartz wackes, gritty quartzites and slates, often showing ripple mark and crossbedding) d. Tuguwali Formation (slates, fine-grained quartz wackes). e. Chak 112 Conglomerates (polymict conglomerate with clasts of dolerite and acid volcanics)
Hachi Volcanics	a. Volcanics (dolerites, andesite, dacite, dacitic tuff, rhyolites and rhyolitic tuff) b. Volcanogenics Slates (often interbedded with rhyolite/rhyolitic tuff and dolerite)

Hachi Volcanic rock units

On the basis of detailed field investigations, petrographic examination and geochemical analysis of the samples collected from Kirana group of hills, namely Kirana, Tuguwali, Shaikh hill, Buland hill, Hachi, Hundawal and hills at Chak 47, Chak 48, Chak 102, Chak 103 and Chak 128, various rock units have been catagories as follows:

Basalts, basaltic andesites and dolerites: These are subvolcanic and intrusive sheet-like bodies and are generally concordant to semi-concordant. Cross-cutting relationships are seen at places. They are fine to medium grained rocks. At places, they become quite coarse-grained like gabbbros. Dolerites are mainly exposed in Hachi, Buland hill, Shaikh hill, Shaheenabad and hills of Chak 127 and Chak 128. They generally trend NW-SE. On the north and northeast side of the Kirana hills dolerites are either absent or occur occasionally as thin bands. Their thickness varies from about 0.5 to 175 meters. Thick intrusions may show chilled margins and may cause some baking of the country rocks. The fresh colour of the unit is green and black whereas the color on the weathering surface is brownish green to grayish green.

Davies and Crawford (1971) considered the mafic rocks as dolerites and gabbros of the 'autometasomatic' type. These rocks were metasomatised during final stages of crystallization due to the concentration of aqueous carbonate-rich fluids and resulted in the breakdown of plagioclase and mafic minerals. These basaltic/doleritic rocks invariably show some alteration, though unaltered dolerites have been recognized at places. Thus, basalts and dolerites can be group into two varieties:

a) *Unaltered basalts/dolerites:* Unaltered dolerites are medium to coarse grained, having ophitic to subophitic texture. These are composed of olivine ± pyroxene ± hornblende + plagioclase ± chlorite. The rock unit is generally hollocrystalline and lacks directional texture. However, at the contacts of these rocks the alignment of minerals or backing effects in the country rocks are observed. Usually laths of plagioclase porphyroblasts are subophitically enclosed within aggregates of amphiboles. Sometimes sericitization of feldspar is very prominent. Calcite is present both in the intracrystalline spaces and along cracks. Partial to complete alteration of ilmenite to leucoxene is common.

b) *Altered basalts and basaltic andesites/dolerites:* The altered basalts and basaltic andesites/dolerites are olivine-pyroxene free. The rock unit has been altered due to extensive chloritization, calcitization, sericitization, epidotization (sassuritization). The altered dolerites are comprised of chlorite, plagioclase, quartz, sericite, calcite, epidote and ilmenite-leucoxene. They are fine to medium grained.

Andesites and Dacites: Occasionally intercalated, conformable bodies of andesites and dacites, having variable thickness, are associated with these dolerites. These are fine to medium grained, chloritised, calcitised, and epidotized variably. Microphenocrysts of quartz, plagioclase, and K-feldspar are subophitically encloses within devitrified microcrystalline to glassy groundmass of microcrystalline texture. Generally these are composed of quartz+plagioclase+K-feldspar ± calcite ± chlorite + microcrystalline glass. Texturally fineness of grains increases from andesites to dacite. Andesites and dacites are

volumetrically minor bodies present at Hachi, Sheikh hill, Chak 128, and Chak 123 of the area.

Felsic Volcanics/Volcanogenics: This rock unit is predominantly composed of rhyolite flows, tuffs/ welded tuffs, pyroclasts and volcanogenic slates. The felsic volcanics are often interbedded with volcanogenic components. The northern and northwestern side of the area is composed of siliciclastic metasediments. In the southern part rhyolites predominates and may form independent hillocks. In the Shaikh hill, Hachi and Shaheenabad, rhyolites occur as alternate bands with volcanogenic slate intercalations and dolerite sills.

Felsic volcanics consist of quartz porphyry, plagioclase porphyry, and rhyolite. In general merrocrystalline and microcrystalline varieties are extensively developed. The volcanics are usually associated with volcanogenic slates and dolerites as alternating bands or beds. Tuffs and tuffaceous rocks are also common. The thickness of individual flows varies from a few centimeters to a few meters. While the grain size of the matrix is often from glassy to microcrystalline, microphenocrysts may be as big as 0.5 cm. Phyllites and wackes predominate in Machh and Chandar hill sections. Slump structures are also visible. Wackes are comprised of fine-grained quartz with iron, microcrystalline calcite and clay groundmass. A conglomerate bed of about 1 to 3 meters thickness is seen in Sharaban hill, which consists of quartzites, slates, dolerites, rhyolites pieces indicating that this conglomeratic bed is younger than volcanics/volcanogenics and dolerites.

AGE RELATIONSHIPS

Davies and Crawford (1971) conducted geochronological studies on the volcanic rocks of Bulland Hill and obtained an Rb-Sr isochron age of 870 ± 40 Ma. They correlated the Kirana volcanism to a period of uplift in the Trans-Aravalli mountain belt within the Vindhyan System of northern India. Recently Ahmad et al. (1997) has determined whole-rock K-Ar ages from two outcrops of Hachi Volcanics and obtained 889 ± 44 Ma and 868 ± 43 Ma dates which are quite comparable with Rb-Sr isochron age.

The available isotope age data indicates that Kirana Volcanics represent the oldest pulses of igneous activity associated within the Kirana-Malani basin. The Neoproterozoic Kirana volcanism is relatively older than magmatism represented by Malani Rhyolite Series of southwest Rajasthan (Rathore et al., 1996, 1999)

PETROGRAPHY

About 200 representative samples were selected for petrographic study after systematic sampling of different rock units covering the whole range of lithologies of the Kirana Volcanics.

Basalts, basaltic andensites/dolerites

Mafic rocks are fine to medium grained and dark green to light greyish green. Basalts and basaltic andesites are non-vesicular to holocrystalline rarely porphyritic. Plagioclase and clinopyroxene may occur as phenocrysts as well as small crystals in the groundmass. The dolerites are hollocrystalline, medium to coarse grained and at places appear to like gabbros. Ophitic to suborphitic textures are common. Mafic suites are grouped into olivine-pyroxene bearing and olivine-pyroxene free types.

The unaltered basalts/dolerites are represented by olivine ± pyroxene (augite) ± hornblende ± calcic plagioclase ± quartz ± ilmenite/leucoxene assemblage. These contain relics of clinopyroxene and calcic plagioclase phenocrysts. The altered dolerites are holocrystalline and composed of chlorite ± Fe-epidote ± hornblende ± plagioclase ± quartz ± ilmenite/leucoxene. The altered dolerites are comparatively more abundant in Bulland hill, Sheikh hill, Hachi and Shaheenabad areas. In these dolerites plagioclase (andesine) and clinopyroxene (augite) may occur as phenocrysts/ microphenocrysts as well as smaller crystals in the groundmass. Ophitic texture is present in these altered dolerites. Usually porphyroblasts/phenocrysts of plagioclase enclose aggregates of chlorite/epidote.

Olivine occurs as anhedral to subhedral, very fine to fine grained crystals, showing alterations at the margin into pyroxene. Very often olivine is preserved as relics in pyroxene. Olivine crystals show typical radial cracks.

Pyroxene is generally subhedral to eumorphic. It may occur as discrete crystals as well as aggregates. The phenocrysts often enclose subophitically, laths of ca-plagioclase of andesine composition. Cracks and fractures of pyroxene may be filled by secondary calcite. Pyroxene is generally augite and may marginally alter to hornblende.

Hornblende occurs as euhedral to subhedral phenocrysts as well as smaller crystals in the groundmass. Hornblende may also ophitically enclose laths of calcic-plagioclase. Rarely acicular to columnar aggregates of actinolite may also occur. Hornblende may show marginal alteration to chlorite.

Plagioclase is subhedral to eumorphic and occurs as well formed prismatic crystals. Plagioclase occurs both as phenocrysts as well as smaller crystals in the groundmass. The crystals of plagioclase are well twinned on albite law. Combined carlsbad-albite twins are rare. The plagiocalse is variably and erratically saussuritised. The products of this alteration are epidote, sericite and calcite. Sericite and

Table 1

Average major and trace element compositions of Kirana volcanic suites and representative data for tholeiitic basalts – granites from different tectonic settings

No. of Samples	Olivine tholeiites [11]	Quartz tholeiites [19]	Basaltic andesites [21]	Andesites [4]	Dacites [5]	Rhyolites [42]	Normal MORB Average	Enriched MORB Average	Back-arc tholeiites Average	Island-arc tholeiites Average	A-type Granites* Average
SiO_2	49.49	50.12	52.86	60.20	68.86	77.08	50.45	51.18			74.82
TiO_2	1.61	1.90	1.82	1.00	0.41	0.29	1.62	1.69			0.17
Al_2O_3	14.93	15.28	14.64	13.25	13.51	12.23	15.26	16.01			13.90
$Fe_2O_3^t$	13.00	13.26	13.38	6.52	5.27	3.44	11.59	9.40			1.68
MnO	0.22	0.24	0.20	0.35	0.16	0.11	0.18	0.16			0.03
MgO	8.25	6.44	5.27	3.49	1.92	0.77	7.58	6.90			0.13
CaO	9.50	9.89	8.36	9.60	2.69	0.90	11.30	11.49			0.77
Na_2O	2.37	1.53	2.17	4.18	0.67	1.19	2.68	2.74			1.72
K_2O	0.63	0.84	1.02	0.99	4.49	4.02	0.10	0.43			5.66
P_2O_5	0.19	0.23	0.24	-	0.40	-	0.12	0.15			0.07
Rb	21	46	44	40	164	108	2.3	10.3	6	4.6	-
Sr	234	155	174	82	40	68	90	155	212	200	48
Ba	160	146	372	222	415	384	13	86	77	110	352
V	244	303	321	-	-	-					6
Cr	376	205	74	-	-	-	346	225			-
Co	46	37	35	-	-	-					-
Ni	128	91	24	-	-	-	177	132			-
Cu	48	42	32	-	-	-					-
Zn	107	137	122	50	81	53					-
Ga	15	16	19	16	-	-					-
Y	23	34	34	38	152	74	28	39	30	12	75
Zr	91	109	164	247	206	340	88	121	130	22	528
Nb	6	13	9	16	21	31	2.5	8.6	8	0.7	37
Th	-	-	-	-	51	26				0.25	23
Ce	41	39	48	67	88	141	10	17.8	119	3.7	137
Nd	17	14	28	26	42	55	7.3	13.6	13.1	3.4	-

* A-type granites, average of 148 samples (Whalen et al., 1987)

epidotes are the major components of this alteration while calcite is minor. Plagioclase crystals and laths are sometimes traversed by epidote, calcite and chlorite vein-lets. These vein-lets are in fact late stage and post consolidation fracture fillings.

Chlorite varies widely in this unit. It may occur as pseudomorphs after amphibole or may develop as aggregates of small flaky crystals. It is strongly pleochroic from neutral green to bright green and shows a variety of interference colours, most common being tobacco green and bluish green. It appears to be Fe-Mg-rich chlorite. It is generally very fine to fine grained and occurs as flake and fibre like aggregate.

Epidote is usually anhedral and occurs as an alteration product of plagioclase and amphibole. It may occur as smaller grains, or granular masses. It varies from colourless to pale. The interference colours show that both zoisite and clinozoisite are present, since both normal and anomalous interference colors are observed. Size of epidote grains ranges from 0.01 mm to 0.52 mm in general. It is pleochroic in various shades of yellow and green.

Calcite is a secondary mineral and occurs as anhedral to subhedral crystals of widely variable size. Its amount varies widely and it may, therefore, occur as an accessory to essential mineral. It either forms extremely fine-grained microcrystalline aggregates or occurs as clear and well-formed discrete crystals and their aggregates. It may also occur as fracture filling mineral within plagioclase.

Dacites and Andesites.

Dacite and andesites occur at Hachi, Chak 123,Chak 128 and Shaikh hill outcrops. These are very fine to medium grained, merrocrystalline, present as intercalations with other volcanics, volcanogenics sediments and dolerites. Generally microporphyritic varieties are seen.

Quartz is anhedral to eumorphic. It also occurs as microphenocrysts in a groundmass of microcrystalline /glassy with chlorite/epidote aggregates. Occasionally a subophitic texture is also observed.

Plagioclase is generally present as microphenocrysts as well as tiny crystals in the groundmass. The groundmass is microcrystalline to glassy. Microcrystalline calcite is generally associated with groundmass. Plagioclases are partially sericitized and fractures are usually filled with microcrystalline calcite. Calcite is present as secondary mineral.

K-feldspars occurs as anhedral to subhedral and present as microphenocryst, embedded within a groundmass of microcrystalline/glass including microcrystalline calcite

Chlorite occurs as a secondary mineral having fibrous as well as flaky nature. It is altered product of both plagioclase and hornblende

Hornblende occurs as subophitic aggregates in the matrix as well as groundmass.

Epidote is present as anhedral to subhedral and varies variably, present as alteration product of plagioclase as well as hornblende.

Felsic volcanics (rhyolite flows, tuffs and pyroclastics)

The rhyolites are characterized by phenocrysts of quartz and feldspar and rarely ferromagnesian mineral phases in microcrystalline or glassy matrix. The rhyolites are generally merrocrystalline, microporphyritic and fluidal. Micro vesicular varieties are also common. The rhyolites, rhyolitic tuffs and rhyolite porphyries are major representatives of silicic volcanic rocks. Rhyolites generally occur in Hachi hill, Shaikh Hill, Chak 120, Buland Hill, Chak 123 out crops, Shaheenabad and Chak 112, whereas they are rarely present in the north and northwest of the area. The rhyolites generally occur as flows interbedded with slates/other volcanogenic slates/fissile volcanics. The volcanics and volcaniclastic rocks vary in color from grey, yellowish brown to reddish brown. At places these are fissile and are difficult to distinguish from slate. While at other localities these are massive and show excellent columnar jointing e.g. at Chak 47 hill and Chak 48 hill. Generally these rhyolites are merrocrystalline to microcrystalline and rarely holohyaline. Notwithstanding physical appearance the volcanics are predominantly rhyolitic in petrographic composition. Generally the rocks are microgranular and composed of minute granules of quartz, altered K-felspar, chlorite and zoisite. Sometimes secondary calcite is present as fracture filling and in the groundmass. Ilmenite/leucoxene occur as subhedral fine crystals. Occasionally microliths of altered feldspar are also seen. Sometimes proportion of microliths increases and the matrix to these microliths is microgranular. The reconstituted texture of the matrix suggests that it represents devitrified and recrystallised glass.

Tuffs are fairly prominent and easy to identify in the field. Generally two textural varieties are identified i.e. lithic felsitic and vitric felsitic. Generally these rocks are typically merrocrystalline i.e. with glassy/spherulitic groundmass and fluidal structure in which are enclosed fragments of K-feldspar/plagioclase and quartz. Haematite/goethite grains may occur along flow foliation.

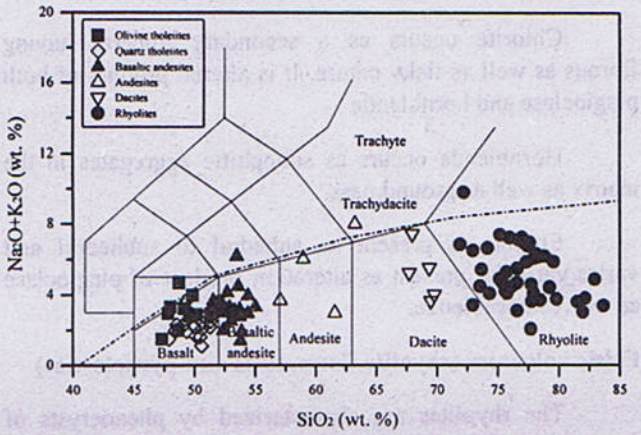

Fig. 2. Total alkali-silica classification diagram (TAS:Le Bas et al., 1986; Le Maitro et al., 1989) Kirana Complex. The dotted dividing line between alkalic and sub alkalic rock series is after Irvine and Baragar (1971).

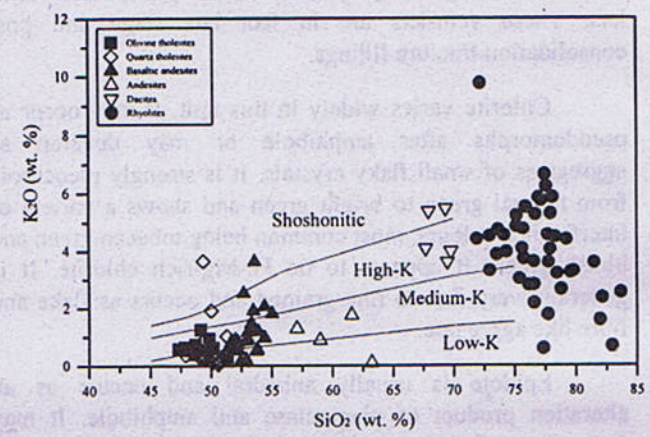

Fig.3 K_2O versus SiO_2 (wt%) diagram for the igneous rocks of the Kirana Volcanics with boundaries for the division into compositional fields of the low-K Calc-alkaline (High-K) and Shoshonitic suits (after Peccerlillo and Taylor 1976; Rickwood 1989).

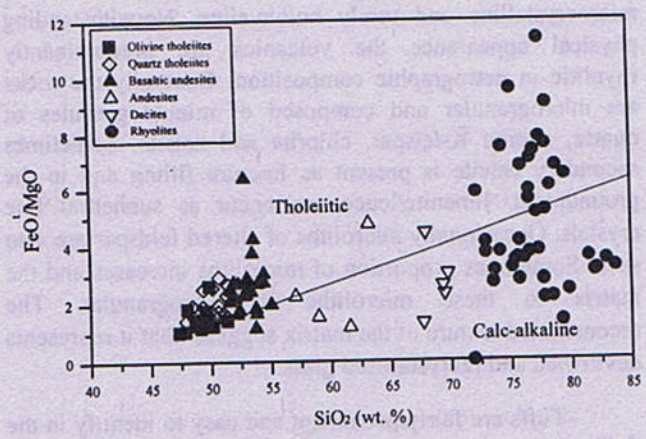

Fig. 4 Classification of Tholeiitic and Calc-alkaline series within igneous rocks of Kirana Volcanics. The dividing line between the two series is taken from Miyashiro (1974).

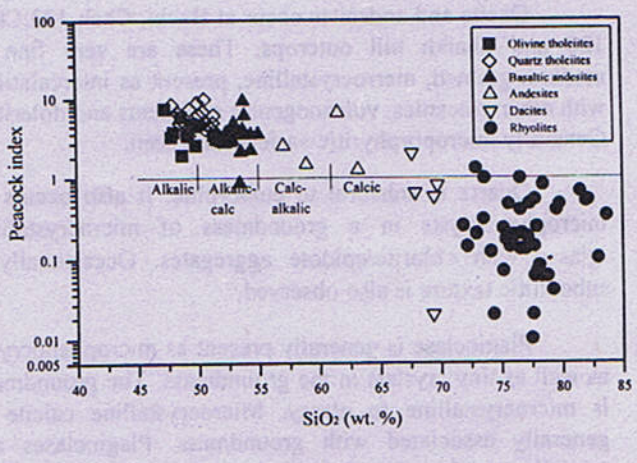

Fig. 5 Peacock index (CaO/Na_2O+K_2O) versus SiO_2 after Brown (1981) for the igneous rocks of the Kirana Volcanics showing the calcic trend for the felsic suites.

The vitric variety of tuff includes compacted tuff, in which shardy fragments have not been deformed, and also welded tuffs or ignimbrites in which considerable plastic flattening of the original shardy elements has taken place. The presence of latter suggests that the deposition of the pile took place under sub-areal conditions. Mineralogical composition of tuffs suggests that they have been derived from magma of acidic composition.

Lava flows are interlayered with slates (metasediments/ volcanogenics). Lava is of acidic composition and represents typical potassic rhyolites. Lava flows are wide spread in Hachi, Buland, Tuguwali, Shaheenabad, Chak 112, and Chak 128 hills. These are generally grayish, pale green and light brown in colour having quartz and K-feldspar microphenocrysts in glassy/microcrystalline groundmass. In flows the glass to microphenocryst ratio ranges up to 85:15.

The general characteristics of individual minerals and textures are as follows:

K-feldspar occurs as subhedral to eumorphic crystals, forming phenocrysts as well as smaller crystals in the groundmass, which are variably sericitized. Some plagiocalse laths enclosing chlorite are embedded in microcrystalline/fine grained quartz groundmass. In some cases porphyroblasts of K-felspar (perthite) enclose anhedral quartz and fine laths of albite.

Microperthitic texture also exists in some samples from Chak 123, 128,and 120. Here we find microphenocrysts of quartz and K-felspar surrounded by very fine anhedral epidote and microcrystalline groundmass composed of quartz and microcrystalline matter. Generally microcrystalline calcite occurs in the groundmass as well as in crystals, filling cracks and spaces.

Plagioclase is subhedral to euhedral, occurs as phenocrysts and in the groundmass. It is variably altered to epidote and sericite. Plagioclase laths may enclose chlorite and anhedral epidote. Sometimes laths of plagioclase are embedded in microcrystalline/fine quartz groundmass forming microphenocrystic texture. At places tiny plagioclase laths along with quartz are enclosed by K-felspar perthite phenocrysts. Microphenocrystic texture is common in samples of hills of Chak 123, 128,and 120.

Quartz occurs as strained, anhedral grains and microphenocrysts. It may enclose calcite and contain gas and fluids inclusions.

Epidote is fine grained and from anhedral to subhedral. Both zoisite and clinozoisite is present. It is secondary mineral formed due to the alteration of plagioclase.

GEOCHEMISTRY

Major and trace element contents in various rock units from Kirana Volcanics were determined by standard X-ray fluorescence technique. Average data of major and trace element compositions for rock suites are presented in Table 1. All major elements have been recalculated on an anhydrous basis as recommended by IUGS (Le Maitre et al., 1989) after adjustment of Fe_2O_3 contents according to the recommendation of Middlemost (1991) for oxidation condition of magma sub. Mg-number Peacock index, per alkalinity index, and Alumina saturation index are worked out and the average values are reported in Table 1.

A major complication in the study of mafic rocks from Kirana Volcanics is to account for the effects of element mobility due to alteration of primary mineralogy. The basaltic rocks from Kirana Volcanics suffered hydrothermal alteration due to carbonate bearing fluids. The analytical data was evaluated with a completely preserved primary mineralogy among the studied rocks (unaltered basalt/dolerites) to check the elements which were mobile during hydrothermal alteration. The majority of the rock samples show conformity with the trends defined by unaltered samples, indicating that there has been minimal element mobility during the secondary geological processes. The field relations indicate that Kirana Volcanics represent distinct mafic and felsic magma activity.

The major rock units have been classified on the basis of petrography and major element chemistry. The analytical data have been plotted on the standard geochemical classification diagrams of total alkali versus silica (Fig 2, TAS diagram after Le Maitre 1989, Middlemost 1991) and K_2O versus SiO_2 (Fig 3, after Rickwood 1989). The subalkaline-alkaline dividing line of Miyashiro (1978) has been marked to define magma series. (Fig 2) using the criteria proposed by Irvine and Barager (1971), the basalts/dolerites are tholeiites which are oliving normatives and quartz normative.

Kirana Volcanic rocks exhibit subalkaline trend and range in composition from tholeiite, basaltic tholeiite, andesite, dacite to rhyolite. The salient geochemical characteristics of Kirana Volcanics summarized below:

The Kirana volcanics fall into two distinct sets of rocks mafic suites (basalts and basaltic andesites) and felsic rocks (dacites and rhyolites). The volcanics exhibit subalkaline tholeiitic magma activity. The mafic rock suites mostly straddle the low-K and medium-K boundary, with a few samples show a trend towards high-K/shoshonites (Fig. 4). With the excepton of a few randam samples of andsitic composition, a distinct compositional gap exists from 56 SiO_2 to 66 wt% SiO_2. Thus the volcanics show bimodality of basalt and rhyolite association.

The mafic suites are represented by ol-tholeiite, q-tholeiite, and basaltic andesites (SiO_2 contents between 47.3 to 55 wt %), sub-aphyric to weakly porphyritic and saturated with mineral phases of olivine, pyroxene and Fe – Ti oxide. The basalts/dolerites have generally low MgO contents (<9 wt % except one sample with MgO=12.46 wt %) and Mg- number ranging from 62.4-20.1, indicating that the mafic rocks represent a range of differentiated tholeiitic trend from relatively primitive basalt (MgO>8%, Cr=236 to 680 ppm, Ni=63 to 272 ppm) to highly fractionated basaltic andesites.

The whole suite of rocks broadly define a negative trend of Fe_2O_3, MgO, and CaO against increasing SiO_2 contents, reflecting differentiation trend dominated by separation of dense phases of olivine, clinopyroxene and iron oxides (Fig 5)

Kirana mafic and felsic volcanic rocks are plotted on the AFM diagram in the Fig. 8, which define Fe-enrichment along the trend demarcating calc-alkaline from tholeiitic rocks. The rocks fall linearly in the tholeiitic field. This also suggests that the major elements were weakly mobile reflecting partial chloritization of mafic rocks.

The tholeiitic trend in Kirana Volcanics is clearly depicted also in the FeO/MgO versus SiO_2 (wt %) diagram (Fig. 4)

Rhyolites are high silica and medium-K to high-K subalkaline rocks. (Fig. 4). They are low in TiO_2 (mostly less than 0.4 wt% TiO_2) and extremely low in P_2O_5 contents.

Major element diagrams (show linear relationships with decreasing Al_2O_3, CaO and TiO_2

Trace element compositions of rhyolites are comparable with A-type granites.

Dacite and rhyolite units are characterized by metaluminous to strongly peraluminous trend (Alumina saturation index =A/CMK ranges from 0.62 to 2.77) and normative corundum values shoot as high as 9.4%. (Fig. 7)

In Peacock (1931) diagram (Fig 7), all the felsic rocks show clear calcic trend in the Peacock diagram (Fig.8)

Some rhyolite flows exhibit extreme depletion of Na_2O, which might have been lost by secondary geological processes (Fig. 6).

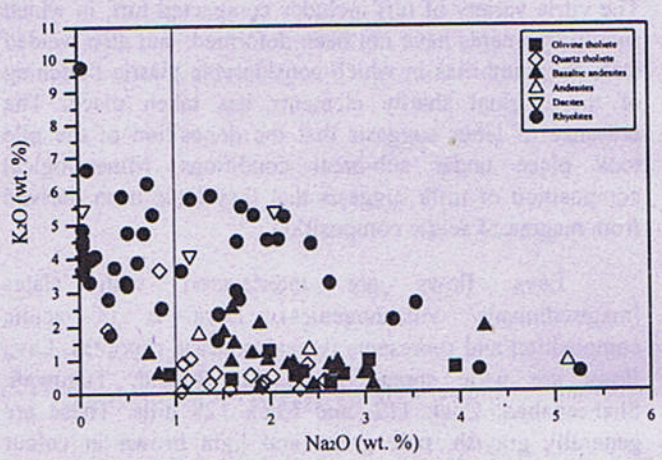

Fig. 6 K_2O/K_2O diagram showing depletion in K_2O due to alteration

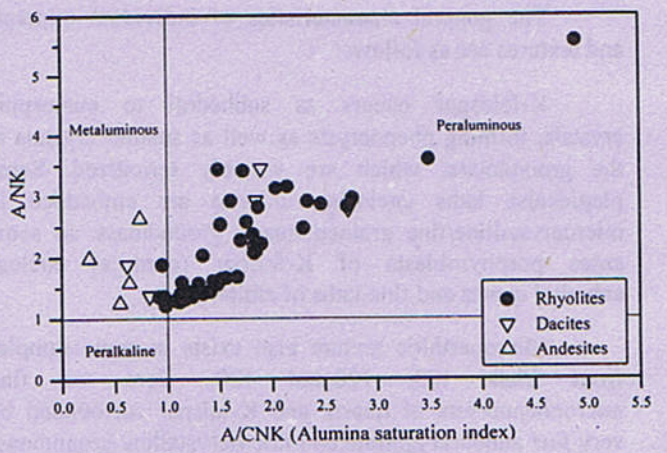

Fig. 7 Plot of A/NK [(mol.% $Al_2O_3/(Na_2O+K_2O)$] versus A/CNK (mol.% $Al_2O_3/CaO+Na_2O+K_2O$)) to show alkalinity index for Kirana Volcanics.

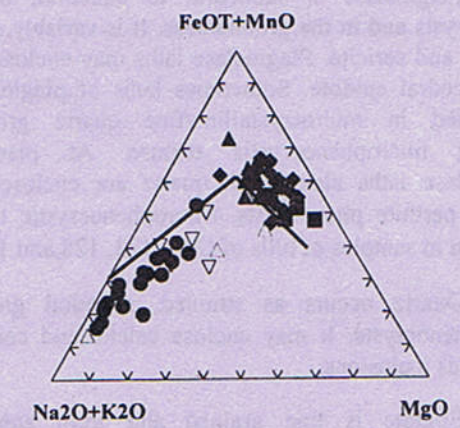

Fig. 8 AFM diagram plots exhibiting tholeiitic to calc alkaline trend.

DISCUSSION

The long-lived magmatism in the Neoproterozoic Kirana-Malani basin necessitates the goechemical and geodynamic conditions that enable melting and igneous activity for extended periods of time. The observed variations in the chemical compositions of Kirana Volcanics require that they are derived by different degrees of melting from heterogeneous mantle source. The petrogenetic interpretation of Kirana Volcanic can be discussed in terms of two main aspects (a) geochemical constraints (b) tectonic considerations. Following brief discussion is presented.

Geochemical constraints

The trends on the major element variations diagrams (Fig.5) can be interpreted either in terms of mafic and felsic volcanics or on overall evolutionary trend. The simplest interpretation of the array of data is that the majority of the samples fall into two distinct sets : (a) mafic suites (basalts and basaltic andesites) (b) felsic rocks (predominantly rhyolites). Geochemically a distinct compositional gap exists from 56 to 66 wt% SiO_2 (with a few randam samples of andesitic composition).

The geochemical distribution patterns of major element, tholeiitic magma affinity and biomadality of mafic and felsic rocks clearly suggest that basalts and rhyolite may have totally unrelated sources. This also supported by petrography and field relationships. Mafic and felsic rock suites may be linked genetically merely by simple thermal processes and may be a situation where anatexis of the felsic lower crust occurred due to the intrusion of a mantle derived mafic magma. Kirana volcanics display distinct tholleiitic trend for mafic suites (Fig. 4) and the felsic dacites and rhyolites are metaeuminous to peraluminous in nature (Fig. 6) Lack of calc-alkaline andesitic suites in the Kirana Volcanics suggest that the volcanics are probably unrelated to typical subduction environment.

Before any further inference can be made on the tectonic setting of the Kirana Volcanics, it is necessary to assess the significance of both the mafic and the felsic rocks. This requires evaluation of the origin of isotopic variations in mafic rocks and their relationships to incompatible trace elements and REE data. (Investigations on REE and isotope systematics for Kirana Volcanics are in progress).

Kirana mafic volcanic suites plot in the subalkaline tholleiitic field (Fig 4). SiO_2 and Mg-numbers has been used as an index of differentiation to identify processes that may be responsible for chemical variations in mafic rocks. Fig.s exhibit chemical compositional trends that can be explained by low-pressure olivine ± pyroxene + titanomagnetite fractionation in magma association. The positive correlation of CaO/Al_2O_3 ratio with MgO (not shown) and decrease in TiO_2 with increasing SiO_2 is consistence with this fractionation trend. The compositional variations of tholeiitic lavas in Kirana may reflect differences in degree of partial melting, source composition and post-melting fractionation and contamination. Low Mg-numbers of the tholeiite indicate that they are mostly fractionated derivatives of primary magma.

In Table 2, the major and trace element composition for Kirana mafic volcanics are compared to normal MORB, enriched MORB, black-arc tholeiite and Island- arc tholeiites. This comparison clearly indicates that trace element data rule out subduction-related origin because the Kirana mafic rocks do not exhibit relatively depletion in high field strength elements (HFSE) especially Nb and LREE and Rb which are characteristic very low for Island – arc tholeiites (Fitton et al., 1991). Nevertheless, the geochemical characteristics of Kirana mafic rocks are closely comparable (particularly trace elements, Table 2) with enriched MORB or back-arc basin tholeiites.

Felsic rocks: The geochemical characteristics indicate that the Kirana rhyolites are medium-K, high-K subalkaline rocks, originate possible from partial melting of continental crust. This conclusion is supported by geochemical data, petrographic and volumetric features which show that they are not genetically related to mafic rocks by fractional crystallization of mafic magma. The existence of a shallow reservior beneath the rhyolitic volcanos is usually assumed by many authors (Cas and Wright, 1988). In the Kirana Volcanics, this can be questioned on account of the textural observations of the pyroclastics, Tuffs and their cogenetie lithic fragments.

Tectonic Implications

Petrographic features and geochemical characteristics of Kirana mafic rocks show that comparable chemistry with enriched MORB or back arc basin tholeiites. The abundant associated rhyolites are genetically unrelated with mafic rocks. Mafic suites do not show relative depletion in HFSE, exemplified by negative NB anomalies, preclude an affinity with subducted-related arc magmatism. The trace element data favours the involvement of rift or plume-related magmatism. It is therefore, considered that such bimodal suites of Kirana volcanics may be produced in extensional environment. It is suggested that ancient ensialic rift zones can be distinguished. Alternatively, back – arcs (Karig, 1971). Mature back-arc basin may be defined to be those where extension is principally accompanied by seafloor spreading (Gribble et al., 1998). Kirana volcanics are interpreted to have been linked with incipient extensional rifting of NE-Gondwana during the Late Proterozoic.

The Kirana felsic volcanics rocks are the part of one of the largest rhyolitic province known in Gondwana, vary considerably in major and trace element composition. The heat source for crustal anatexis is problematical, unless produced by unrelated but contemporaneous mantle-derived basalt magmatism. The basalts/dolerites and related mafic rocks were formed by mantle-derived magmas with the Kirana-Malani basin. Circumstantial geochemical evidences support that extensive lower crustal melting was related to the tectonic environment associated with the rifting and incipient break-up of the Late-Proterozoic Gondwana supercontinent (Storey et al., 1992). Evidence from experimental petrology has shown that fluid-absent partial melting of amphibolite crust at about 30 Km depth can reach large degrees at relatively low temperatures (Rushmer, 1991). This may be triggered by crustal thinning processes without too much additional heat input.

CONCLUSION

The Kirana Volcanics in Pakistan felsic Volcanic associations of Tosham in Haryana and Gurapratap Singh and Diri of Pali district in Rajasthan are part of widespread volcanic activity in Kirana-Malani basin, probably initiated by mantle plume along the western flanks of post-Delhi Trans-Aravalli belt. Subalkaline tholeiitic basaltic and rhyolitic volcanism probably commenced around 950 Ma. The centres of magmatic actively were Kirana in Pakistan (873 ± 40 – 870 ± 40 Ma, Ahmad et al., 1997), Tosham in Haryana (1940 ± 20 Ma, modal age, Kochhar 1974, calculated isochron age of 770 Ma, Eby, 1990) and Pali district of western Rajasthan (779 Ma ± 10). Extensive volcanism in the region is probably linked with initial stages of rifting / back-arc extension triggered by rising mantle plume with Late Proterozoic Gondwanan configuration of Greater India.

AKNOWLEDGEMENTS

This research work was carried out under financial support of Punjab University research grant no 16/96,8/97 R-I and 211-222-P&D dated 25 6 99.

REFERENCES

Ahmad, M. N., Yoshida, M. and Khadim, I. M., 1997. Paleomagnetic reconnaissance and K-Ar dating of Late Proterozoic Hachi Volcanics, Kirana Hills, Sargodha District, Pakistan. In: Proceedings of Inter-PARMAGS: Paleomagnetism of Collision Belts, Recent Progress in geomagnetism, rock Magnetism and Paleomagnetism, **1, 171-176.**

Alam, G.S., 1987. Geology of Kirana Hills, Sargodha, Punjab, Pakistan. *Information release. GSP. Quetta, Pakistan.* **201 1-37.**

Alam, G.S., Jaleel, A. and Ahmad, R. 1992. Geology of the Kirana area, District Sargodha Punjab, Pakistan. Acta Miner. Pak., **6, 93-100.**

Brown, G.C., Thorpe, R.S. and Webb, P.C., 1984. The geochemical characteristics of granitoids in contrasting arcs and comments on magma sources. *Jour. Geol. Soc. London*, **141,** 411-426.

Cas, R. A. F. And Wright, J. V., 1988. Volcanic Successions Modern and Aricient: A Geological Approach to Processes, Products and Successions Allen and Unwin, London.

Chaudhry, M.N., Ahmad, S.A. and Mateen, A., 1999. Some postulates on the tectonomagmatism, tectonostratigraphy and economic potential of Kirana-Malani-Basin, Indo-Pakistan. *Pakistan. Jour. Hydrocarbon.Res. Islamabad, Pakistan,* **11, 52-68.**

Davies, R.G. and Crawford, A.R., 1971. Petrography and age of the rocks of Buland Hills, Sargodha Districts West Pakistan. *Geol. Mag;* **108 (3), 235-246.**

Eby, G.N. and Kochhar. 1990. Geochemistry and petrogenesis of the Malani igneous suite,north penisular India.*Jour.Geol.Soc.India.***36, 109-130.**

Fitton, J. G., Jame, D. and Leeman, W. P. 1991. Basic magmatism associated with late Cenozoic extension in the Western United States: compositional variation in space and time. *Jour. Geophys. Res* **9, 13693-13711.**

Gribble, R. F., Stern, R. J., Newman, S., Bloomer and Hearn 1998. Chemical and isotopic compositional of lavas from the northern Mariana Trough: Implications for magmagenesis in back-arc basins. *Jour. Petrol.*, **39, 125-154.**

Heron, A.M., 1913. The Kirana and other hills in the Chej and Rachna Doabs. *Memoirs, Geil.Surv.India,, Records,* **43(3) 229-236.**

Heron, A. M., 1953. The Geology of Central Rajputana. Mem. *Geol., Surv. Inida*,. 79, 1-339.

Hofmann, A.W., 1988. Chemical differentiation of the earth: The relationship between mantle, continental crust and occanic crust. *Earth Planet. Sci. Lett.*, **90,** 297-314.

Irvine, T.N. and Baragar, W.R.A., 1971. A guide to the chemical classification of the common volcanic rocks. *Can.Jour.Earth. Sci.*,**8, 523-548.**

Karig, D.E., 1971. Origin and development of marginal basins in the western Pacific. *Jour. Geophys. Res.*, **76,** 254-261.

Khan, Z.K. and Chaudhry, M.N., 1991. Engineering geological and petrographic evaluation of metadolerites of Buland Hill and Chak 123 Quarries of Kirana Hills, District, Sargodha, Pakistan. *Kashmir Jour. Geol:*, **8, & 9, 181-184.**

Kochhar, N., 1973. On the occurrence of a ring dyke in the Tosham igneous Complex, Hisar (Haryana). *Jour. Geol. Soc. India.*,.**14(2), 190-193.**

Kochhar, N., 1974. The age of the Malani series.*Jour.Geol.Surv.India:* **15, 316-317.**

Kochhar, N., 1984. Malani igneous suite: Hotspot magmatism and Cratonization of the northern part of Indian Shield. *Journal of Geological Survey of India:* **25(3), 155-161.**

Le Bas M.J, Le Maitre,R.W., Streckeisen, A and Zanettin, B., 1986. A chemical classification of volcanic rocks based on the total alkali silica diagram.*Jour.Petrol:* **27, 745-750.**

Le Maitre, R.W., Baterman P.,Dudec, A.,Keller, J.,Lameyre, Le Bas, M.J,SabineP.A,Schmid, R.,Sorensen, H.,Streckeisen, A.,Wooley, A.R. and Zanettin B.,1989. A classification of igneous rocks and glossary of terms. Blackwell ,Oxford.

Miyashiro, A., 1978. Nature of alkalic volcanic rock series. *Contrib. Mineral. Petrol.*, **66, 91-104.**

Middlemost, E.A.K., 1991. Towards a comprehensive classification of Igneous rocks and magmas. In: Earth Science Reviews: **31, 73-87**.Elsevier Science Publishers, B. V, Amsterdam, Australia.

Peacock, M.A., 1931. Classification of igneous rock series. *Jour, Geol.*, **39, 65-67.**

Peccerillo, R.and Taylor, S.R., 1976. Geochemistry of Eocene calc-alkaline rocks from the Kastamonu area, northern Turkey. *Contrib. Mineral. Petrol.*, **58, 63-81.**

Rathore, S. S., Venkatesan, T. R. and Srivastava, R. K., 1996. Rb-Sr and Ar-Ar systematics of Malani volcanic rocks of southwest Rajasthan: Evidence for a younger post-crystallization thermal event. *Proc. Indian Acad. Sci., Earth Planet. Sci, Lett.*. **105, 131-141.**

Rathore, S. S., Venkatesan, T. R. and Srivastava, R. K., 1999. Rb-Sr isotope dating of Neoproterozoic (Malani Group) magmatism from southwest Rajasthan, India: Evidence of younger Pan-African thermal event by ^{40}Ar-^{39}Ar studies. *Gondwana Research*, **2, 271-281.**

Rickwood, P.C., 1989. Boundary lines within petrologic diagrams, which use oxides of major and minor elements. *Lithos,* **22, 247-263.**

Shah, S.M.I., 1973. Occurrence of gold in the Kirana group, Sargodha (Punjab) Pakistan. *Inform Release, GSP, Quetta, Pakistan:* **68, 1-14.**

Storey, B. C., 1995. The roal of mantle plumas in the continental breakup: Case histories from Gondwanaland. *Nature*, **377,** 301-308.

Whalen, J. B, Currie, K. L. And Chappel B. W., 1987. A type granites: Geochemical characteristics, discrimination and petrogenesis. Contrib. Mineral. Petrol: 95 407-419.

Geol. Bull. Punjab Univ. 35, 2000.

TECTONO-MAGMATIC ENVIRONMENT OF THE PANJAL VOLCANICS IN AZAD KASHMIR AND KAGHAN AREAS, PAKISTAN.

BY

MOHAMMAD SABIR KHAN

Institute of Geology, University of Azad Jammu and Kashmir, Muzaffarabad.

MOHAMMAD ASHRAF AND M. N. CHAUDHARY

Institute of Geology, University of the Punjab, Lahore.

Abstract:- *The Panjal volcanivs (lava flows) in Lesser Himalaya are basalts to basaltic andesites in composition (SiO2 ranges from 42 - 56 wt.%). A more petrological and geochemical data is used to determine the tectonic setting of the Panjal volcanic rocks. Petrology and geochemical investigations show that the Panjal volcanics are mainly tholeiitic to slightly alkalic basalts. The volcanics are enriched in incompatible trace elements and the light rare earth elements (LREE) relative to heavy rare earth elements (HREE).*

When geochemical data for the Panjal volcanic rocks are plotted on different geochemical discriminant diagrams which have been used to infer tectonic environment, some of them plot in the compositional fields designated as characteristics of "within-plate" basalts. In contrast, the remaining most of data plot largely in the "MORB" fields on geochemical discriminant diagrams.

The trace element variations in the Panjal volcanic rocks show compositional differences which occur throughout the region. The immobile element ratios and rare earth element (REE) contents demonstrate that they are enriched in the Panjal volcanics.The Panjal volcanics are characterized with Zr/Nb from 5 to 11, Y/Nb 1 to 2.7, Zr/Y from 3.8 to 4.16 and Ti/Y ratios from 331 to 371. The Panjal volcanic rocks show fractional crystallization which was dominated by the removal of olivine and pyroxene. Most of the Panjal volcanics are evolved in terms of Mg number (38 - 66) and low Ni (316 - 24 ppm) and Cr (541 - 34 ppm) values. Geochemical variation of the Panjal volcanics can be attributed to varying degrees of partial melting and fractionation. Trace elements and REE data like La/YbN, Ce/YbN (2.83 - 8.82) and La/SmN (1.96 - 4) for the Panjal volcanics support the concept that the melt have been derived from an 'enriched' source region, such as mantle plume P. type MORB.

The geochemistry and tectonics of the Panjal volcanics suggest that they were generated during Permian rifting of the northern periphery of Gondwana with the development of shallow marine conditions.

INTRODUCTION

The Panjal volcanic rocks of the Kahuta, Muzaffarabad and Kaghan areas are largely altered, spilitized and metamorphosed.

Basaltic rocks similar to those like the Panjal volcanics with large-ion lithophile (LIL) and light rare earth elements enrichment (LREE) are reported from spreading centers in main ocean basins like Iceland (Wood, 1976), Mid Atlantic Ridge (Wood et al., 1979; Schilling et al., 1983), in back arc basins (Tarney et al., 1981) and ocean islands. The Panjal volcanic rocks have geochemical characteristics similar to P-type mid ocean ridge basalts (MORB) although similar rocks are also observed in continental flood basalts.

Geochemistry of the Panjal volcanic rocks were studied by other workers (Nakazawa and Kapoor, 1973; Bhat and Zainuddin, 1978, 1979); Honegger et al., 1982) from the Srinagar region in the valley of Kashmir.

The geology of the Panjal volcanic rocks in the Lesser Himalaya was studied by Lydekker (1883), Wadia (1928, 1934), Ghazanfar and Chaudhry (1984), Ghazanfar and Chaudhry (1985), Greco (1989), Ashraf and Khan (1991). The geochemical characteristics of the Panjal volcanic rocks in the Lesser Himalaya have been described by Butt et al. (1985), Chaudhry and Ashraf, (1980), Khan

and Ashraf (1989), Papritz and Rey (1989). Khan et al. (1991), Khan (1994) and Khan et al (1997). There has been a controversy about the tectonic setting of these rocks. To infer tectonic setting of these rocks a new geochemical data of major and trace elements was obtained. In the Panjal volcanics the degree of alteration and metamorphism is such that abundances of all mobile elements are likely to have been altered from original magmatic values.

Since the aim of this paper is to identify the original tectonic setting of eruption of the Panjal volcanics, emphases is placed on the immobile elements, high field strength elements and the rare earth elements (REE) which are not affected by alteration and low grade metamorphism.

The immobile elemental abundances of the Panjal volcanic rocks were plotted on tectonic discrimination diagrams, multielement diagrams and rare earth element plots to find out the true tectonic setting of the Panjal volcanics.

GEOLOGICAL SETTING

The Panjal volcanics are exposed in the Lesser Himalaya (Fig. 1). They form a parallel belt, extending from Kahuta to Kaghan (Fig. 1), imbricated and bound between the Main Boundary Thrust (MBT) and the Panjal Thrust (PT). Along the PT the older metasedimentary rocks were thrust over the Panjal volcanics. These metasediments were derived from advancing thrust sheets during Himalayan orogeny. Overthrusting of the older metasediments onto the Panjal volcanics which are stratigraphically younger might have affected thickness of these rocks and their paleotectonic position.

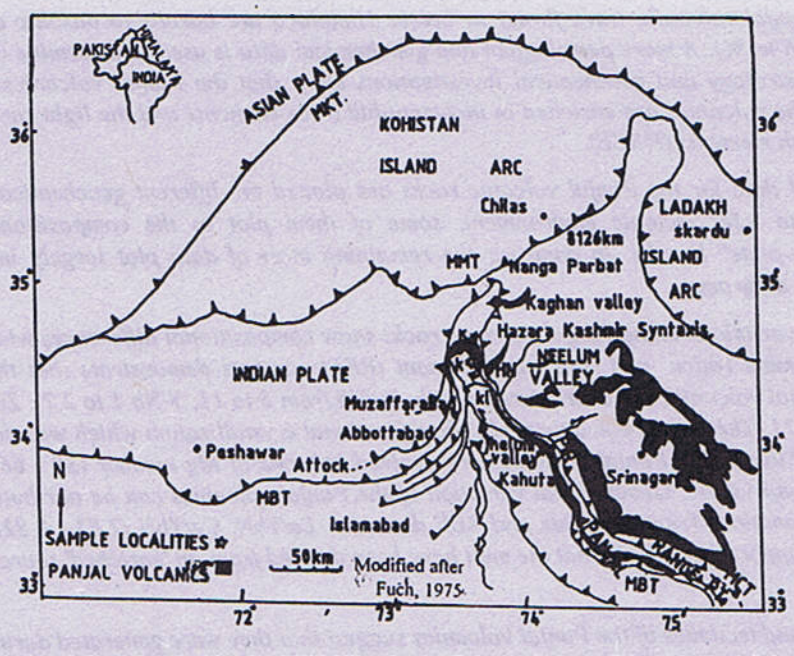

Fig. 1. Distribution of the Panjal Volcanics in the NW Himalayas Stippled area. Occurrence of the Panjal Volcanics, MMT= Main Mantle Thrust, MKT=Main Karakoram Thrust, MCT=Main Central Thrust. PT Panjal Thrust and MBT=Main Boundary Thrust.

In this area a sequence of the pryroclastic rocks, agglomerates and predominantly Panjal volcanic rocks (lava flows) are exposed on the eastern and western flanks of the Hazara-Kashmir Syntaxis. The area between the PT and MBT comprises a lower unit of Agglomeratic slates followed by the Panjal volcanic rocks. The Panjal volcanic rocks comprise, massive basaltic lava flows with pillow structures. The Panjal volcanic rocks are altered, metamorphosed to greenschist facies and are subordinately spilitized. They were first altered and reconstituted in the submarine conditions and metamorphosed during Himalayan orogeny.

The Panjal volcanics in the Kaghan area are associated with turbidite beds. The carbonate bands occur as interbeds within the volcanics. After magmatic effusion when eruption ceased in late Permian and early Triassic, the volcanics in some parts were covered with Triassic limestone. However, at some places, in the Muzaffarabad and Kaghan areas after deposition of Triassic limestone volcanism was again active at least at local scale which is reflected by the presence of thin lava flows and limestone intercalation in this area. Greenish to reddish chert interbedded with the Panjal volcanics and lava flows with pillow structures, at places associated with black shales are also found.

A Permian to Triassic age for the Panjal volcanic rocks in the Lesser Himalaya is based (1) on correlation of these rocks in Baramula and Srinager region where a Permian to Triassic age has been accepted (Wadia, 1934) and (2) radiochronological dating (Ar^{40}/Ar^{39}) have established the age of these rocks 284±4 to 262±1 Ma (Baig, 1991).

METHOD OF STUDY

Fresh and representative rock samples of lava flows of the Panjal volcanics were selected for chemical analysis after petrographic studies. Rock samples were crushed in the geochemical laboratory of Pakistan Atomic Energy Mineral Center, Lahore. The samples were ground in the tungsten carbide Tma mill in the geochemical laboratories of Sarhad Development Authority (SDA) in Abbottabad, for inductively coupled plasma (ICP) analysis, for major and trace elements. Rare earth elements were determined by mass spectrometry inductively coupled plasma (ICP/MS) techniques. For analysis by the ICP method, a 0.2 gram sample was fused with 0.60 gram of LiBO2 and was dissolved in 100 mls 5% HNO_3. The samples prepared were thus analysed by ICP method. Rock samples MRG-1 and SY-2 (Abbey, 1979) were analysed for calibration.

PETROGRAPHY

The Panjal volcanic rocks are altered and metamorphosed to lower greenschist facies. They are plagioclase phyric basalts in the Muzaffarabad and Kaghan areas, and Plagioclase and clinopyroxene phyric basalts in the Kahuta area. Plagioclase has been altered to epidote, chlorite, sericite and calcite. Pyroxene alters to chlorite and actinolite. Thinsection studies show the mineral assemblages of albite-epidote-chlorite-actinolite-quartz-calcite-sphene.

Normative (CIPW) composition of the chemically analysed Panjal volcanic rocks and Mg number (100MgO/Mg+Fe+), were calculated using Fe2O3/FeO ratio 0.15. The normative minerals diopside (Di), olivine (Ol), hypersthene (Hy), nepheline (Ne) and quartz (Q) are formed (Fig. 2). Thus the normative mineralogy of the Panjal volcanics indicate that these rocks are quartz tholeiites, olivine tholeiites and hypersthene tholeiites in nature. Although olivine is a normative phase, but no modal olivine was found in these rocks. However, the widespread chlorite clots within the Panjal volcanics could have in part replaced primary magmatic olivine. The scatter of the major element data (Khan, 1994) indicate a considerable effect of the mobility of these elements in the Panjal volcanic rocks.

GEOCHEMISTRY

One hundred and twenty rock samples of the Panjal lava flows were analysed by ICP for major elements SiO_2, TiO_2, Al_2O_3, Fe_2O_3 (Fe_2O_3 was analysed as total iron), MnO, MgO, CaO, Na_2O, K_2O, P_2O_5 and trace elements like Ba, Sr, Cr, Ni, La, Ce, Y, Nb, Zr, V, Co, Cu and Zn The average geochemistry of the Panjal volcanic rocks is given in Table 1. In addition repre-sentative rocks were analysed for rare earth elements (La, Ce, Pr, Nd, Sm, Eu, Gd, Dy, Er and Yb) by ICP/MS. Major oxides are presented in wt.% while trace and rare earth elements are in ppm.

Table-1

Average chemical analyses of the Panjal volcanics. (1) Kahuta (2) Khatir Nar (3) Lamnian (4) Nauseri (5) Manj Hotor (6) Kaghan. (7) Kaghan (number in parentheses indicate number of samples).

Wt.%	(n=18)1	(n=16)2	(n=18)3	(n=13)4	(n=16)5	(n=16)6	(n=20)
SiO_2	49.40	50.42	50.12	49.74	48.88	50.10	49.33
TiO_2	1.42	1.43	1.53	1.66	1.67	1.61	1.45
Al_2O_3	15.49	16.03	15.08	14.28	15.08	15.22	14.93
Fe_2O_3	10.58	10.55	10.97	12.07	12.03	11.09	11.17
MnO	0.16	0.15	0.17	0.17	0.22	0.18	0.17
MgO	6.13	6.29	6.22	5.88	6.44	6.77	6.12
CaO	7.86	6.14	7.71	7.78	7.91	7.44	6.95
Na_2O	2.71	4.12	3.08	2.95	3.13	3.64	3.14
K_2O	1.53	1.52	1.01	1.19	0.90	0.74	0.74
P_2O_5	0.16	0.18	0.17	0.18	0.16	0.16	0.18
LOI	4.31	2.90	3.45	3.78	3.04	2.76	-

Mg #	57.50	58.10	56.90	53.20	55.50	58.70	56
Al_2O_3/TiO_2	10.91	11.21	9.86	8.60	9.03	9.45	10.29
CaO/TiO_2	5.53	4.29	5.04	4.69	4.74	4.62	4.79
TiO_2/P_2O_5	8.88	7.94	9.00	9.22	10.44	10.06	8.05
ppm							
Rb							7
Ba	352	306	220	215	260	178	415
Sr	373	368	282	218	178	170	163
Cr	325	236	190	235	321	204	243
Ni	100	116	86	93	113	83	63
La	18	23	14	18	18	16	23
Ce	50	37	35	40	33	29	50
Y	25	25	26	30	27	26	28
Nb	<13	<16	<11	<18	<10	<13	9
Zr	104	95	107	123	111	107	99
Co	64	52	41	53	59	54	35
Cu	109	76	68	(518)68	97	74	43
Zn	106	97	110	112	114	119	93
Zr/Nb	8	5.9	9.7	6.8	11	8.2	11.2
Zr/Y	4.16	3.8	4.12	4.1	4.1	4.12	3.5
Ti/Y	340	342.5	352	331	370	371	310
Ti/Zr	81.75	90.13	85.62	80.81	90	90	88
Y/Nb	1.92	1.56	2.36	1.66	2.7	2	3.1
Nb/Y							0.31
Rb/Nb							0.9
Rb/Y							0.3

Cu in Nauseri is 68ppm of average 12 rocks excluding one sample which has high value of copper (5912ppm). Average Cu of 13 samples is 518 ppm. Rb in one sample is 244ppm. Excluding this sample average Rb is 7ppm. Rb\Nb and Rb\Y in this sample is 56, and 13.17 respectively.

MAJOR AND TRACE ELEMENT GEOCHEMISTRY

Geochemical data of the Panjal volcanic rocks are discussed mainly for interpretation of tectonic environment. An average number of analyses is presented from Kahuta, Muzaffarabad and Kaghan areas (Table 1). Therefore, a brief introduction of major and trace elements are given in this section for general consideration.

The Panjal volcanic rocks reveal a wide range in major element composition. SiO_2 contents of the volcanics range between 42.01 to 52% except three rocks in which SiO_2 is from 52.44 to 54.10%. Al_2O_3 varies from 11.72 to 18.02% in these rocks. Fe_2O_3 has values from 8.27 to 13.72%, MgO ranges from 3.14 to 9.44%, CaO shows variation from 3.46 to 12.62%, Na2O ranges from 0.05 to 6.41%, K2O varies from 0.05 to 4.61%. TiO_2 ranges from 1.11 to 2.69%, P_2O_5 shows variation from 0.09 to 0.41%. MnO exhibits values from 0.07 to 0.29% in the Panjal volcanic rocks. Variation in total alkalies, silica, calcium and other elements indicate mobility of these elements during alteration of the Panjal volcanics.

In the Panjal volcanics Rb values range from <2 to 224 ppm. It shows scattered but positive correlation with Zr. Sr values range from 49 to 360 ppm, however, few samples show values >400 to 1244 ppm. The variation in the value of the Sr in the Panjal volcanics is due to spilitization, alterations and probably due to contamination.

Ba values range from 23 to 687 ppm. It shows good positive correlation with K_2O.

Nb content ranges from <2 to 33 ppm in the Panjal volcanics. In one rock (Nus-9) the Nb content is 44 ppm. La ranges from 4-40 ppm. The Ce contents are present from 20 to 123 ppm. Zr values in the Panjal volcanics occur from 53 to 209 ppm while one sample has Zr content 253 ppm. Y ranges from 19 ppm to 57 ppm. Zr shows positive correlation Nb, Y, TiO_2 and P_2O_5.

The variation in the Ni abundances of the Panjal volcanics vary between 24 to 316ppm. The Ni content decreases with decreasing MgO. The Ni and MgO contents suggests the presence of olivine in the fractionating assemblage. Cr contents decrease with decreasing MgO wt.% in the Panjal volcanic rocks. Cr abundances vary between 34 to 541 ppm in these rocks. This suggests that clinopyroxene was an important component in the fractionating assemblage. Co values range from 10 to 92 ppm in the Panjal volcanics. Copper contents show values from 5-5912 ppm. V ranges from 121 to 284 ppm while the constituents of Zn in the Panjal volcanics ranges from 71-200 ppm.

Geochemical variations in the Panjal volcanics indicate that they have been effected by fractional crystallization. Fractional crystallization was accompained by olivine and clinopyroxene fractionation (Khan, 1994). Fractionation is also evident in the trace element patterns of these rocks from different sections (Fig. 13). The panjal volcanic rocks reveal minor crustal contamination as indicated by high values of K2O (0.74 - 1.53), Rb/Y (0.05 - 1.08, one sample 13), Nb/Y (0.1 - 0.4) and Rb/Nb (0.2 - 2, one sample 56) ratios table -1.

In order to evaluate the tectonic environment of these rocks their geochemical data were plotted on different tectonomagmatic discriminant diagrams.

DISCRIMINANT DIAGRAMS

The Panjal volcanics have mainly normative composition characteristics of tholeiitic basalts. Tholeiites are quartz normative, hypersthene and olivine normative (Fig. 2). The normative compositional data demonstrates mobility to some extent of the major elements in the Panjal volcanic rocks.

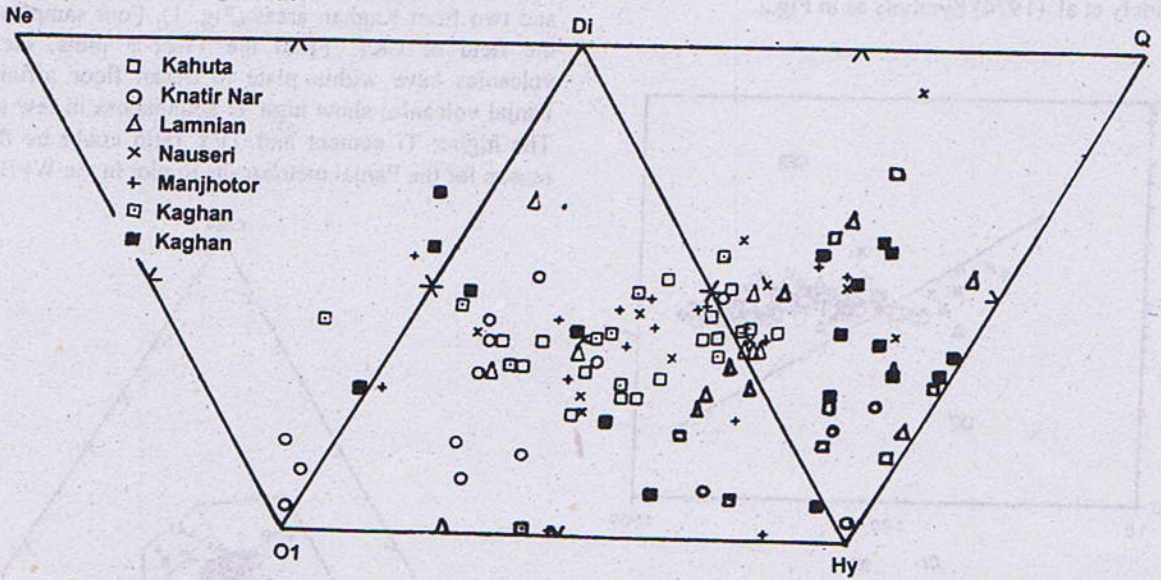

Fig. 2 CIPW normative composition of the Pajal Volcanic rocks. All Fe as Fe_2O_3. Fe_2O_2 is calculated as 0.15.

The Panjal volcanic rocks are tholeiitic to slightly alkalic basalts. The alkalic and tholeiitic character of the Panjal volcanic rocks was determined by using TiO_2 - P_2O_5/Zr ratios.

On the TiO_2-P_2O_5 diagram (Fig. 3) after Ridley et al. (1974) the Panjal volcanic rocks largely plot in the field of MORB. Only two samples fall in ocean island tholeiites (OIT) and one in the field of ocean island alkali basalts (OIAB). One of the Panjal volcanic rocks lie outside these fields. When TiO_2 is plotted against Cr (Fig. 4) after Pearce (1975) most of the Panjal volcanics geochemical data fall in OFB fields. Only a few samples are plotted in island arc field. This may be due to low content of Cr observed in these rocks. This diagram shows the Panjal volcanics in the field of OFB. The average values of Ni in these rocks is

significantly higher from island arc volcanics in which average Ni content is 30 ppm (Jakes and White, 1972). These diagrams show the tholeiitic composition of the rocks.

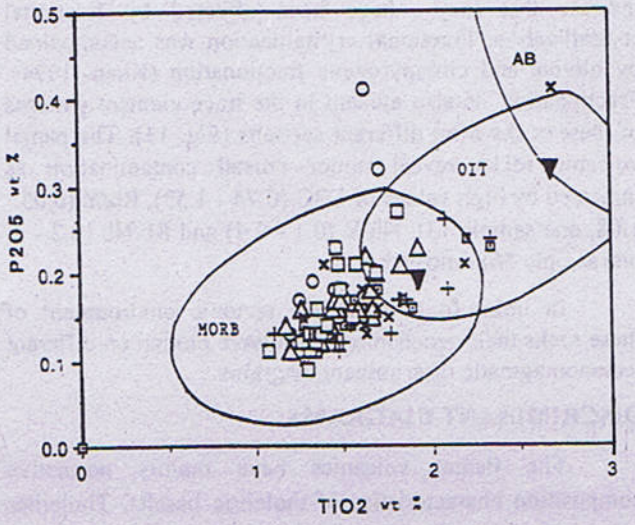

Fig. 3 Chemistry of the Panjal Volcanics and hypabyssal intrusive rocks in P_2O_5 versus TiO_2 diagram. Fields for mid ocean ridge tholeiites (MORB) ocean island thoieites (OTT) and alkali basalts (AB) are after Ridely et al. (1974) Symbols as in Fig.2.

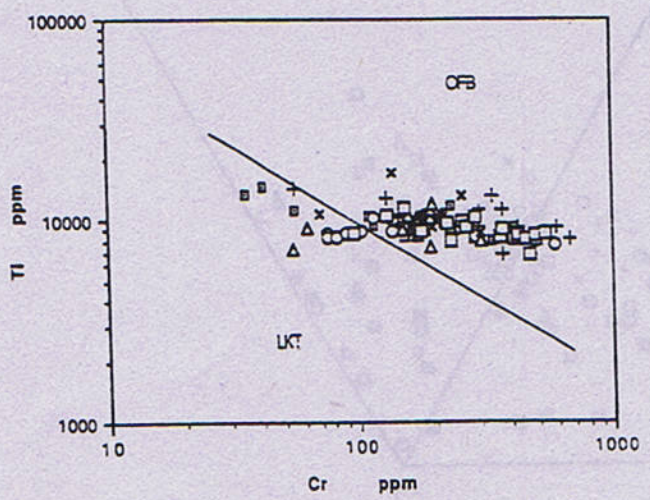

Fig.4 Log Ti versus log Cr diagram for the Panjal Volcanics ocean floor basalts (OFB) and low-postassium tholeiites (LKT) divide is after Pearce (1975). Symbols as in Fig.2.

Various tectonic discrimination diagrams are used to identify the altered and metamorphosed basaltic rocks by different workers.

immobile by processes of alteration and metamorphism up to greenschist facies (Pearce and Cann, 1971, 1973; Floyd and Winchester, 1975; Smith and Smith, 1976; Pearce and Norry, 1979; Pearce, 1982; Mullen, 1983; Meschede, 1986). These elements serve in determining paleotectonic setting of metavolcanic rocks (Pearce and Cann, 1971, 1973; Pearce, 1975; Bickle and Nesbitt, 1972; Wilson, 1989).

After determining the petrologic character of the volcanics as tholeiitic to mildly alkalic, the geochemical data of the Panjal volcanics from the Kahuta, Muzaffarabad and Kaghan areas, were plotted on various tectono-magmatic discriminant diagrams. Pearce and Cann (1973) used Ti, Zr, Y and Nb ratios to determine the paleotectonic environment of the altered volcanic rocks. By using these elements they distinguished island arc (low-potassium tholeiite (LKT), ocean floor basalts (OFB), calc-alkaline basalts (CAB) and within plate basalts (WPB).

On the Ti-Zr-Y diagram (Fig. 5) after Pearce and Cann (1973) the Panjal volcanics geochemical data mainly plot in ocean floor basalts (OFB) field. Eighty eight out of 116 Panjal volcanic rocks fall in the field of OFB. Only nineteen volcanic rocks fall in the field of WPB. The remaining 5 rocks plot in the field of calc-alkali basalts (CAB). Of these one is from Nauseri, two from the Kahuta and two from Kaghan areas (Fig. 1). Four samples plot in the field of LKT. From the Ti-Zr-Y plots, the Panjal volcanics have within plate to ocean floor affinity. The Panjal volcanics show high Ti abundances in few samples. The higher Ti content and Ti/Y ratio could be the main reason for the Panjal metabasalts to plot in the WPB fields.

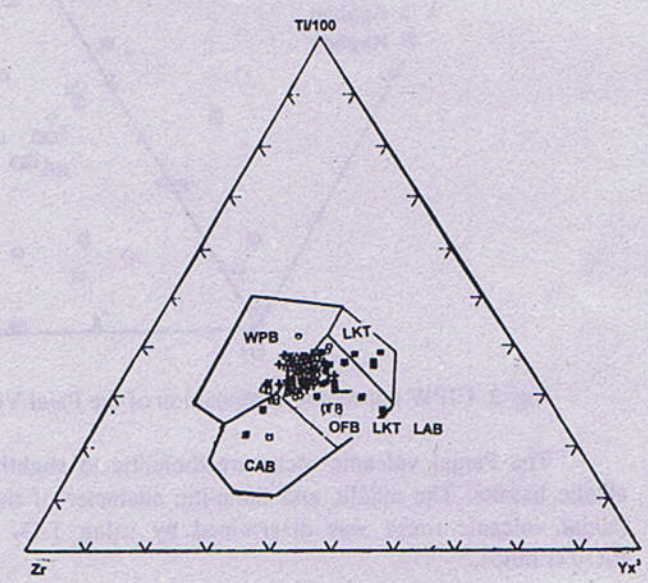

Fig.5 Plot of the Panjal Volcanics in Ti-Zr-Y diagram. Fields discriminating ocean floor (OFB), continental

Mg #	57.50	58.10	56.90	53.20	55.50	58.70	56

The Panjal volcanics fall almost entirely in the field of OFB on the Ti-Zr diagram (Fig. 6) of Pearce and Cann (1973). The geochemical data of the volcanics either plot in the OFB or in its extension away from the field of calc-alkaline rocks. Only one sample falls in the field of calc-alkaline environment and one in its extension away from it. The Ti and Zr enriched samples fall outside the designated tectonic discrimination fields. The enrichment trend on the Ti-Zr plot is a result of fractionation. As a whole many of the Panjal volcanics show OFB affinity while seven samples lie outside the field of OFB.

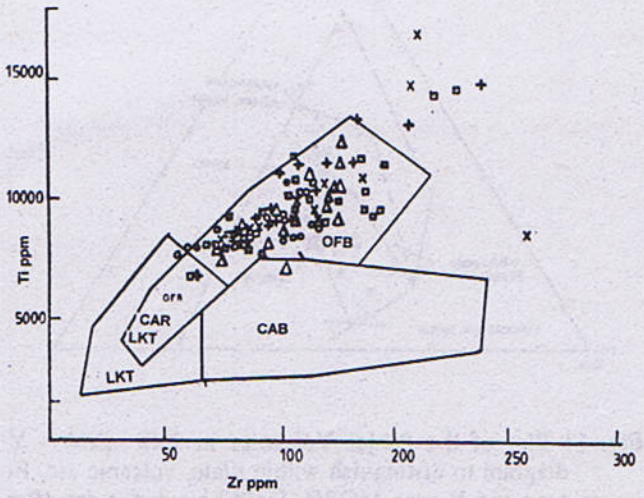

Fig. 6 Ti versus Zr diagram for the Panjal Volcanics. Fields like ocean floor basalts (OFB), low potash island arc tholeiites (LKT) and calc-alkaline basalts are from Pearce and Cann (1973). Symbols as in Fig. 2.

Pearce (1980) used Ti-Zr diagram to discriminate between arc basalts, within plate basalts and mid ocean ridge or ocean floor basalts. When the samples of the Panjal volcanics are plotted on the Ti-Zr diagram, (Fig. 7) most of them fall within the field of MORB and only 3 rocks of the Panjal volcanics lie exclusively in the field of WPB (Fig.7). This diagram indicate the ocean floor affinity of the Panjal volcanic rocks.

Plots of the Panjal volcanics on the TiO_2 -MnO-P_2O_5 diagram of Mullen (1983) are shown in Fig. 8. The major population of the geochemical data lie in the field of MORB. The geochemical data straddles MORB and IAT boundary. The rocks which occupy the field of IAT have high MnO contents relative to P2O5 in the Panjal volcanics. The high concentration of MnO in the Panjal volcanic rocks may be due to post-magmatic processes. The Panjal volcanic rocks are altered and metamorphosed due to which they show enrichment of MnO in some rocks which fall in IAT field. In contrast, to IAT field in TiO_2-MnO-P_2O_5 discriminant diagram majority of the Panjal volcanic rocks geochemical data lie in OFB field while some of them reflect ocean island type environment.

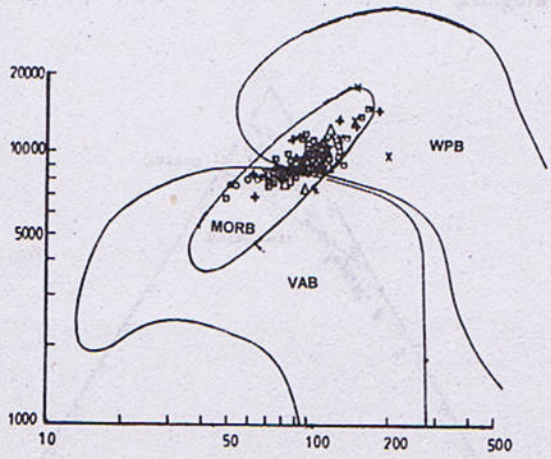

Fig. 7 Plot of the Panjal Volcanics in the Ti versus Zr tectonic discriminant diagram. Fields distinguishing mid ocean ridge basalts (MORB), within plate basalts (WPB), and volcanic arc basalts (VAB) are after Pearce (1980). Symbols as in Fig. 2.

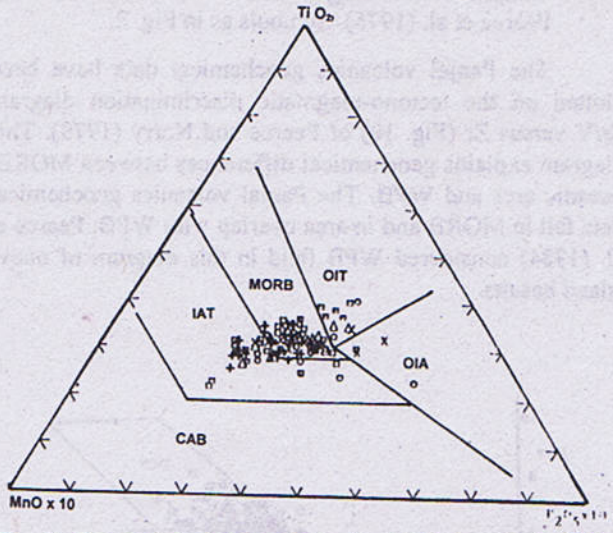

Fig. 8 Geochemical data of the Panjal Volcanics in TiO_2-MnO-P_2O_5 discrimination diagram. Fields of ocean island arc tholeiites (OIT), mid ocean ridge basalts (MORB), island arc tholeiites (IAT), calc-alkali basalts (CAB), and ocean island alkali basalts (OIA) are from Mullen (1983). Symbols as in Fig. 2.

Pearce et al. (1975) used TiO_2-K_2O-P_2O_5 contents (Fig. 9) to discriminate tectono-magmatic environment of oceanic and non-oceanic basalts (WPB). The Panjal volcanic rocks from the Kahuta and Muzaffarabad (Jhelum & Neelum valleys) in Azad Jammu and Kashmir Himalayas and the Kaghan area on the western side of the Hazara-

Kashmir syntaxis, plot both in the non-oceanic and oceanic fields. This diagram is consistent with other diagrams used for the Panjal volcanics. The high K_2O content of the Panjal volcanics is reflected by their plot in non oceanic field in this diagram.

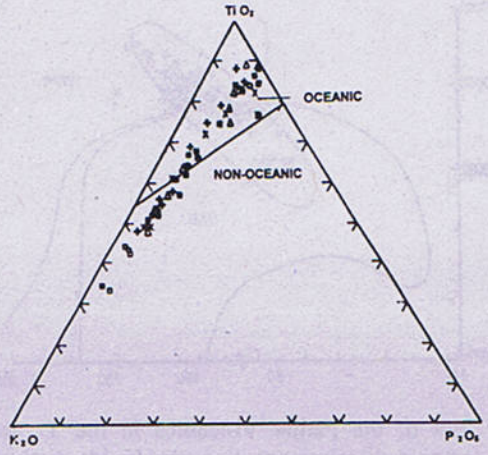

Fig. 9 TiO_2-K_2O-P_2O_5 diagram to distinguish oceanic and non-oceanic tectonic setting for the Panjal Volcanics. Dividing line for two fields is from Pearce et al. (1975). Symbols as in Fig. 2.

The Panjal volcanics geochemical data have been plotted on the tectono-magmatic discrimination diagram Zr/Y versus Zr (Fig. 10) of Pearce and Norry (1979). This diagram explains geochemical differences between MORB, oceanic arcs and WPB. The Panjal volcanics geochemical data fall in MORB and in area overlap with WPB. Pearce et al. (1984) considered WPB field in this diagram of ocean island basalts.

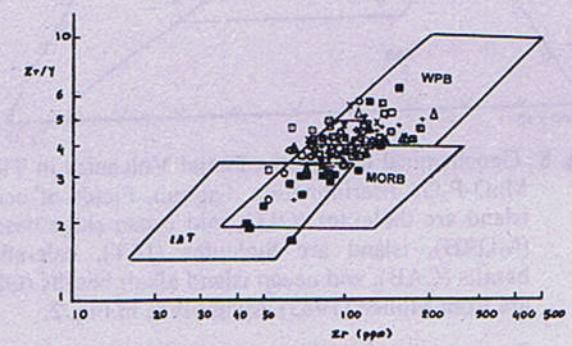

Fig. 10 Geochemical data of the Panjal Volcanics in Zr/Y versus Zr diagram. Field boundaries separating mid ocean ridge basalts (MORB), island arc tholeiites (IAT), and within plate basalts (WPB) are after Pearce and Norry (1979), Symbols as in Fig. 2.

The proportions of 2Nb-Zr/4-Y (Fig. 11) after Mesched, (1986) for the Panjal volcanics are shown. Most of the geochemical data fall in the P-type MORB field. Other samples plot in the field of within plate tholeiites whereas some samples lie in the field of within plate alkalic basalts.

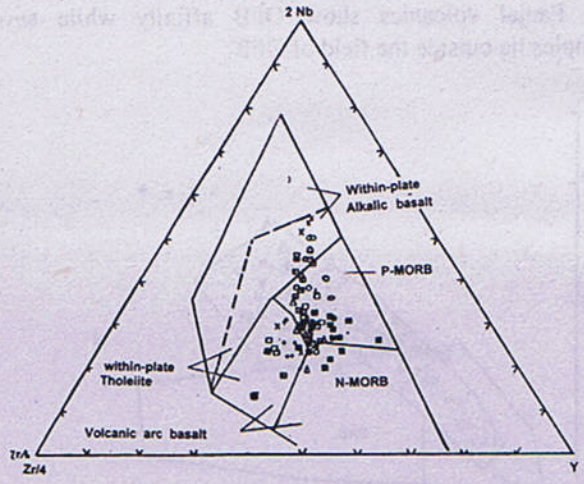

Fig. 11 Plot of the Panjal Volcanics in 2Nb –Zr/4 – Y diagram to distinguish within plate, volcanic arc, P-type and N-type MORB. Field boundaries are after Mesched (1986). Symbols as in Fig. 2.

Jones et al. (1993) discriminated between OIT (tholeiitic shield basalts of Hawaiian chain) and P-type MORB basalts by using La/Sm and Sm/Yb ratios. When the (Sm/Yb)N vs (La/Sm)N ratios of the Panjal volcanics are plotted the geochemical data of the Panjal volcanics fall in the field of P-type MORB field (Fig. 12).

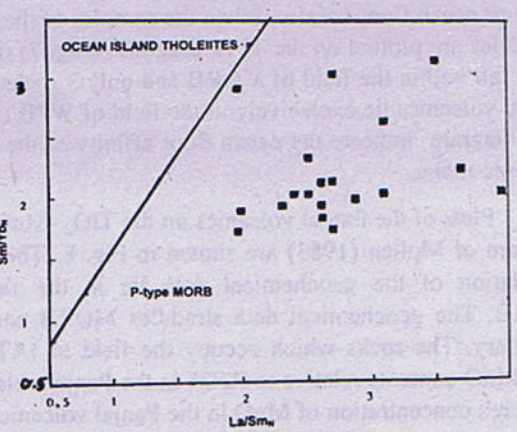

Fig. 12 Discrimination diagram of Sm/Yb versus La/Sm for the Panjal Volcanic rocks. Field for OIT and P-type MORB are after Jones et al. (1993).

The geochemistry indicates that these rocks were not erupted in calc-alkaline and low K-tholeiite island arc environment.

SPIDERDIAGRAMS

Trace element patterns of the Panjal volcanics normalized to MORB values after Pearce (1982) are shown in Figs. 13. Elements like Sr, K, Rb, Ba, Ce, P, Zr, Sm, Ti, Y, Yb, Ni and Cr, normalized to MORB values, are plotted for the Panjal volcanics from the Kahuta, Muzaffarabad (Jhelum & Neelum valleys) and the Kaghan area. The large ion lithophile (LIL) elements (Sr, Rb and Ba), which are mobile during hydrothermal alteration and metamorphism are plotted on the left side of the diagram. The immobile, high field strength (HFS) elements, are plotted to the right side in these patterns. Pearce (1980) demonstrated that characteristic of WPB relative to MORB, is the higher content of all elements, except those compatible with garnet lherzolite (Y, Yb, Sc and Cr). IAT basalts have a distinguishing feature which is reflected in depletion of immobile elements with higher concentration of alkali elements. The elements commonly thought to be relatively mobile like Sr, K, Rb and Ba are enriched in the Panjal volcanics. These alkali elements are generally affected by alteration processes. The increase in elemental abundances are attributed to varying degree of crystal fractionation (Pearce, 1982). These rocks show some depletion in Cr and an enrichment of mobile elements relative to immobile elements. The alteration and crustal contamination could cause K2O enrichment in rocks. The enrichment of K, Rb, Sr and Ba due to alteration processes and mobility of these elements under greenschist conditions. The Panjal volcanic rocks are spilitized. This process may cause Sr depletion and both enrichment and depletion of K2O, Rb and Ba. Therefore, another possibility of enrichment of K2O and Ba in some of the Panjal volcanic rocks may be related with alteration processes. These rocks are depleted in the Y and enriched in Nb, La and Ce (Fig 13). Some rocks have low Ba and K content. The general depletion of Y in these rocks show the presence of garnet in the source region.

Fig. 15 shows a composite chondrite normalized REE diagram for the Panjal volcanics. The shape of the REE patterns indicate that LREE are enriched relative to HREE. La/SmN in the Panjal volcanics ranges from 1.96 to 4.09 . LREE enrichment in the Panjal volcanics are also shown by La/YbN ratios ranging from 3.29 to 11.16 whereas Ce/YbN ratios from 2.83 to 8.62. The shape of rare earth elements and the La/SmN ratios for the Panjal volcanics are similar to P-type mid ocean ridge basalts.

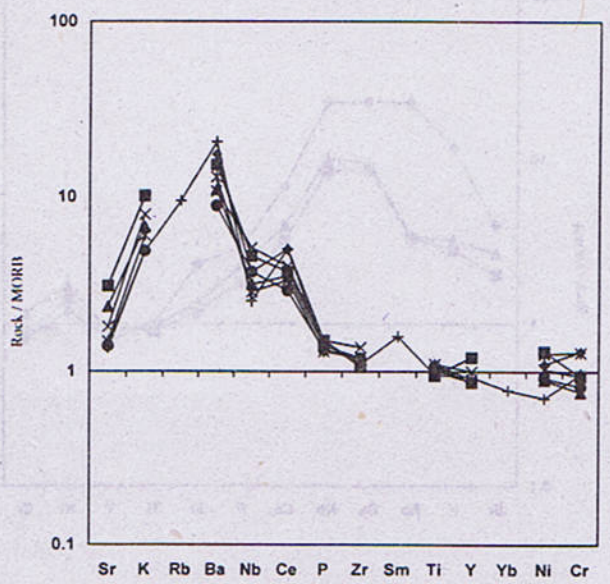

Fig. 13 MORB normalized spidergram of the Panjal Volcanics (average values). Normalizing factors after Pearce (1982).

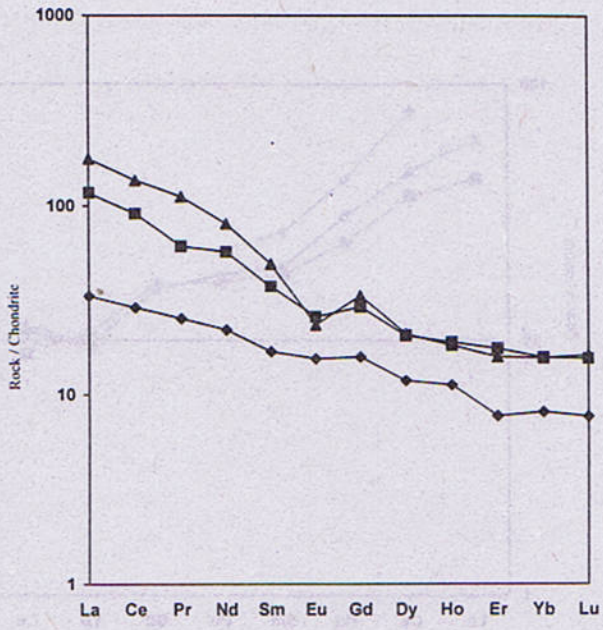

Fig. 14 Chondrite normalized composite REE patterns of the Panjal Volcanics. Normalizing values are from Nakamura (1974).

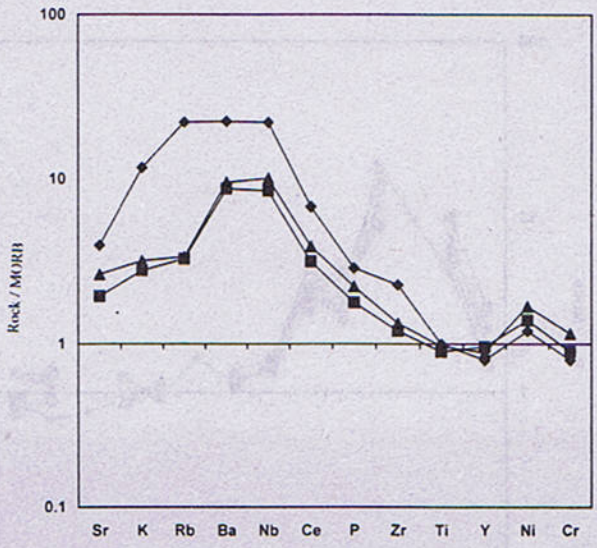

Fig. 15 Trace elements diagram of mid ocean ridge basalts 45°N (Wood et al., 1979) normalized to MORB values of Pearce (1982).

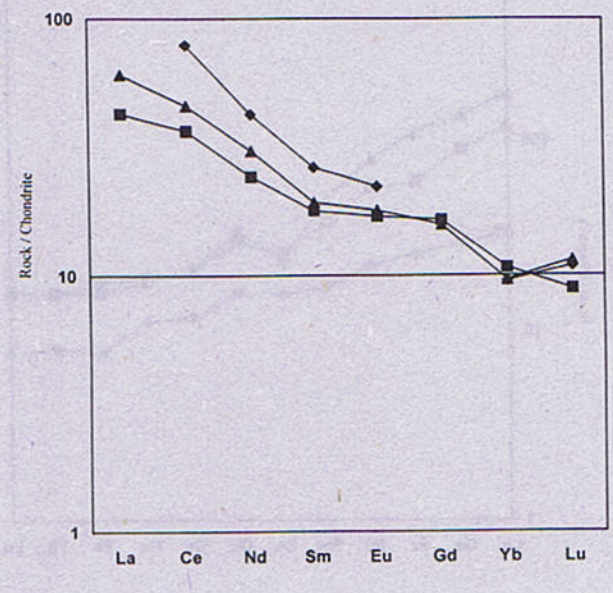

Fig. 16 Chondrite normalized REE patterns of the Mid Atlanic Ridge basalts 45°N (Wood et al., 1979).

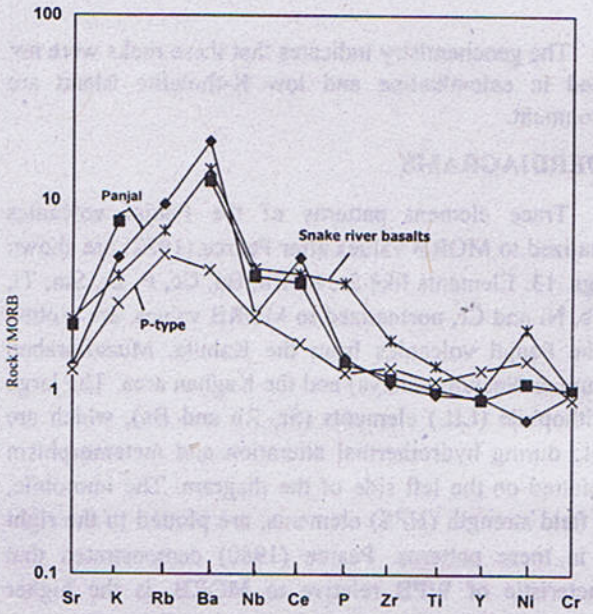

Fig. 17 MORB normalized trace element patterns of the Panjal Volcanics for comparision with P-type and continental flood basalts.

DISCUSSION

Geochemical data of the Panjal volcanics is used to infer their tectonic setting. Immobile elements data mainly fall in the mid ocean ridge basalts and within plate basalts fields. On the basis of geochemical data Panjal volcanic rocks can be considered as within plate basalts to ocean floor basalts. The Immobile element ratios such as Zr/Nb and Y/Nb indicate an enriched mantle source region for the generation of the Panjal magma. This is also supported by REE data that indicate an enriched or plume type mantle source for these rocks. Sm/yb ratios indicate depth of melting of basaltic rocks (White et al., 1993). For the Panjal volcanics Sm/Yb ratios vary from 1.68 to 2.94 indicative of melting in the garnet stability field. The higher Sm/Nd ratios represent different degrees of partial melting and rifting (Furnes et al., 1994). In the Panjal volcanics the Sm/Nd ratios ranges from 0.20 to 0.25. This may represent more advanced stages of rifting.

The trace element patterns (Fig. 13) of the Panjal volcanic rocks show crystal fractionation as indicated by Ni, Cr and Co variable values (Table 1). Ni is partitioned in olivine while Cr and Co are strongly partitioned into garnet and clinopyroxene, so garnet clinopyroxene rapidly depletes a residual liquid in these elements (Gast, 1968). The Mg-rich samples have high Ni and Cr contents. Ni, Cr and Sc, which are accommodated in early crystallizing phases, decrease during fractionation in the Panjal volcanics.

It is, therefore, envisaged that both processes of crystal fractionation and different degrees of partial melting of soucre region (lherzolite or probably garnet lherzolite) have been operated together, resulting into slight alkalinity and LREE enrichment of the Panjal volcanics. Pearce (1982) showed that alkalic basalts have strong enrichment of Nb relative to tholeiitic basalts. Nb is enriched in some of the Panjal volcanics with respect to other incompatible elements. Zr, Nb, P, Ti, Y, Ba and LREE remains incompatible elements in tholeiitic basalts during fractional crystallization. Therefore, a higher, content of the incompatible elements in the Panjal volcanics show higher degree of fractionation.

However, the highly incompatible elements in the Panjal volcanics and Zr/Nb= 5.9 -11, Zr/Y= 3.8- 4.16, Ti/Y= 331-370, Ti/Zr= 81-90, Y/Nb= 1.56-2.70, ratios (Table 1) may reveal that only factors like fractional crystallization and alkalic nature alone cannot explain the variation in bulk chemistry of these rocks. These rocks are also enriched in K2O, Rb, Sr and Ba. These elements are highly mobile during alteration processes. The variation in the trace element abundances may have been caused by addition of crustal melt component to the mantle derived basaltic magma. The affects upon the trace elements by crustal contamination of the basalts is the pronounced increase in incompatible elements (Thompson, 1982). Trace elements (Table 1) indicate crustal contamination for some of the Panjal volcanics whereas other samples do not show significant contamination. Thus increase in incompatible elements in some of the Panjal volcanic rocks may show affects of contamination to some degrees.

When the Panjal volcanics geochemical data are plotted on the different tectono-magmatic discrimination diagrams, some samples fall outside the designated fields and a few show scattering and fall in calc-alkaline and island arc tholeiitic fields (Figs. 3 to 11). The Panjal geochemical data which fall outside the designated fields and scatter into different fields simultaneously reveal the mantle heterogeneity. Ti/Y, Zr/Y and Nb/Y ratios (Table 1) and geochemical patterns for the Panjal volcanics further indicate mantle heterogeneity.

Therefore, the variation of the elements in the Panjal volcanics indicate different degrees of partial melting, fractionation, crustal contamination and mantle heterogeneity. The incompatible elements Zr/Nb, Y/Nb and REE data support for enriched mantle source for these rocks.

GEOCHEMICAL COMPARISON

A comparison of chemical Composition of the Panjal volcanics is made with Major recognized basalt types from different tectonic settings for example MORB, P-type MORB, OIT and continental flood basalts (Table 2). The comparison is also made by using spider diagrams of the Panjal volcanics and other basalts normalized with MORB. The results of the comparisons of these different basaltic types with the Panjal volcanics are summarised as follows.

Geochemical composition of basalts from North Atlantic Ridge 45oN have been discussed by Sun et al. (1979), Wood et al. (1979), White and Schilling (1978), Tarney et al. (1979), Pearce (1982) and 43oN by Shibata et al. (1979). Trace elements and REE data of the MAR 45oN have been shown for comparison with trace element and REE data of the Panjal volcanics (Table 2). The mid ocean ridge normalized trace element patterns (Fig. 15) of MAR 45oN (410-2, 410A-2, 410A-1 after Wood et al. 1979) and chondrite normalized REE patterns (Fig. 16) are similar to the trace elements (Fig. 13) and REE (Fig. 14) of the Panjal volcanics normalized with MORB and chondrite respectively. Trace element patterns are enriched in incompatible elements whereas REE are enriched in LREE in the Panjal volcanics with respect to N-type MORB and appear similar to those of the MAR 45oN.

Table-2

Average chemical analyses of the Panjal Volcanics compared with chemical analyses of continental flood basalts, ocean island tholeiites, N-type MORB, P-type MORB and Mid Atlantic Ridge 45 N. (1) Snake River Plain, (2), ocean island tholeiites, (3) N-MORB, (4) P-MORB, (5) MAR 45 N and (6) Panjal Volcanics.

Wt.%	1	2	3	4	5	6
SiO_2	46.18	50.36	50.40	51.18	50.16	49.77
TiO_2	2.06	3.62	1.36	1.69	1.51	1.55
Al_2O_3	14.47	13.41	15.19	16.01	17.71	15.23
Fe_2O_3	13.52	13.63	10.01	9.40	3.59	11.22
FeO	-	-	-	-	4.36	-
MnO	0.19	0.18	0.18	0.16	0.17	0.18
MgO	9.99	5.52	8.96	6.90	3.77	6.29
CaO	9.88	8.80	11.48	11.48	10.07	7.47
Na_2O	2.63	2.80	2.30	2.74	3.98	3.27
K_2O	0.61	0.77	0.09	0.43	1.76	1.15
P_2O_5	0.44	0.42	0.14	0.15	0.35	0.17
Table 5.8 (contd.).						
ppm						
Ba	298	191	<20	86	447	255
Sr	285	395	98	155	28.9	265
Cr	256	81	346	225	206	252
Ni	193	78	177	132	108	99
La	18.3	24	2.95	6.92	42.2	18
Ce	41.2	53	12	17.8	68.	237
Y	31	42	37	39	28.9	27
Nb	15.1	21.5	2.1	8.6	77.2	<14
Zr	167	227	97	121	206	108
Co	-	-	-	-	-	54

Cu	59	98	-	-	-	85
Zn	97	119	-	-	33	110

Data source (Table-5.8):1, Thompson et al. (1983); 2, Thompson et al. (1984); 3, 4, Humphris et al. (1985); 5, Wood et al. (1979).

Comparison of the Panjal volcanics with OIT (Table 2) show that OIT are slightly enriched in incompatible and compatible elements than the Panjal volcanics. P-type MORB rocks show a close similarity to the Panjal volcanics.(Fig.17) Elements like P, Zr, Ti and Y in the Panjal volcanics resemble with the P-type MORB (Table 2). This probably represents P-type source for these rocks. Geochemical comparison with modern oceanic plume influenced basalts using La/Sm - Sm/Yb ratios (Fig. 12) suggest that the Panjal volcanics are similar to the volcanics erupted along P-type MORB than the basalts generated in intra plate (OIT).

The incompatible elements like K, Rb and Ba of the Panjal volcanics compare well with the continental flood basalts (Fig.17). The continental flood basalts are enriched in whole spectrum of incompatible elements, other than Y and Yb.(Table 2) The Panjal volcanics are enriched in the incompatible elements. The incompatible elements like K, Rb and Ba of Panjal volcanics have been affected by hydrothermal alteration, metamorphism and to some extent by crustal contamination. These processes have certainly caused enrichment of Sr, K, Rb and Ba in the Panjal volcanic rocks. Due to this reason the incompatible elements show similarity with the flood basalts. Nb in the Panjal volcanics show a trough in some rocks with respect to the other elements. Elements like, P, Zr, Ti, Y and Yb show flat patterns as compared to continental flood basalts which have rather steep slope. Sm shows a positive anomaly in the Panjal volcanics.

The Panjal volcanics reveal characteristics which indicate their within plate setting to marine conditions. Marine conditions are indicated because of (1) the submarine nature of the volcanic rocks indicated by presence of pillow lavas (2) the associated marine sediments which include bedded chert and limestone. Both the carbonate and siliceous facies associated with the Panjal volcanics suggest that the volcanic rocks were erupted in a submarine environments. Their submarine origin is discussed by Khan and Ashraf (1989), Khan et al. (1991) and Khan et al. (1992). Pillow basalts are widely formed in marine conditions. Although some flows are highly vesiculated and can form in deep waters. The discrimination diagrams (Figs. 3 to 12), on which the Panjal volcanics geochemical data was plotted and the elemental abundances of the Panjal volcanics reflected by the shape of multi-element patterns (Fig. 13), REE (Fig. 14) are indicative of within plate to oceanic environment (P-type MORB). Hygromagmatic elements are strikingly similar to those of P-type MORB. Geochemical patterns of the Panjal volcanics normalized to MORB (Fig. 13) also show a close similarity to the Mid Atlantic Ridge 45o N patterns of Pearce (1982) and Wood et al. (1979) for 45oN MAR (Fig.15).

In genernal the early development of the Panjal volcanics appears to be shallow water, associated with limestones and shallow water sediments. The earlier formed basalts are transitional and are typically of within plate affinity. The late stage lava flows of the Panjal volcanics show pillow structures. These lava flows are associated with chert bands, at places, turbiditic rocks and black shales. This stage represents deeper water conditions. Therefore, the Panjal volcanics started from within plate rifting leading to opening of a narrow ocean basin.

However, field evidence presented earlier in combined with the geochemical characteristics, it may be suggested that the Panjal volcanic rocks were erupted in the northern margin of India in a rapidly widening continental rift, which had developed into oceanic conditions in later time.

CONCLUSIONS

The Panjal volcanics in Lesser Himayala represent an important exposure of the major geological and geotectonic event in the NW Himalayan region that occurred during late Palaeozoic to early Mesozoic time. They are thrust bound by the Panjal Thrust on the northeast and the Main Boundary Thrust on the southwest. The volcanics are altered, metamorphosed to greenschist facies and are subordinately spilitized. They were first altered and reconstituted in the submarine conditions and metamorphosed during Himalayan orogeny.

Geochemically the Panjal volcanics can be divided into tholeiitic to mildly alkalic basalts or transitional between alkalic and tholeiitic basalts.

The Panjal volcanics in the Kaghan area are associated with turbidite beds. These interbedded turbiditic deposits indicate submarine origin of the Panjal volcanics.

The carbonate bands occur as interbeds within the volcanics. Such intert-rappean limestone bands indicate pause in volcanism.

Greenish to reddish chert interbedded with the Panjal volcanics and lava flows with pillow structures, at places associated with black shales and turbiditic rocks also support their submarine origin.

These rocks have been fractionated. The high pressure fractionation was dominated by the removal of

olivine and pyroxene. Most of the Panjal volcanics are evolved in terms of Mg number and low Ni and Cr values.

It is suggested that 13 to 28 % partial melting of the source material (garnet lherzolite and lherzolite) occurred for these rocks.

Partial melting process cannot sufficiently account for variation in trace elements on large scale as in the Panjal volcanics. These chemical characters imply source inhomogeneity. The Panjal magma source heterogeneity is expressed by large variation in their incompatible element ratios.

Discrimination diagrams, trace element patterns, rare earth element patterns all favour source heterogeneity and fractionation.

The Zr/Nb, Zr/Y and Zr/Ti ratio of the Panjal volcanics indicate their P-type MORB character.

Tectonomagmatic discrimination diagrams indicate that the Panjal volcanic rocks were erupted in a within plate to oceanic environment. This view is further strengthened by their multi-element patterns and REE abundances plots.

The chemical characteristics of the Panjal volcanics and associated sedimentary rocks invokes a progressive rifting initially in a continental setting. The continental rifting at later stages opened into a small ocean basin. Moreover, it is concluded that variation in the trace element abundances of the Panjal volcanics is attributed by partial melting, fractionation and to some degrees of contamination but mainly due to source heterogeneity.

ACKNOWLEDGEMENTS

The data used in this paper was obtained during Ph.D research by M.sabir Khan. Financial support for this programme was sponsored by the Pakistan Science Foundation.

REFERENCES

Abbey, S., (1979). Reference materials-rock samples SY-2, SY-3, MRG-1. Canada Centre for Mineral and Energy Technology, Canmet Report 79-35, pp. 53-54.

Ashraf, M., and Khan, M. S., (1991). Geology of Panjal volcanics in Azad Jammu and Kashmir, Pakistan. Min. Assoc. Canada. *SEG. Abst. Programs,*. **16**, A5, P9.

Baig, M. S., (1991). Geochronology of Pre-Himalayan and Himalayan tectonic events, northwest Himalaya, Pakistan. *Kashmir Jour. Geol.*, **8, & 9,** . 197.

Bhat, M. I., and Zainuddin, S.M., (1979). Environment of eruption of the Panjal Traps. *Him. Geol.*, **8,** pp. 728-738.

Bhat, M. I., and Zainuddin, S. M., (1978). Geochemistry of the Panjal Traps of Mount Kalol, Lidderwat , Pahalgam, Kashmir. *Geol. Soc. India,* **19,** pp. 403-420.

Bickle, M. J., and Nisbet, E. G., (1972). The oceanic effinities of some alpine mafic rocks based on their Ti-Zr-Y contents. Jour. *Geol. Soc. London,* **128,** pp. 267-271.

Butt, K. A., Chaudhry, M., and Ashraf, M., (1985). Evidence of an incipient Palaeozoic ocean in Kashmir, Pakistan. *Kashmir Jour. Geol.*, **3,** pp.87-103.

Chaudhry, M. N., and Ashraf, M., (1980). The volcanic rocks of Poonch District, Azad Kashmir. *Geol. Bull. Univ. Peshawar,* **13,** pp. 121-128.

Floyd, P. A., and Winchester, J. A., (1975). Magma type and tectonic setting discrimination using immobile elements. *Earth Planet. Sci. Lett.*, **27,** pp. 211-218.

Fuchs, G., (1975). Contributions to the geology of the North Western Himalaya. Abh. Geol. *Bundensanstalt,*. **32,** pp. 1-59.

Furnes, H., Kryza, R., Muszynski, A., Pin, C. and Garmann, L.B. (1994). Geochemical evidence for progressive, rift related early Palaeozoic volcanism in the western Sudentes. Jour., *Geol. Soc., London,* **151,** pp. 91-109.

Gast, P. W., (1968). Trace element fractionation and the origin of tholeiitic and alkaline magma types. *Geochim. Cosmochim. Acta,* **32,** pp. 1057-1086.

Ghazanfar, M., and Chaudhry, M. N., (1985). A third suture in northwest Himalaya. *Kashmir Jour. Geol.*, **3,** pp. 103-108.

Ghazanfar, M., and Chaudhry, M. N., (1984). A Paleozoic ophiolite and island arc sequence of Hazara - Kashmir syntaxis, District Mansehra. *Kashmir Jour. Geol.*, **2, (1),** pp. 37-38.

Greco, A. M., (1989). Tectonics and metamorphism in the Western Himalayan syntaxis area (Azad Kashmir, NE-Pakistan). Ph.D Dissertation ETH - Zurich , Nr. 8779, Zurich, 193p.

Honeggger, K., Dietrich, V., Frank, W., Gansser, A., Thoni, M., and Trommsdorff, V., (1982). Magmatism and metamorphism in the Ladakh Himalayas (the Indus-Tsangpo suture zone). *Earth Planet. Sci. Lett.*, **60**, pp. 253-292.

Humphris, S. E., Thompson, G., Schilling, J. G., and Kingsley, R. A., (1985). Petrological and geochemical variations along the mid Atlantic ridge between 460s and 320s: Influence of the Tristan da Cunha mantle plume. *Geochim. Cosmochim. Acta,* **49**, pp 1445-1464.

Jakes, P., and White, A. T. R. , (1972). Major and trace element abundances in volcanic rocks of orogenic areas. *Geol. Soc. Am. Bull.*, **83**, pp. 29-40.

Jones, G, Sano, H. and Valsami-Jones, E., (1993). Nature and tectonic setting of accreted basalts from the Mino terrane, central Japan. Jour. *Geol. Soc. London,* **150**, pp. 1167-1181.

Khan, M. S., and Ashraf, M., (1989). Panjal volcanics: geochemistry and tectonic setting in Azad Jammu and Kashmir and Kaghan valley. *Kashmir Jour. Geol.*, **6 & 7**, pp. 61-81.

Khan, M. S., Ashraf, M., and Chaudhry, M. N., (1991). Geochemical evidence for an oceanic affinity of the Panjal volcanics in Kaghan valley, Pakistan. *Kashmir Jour. Geol.*, **8 & 9**, pp. 1-18.

Khan, M. S., Ashraf, M., and Chaudhry, M. N., (1992). Geochemical evidence for an oceanic affinity of the Panjal volcanics in Azad Kashmir and Kaghan area. *First South Asia Geol. Cong. Abst. Programs,* pp. 24.

Khan, M. S., (1994). Petrlogy and geochemistry of the Panjal volcanics in the Azad Kashmir and Kaghan areas, the NW Himalaya, Pakistan. Unpublished Ph.D. thesis, Punjab university, Lahore, Pakistan, 233p.

Khan, M. S., Ashraf, M., and Chaudhry, M. N., (1997). Geochemical evidence for the tectonic setting of the Panjal volcanics in Azad Kashmir and Kaghan area.

Lydekker, R., (1883). The geology of Kashmir and Chamba territories and the British Districts of Kaghan. Mem. *Geol. Surv. India,* **22**, pp. 31-34.

Mesched, M. A., (1986). A method of discriminating between different types of mid-ocean ridge basalts and continental tholeiites with Nb-Zr-Y diagram. *Chem. Geol.* **56**, pp. 207-218.

Mullen, E. D., (1983). MnO-TiO2-P2O5: a minor element discriminant for basaltic rocks of oceanic environments and its implications for petrogenseis. *Earth Planet. Sci. Lett.*, **62**, pp. 53-62.

Nakamura, N., (1974). Determination of REE, Ba, Mg, Na and K in carbonaceous and ordinary chondrites. *Geochim. Cosmochim. Acta,* **38**, pp. 757-775.

Nakazawa, K., and Kapoor, H. M., (1973). Spilitic pillow lava in Panjal Trap of Kashmir, India. Mem. Fac. Sci. Kyoto University, Ser. *Geol. Mineral.*, **39(2)**, pp. 83-98.

Papritz, K., and Rey, R., (1989). Evidence for the occurrence of Permian Panjal Trap basalts in lesser and higher Himalayas of the western syntaxis area, NE Pakistan. *Eclogae Geol. Helv.*, **82**, part-2, pp. 603-627.

Pearce, J. A., and Cann, J. R., (1971). Ophiolite origin investigated by discriminant analyses using Ti, Zr and Y. *Earth Planet. Sci. Lett.*, **12**, pp. 339-349.

Pearce, J. A., and Cann, J. R., (1973). Tectonic setting of basic volcanic rocks determined using trace element analyses. *Earth Planet. Sci. Lett.*, **19**, pp. 290-300.

Pearc, J. A., (1975). Basalt geochemistry to investigate past tectonic environment on Cyprus. *Tectonophysics,* **25**, pp. 41-67.

Pearc, J. A., Gorman, B. E., and Birkett, T. C., (1975). The TiO2- K2O - P2O5 diagram. A method of discriminating between oceanic and non-oceanic basalts. *Earth Planet. Sci. Lett.*, **24**, pp. 419-426.

Pearce, J. A., and Norry, M. J., (1979). Petrogenetic implications of Ti, Zr, Y and Nb variations in volcanic rocks. *Contrib. Mineral. Petrol.*, **69**, pp. 33-47.

Pearce, J. A., (1980). Geochemical evidence for the genesis and eruptive setting of lavas from Tethyan ophiolites. In: Panoyiotou, A., (ed.), proceedings of the seminar on ophiolites. *Geol. Surv. Depart., Nicosia, Cyprus,* pp. 261-272.

Pearce, J. A., (1982). Trace element charac-teristics of lavas from destructive plate boundaries. In Thorpe, R. S., (ed.), Andesites: Orogenic andesites and related rocks. John Wiley and Sons, New York, pp. 525-548.

Pearce, J. A., Lippard, S. J., and Roberts, S., (1984). Characteristics and tectonic significance of supra-subduction zone ophiolites. In: Kokelaar, B. P., and Howells, M. F., (eds.), Marginal basin geology. Blackwell, Oxford, pp. 77- 94.

Ridley, W. I., Rhodes, M. J., Reid, A. M., Jakes, P., Shih, C., and Bass, M. N., (1974). Basalts from Leg 6 of the Deep sea Drilling Project. *Jour. Petrol,* **15,** pp. 140-159.

Schilling, T. G., Zajac, M., Evans, R., Johnston, T., White, W., Devine, J. D., Kingsty, R., (1983). Petrologic and geochemical variation along the Mid-Atlantic Ridge from 29o N to 73o N. *Am. Jour. Sci.,* **283,** pp. 510- 586.

Shibata, T., Thompson, G., and Frey, F. A., (1979). Tholeiitic and alkalic basalts from the Mid-Atlantic ridge at 43o N. Contrib. *Mineral. Petrol.,* **70,** pp. 127-141.

Smith, R. E., and Smith, S. E., (1976). Comments on the use of Ti, Zr, Y, Sr, K, P and Nb in classification of basaltic magma. *Earth Planet. Sci. Lett.,* **32,** pp. 114-120.

Sun, S. S., and Nesbitt, R. W., and Sharaskin, A. Ya., (1979) Geochemical charac-teristics of mid-ocean-ridge basalts. *Earth Planet. Sci. Lett.,* **44,** pp. 119-138.

Tarney, J., Saunders, A. D., Mattey, D. P., Wood, D. A., and Marsh, N. G., (1981). Geochemical aspects of back-arc spreading in the Scotia Sea and Western Pacific. Philos. Trans. R. Soc. London, A 300, pp. 263-285.

Tarney, J., Wood, D. A., Saunders, A. D., Cann, J. R., and Varet, J., (1979). Nature of mantle heterogeneity in the North Atlantic: evidence from deep-sea drilling. Philos. Trans. R. Soc. London, A 279, pp. 179-202.

Thompson, R. N., (1982). Magmatism of the British Tertiary Province. *Scottish Jour. Geol.,* **18,** pp. 49-107.

Thompson, R. N., Morrison, M. A., Dickin, A. P., and Hendry, G. L., (1983). Continental flood basalts... arachnids rule OK? In: Hawkesworth, C. J., and Norry, M. J., (eds.), Continental basalts and mantle xenoliths. Shiva, Nantwich,U.K., pp. 158-185.

Thompson, R. N., Morrison, M. A., Hendry, G. L., and Parry, S. J., (1984). An assessment of the relative roles of a crust and mantle in magma genesis an elemental approach. Phil. Trans. R. Soc. Lond., A 310, pp. 549-590.

Wadia, D. N., (1928). The geology of Poonch state (Kashmir) and adjacent portions of Punjab. *Mem Geol. Surv. India,* **51,** part-2, pp. 184-370.

Wadia, D. N., (1934). The Cambrian-Trias Sequence of North-Western Kashmir (parts of Muzaffarabad and Bramula Districts). Rec. *Geol. Surv. India,* **68,** part-2, pp. 121-176.

White, W. M., and Schilling, J. G., (1978). The nature and origin of geochemical variation in Mid Atlantic Ridge basalts from central North Atlantic. *Geochim. Cosmochim. Acta,* **42,** pp. 1501-1516.

White, W. M., McBirney, A. R. and Duncan, R. A., (1993). Petrology and geochemistry of the Galapagos Islands: Portrait of a pathological mantle plume. *Jour. Geophy. Res.,* **98(B11),** pp. 19533-19563.

Wilson, M., (1989). Igneous petrogenesis: a global tectonic approach. Unwin Hyman inc., Publ. Winchester U.S.A. 466p.

Wood, D. A., (1976). Spatial and temporal variations in the trace element geochemistry of the eastern Iceland flood basalt succession. *Jour. Geophys. Res.,* **81,** pp. 4353-4360.

Wood, D. A., Tarney, J., Varet, J., Saunders, A. D., Bougault, H., Joron, J. L., Treuil, M., and Cann, J. R., (1979). Geochemistry of basalts drilled in the north Atlantic by IPOD leg 49: implications for mantle heterogeneity. *Earth Planet. Sci. Lett.,* **42,** pp. 77-97.

Geol. Bull. Punjab Univ. 35. 2000.

BIOSTRATIGRAPHY OF THE UPPER PALEOCENE PATALA FORMATION, JABRI AREA, HAZARA, NORTHERN PAKISTAN.

BY

KAMRAN MIRZA, SHAHID JAMIL SAMEENI AND SAJID RASHID
Institute of Geology, Punjab University, Lahore, Pakistan.

Abstract : *A section of the Upper Paleocene Patala Formation from Jabri area, southeastern Hazara, northern Pakistan was measured for palaeontological and palynological research. The formation is mainly composed of shale with subordinate limestone and marl. It is about 82 m thick in this area with well-defined overlying and underlying contacts. Thirty samples were collected from bottom to top at regular intervals for biostratigrahic study. Eight age diagnostic benthic larger foraminiferal species were encountered while the formation happened to be devoid of palynoflora. The foraminferal evidence confirms the Upper Paleocene age of the Patala Formatiom which has been deposited in shallow water marine environments.*

INTRODUCTION

The name Patala Formation was formalized by the Stratigraphic Committee of Pakistan (Fatmi, 1973) for the " Patala Shales" of Davies and Pinfold (1937) from its type locality Patala Nala in the western Salt Range. The stratigraphic name had been extended to similar succession in the Hazara Mountains for the " Nummulitic Formation" of Waagen and Wynne (1872) , part of the Nummulitic Series of Middlemiss (1896) and the "Kuzagali Shale" of Latif (1970).

The Hazara Mountains form the northern border of the Potwar Basin. It is a NE-SW trending arcuate trough situated along the northern margin of the Indo-Pakistan Plate and has been formed as a result of continent to continent collision. The Jabri Village is located in the southeastern part of the Hazara (long. 75 10 33 lat. 33 54 45) along the Lora-Maqsood Road (Fig.I). The area is easily accessible throughout the year.

The Patala Formation near Jabri Village is well exposed in an inverted sequence with well-defined upper and lower contacts. It, therefore, underlies the Upper Paleocene Lockhart Limestone and overlies the Lower Eocene Margalla Hill Limestone. This formation is the source rock for the adjacent hydrocarbon bearing Potwar Basin and the Kohat region. It also contains economic deposits of coal in the eastern Salt Range.

GEOLOGY AND PALAEONTOLOGY

As has been mentioned earlier about the inverted sequence of the Patala Formation , the upper contact with the Lockhart Limestone is transitional with the shales decreasing and limestone increasing in amount. The lower contact with the Margalla Hill Limestone is sharp. Both the underlying and the overlying contacts are conformable in the area.

The lower part of the formation is mainly composed of brownish gray to greenish gray shales with intercalations of marl. These intercalations are 70 cm to more than 2m thick, which decrease in thickness as well as their frequency towards the contact with the Margalla Hill Limestone. The intercalations, however, increase towards the contact with the Lockhart Limestone. The intercalated beds of limestone are slightly greenish gray to brownish gray on weathered surface and dark gray on fresh surface.

In the middle part, the formation is composed of shale with thin to thick bedded nodular but at places marly limestone which is dark gray in color. The upper part of the formation is mainly composed of greenish gray shale along with reddish gray marl and the intercalations of thin-bedded limestone. Occasionally pyrite nodules are present at number of places.

The formation is fossiliferous and the following age diagnostic benthonic larger foraminifera were encountered.

Miscellanea miscella (d, Archaic and Haime)

Lockhartia haimei (Davies)

Lockhartia tipperi (Davies)

Lockhartia conditi (Nuttal)

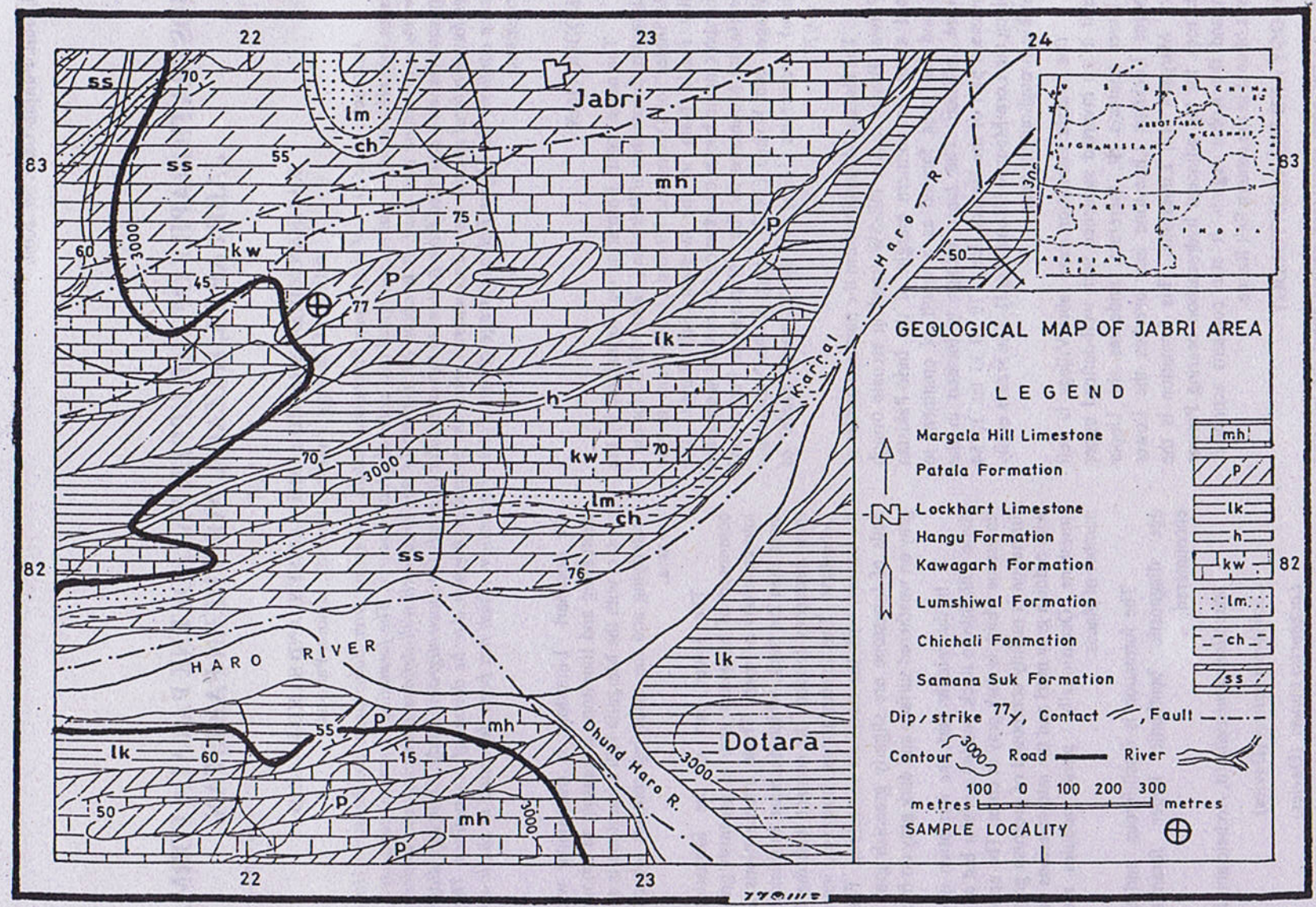

Fig. 1 Geological Map of Jabri Hazara, Northern Pakistan.

Plate 1

X 20

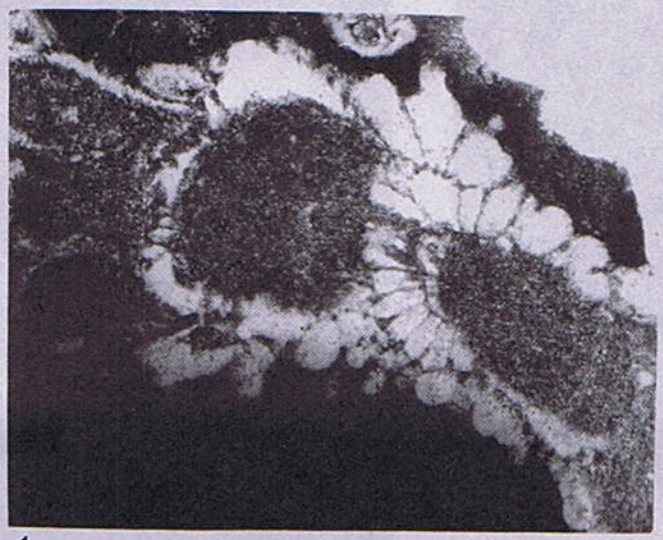

1

2

3

4

5

6

7

Plate 2

X 20

1

2

3

4

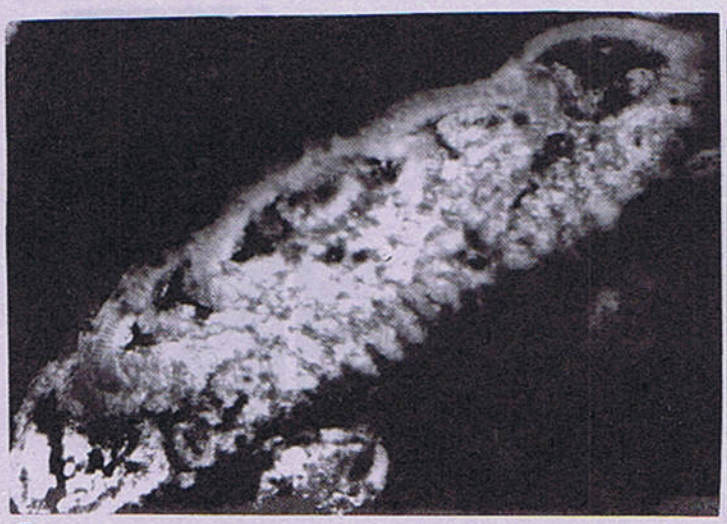

5

6

Discocyclina ranikotensis (Davies)

Operculina subsalsa (Davies and Pinfold)

Actinosiphon tibetica (Douville)

Ranikothalia sindensis (Davies)

The foraminiferal species mentioned above have already been reported and illustrated from this formation by Davies and Pinfold (1937) from the Salt Range. On the basis of the foraminiferal assemblage the age of the Patala Formation at Jabri area is Upper Paleocene.

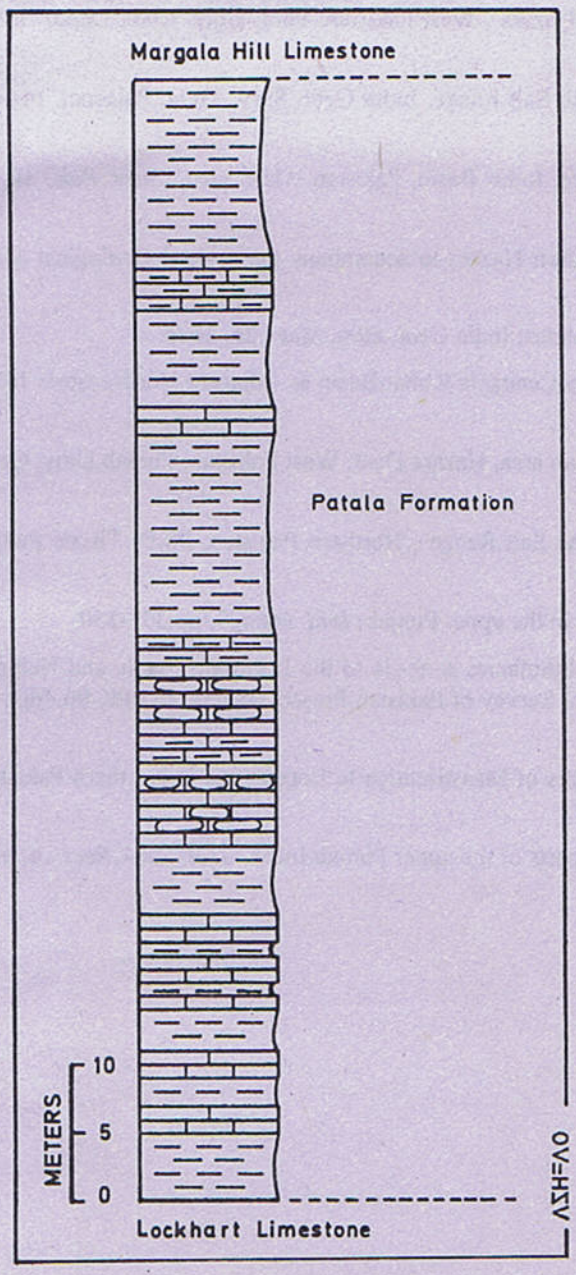

Fig. 2 Stratigraphic column of the Patala formation, Jabri Bazar, Northern Pakistan

Explantion of Plates

Plate 1

1.1& 1.2 *Miscellanea miscella* (d'Archaic & Haime)
1.3 *Miscellanea miscella* (d'Archaic & Haime) Oblique view
1.4 *Operculina subsalsa* (Davies and Pinfold) Horizontal view
1.5 *Ranikothalia sindensis* (Davies)
1.6 *Miscellanea miscella* (d'Archaic & Haime) Horizontal view
1.7 *Actinosiphon tibetica* (Douville)

Plate 2

2.1 *Operculina subsalsa* (Davies and Pinfold)
2.2 Top *Ranikothalia sindensis* (Davies)
Bottom *Operculina subsalsa* (Davies and Pinfold)
2.3 Top *Discocyclina ranikotensis* (Davies)
Bottom *Lockhartia conditi* (Nuttal)
2.4 & 2.6 *Lockhartia tipperi* (Davies)
2.5 *Lockhartia haimei* (Davies)

DISCUSSION

There is a general agreement of most of the workers that the Paleocene-Eocene boundary is marked by the appearance of the genus *Nummulites* which is thought to be associated with the beginning of the Eocene (Cavelier and Pomerol, 1983). Although the formation has been reported to extend into the Lower Eocene in the Salt Range on the basis of Alveolinid biostratigraphy (Sameeni, 1997) and the planktonic foraminiferal biostratigraphy (Afzal ,1997). Sameeni (1997) indicated the extension into the Lower Eocene in the Trans Indus Salt Range at Makerwal, while Afzal (1997) mentioned part of it from the Nammal Gorge and further western Salt Range. It is worth mentioning that the present authors did not record any Eocene fauna from the formation in Jabri area which clearly indicates that the development of the Patala Formation in Jabri area is restricted only to the Upper Paleocene period.

The formation at this locality is an argillaceous facies and mainly composed of shale. Most of the shales are thought to be generated in deep water environments but the presence of larger benthic foraminifera in the formation in Jabri area safely suggests that the formation was deposited in shallow shelf (open marine) environments.

Extensive palynological studies were also carried out for further refinement of the above mentioned results but no spores or pollen were observed in the Patala Formaion at this locality. This might be because of the reason that there was no vegetation in the area at that time and the sediments did not receive any spore or pollen.

REFERENCES

Afzal ,J.(1997) Planktonic Foramieiferal Biostratigraphy of the Paleocene to Eocene Patala Formation, Western Salt Range, Pakistan.

Butt, A.A.(1990) The Paleogene Stratigraphy of the Kala Chitta Range , Northern Pakistan. *Acta Mineralogica Pakistanica* **3**, pp.97-110.

Butt, A.A.(1991). Ranikothalia sindensis zone in late Paleocene biostratigraphy. *Micropal. U.S.A.* **37**, No.1, pp.77-85.

Cavelier C. and Pomerol Ch. (1983) Echelle de Correlation Stratigraphique Paleogene, stratotypes , etages standards, biozones, chimigones et anomalies magnetiques. Geologie de la France, 3, pp.261-262.

Cheema, M.R. (1968) Biostratigraphy of Changla Gali area , Distt. Hazara , West Pakistan. Punj. Univ. Geol. Deptt. M.Sc. Dissert ., Unpub.

Davies L.M. and Pinfold E.S. (1937) The Eocene beds of the Punjab Salt Range, India Geol. Surv. Mem. Palaeont. Indica, New Series, 24, No.1, 79p.

Fatmi A.N. (1974) Lithostratigraphic units of Kohat-Potwar Province, Indus Basin, Pakistan. *Mem. Geol. Surv. Pak.*, **10**, 1-63.

Latif M.A. (1970a) Explanatory notes on the geology of South Eastern Hazara to accompany the revised Geological Map; Wein Jb. Geol. B.A., Sonderb. 15, pp.5-20.

Middlemiss C.S. (1896) The Geology of Hazara and the Black Mountains; India *Geol. Surv. Mem.*,**26**, 302p.

Neil, A.W.(1984) Marine and Continental Sedimentation in the Early Cenozoic Kohat Basin & Adjacent Northwestern Indo-Pakistan. Ph.D. Dissert Mischigan Univ.(Unpub.).

Raza S.M. (1967) Stratigraphy and palaeontology of Gandhian-Dartian area, Hazara Distt. West Pakistan, Punjab Univ. Geol. Deptt. M.Sc. Dissert.,Unpub.

Sameeni, S.J. (1997) Biostraigraphy of the Eocene succession of the Salt Range , Northern Pakistan, Ph.D. Thesis Punjab Univ.

Waagen W., and Wynne A.B. (1872) The geology of Mount Surben in the upper Punjab; *Ibid. Mem.*,**9**, pp.331-350.

Wardlaw, B.R., Martin, W.E., and Haydri, I.H.(1990) Preliminary lithofacies analysis of the Lockhart, Patala and Nammal formations (Paleocene-Eocene) of the Salt Range , Geological Survey of Pakistan Project Report (IR) PK-90,40p., on file in Reston, Virginia, U.S. Geological Survey.

Weiss, W.(1993) Age assignments of larger foraminiferal assemblages of Maastrichtian to Eocene age in Northern Pakistan, Munchen.,Zitteliana,20.(HAGN/HERM-Festschrift): 223-252.

Wynne A.B. (1873) Notes from a progress report on the geology of parts of the upper Punjab,India. *Geol. Surv.,Recs.*, **6**, pt.3, pp.59-64.

Geol. Bull. Punjab Univ. 35, 2000.

GEOCHEMICAL STUDIES OF THE DUNGAN FORMATION, EASTERN SULAIMAN RANGE, PAKISTAN.

BY

NAZIR AHMAD
Institute of Geology, Punjab University, Lahore-54590, Pakistan.

A.C. DUNHAM, J.D. HUDSON
Department of Geology, Leicester University, Leicester, U.K.

AND

SHAFEEQ AHMAD
Institute of Geology, Punjab University, Lahore-54590, Pakistan.

Abstract:- *Geochemical investigations of the Dungan Formation were carried out from three sections, namely, Raghasar, Zinda Pir and Rakhi Nala in the Eastern Sulaiman Range. X-ray diffraction revealed the presence of mainly calcite and in few cases clay minerals are present. The mineral chemistry of different calcite grains and cements present in the Dungan Formation indicates that the skeletal grains are originally of high magnesium calcitic, and after diagenesis (fresh water) they lose their magnesium content which established the new equilibrium with the fresh water and the drusy cement (non-ferroan) is formed with 1.2 mole% of $MgCO_3$, and ferroan drusy cement with 1.90 mole% of $MgCO_3$. The skeletal grains become stable at the present mole percentage of magnesium carbonate. X-ray fluorescence analyses were used to determine the major elements (as oxides), of the whole rock. This study shows that the detrital material (quartz) is high in inner ramp facies, the middle ramp facies are the pure carbonate facies and the impurities are very low. The outer ramp facies are the argillaceous carbonate. These results also demonstrate a relationship between mineralogy and geochemical composition, and geochemical composition and the diagenetic events.*

INTRODUCTION

The Sulaiman Range lies on the northwestern margin of the Indo-Pakistani Plate. The geochemical studies of the eight microfacies, (peritidal, inner lagoon, oolitic, outer lagoon, rhodolith platform, nummulitic, larger benthonic foraminiferal and planktonic foraminiferal) of the Dungan Formation, which has already been interpreted within a homoclinal, ramp model are discussed (Ahmad and Pedley, 1997). The samples are taken from three sections Raghasar, Zinda Pir and Rakhi Nala (Ahmad 1996).

This paper deals with the results and interpretation of the geochemical investigations of the Dungan Formation. The whole rock mineralogy and mineral chemistry is determined by x-ray diffraction and electron microprobe analysis while the whole rock geochemistry is determined by x-ray fluorescence.

METHODS AND TECHNIQUES

Three sections Raghasar, Rakhi Nala and Zinda Pir have been studied thoroughly and more than 150 samples were taken from these sections on the basis of lithologic variations. Each sample was crushed to about 1 cm. in diameter in a flypress. The flypress was cleaned after each sample crushing to prevent contamination. About 50 to 70 grams of the sample was ground to a fine powder in tungsten-carbide mill. This fine powder was used for the investigation of whole rock chemistry by x-ray fluorescence techniques. For whole rock mineralogy, about 10 gram of fine powder sample was micronised in the microniser and kept them in the oven over night to become dry. This dried material was used for the analysis of whole rock mineralogy by x-ray diffraction techniques. Carbon coated polished thin sections were used for the analysis of mineral chemistry of the carbonate grains and cements by electron microprobe techniques.

More than 50 samples were prepared for x-ray diffraction techniques. The analyses were carried out on a Philips PW 1729 x-ray diffractometer generator attached to PW diffractometer controlled by Sieronois Sie 1710 Software running on a Viglen 386 computer. The accuracy of the analyses deviates about 5%.

Polished thin sections 50 in number were prepared for electron microprobe analysis. They are coated with carbon before performing the analyses. The analyses were carried out through Jeol Superprobe model JXA-8600S with an on-line computer for ZAF corrections and six major oxides (i.e.,CaO, MgO, FeO, MnO, SrO, and BaO) were determined. The accuracy of the analyses deviates about 5%.

A total of ten major oxides (SiO_2, TiO_2, Al_2O_3, Fe_2O_3, MnO, MgO, CaO, Na_2O, K_2O, and P_2O_5) were determined by using a Philips 1400 x-ray spectrometer and ARL 8420 spectrometer, each equipped with a rhodium anode x-ray tube. The detection limits are generally low, .01 for SiO_2; .0016 for TiO_2; .005 for Al_2O_3; .002 for Fe_2O_3; .002 for MnO; .011 for MgO; .003 for CaO; .016 for Na_2O; .002 for K_2O; and .002 for P_2O_5. However, the accuracy of the results is generally dependent upon the accuracy of calibrations used and the effect of mineralogical variations within the sample analysed. The accuracy of the analyses deviates about 4% in the case of major oxides. The analyses were performed on fused glass bead made up of 1.0 gram of 100 mesh dried rock powder and 5.0 gram of spectroflux (lithium tetraborate). All major oxides are reported in weight percent (wt.%).

RESULTS AND INTERPRETATION

MINERALOGY

More than 50 randomly oriented samples were analysed by XRD method for qualitative identification of minerals present in the Dungan Formation. The minerals were identified from the tables given in International Centre for Diffraction Data (ICDD). The facies type describes the whole rock mineralogy of the Dungan Formation.

In the inner ramp facies the minerals are quartz, calcite and clay minerals, in the middle ramp facies the mineral present is the calcite and in the outer ramp facies the minerals are calcite and clay minerals. It is clear that the inner ramp facies are close to the shore and the quartz grains are transported from shore line to the depositional area. The middle ramp facies are pure limestone and these facies represent the main "carbonate factory". This limestone has mainly skeletal allochems of algae and benthonic foraminifera. The outer ramp facies are the deep-water facies, which are slightly argillaceous, thus showing the presence of clay minerals with calcite.

Nine samples which are the representative of facies 4, 7, and 8 are dissolved in 10% HCl to remove the carbonate. When the samples are free from carbonates, they are washed and dried overnight at 100 °C. These samples are analysed using XRD techniques. Similar to whole rock mineralogy, the residue confirms the presence of clay minerals (kaolonite, montmorillonite, and illite) in carbonates.

Two calcium carbonate minerals aragonite and calcite predominate in modern carbonate sediments. Two types of calcite are recognised depending on magnesium content; low magnesium calcite, having less than 4 mole% $MgCO_3$, and high magnesium calcite having more than 4 mole% $MgCO_3$. The mineralogy of a modern carbonate sediment depends largely on the skeletal grains present in the sediments. The carbonate skeletons of organisms have a specific mineralogy or a mixture of mineralogies. The original mineralogy of the skeletal grains present in the Dungan Formation is mainly high-Mg calcitic (Tucker, 1981), although the actual magnesium content of the calcite may vary, being partly dependent on water temperature. Since aragonite is metastable and in time high-Mg calcite loses its magnesium, and thus all carbonate sediments are eventually converted to low-Mg calcite.

The mean values of oxides of Ca, Mg, Fe, Mn, Sr, and Ba of the skeletal allochems, and cement of the Dungam Formation are listed in Table 1. The probe data shows the average mole% $MgCO_3$ of coralline algae, 2.01; bryozoa, 2.25; coral, 0.89; echinoids, 4.34; benthonic foraminifera (non-ferroan), 2.08; benthonic foraminifera (ferroan), 2.37; and planktonic foraminifera 0.90.

Coralline algae is thought to be totally high magnesium calcite ,(Vinogradov, 1953; Goldsmith and others 1955; Thompson and Chow, 1955; Schmalz 1965; Keith and Weber 1965). Chave (1954a) has done a lot of work on recent coralline algae of different areas and he found the wt. percentage of $MgCO_3$ from 8.0 to 21.0 at different water temperature ranges from 5.2 to 28.0 °C, the content of $MgCO_3$ increasing with temperature. The calcitic forms of calcareous algae such as *Lithothamnium* and *Lithophyllum*, contain a wide range of magnesium values, extending from 7.0 to almost 30.0 percent magnesium carbonate. The calcareous algae dominantly present in the Dungan sediments are *Lithothamnium*, *Lithophylum* and *Archaeolithothamnium*. Originally they were deposited as high magnesium calcitic and after diagenetic processes they lost their magnesium content and became stable at 2.0 mole% of $MgCO_3$. The recent foraminiferal sediments collected at different localities show $MgCO_3$ from 0.33 to 16.0 at different water temperature ranges from 0 to 28 °C (Chave, 1954a). From Bermuda eleven foraminifera were analysed and found to contain a range of magnesium

Table 1.

Mean values of different carbonate grains present in the Dungan Formation analysed by electron microprobe.

Grain	Algae	Bryozoa	Coral	Ech	F	F F	F(PL)
n	13	6	3	19	24	25	1
CaO	54.87	53.94	54.5	53.55	54.85	53.83	55.15
MgO	0.81	0.89	0.35	1.75	0.84	0.94	0.36
FeO	0.29	0.57	0.79	0.32	0.16	0.96	0.03
MnO	0.08	0.35	0.19	0.17	0.02	0.15	0.02
SrO	0.04	0.06	0.11	0.05	0.07	0.1	0.14
BaO	0.09	0.16	0.1	0.12	0.1	0.11	0.05
TOTAL	56.18	55.97	56.03	55.96	56.05	56.09	55.74
$CaCO_3$%	97.93	96.26	97.26	95.58	97.9	96.08	98.42
$MgCO_3$%	1.69	1.87	0.74	3.66	1.75	1.97	0.75
Mol%$MgCO_3$	2.01	2.25	0.89	4.34	2.08	2.37	0.9

Grain	C	C F	V	V F	Micrite
n	207	198	47	43	8
CaO	55.38	53.72	55.68	54.86	54.49
MgO	0.49	0.75	0.37	0.57	0.73
FeO	0.11	1.08	0.05	0.68	0.19
MnO	0.04	0.25	0.03	0.03	0.02
SrO	0.08	0.08	0.14	0.09	0.06
BaO	0.11	0.1	0.09	0.11	0.19
TOTAL	56.2	55.97	56.36	56.35	55.69
$CaCO_3$%	98.84	95.87	99.38	97.92	97.25
$MgCO_3$%	1.02	1.56	0.76	1.2	1.52
Mol%$MgCO_3$	1.21	1.9	0.9	1.43	1.83

$CaCO_3$%=CaO*100.09/56.08; $MgCO_3$%=MgO*84.32/40.31

Mol% $MgCO_3$=Mol.$MgCO_3$*100/(Mol.$CaCO_3$+Mol.$MgCO_3$)

Ech=Echinoderm C=Drusy Cement; C F=Ferroan Drusy Cement

F=Foraminifera; F F=Ferroan Foraminifera F(PL)=PlanktonicForaminifera V=Veins; VF=Ferroan Veins.

n =No. of analysis

carbonate from 10.8 to 15.2 percent. The benthonic foraminifera of the Dungan Formation were originally high magnesium calcitic as shown by the recent foraminiferal sediment, but after diagenesis they lost their magnesium content and became stable at 2.2 mole% of magnesium carbonate. In the echinoids the magnesium contents of both the tests and the spines are different. The recent sediments of echinoids from Florida has a test with 10.2 percent magnesium carbonate and a spine with a very close 10.9 percent of magnesium carbonate. In the Dungan Formation the same is assumed, the echinoids are originally deposited as high magnesium calcitic grains, and later on after diagenesis they lose their magnesium content and become stable at 4.34 mole% of magnesium carbonate. Due to the dense structure of echinoids they lose less magnesium as compared to algae. The bryozoa consists of calcite, aragonite or a mixture of the two, preliminary investigations indicate that the magnesium content of the calcite is above 4 percent. The bryozoa skeletal grains of the Dungan Formation were originally of high magnesium calcitic which after diagenesis became stable at 2.25 mole% of $MgCO_3$.

In summary all these skeletal grains are originally of high magnesium calcitic, and after diagenesis (fresh water) they lose their magnesium content (Stehli and Hower,1961), which established the new equilibrium with the fresh water and the drusy cement (non-ferroan) is formed with 1.2 mole% of $MgCO_3$, and ferroan drusy cement with 1.90 mole% of $MgCO_3$. The skeletal grains become stable at the present mole percentage of magnesium carbonate. From the data it is noted that the ferroan skeletal allochems, ferroan cement and ferroan veins have more mole% of $MgCO_3$ as compared to that of non-ferroan. It is similar to the findings of (Richter and Fuchtbauer, 1978), that the organisms having a skeleton originally of high magnesium calcite become ferroan during diagenesis, and the low magnesium calcite skeletons do not.

GEOCHEMISTRY

The main element selected for this study is magnesium, chosen because of its ability to substitute for calcium in the carbonate lattice and its expected variability with mineralogical changes. Magnesium and strontium are common elements in the metastable carbonate minerals, magnesium in Mg-calcite and strontium in aragonite and Mg-calcite. Hence these elements can be used as geochemical indicators of diagenetic trends.

Stehli and Hower (1961) studied the effects of diagenesis on the distribution of magnesium, strontium, barium, and manganese in Florida carbonates. They compared recent carbonate sediments in Florida with Pleistocene rocks from the same area. They found a reduction in the abundance of these elements from the recent to the Pleistocene.

The whole rock chemical analyses are determined by XRF. The mean, standard deviation, maximum and minimum of these analyses are presented by facies in Table 2. The major element oxides are reported on a 100% anhydrous basis and are in weight percent.

Hirst and Nicholls (1958) point out that many impure limestones can be considered to consist of two distinct fractions, an essentially carbonate fraction, such as $CaCO_3$, of non-detrital origin, and a detrital fraction made up of essentially of silicates, clay minerals or quartz.

The chemical composition varies remarkably between the facies. The plots are drawn against the mean values of major oxides present in different facies of the Dungan Formation (Fig.1). The peritidal facies (inner ramp) are rich in SiO_2, TiO_2, Al_2O_3, Fe_2O_3 and MnO. The plots of Al_2O_3 against K_2O (Fig. 1A); SiO_2 against TiO_2 (Fig.1B); TiO_2 against Fe_2O_3 (Fig. 1C); and SiO_2 against MnO (Fig. 1D) show strong correlation. The plot of Al_2O_3 against K_2O (Fig. 1A) presumably shows that K and Al are both present in clays and in feldspars. The plot (Fig. 1B) of SiO_2 and TiO_2 indicate the presence of quartz sand content and the heavy minerals (such as rutile). The plot of TiO_2 and Fe_2O_3 (Fig. 1C) indicate the presence of quartz and feldspars. The plot of SiO_2 and MnO (Fig. 1D) also indicates the presence of quartz sand. These plots suggest, the inner ramp facies are rich in quartz, and low in carbonates and argillaceous material. It is also high in iron and manganese. The same observations are given by XRD. The middle ramp facies are low in SiO_2, TiO_2, and Al_2O_3, and the outer ramp facies are low in TiO_2 but moderate in SiO_2, Al_2O_3 and K_2O. The plot of Al_2O_3 against K_2O shows the strong relation between them. The middle ramp facies are pure limestone, it is the main carbonate factory so they are poor in all these oxides. The outer ramp facies, which are deeper facies, are poor in TiO_2, and moderate in SiO_2, Al_2O_3 and K_2O. It suggests that outer ramp facies have more argillaceous than the inner and middle ramp facies, has very few detrital material. This observation is in agreement with XRD findings.

In summary, the detrital material (quartz) is high in inner ramp facies, the middle ramp facies are the pure carbonate facies and the impurities are very low, and the outer ramp facies are the argillaceous carbonate.

Magnesium

Magnesium is sufficiently abundant in modern sediments (Milliman, 1974) to be of major importance. Mineralogical and the trace element analyses show that the bulk of the magnesium is incorporated in high-Mg calcite, and a lesser amount in low-Mg calcite. From the conversion of high to low Mg-calcite, most of the magnesium is lost from the system. Early diagenesis reduces the magnesium level. The magnesium released by conversion of high-Mg

Table 2.

Mean, standard deviation, maximum and minimum values of major elements in different facies obtained by XRF analyses, with calculated Ca/Mg ratio.

Facies	1	1	1	1	2	2	2	2	3	3	3	3
n	9	9	9	9	14	14	14	14	11	11	11	11
	Mean	Std.	Max.	Min.	Mean	Std.	Max.	Min.	Mean	Std.	Max.	Min.
SiO_2	85.41	3.47	89.43	81.12	63.96	15.95	82.78	37.72	43.67	14.54	68.53	18.09
TiO_2	0.29	0.11	0.48	0.17	0.3	0.22	0.89	0.12	0.26	0.2	0.81	0.11
Al_2O_3	3.85	1.98	8.39	2.03	2.67	1.83	6.83	0.95	2.42	1.85	7.42	0.97
Fe_2O_3	5.82	1.74	8.96	3.62	6.72	3.01	12.35	1.58	7.36	4.81	19.65	2.75
MnO	0.37	0.27	0.8	0.09	0.32	0.17	0.64	0.05	0.37	0.15	0.77	0.24
MgO	0.82	0.22	1.2	0.56	1.44	1.24	5.6	0.57	1.24	0.3	1.76	0.89
CaO	2.92	2.27	6.89	0.58	15.46	9.46	27.29	0.13	25.9	7.63	40.48	11.81
Na_2O	0.02	0.04	0.11	0	0.05	0.08	0.21	-0.02	0.06	0.07	0.23	0.01
K_2O	0.29	0.25	0.9	0.11	0.26	0.18	0.67	0.04	0.23	0.27	0.98	0.02
P_2O_5	0.05	0.02	0.1	0.03	0.16	0.12	0.4	0.04	0.23	0.39	1.42	0.08
Ca/Mg ratio	2.59	2.02	6.12	0.63	10.2	8.01	24.29	0.07	15.59	5.04	23.12	4.77

Facies	4	4	4	4	5	5	5	5	6	6	6	6
n	10	10	10	10	29	29	29	29	24	24	24	24
	Mean	Std.	Max.	Min.	Mean	Std.	Max.	Min.	Mean	Std.	Max.	Min.
SiO_2	15.3	12.93	31.94	0.29	0.42	0.17	0.9	0.23	1.94	1.47	4.69	0.26
TiO_2	0.1	0.11	0.34	0	0	0	0.02	0	0.04	0.06	0.2	0
Al_2O_3	0.91	0.63	2.24	0.2	0.27	0.09	0.57	0.17	0.97	1.01	3.5	0.19
Fe_2O_3	3.02	2.08	5.89	0.06	0.11	0.08	0.32	0.02	0.66	0.63	1.89	0.01
MnO	0.16	0.13	0.32	0.01	0.01	0	0.02	0.01	0.02	0.01	0.03	0
MgO	1.47	0.62	2.82	0.83	1.03	0.19	1.39	0.77	1.33	0.36	2.59	0.79
CaO	42.39	9.45	53.86	30.18	54.52	0.77	55.64	53.12	52.61	1.84	55.45	48.78
Na_2O	0.15	0.09	0.24	0.01	0.22	0.03	0.31	0.17	0.24	0.02	0.29	0.19
K_2O	0.08	0.04	0.15	0.01	0.02	0.02	0.09	0.01	0.08	0.07	0.27	0.01
P_2O_5	0.14	0.18	0.63	0.03	0.04	0.03	0.13	0.02	0.07	0.07	0.26	0.02
Ca/Mg ratio	24.3	12.28	43.64	11.48	38.88	7.25	51.03	27.26	30.13	8.39	49.91	14.71

Facies	7	7	7	7	8	8	8	8
n	13	13	13	13	13	13	13	13
	Mean	Std.	Max.	Min.	Mean	Std.	Max.	Min.
SiO_2	4.54	2.11	9.14	1.61	9.49	7.72	31.39	2.62
TiO_2	0.11	0.08	0.32	0.02	0.18	0.27	0.97	0.01
Al_2O_3	2.37	1.26	4.15	0.56	3.07	4.07	15.04	0.53
Fe_2O_3	1.84	1.01	3.81	0.54	1.68	1.88	6.5	0.21
MnO	0.02	0.01	0.04	0.01	0.02	0.01	0.04	0
MgO	1.68	0.29	2.09	1.08	1.64	0.67	3.04	0.98
CaO	48.44	3.21	52.77	41.13	45.23	8.61	52.01	20.64
Na_2O	0.25	0.05	0.32	0.17	0.31	0.11	0.54	0.2
K_2O	0.2	0.12	0.4	0.03	0.33	0.47	1.66	0.04
P_2O_5	0.22	0.2	0.64	0.03	0.12	0.09	0.38	0.04
Ca/Mg ratio	21.32	5.5	34.5	15.32	23.37	10.53	36.62	5.87

Major elements values are in weight %.

n=No. of Samples Std.=Standard Deviation

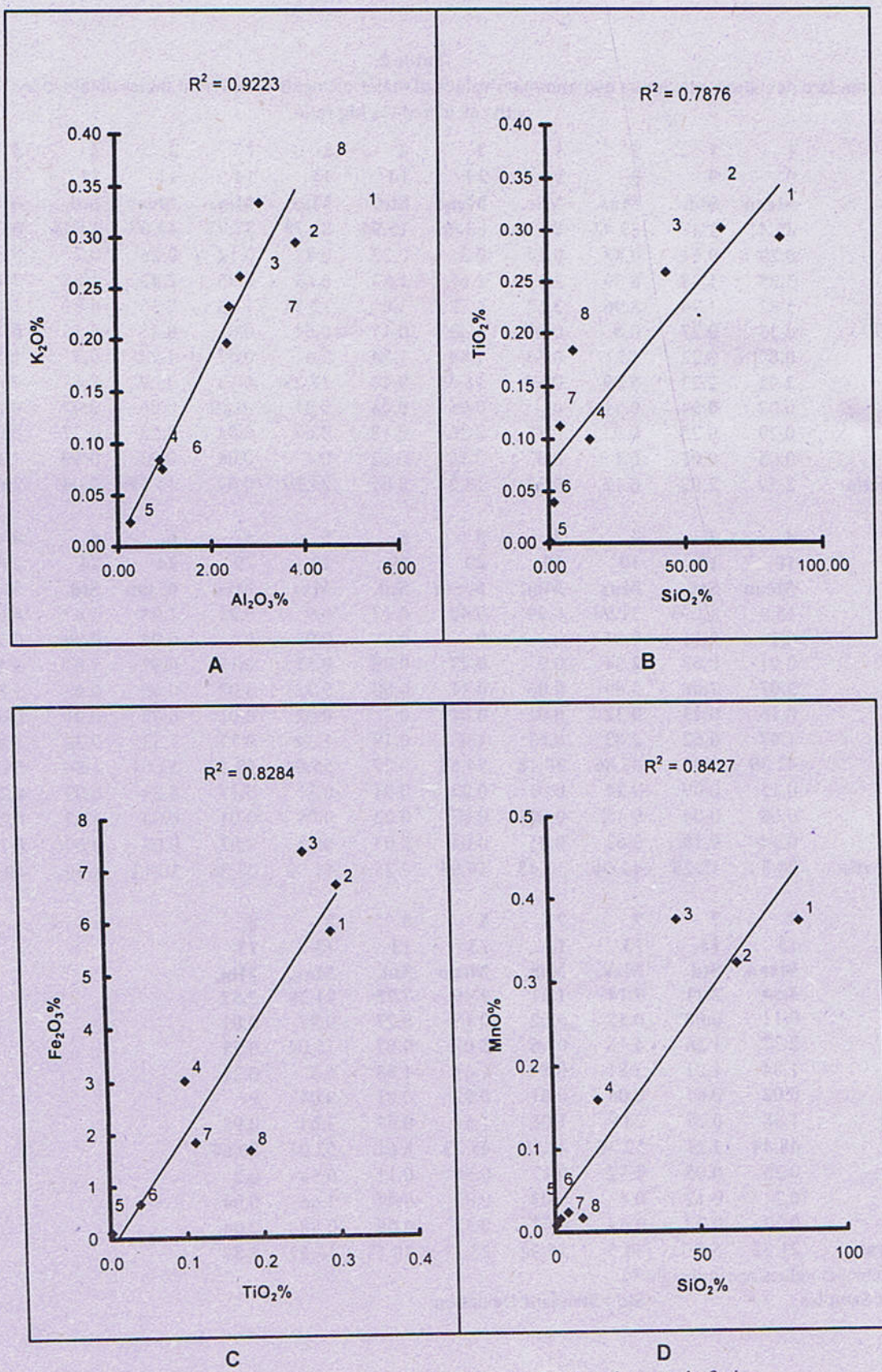

Fig. 1. Plots showing the relationship between the oxides of major elements in facies 1 to 8, present in Dungan Formation. A, between Al2O3 and K2O; B, between SiO2 and TiO2; C, between TiO2 and Fe2O3; and D, between SiO2 and MnO.

calcite may ultimately contribute to dolomite formation, but it does not generally do so in the rocks in which it originates (Stehli and Hower, 1961).

Three processes appear to be active in bringing the magnesium to an equilibrium state. These are the removal of the magnesium from the fossils and deposition in the nearby matrix, i) as dolomite or some other magnesium mineral, ii) the reorganization of the material of the fossil to form two stable phases, low magnesium calcite and dolomite and, iii) the removal of magnesium from the rock by moving pore water.

Magnesium, originally deposited within the skeletons of living organisms, commonly remains within the rock throughout the processes of lithification and uplift. In many cases fossils of Cenozoic sediments contain magnesium still in its original form in solid solution with calcite (Chave, 1954a).

Clarke and Wheeler (1922), Chave (1954b), Pilkey and Hower (1960), studied the magnesium distribution in carbonate rocks. These early studies involving distribution of calcite and magnesium in carbonate rock, investigated the role of their ratio in the precipitation of calcite and aragonite. This has been supported by other investigations which suggest a relationship between evaporite conditions and a low Ca/Mg ratio (Bordine, 1965). The Ca/Mg ratio of carbonates corresponds to definite stability conditions during their formation and is thus of particular interest. Bordine (1965), showed an inverse relationship between Ca/Mg ratio and the insoluble material (clays and detrital sediments). In general if the Ca/Mg ratio is high, the residual material is low; and in low Ca/Mg ratio the residual material (clay and detrital material) is high (Bordine, 1965). The similar relationship is found in the Dungan Formation. The distribution of Ca/Mg ratio in different facies of the Dungan Formation is shown in Table 2. The mole% of $MgCO_3$ is high in inner ramp facies, low in middle ramp facies and moderate in outer ramp facies. In general magnesium content is considerably low in normal shallow marine conditions. In the inner ramp facies the mole% of $MgCO_3$ is high and the Ca/Mg ratio is low, which indicate more detrital material. In the middle ramp facies the mole% of $MgCO_3$ is low and the Ca/Mg ratio is high, which indicates normal salinity and very few detrital materials. It is mainly the pure limestone. In the outer ramp facies the mole% of $MgCO_3$ is low and Ca/Mg ratio is moderate which indicates normal salinity conditions and slightly more residual material mainly clays than the mid ramp facies.

CONCLUSIONS

In the inner ramp facies, the mole% of $MgCO_3$ is high, the Ca/Mg ratio is low and detrital material (quartz) is high. The carbonate is admixed with terrigenous debris. This indicates the shoal environments.

In the mid ramp facies the mole% of $MgCO_3$ is low and the Ca/Mg ratio is high which indicates normal salinity and very few detrital materials. It is the pure carbonate facies. The impurities are very low and this shows the shallow fresh water diagenesis.

In the outer ramp facies the mole% of $MgCO_3$ is low and Ca/Mg ratio is moderate which indicates normal salinity conditions and slightly more residual material mainly clays than the middle ramp facies. The carbonate is argillaceous, this indicates the fresh water diagenesis under burial conditions.

All the skeletal grains are originally of high magnesium calcitic (except in facies 8, which had a mixture of low and high magnesium calcite) and after diagenesis they became stable at the present mole percentage of magnesium carbonate. After fresh water diagenesis, the drusy cement (non-ferroan) is formed with 1.2 mole% of $MgCO_3$, and ferroan drusy cement with 1.90 mole% of $MgCO_3$.

REFERENCES

Ahmad, N. 1996. Palaeoenvironments, diagenesis and geochemical studies of the Dungan Formation (Palaeocene), Eastern Sulaiman Range, Pakistan. Ph.D. Thesis, Leicester University.

Ahmad, N. and Pedley, M. 1997. Facies and Palaeoenvironments of the Dungan Formation, Eastern Sulaiman Range, Pakistan. *Geological Bulletin of the Punjab University, Lahore,* **31 & 32**, 79-102.

Bordine, B. W. 1965. Paleoecological implications of Strontium, Calcium and Magnesium in Jurrasic Rocks near Thistle, Utah. Brigham Young University, *Geology Studies,* **12**, 91-120.

Chave, K. E. 1954a. Aspects of biogeochemistry of magnesium 1. Calcareous marine organisims. *Jour. Geol.*, **62**, 266-287.

Chave, K. E. 1954b. Aspects of biogeochemistry of magnesium 2. Calcareous sediments and rocks. *Jour. Geol.*, **62**, 587-599.

Clarke, F. W. and Wheeler, W. C. 1922. The inorganic constituents of marine invertebrates. U.S.G.S., Profess. Papers, **124**, 1-62.

Goldsmith, J. R., Graf, D. L. and Joensuu, O. I. 1955. The occurance of magnesian calcites in nature. *Geochim Cosmochim Acta*, **7**, 212-230.

Hirst, D. M., and Nicholls, G. D. 1958. Techniques in sedimentary geochemistry. (1) Separation of the detrital and non-detrital fractions of limestones. *Jour. Sed. Pet.*, **28**, 461-468.

Keith, M. L. and Weber, J. N. 1965. Systematic relationships between carbon and oxygen isotopes in carbonates deposited by modern corals and algae. *Science*, **150**, 498-501.

Milliman, J. D. 1974. Marine Carbonates. Springer-Verlag, New York, 1-375.

Pilkey, O. H. and Hower, J. 1960. The effect of environment on the concentration of skeletal magnesium and strontium in *Dendraster*. *Jour. Geol.*, **68**, 203-216.

Richter, D. K. and Fuchtbauer, H. 1978. Ferroan calcite replacement indicates former magnesian calcite skeletons. *Sedimentology*, **25**, 843-860.

Schmalz, R. F. 1965. Brucite in carbonate secreted by the red alga *Goniolithon* sp. *Science*, **149**, 993-996

Stehli, F. G. and Hower, J. 1961. Mineralogy and early diagenesis of carbonate sediments. *Jour. Sed. Pet.*, **31**, 358-371.

Thompson, T. G., and Chow, T. J. 1955. The strontium-calcium atom ratio in carbonate-secreting marine organisms. *Deep-Sea Res., Suppl.*, **3**, 20-39.

Tucker, M. E. 1981. Sedimentary Petrology. Blackwell Scientific Publications, London, 1-252.

Vinogradov, A. P. 1953. The Elementary Chemical Composition of Marine Organisms. Sears Foundation for Marine Research, Yale Univ., New Haven, Conn.,Mem., **2**, 1-647.

Geol. Bull. Punjab. Univ. 35, 2000.

FORAMINIFERA IN THE ZALUCH GROUP OF THE SALT RANGE AND TRANS INDUS RANGES, PAKISTAN.

BY

SARFRAZ AHMED

Institute of Geology, University of the Punjab, Quaid-e-Azam Campus, 54590 Lahore, Pakistan

AND

MERTMANN DOROTHEE

Institut für Geologie, Geophysik und Geoinformatik, FR Allgemeine Geologie, Freie Universitat Malteserstr. 74-100, 12249 Berlin, Germany.

Abstract:- *The marine Permian sediments (Amb-, Wargal- and Chhidru Formations) of the Salt Range and the Trans Indus Ranges yield an abundant fauna of foraminifera. Main groups include Fusulinina, Miliolina and Rotaliina. The fauna occur as benthic organisms settling under open marine to lagoonal conditions in a temperate to warm tethyan sea. Fusulinaceans - Parafusulina (Monodiexodina) kattaensis (Schwager) and Codonofusiella laxa Douglass - are rare in the Amb Formation due to strong clastic input and an agitated coastal water. In the lower Wargal Formation the association comprises Neoschwagerina margaritae Deprat, Sphaerulina sp. and Schubertella sp.. Therefore a Guadalupian age is evident. In the upper part of the Wargal Formation and in the Chhidru Formation Nanlingella simplex Sheng & Chang, Reichelina sp., Nankinella sp. and Staffella sp. indicate a Lopingian age. Small foraminifera include a variety of long ranging species from Parathuramminidae, Earlandiidae, Nodosinellidae, Endothyridae, Lasiodiscidae, Hemigordiopsidae and Fischeridae. Globivalvulina vonderschmitti Reichel and Dagmarita chanakchiensis Reitlinger are present in the Amb-, and Wargal- Formation. Paraglobivalvulina mira Reitlinger occurs from the Upper Wargal onward. Colaniella ex gr. lepida Wang and Colaniella ex gr. minima Wang are restricted to the Upper Wargal and the Chhidru Formation.*

INTRODUCTION

The well exposed marine Permian rocks along the Salt Range and the Trans Indus Ranges (Fig. 1) provide a good field for investigations. The various carbonates and mixed carbonate/siliciclastic facies yield a diverse fauna of larger and smaller foraminifera. They constitute an interesting part in the rich faunal and floral content. For the first time their distribution is evaluated all along the Salt Range and the Trans Indus Ranges.

During the Permian, a large carbonate platform developed on Gondwana continental crust in front of the Indian Shield (Pakistani Japanese Research Group - P.J.R.G. 1985). The platform was influenced both by sea-level fluctuations and by repeated intervals of hinterland uplift associated with an increase in clastic terrigenous input The major depositional sequences illustrate sedimentary responses to variations in the depositional environment (Mertmann & Sarfraz 1999).

The marine Permian rocks of the Salt Range and Trans Indus Ranges are grouped into the Zaluch Group with the Amb-, Wargal- and Chhidru Formation (Kummel & Teichert 1970, Fatmi 1974, Gee 1980). Foraminifera from the Salt Range and the Trans Indus Ranges were mainly described by Dunbar (1933), Douglass (1970), P.J.R.-G. (1985) and Jenny-Deshusses & Baud (1989). The first two authors concentrated on the fusulinids of the Amb Formation: *Monodiexodina* (*Parafusulina*) *kattaensis* (Schwager) and *Codonofusiella laxa* Douglass. P.J.R.-G. (1985) recognized a *Neoschwagerina* assemblage in the lower Wargal Formation and a *Codonofusiella-Reichelina-Colaniella* assemblage in the Chhidru Formation out of the sections of Zaluch, Nammal and Chhidru. Jenny-Deshusses & Baud (1989) used material from Pakistan for their analysis of the genus *Colaniella*, also. Mainly fusulinids and brachiopods were used for stratigraphic dating (e.g. P.J.R.-G. 1985). Due to conodont determinations (Wardlaw & Pogue 1995, Mei Shilong et al. 1999, Wardlaw & Mei Shilong 1999) stratigraphic attributions were revised

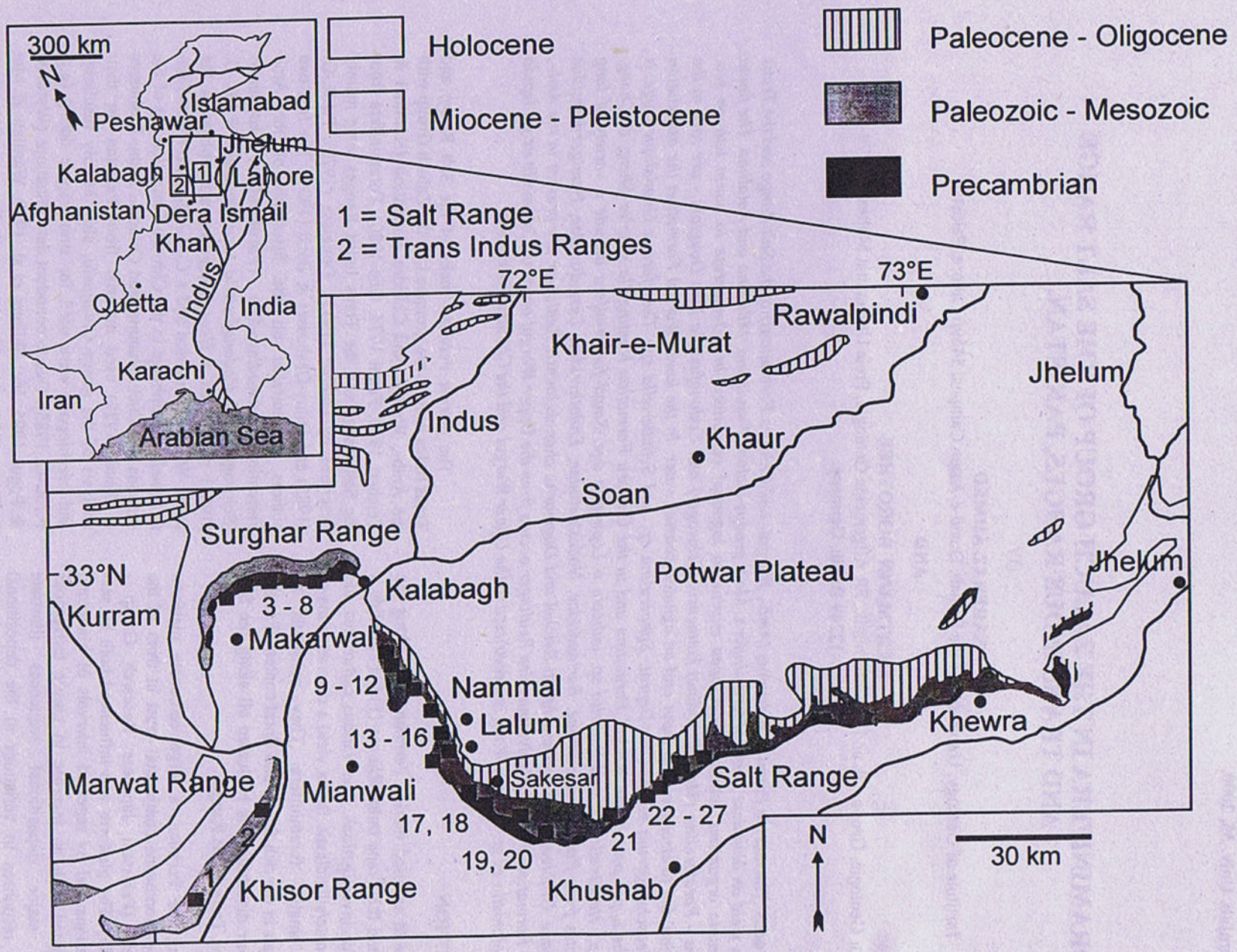

Fig. 1 Map of Pakistan showing the position of the studied areas. Larger map represents a simplified geological map of the Salt Range and the Trans Indus Ranges (modified from Gee 1990) with the locations of the measured sections. 1-Tapan Wahan, 2-Saiyiduwali, 3-Landa Pusha, 4-Landu Nala, 5-Gulakhel, 6-Narmia, 7-Narmia Spring, 8-New Narmia, 9-Thatti, 10-Zaluch Nala, 11-S-Lakriki Nala, 12-Buri Khel, 13-Nammal Gorge, 14-Ratti Wahan, 15-Kasanwal, 16-Chhidru Nala, 17-Sarai, 18-Sakesar, 19-Jan Sukh Nala, 20-Choha, 21-Jallhar, 22-Khura, 23-Choi, 24-Kathwai, 25-Chambalwal Nala, 26 Kattha, 27-Pail.

(Fig.2). A Wordian age is assigned to the Amb Formation, a Capitanian to Wuchiapingian age to the Wargal Formation and a Wuchiapingian to lower Changhsingian age to the Chhidru Formation. The lowermost part of the Kathwai Member (Kathwai A) is still Changhsingian in age. The Permian/Triassic Boundary is situated in between the Kathwai Members A and B (P.J.R.-G. 1985, Wignall & Hallam 1993). Various hiati occur as well between the formations and even between members (Fig.2).

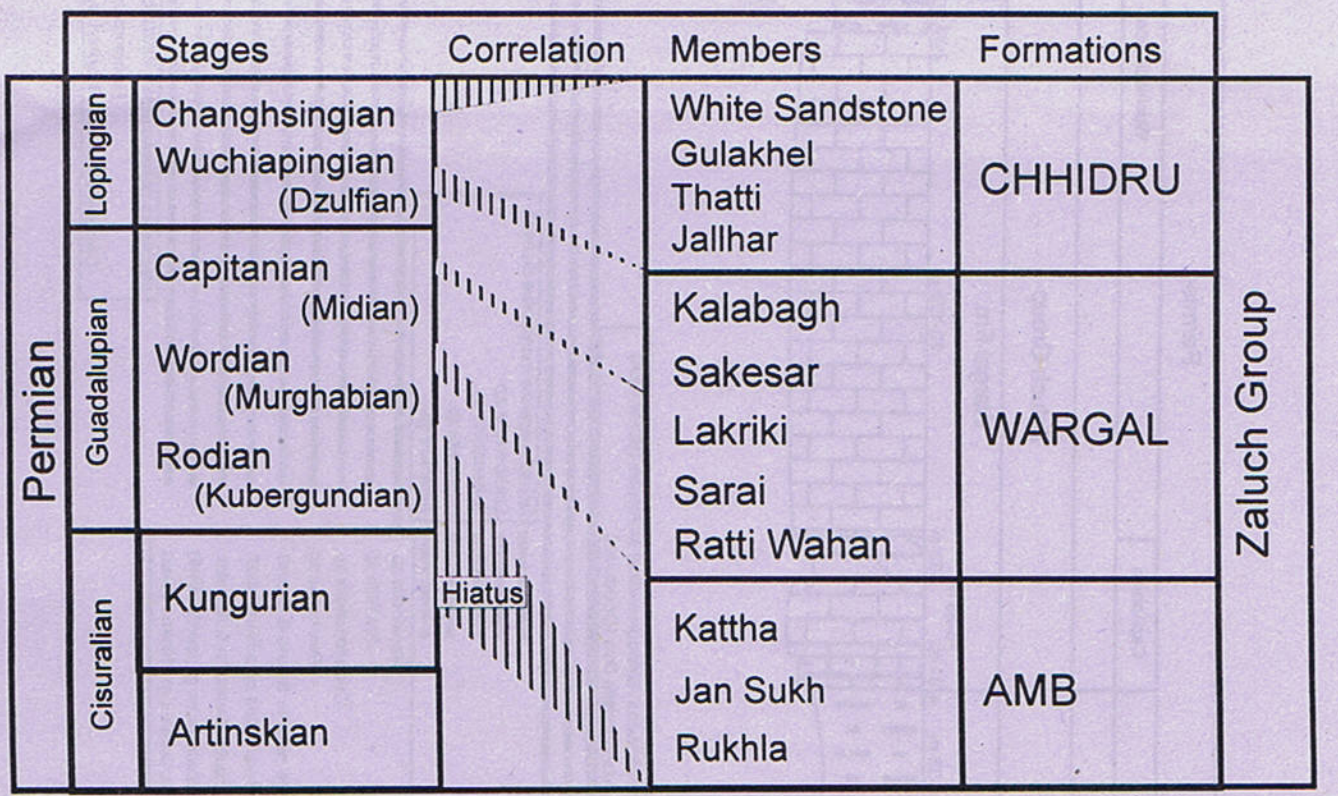

Fig. 2 Conodont biostratigraphy of the Salt Range and Khisor Ranges, Pakistan. (after Wardlaw and Mei Shilong 1999

METHODOLOGY

Along the Salt Range and the Trans Indus Ranges 27 sections have been studied through field observations (Fig. 1), and 400 thin sections and polished slabs have been analysed. Each sample has been described with its skeletal content with special emphasis on the foraminifera. Main literature used for determinations include Douglass (1970), Bozorgnia (1973), Rozovskaya (1975), Kahler & Kahler (1979), Nguyen (1979), Vachard (1980), Altiner (1981), Kahler (1983), Jenny-Deshusses (1983), Noe (1987), Lys (1977, 1987, 1988 a and b), Ishii et al. (1975), Jenny-Deshusses & Baud (1989), Lys et al. (1990). Within the following two chapters a brief description of the main characteristics of the formations and a listing of foraminifera is given (Figs. 3 & 4).

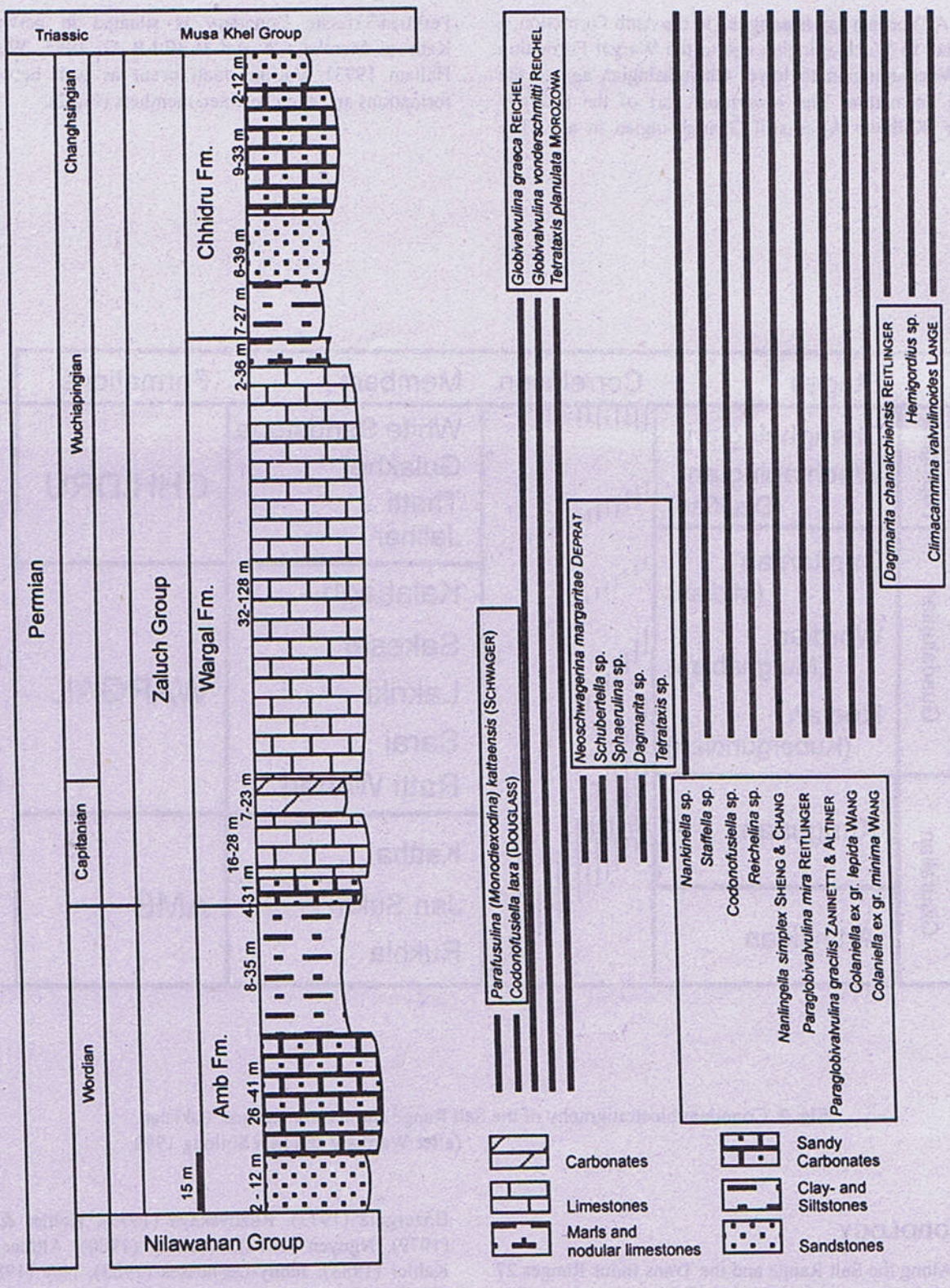

Fig. 3 Composite section of the Zaluch Group based on the sections Chhidru Nala, Sarai, Jan Sukh Nala and Zaluch Nala. Thickness variations of the members from all sections are given. Distribution of the main genera and species of foraminifera is indicated. Members of the Amb Formation: 1-Rukhla, 2-Jan Sukh, 3-Kattha. Members of the Wargal Formation: 1-Ratti Wahan, 2-Sarai, 3-Lakriki, 4-Sakesar, 5-Kalabagh. Members of the Chhidru Formation: 1-Jallhar, 2-Thatti, 3-Gulakhel, 4-White Sandstone.

Sections/ Foraminifera	1	2	3	4	5	6	7	8	9	10	11	12	13	14	15	16	17	18	19	20	21	22	23	25	26	27
Bisphaera irregularis	x	x	x	x		x			x	x	x	x	x	x		x	x	x	x	x	x	x		x		
Earlandia sp.	x	x				x			x	x	x	x	x	x		x	x	x	x	x	x	x		x		
Tuberitina sp.										x						x										
Tuberitina conili																x										
Eotuberitina reitlingerae	x	x	x	x	x		x		x	x	x	x	x	x		x	x	x	x	x	x	x	x	x		
Umbellina sp.	x	x		x					x	x	x		x			x	x	x		x	x	x	x	x		
Geinitzina sp.	x		x		x	x	x		x	x	x		x			x	x	x		x	x	x	x	x	x	
Geinitzina postcarbonica		x								x									x						x	
Pachyphloia sp.	x	x	x	x	x	x	x	x	x	x	x	x	x	x	x	x	x	x	x	x	x		x	x	x	
Langella sp.	x		x	x	x			x	x	x	x	x								x				x		
Frondina permica						x	x		x	x			x			x	x			x	x	x				
Ichthyolaria latilimbata	x								x				x				x	x		x	x	x				
Colaniella ex gr. *minima*	x	x		x	x			x	x	x		x	x			x	x	x		x	x	x	x			
Colaniella ex gr. *lepida*	x	x											x			x	x	x		x				x		
Palaeonubecularia sp.					x																x			x		
Climacammina elegans		x	x	x	x		x		x	x			x	x		x	x	x			x		x			
Climacammina valvulinoides				x									x				x						x			
Monogenerina sp.				x	x				x				x				x		x	x	x					
Tetrataxis planulata		x				x				x	x		x	x		x		x		x		x		x		
Globivalvulina graeca		x							x	x	x		x	x		x	x	x	x	x	x	x	x	x		
Globivalvulina vonderschmitti	x	x	x	x	x	x	x		x	x		x	x			x	x	x		x	x	x	x	x		
Paraglobivalvulina mira				x	x	x	x		x								x				x					
Paraglobivalvulina gracilis	x			x		x	x										x					x	x			
Dagmarita sp.		x							x				x				x									
Dagmarita chanakchiensis	x	x		x	x				x	x	x		x					x		x	x	x				
Neoendothyra sp.	x	x		x	x				x	x			x			x	x	x		x	x	x	x	x		
Robuloides sp.	x	x			x	x				x	x		x				x		x	x	x	x		x		
Lasiodiscus sp.	x		x		x	x	x		x	x	x		x	x			x			x	x	x	x	x		
Reichelina sp.													x	x												
Schubertella sp.	x	x	x	x	x	x	x		x	x		x	x			x	x	x		x	x	x	x			
Codonofusiella sp.		x									x															
Codonofusiella laxa	x	x		x	x	x			x	x			x				x									
Nanlingella simplex		x								x	x			x		x			x					x	x	x
Parafusulina (Monodiexodina) kattaensis																								x		
Chusenella sp.	x			x	x					x			x			x	x	x				x	x			
Staffella sp.	x	x	x	x	x	x	x	x	x	x	x	x	x	x	x	x	x	x		x	x	x	x			
Nankinella sp.		x									x			x		x	x	x	x					x		
Sphaerulina sp.											x		x			x		x		x				x		
Neoschwagerina margaritae																										
Hemigordius sp.	x	x	x	x	x			x	x	x	x	x	x			x	x	x	x		x	x	x	x		
Agathammina sp.	x	x		x	x	x		x	x	x	x	x	x	x		x	x	x	x	x	x	x	x	x		
Calcitornella heathi		x	x			x			x	x	x	x	x	x		x	x	x	x	x	x	x		x	x	
Nodosaria sp.	x	x	x		x		x		x	x	x	x	x	x									x			
Nodosaria longissima										x																

Fig. 4 Distribution of the foraminifera in the measured sections of the Salt Range and Trans Indus Ranges. (Abbreviations Fig. 1)

GEOLOGICAL SETTING OF THE ZALUCH GROUP

Amb Formation

The Amb Formation represents the effects of a widespread transgression of the Tethys ocean into the todays Salt Range and Trans Indus Ranges. The basal member - composed mainly of sandstones - thins towards the west and disappears. It forms part of a shallow subaqueous delta. The middle facies directly overlies the delta deposits with no signs of reworking. It is distributed thoughout the area and therefore in part overlies the Sardhai Formation as well with a thin sandstone horizon and locally with a lithoclastic rudstone at the base. Sandy bioclastic rudstones with abundant brachiopods and fusulinids are characteristic. In the east the quartz content increases. The sedimentation happened in a shallow subtidal nearshore area. The water was generally agitated, so that abundant bioclasts were produced and only minor amounts of micrite were preserved. The third facies was deposited in a subtidal, partly intertidal shore environment. The progradational setting was achieved by an increased input of terrigenous material and by a pronounced regression of the sea.

Wargal Formation

The boundary between the Amb Formation and the overlying Wargal Formation is associated with a hiatus. Two sequences are discernible from the rocks of the Wargal formation. The first one is represented sandy shoreline deposits and continue with subtidal open marine carbonates with diverse bioclastic packstones to grain- and rudstones and subordinate bafflestones and framestones. The third facies shows a separate tidal flat and lagoonal environment with stromatolitic boundstones, micrites, oolites and gastropodal to foraminiferal grain- to rudstones. The second transgression led to the accumulation of migrating barriers on the shelf consisting mainly of echinodermal debris. Furthermore coral reefs developped on the platform. In the deeper environment of the todays Khisor Range bryozoan mounds predominate in an equivalent position. Interreef carbonates and nodular marls are present in the uppermost Wargal Formation (Kalabagh Member).

Chhidru Formation

The Wargal Formation and the overlying Chhidru Formation are interfingering. A continuous increase in terrigenous input into the basin is typical for the transitional stage. The hinterland was reactivated. Deposition took place in a relatively near-shore position. Sandstones and finer clastics are developped and increase in their amount towards the top. The fauna reveals an open marine realm, but its quantity diminishes towards the top. Locally fresh water influences occur. The topmost so-called "White Sandstone Unit" is barren or only few fossils are preserved.

Permian-Triassic Boundary

The boundary between the upper permian Chhidru and the lower triassic Mianwali Formations is an erosional unconformity. The overlying Kathwai Member is developped in 3 subsequent phases. The Kathwai Unit A with dolomitic sandstones is only locally preserved. It still belongs to the Permian. Kathwai Unit B is distributed throughout the area and is composed mainly of secondary dolomites and dedolomites with a lot of echinodermal debris.

FORAMINIFERA OF THE ZALUCH GROUP

The foraminifera determined out of the thin sections are listed below (Fig. 3, 4):

Fusulinina

Parathuramminacea Bykova
Parathuramminidae Bykova
Bisphaera irregularis Birina (plate 1.4)

Earlandiidae Cummings
Earlandia Plummer
Earlandia sp. (plate 1.5)

Endothyracea Brady
Nodosinellidae Rhumbler
Tuberitina Galloway & Harlton
Tuberitina sp. (plate 1.6)
Tuberitina conili Nguyen (plate 1.7)

Eotuberitina reitlingerae Miklukho-Maklay (plate 1.8-9)

Umbellina Loeblich & Tappan
Umbellina sp. (plate 1.10)

Geinitzina Spandel
Geinitzina sp. (plate 1.11)
Geinitzina postcarbonica Spandel

Pachyphloia Lange
Pachyphloia sp. (plate 2.1)

Langella Sellier de Civrieux & Dessauvagie
Langella sp. (plate 2.2)

Frondina permica Sellier de Civrieux & Dessauvagie (plate 2.3)

Ichthyolaria latilimbata Sellier de Civrieux & Dessauvagie (plate 2.4)

Colaniellidae Fursenko
Colaniella Likharev.
Colaniella ex gr. *lepida* Wang (plate 2.5-6)
Colaniella ex. gr. *minima* Wang

Ptychocladiidae Elias
Palaeonubecularia Reitlinger
Palaeonubecularia sp. (plate 2.7)

Palaeotextulariidae Galloway
Climacammina elegans (Moeller)
Climacammina valvulinoides Lange (plate 2.8, 10)

Monogenerina Spandel
Monogenerina sp. (plate 3.1)

Tetrataxidae Galloway
Tetrataxis planulata Morozova. (plate 2.9, 11)

Biseriamminidae Chernysheva
Globivalvulina graeca Reichel (plate 3.4)
Globivalvulina vonderschmitti Reichel (plate 3.2)
Paraglobivalvulina mira Reitlinger (plate 3.3)
Paraglobivalvulina gracilis Zaninetti & Altiner (plate 3.5)

Dagmarita Reitlinger
Dagmarita sp.
Dagmarita chanakchiensis Reitlinger (plate 3.10)

Endothyridae Brady
Neoendothyra Reitlinger
Neoendothyra sp. (plate 3.7)

Robuloides Reichel
Robuloides sp. (plate 3.6, 9)

Lasiodiscidae Reitlinger
Lasiodiscus Reichel
Lasiodiscus sp. (plate 3.8)

Fusulinacea von Möller
Ozawainellidae Thompson & Foster
Reichelina Erk
Reichelina sp. (plate 4.1)

Schubertellidae Staff & Wedekind
Schubertella Staff & Wedekind
Schubertella sp.

Codonofusiella Dunbar & Skinner
Codonofusiella sp. (plate 4.2)

Codonofusiella laxa Douglass

Nanlingella simplex Sheng & Chang (entsprechend *Palaeofusulina simplex*) (plate 4.3)

Fusulinidae von Möller
Parafusulina (Monodiexodina) katta-ensis (Schwager) (plate 4.5, 7)

Schwagerinidae Dunbar & Henbest
Chusenella Hsu
Chusenella sp. (plate 4.4)

Staffellidae Miklukho-Maklay

Staffella Ozawa
Staffella sp. (plate 4.6)

Nankinella Lee
Nankinella sp.

Sphaerulina Lee
Sphaerulina sp. (plate 4.8)

Verbeekinidae Staff & Wedekind
Neoschwagerina margaritae Deprat (plate 4.9)

Miliolina

Hemigordiopsidae Nikitina
Hemigordius Schubert (plate 1.2)

Fischerinidae Millet
Agathammina Neumayr
Agathammina sp. (plate 3.11)

Sessile miliolide Foraminiferen
Calcitornella heathi Cushman & Waters (plate 1.3)

Rotaliina

Nodosaria Lamarck

Nodosaria sp. (plate 1.1)
Nodosaria longissima Suleimanov

INTERPRETATION

The described foraminifera were benthic organisms, living partly sessile and settling under marine, temperate to warm water conditions. Sandy carbonates of the Amb and Chhidru Formation indicate agitated water, Moreover, Out of the different settling areas of fusulinaceans described by Ishii et al. (1985) a cratonic shelf is the most suitable.

Larger Foraminifera

In comparison to other Thethyan regions fusulinaceans are rare, mainly due to the paleogeographical peri-gondwanian position of the platform (Shi et al. 1994). *Monodiexodina kattaensis* (Schwager) and *Codonofusiella laxa* (Douglass) are present in the middle facies of the Amb Formation. The water temperature was temperate. They have only minor stratigraphic significance (pers. comm. Baud, 1999). In the lower Wargal Formation the association comprises *Neoschwagerina margaritae* Deprat, *Sphaerulina* sp., and *Schubertella* sp.. The occurence of the *Neoschwagerina* assemblage is related to a spread of warm ocean waters in connection with a major transgression of the Tethyan sea along the margin of Gondwana during the Capitanian. *Nanlingella simplex* Sheng & Chang, *Reichelina* sp., *Nankinella sp., Codonofusiella sp.* and *Staffella* sp. indicate a Lopingian age (P.J.R.-G. 1985).

Plate 1

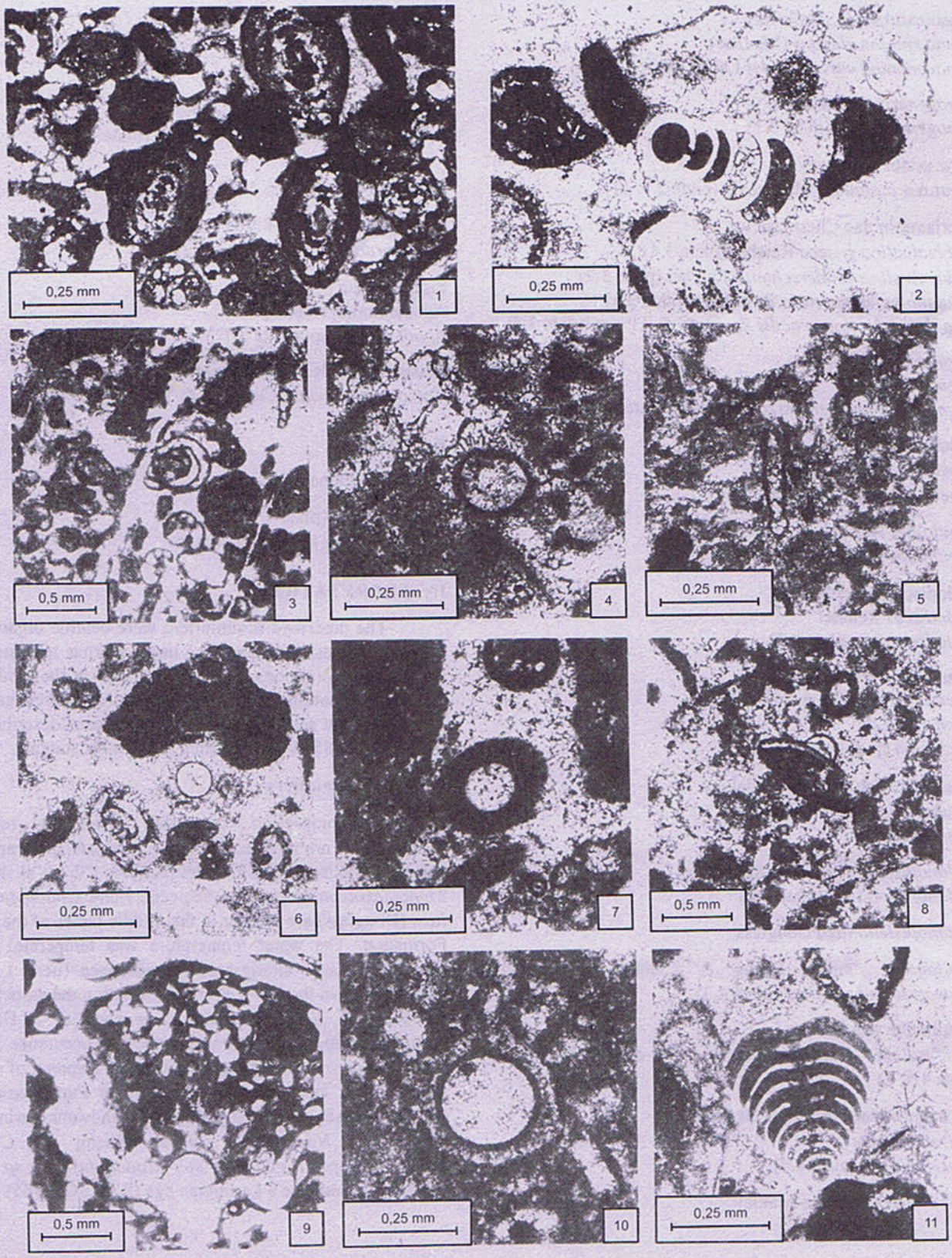
0,25 mm
1
0,25 mm
2
0,5 mm
3
0,25 mm
4
0,25 mm
5
0,25 mm
6
0,25 mm
7
0,5 mm
8
0,5 mm
9
0,25 mm
10
0,25 mm
11

Plate 2

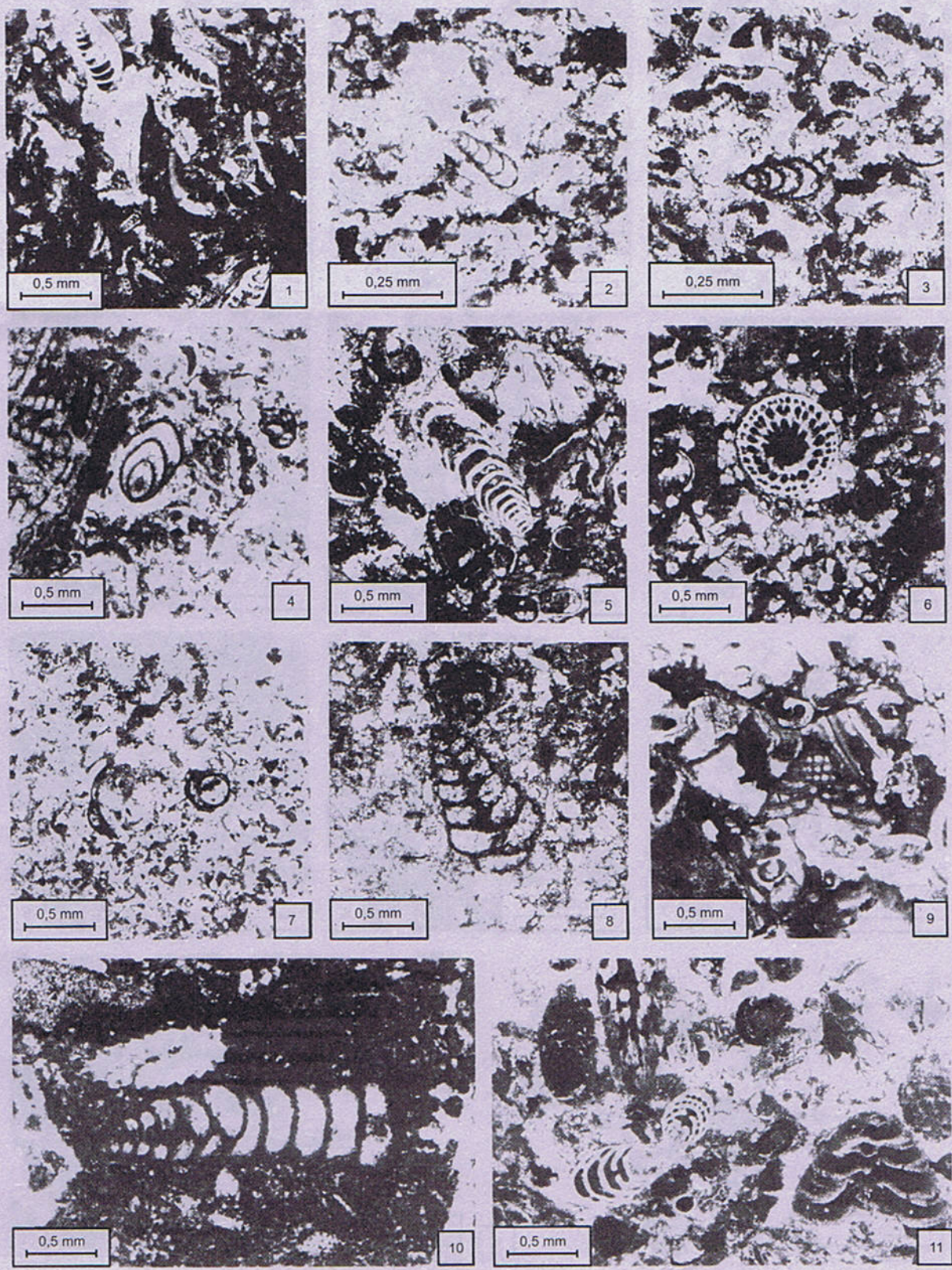
0,5 mm
1
0,25 mm
2
0,25 mm
3
0,5 mm
4
0,5 mm
5
0,5 mm
6
0,5 mm
7
0,5 mm
8
0,5 mm
9
0,5 mm
10
0,5 mm
11

Plate 3

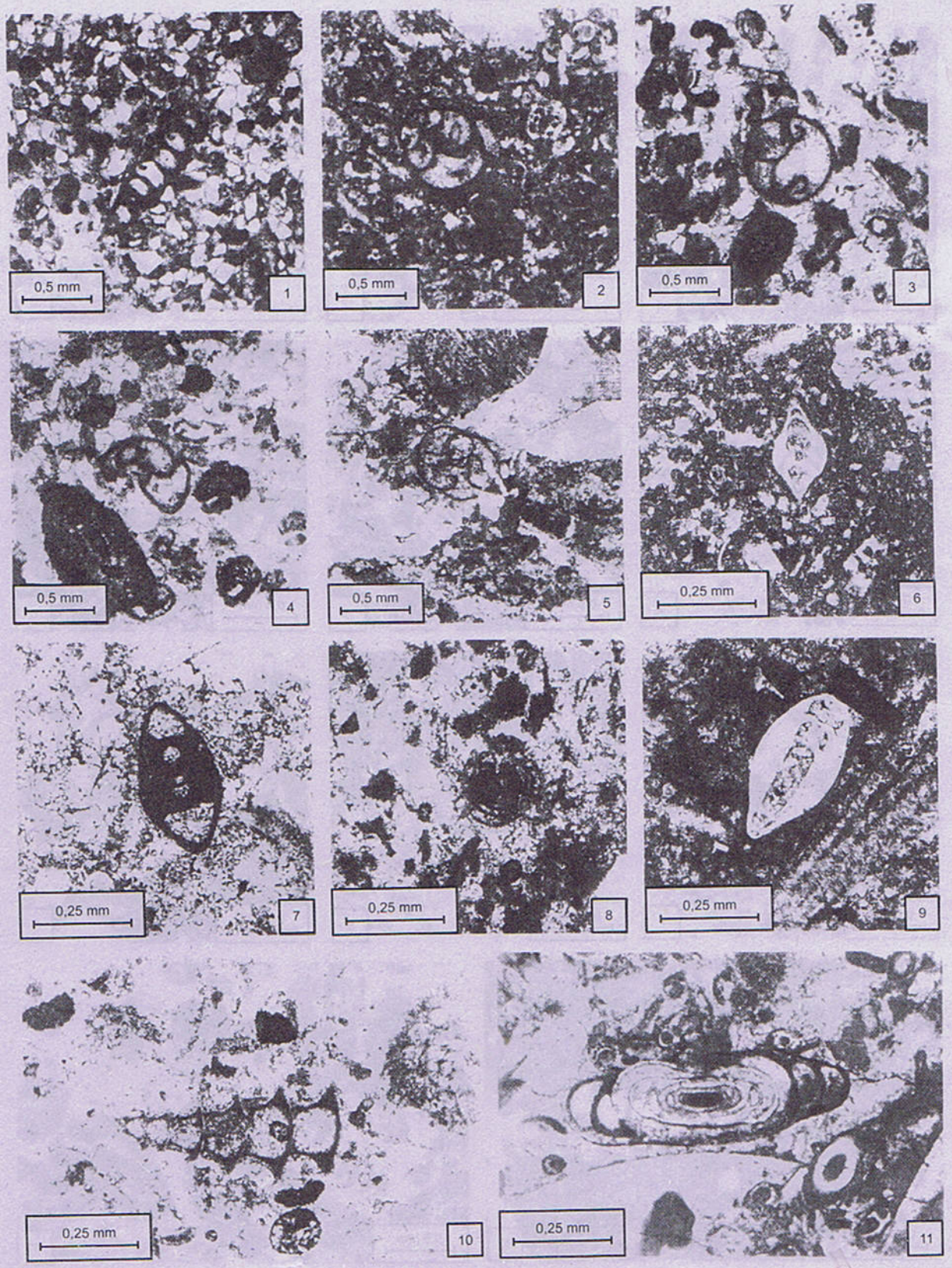
0,5 mm
1
0,5 mm
2
0,5 mm
3
0,5 mm
4
0,5 mm
5
0,25 mm
6
0,25 mm
7
0,25 mm
8
0,25 mm
9
0,25 mm
10
0,25 mm
11

Plate 4

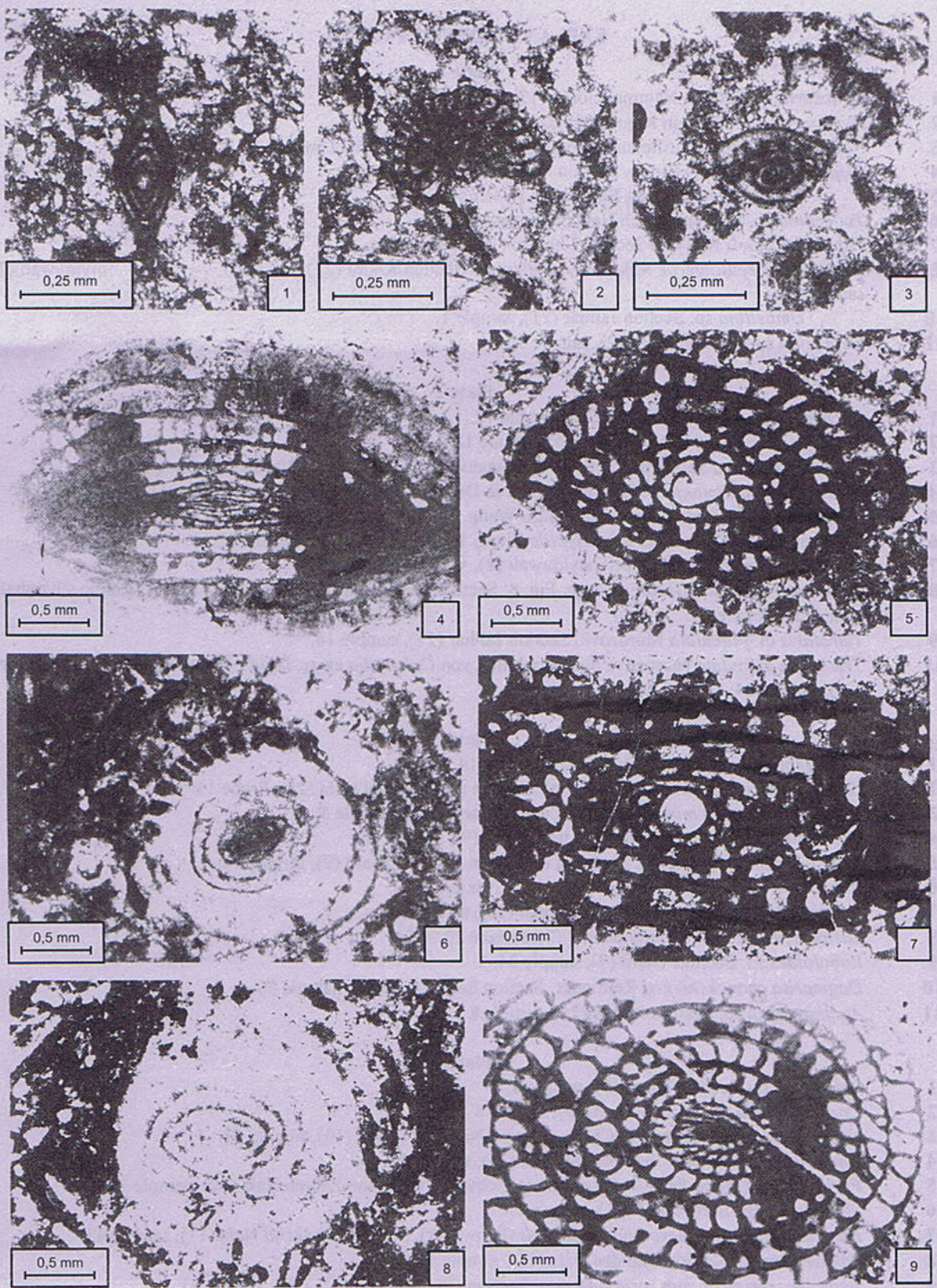

EXPLANATIONS OF PLATES

Plate 1

Fig. 1 *Nodosaria* sp. Section Nammal Gorge (13), sample 4.
Fig. 2 *Hemigordius* sp. Section Khura (22), sample 19.
Fig. 3 *Calcitornella heathi* Cushman & Waters. Section Chhidru (16), sample 32.
Fig. 4 *Bisphaera irregularis* Birina. Section Nammal (13), sample 54.
Fig. 5 *Earlandia* sp. Section Nammal (13), sample 7.
Fig. 6 *Tuberitina* sp. Section Zaluch Nala (10a), sample 32.
Fig. 7 *Tuberitina conili* Nguyen. Section Chhidru (16), sample 32
Fig. 8, 9 *Eotuberitina reitlingerae* Miklukho-Maklay. 8 - Section Khura (22), sample 6; 9 - Section Saiyiduwali (2), sample 14.
Fig. 10 *Umbellina* sp. Section Jallhar (21), sample 1.
Fig. 11 *Geinitzina* sp. Section Thatti (9), sample 26.

Plate 2

Fig. 1 *Pachyphloia* sp. Section Khura (22), sample 12.
Fig. 2 *Langella* sp. Section Ratti Wahan (14), sample 18.
Fig. 3 *Frondina permica* Sellier de Civrieux & Dessauvagie. Section Ratti Wahan (14), sample 18.
Fig. 4 *Ichthyolaria latilimbata* Sellier de Civrieux & Dessauvagie. Section Nammal Gorge (13), sample 22.
Fig. 5 Längsschnitt von *Colaniella* ex gr. *lepida* Wang. Section Khura (22), sample 16.
Fig. 6 Kopfschnitt von *Colaniella* ex gr. *lepida* Wang. Section Chhoi (23), sample 13.
Fig. 7 *Palaeonubecularia* sp. Section Saiyiduwali (2), sample 20.
Fig. 8, 10 *Climacammina valvulinoides* Lange. Fig. 8: Section Landu Nala (4), Probe 55. Fig. 10: Section Chambalwal Nala (25), sample 13.
Fig. 9 *Tetrataxis* cf. *planulata* Morozova. Section Jallhar (21), sample 14.
Fig. 11 *Tetrataxis planulata* Morozova und Anschnitte von *Colaniella* ex gr. *lepida* Wang. Section Nammal Gorge (13), sample 94.

Plate 3

Fig. 1 *Monogenerina* sp. Section Chhoi (23), sample 14.
Fig. 2 *Globivalvulina vonderschmitti* Reichel. Section Chambalwal Nala (25), Probe 13.
Fig. 3 *Paraglobivalvulina mira* Reitlinger. Section Narmia (6), sample 5.
Fig. 4 *Globivalvulina graeca* Reichel. Section Thatti (9), sample 15.
Fig. 5 *Paraglobivalvulina gracilis* Zaninetti & Altiner. Section Thatti (9), sample 14.
Fig. 6 *Robuloides* sp. Section Nammel Gorge (13), sample 84.
Fig. 7 *Neoendothyra* sp. Section Nammal Gorge (13), sample 90.
Fig. 8 *Lasiodiscus* sp. Section Saiyiduwali (2), sample 20.
Fig. 9 *Robuloides* sp. Section Thatti (9), sample 34.
Fig. 10 *Dagmarita chanakchiensis* Reitlinger. Section Saiyiduwali (2), sample 30.
Fig. 11 *Agathammina* sp. Section Jallhar (21), sample 8

Plate 4

Fig. 1 *Reichelina* sp. Section Thatti (9), sample 8.
Fig. 2 *Codonofusiella* sp. Section Thatti (9), sample 8.
Fig. 3 *Nanlingella simplex* Sheng & Chang. Section Nammal Gorge (13), sample 62.
Fig. 4 *Chusenella* sp. Section Chambalwal Nala (25), sample 13.
Fig. 5 *Parafusulina* (*Monodiexodina*) *kattaensis* (Schwager). Section Zaluch Nala (10), sample 10.
Fig. 6 *Staffella* sp. Section Jallhar (21), sample 1.
Fig. 7 *Parafusulina* (*Monodiexodina*) *kattaensis* (Schwager). Section S-Lakriki Nala (11), sample 43.
Fig. 8 *Sphaerulina* sp. Section Chhidru Nala (16), sample 17.
Fig. 9 *Neoschwagerina* cf. *margaritae* Deprat. Section Chambalwal Nala (25), sample 13.

Smaller Foraminifera

Smaller foraminifera include a variety of long ranging species from Parathuramminidae, Earlandiidae, Nodosinellidae, Endothyridae, Lasiodiscidae, Hemigordiopsidae and Fischerinidae.

Others are more interesting: The globivalvulinids evolved in several phases (Altiner 1981, Zaninetti & Altiner 1981, Zaninetti & Jenny-Deshusses 1985). *Globivalvulina* occurred with different species from the Middle Carboniferous to Upper Permian. *Globivalvulina vonderschmitti* Reichel is typical for the Wordian to Wuchiapingian from Taurus, Oman, Iran, Afghanistan, and Thailand (Altiner 1981). *Paraglobivalvulina mira* Reitlinger had its first occurrence in the Capitanian (Altiner 1981, Jenny-Deshusses 1983). In the study area *Globivalvulina vonderschmitti* Reichel allready occurs in the Amb Formation together with *Globivalvulina graeca* Reichel; *Paraglobivalvulina mira* Reitlinger from the upper Wargal onward. *Dagmarita chanakchiensis* Reitlinger is another species indicating a Capitanian to Changhsingian age. Within the sections they were detected in the Chhidru Formation.

The distribution of the colaniellids with *Colaniella* ex grupo *lepida* Wang and *Colaniella* ex grupo *minima* Wang is restricted to the upper Wargal and the Chhidru Formation. Their stratigraphical range is confined to the Capitanian to Changhsingian (Jenny-Deshusses & Baud 1989). However the oldest ones are present e.g. in the Pamir and Caucasus. With the Wuchiapingian they appeared in several Tethyan regions, including the Salt Range and the Trans Indus Ranges. The youngest forms of the Changhsingian are restricted to the central Tethyan sea present in China (Jenny-Deshusses & Baud 1989). Within the Wargal Formation they are often distributed in a coral reef facies.

ACKNOWLEDGEMENTS

The research work was carried out with the financial support of the "Deutsche Forschungsgemeinschaft" and the "Deutsche Akademische Austauschdienst". We like to thank Prof. Dr. F.A. Shams, Prof. Dr. Nawaz Chaudry, Prof. Dr. Aftab A. Butt and all members of the Institute of Geology, Punjab University, Lahore for their substantial help.

REFERENCES

Altiner, D., 1981. Recherches stratigraphiques et micropaléontologiques dans le Taurus Oriental au NW de Pinarbasi (Turquie). Thèse Univ. Genève, No 2005, 1-450

Bozorgnia, F., 1973. Paleozoic foraminiferal biostratigraphy of Central and East Alborz Mountains, Iran. *Nat. Iranian Oil Comp., Geol. Lab. Publ.*, **4**, 1-185

Douglass, R.A., 1970. Monographic studies of fusulinids from the lower Permian of West Pakistan. *Prof. Papers U.S. Geol. Surv.*, 643 G, 1-11

Dunbar, C.O., 1933. Stratigraphic significance of the fusulinids of the lower Productus Limestone of the Salt Range. *Records Geol. Surv. India,* **66,** 405-413

Fatmi, A.N., 1974. Lithostratigraphic units of the Kohat-Potwar province, Indus Basin, Pakistan. *Memoirs Geol. Surv. Pakistan,* **10,** 1-80

Gee, E.R., 1980. Salt Range Maps. *Geol. Surv. Pakistan.*

Gee, E.R., 1989. Overview of the geology and structure of the Salt Range, with observations on related areas of northern Pakistan. Tectonics of the western Himalayas. In: Malinconico, L.L. and Lillie, R.J. (eds.). *Geol. Soc. Amer. Special Papers,* **232,** 95-112

Ishii, K., Okimura, Y. and Ichikawa, K., 1985. Notes on Tethys biogeography with reference to Middle Permian fusulinaceans. In: The Tethys, Nakazawa, K. & Dickins, J.M. (eds.). 139-155

Ishii, K., Okimura, J. and Nakazawa, K., 1975. On the genus *Colaniella* and its biostratigraphic significance. *Jour.. Geosci. Osaka City Univ.*, **19,** 107-129

Jenny-Deshusses, C., 1983. Le Permien de l'Elbourz Central et al Oriental (Iran): Stratigraphie et micropaléontologie (Foraminifères et Algues). These Univ. Genève, No. 2103, 1-265 (unpubl.)

Jenny-Deshusses, 1988. Approche nouvelle de la structure interne de *Paraglobivalvulina mira* Reitlinger, foraminifère benthique du Permien supérieur tethysien.- *Revue de Paléobiologie,. Spec. 2, Benthos* **86,** 69-74

Jenny-Deshusses, C. and Baud, A. 1989. *Colaniella*, foraminifère index du Permien tardif tethysien: propositions pour une taxonomie simplifiée, repartition géographique et environnements. *Eclogae geol. Helv.*, **82,** 869-901

Kahler, F., 1983. Fusuliniden aus Karbon und Perm der Karnischen Alpen und der Karawanken. *Carinthia* II, 41, *Sonderheft,* 5-106

Kahler, F. and Kahler, G., 1979. Fusuliniden (Foraminifera) aus dem Karbon und Perm von Westanatolien und dem Iran. *Mitt. österr. geol. Ges.,* **70,** 187-269

Kummel, B. and Teichert, C., 1970. Stratigraphy and paleontology of the Permian-Triassic boundary beds, Salt Range and Trans Indus Ranges, West Pakistan. Stratigraphic boundary problems - Permian and Triassic of West Pakistan. In: Kummel, B. & Teichert, C. (eds.). University of Kansas, Spec. Publ. 4, 1-110

Lys, M., 1977. Biostratigraphie du Carbonifère et du Permien d'Afghanistan (Micropaléontologie). *Mém. h. ser. Soc. géol. France.,* **8,** 291-308

Lys, M., 1987. Comparaison de biocoenoses du Permien supérieur des domaines mésogéen (en Mediterranée centrale et orientale) et tethysien. Intérêt paléogéographique. *Ann. Soc. Géol. Nord, CV,* 259-267

Lys, M., 1988a. Biostratigraphie des dépôts marins du Carbonifère et du Permien du Sud-Tunisien - Micropaléontologie (Foraminifères) et paléobiogéographie. *Bull. Centres Rech. Explor.-Prod. Elf-Aquitaine,* **12,** 601-659

Lys, M., 1988b. Biostratigraphie du Carbonifère et du Permien en Mésogée (Espagne, Afrique du Nord, Régions Egéennes, Proche Orient) - Étude micropaléontologiques (Foraminifères) - paléobiogéographique. *Docum. B.R.G.M.,* **147,** 1-292

Lys, M., Bouyx, E. and Boulin, J. 1990. La biozone à *Cancellina* (Permien moyen, Kubergandien) dans le versant méridional de l'Hindou Kouch (Afghanistan). *Facies,* **23,** 37-56

Mei Shilong, Henderson, C.M., Wardlaw, B.R. and Shi Xiaoying, 1999. On provincialism, evolution and zonation of Permian and Earliest Triassic Conodonts. *Proc. Int. Conf. Pangea and Paleozoic-Mesozoic Transition,* China University of Geosciences, Wuhan Hubei, 22-28

Mertmann, D. and Sarfraz, A. 1999. Depositional evolution of the marine Permian sequence of the Salt Range and the Trans Indus Ranges, Pakistan. *Int. Conf. Pangea and Paleozoic-Mesozoic Transition,* 130-131

Nguyen, D. T., 1979. Étude micropaléontologique (Foraminifères) de materiaux du Permien du Cambodge. Thèse Univ. de Paris Sud Centre d'Orsay, 1-166 (unpubl.)

Noe, S.U., 198. Facies and paleogeography of the marine Upper Permian and of the Permian-Triassic boundary in the southern Alps (Bellerophon Formation, Tesero Horizon). *Facies,* **16,** 89-142

P.J.R.-G. (Pakistani Japanese Research-Group), 1985. Permian and Triassic system in the Salt Range and the Surghar Range, Pakistan. The Tethys, 221-312 Rozovskaya, S.E. 1975. Composition, phylogeny and system of the order Fusulinida. In: Nakazawa, K. and Dickins, J.M. Eds., *Acad. Sci. USSR, Paleontological Institute,* **149,** 1-267

Shi, G.R., Archbold, N.W. and Zhan, L.-P. 1995. Distribution and characteristics of mixed (transitional) mid-Permian (Late Artinskian-Ufimian) marine faunas in Asia and their palaeogeographical implications. *Palaeo, Palaeo, Palaeo,* **114,** 241-271

Vachard, D., 1980. Tethys et Gondwana au Paleozoique supérieur: les données afghanes - biostratigraphie, micro-paléontologie, paléogéographie. *Docum. Trav. IGAL (Institut Géologique Albert de Lapparent),* **2,** 1-463

Wardlaw, B.R., 1995. Permian conodonts.- The Permian of northern Pangea. In: Scholle, P.A., Peryt, T.M. and Ulmer-Scholle, D.S. eds. *Paleogeography, Paleoclimate, Stratigraphy,* **1,** 186-195

Wardlaw, B.R. and Mei Shilong, 1999. Refined Condont biostratigraphy of the Permian and Lowest Triassic of the Salt and Khizor Ranges, Pakistan. *Proc. Int. Conf. Pangea and Paleozoic-Mesozoic Transition,* 154-156

Wardlaw, B.R. and Pogue, K.R., 1995. The Permian of Pakistan. The Permian of northern Pangea. In: Scholle, P.A., Peryt, T.M. & Ulmer-Scholle, D.S. eds. *Sediment. Basins Econ. Resour,* **2,** 215-224

Wignall, P.B. and Hallam, A. 1993. Griesbachian (Earliest Triassic) palaeoenvironmental changes in the Salt Range, Pakistan and southeast China and their bearing on the Permo-Triassic mass extinction. *Palaeo., Palaeo., Palaeo.,* **102,** 215-237

Zaninetti, L. and Altiner, D., 1981. Les Biseriamminidae (Foraminifères) dans le Permien supérieur mésogéen: évolution et biostratigraphie. *Notes du Lab. Pal. Univ. Genève,* 7, 39-47

Zaninetti, L. & Jenny-Deshusses, C., 1985. Les Paraglobivalvulines (Foraminifères) dans le Permien supérieur tethysien; répartition stratigraphique, distribution géographique et describtion de *Paraglobivalvulinoides* n. gen. *Rev. Paléobiologie,* **4,** 343-346

Geol. Bull. Punjab Univ. 35, 2000.

FELDSPATHOIDS MINERAL CHEMISTRY IN THE KOGA UNDERSATURATED ALKALINE COMPLEX, BUNER SWAT, NW PAKISTAN

BY

IFTIKHAR H. BALOCH, NASIR AHMAD, M. NAWAZ CHAUDHRY
Institute.of Geology, University of the Punjab, Quaid-e-Azam Campus, Lahore, 54590, Pakistan

AND

ABDUL MATEEN
Pakistan Institute of Engineering and Applied Sciences P.O. Nilore, Islamabad, Pakistan.

Abstract:- *Mineral chemistry of feldspathoids in the Koga undersaturated alakaline igneous complex Buner Swat, northwest Pakistan has been investigated to determine the crystallization history of the undersaturated alkaline magma in the region. The Koga feldspathoidal complex consists of sodalite-cancrinite rich pegmatites, foyaites, feldspathoidal syenites, pulaskites, garnet bearing nepheline syenites and alkali syenites, which are genetically associated with ijolites , carbonatites and fenites. The feldspathoidal rocks are essentially pyroxene nepheline syenites containing minor and accessory biotite, magnetite, garnet, sphene, apatite and zircon. Electorn microprobe analyses show that the Koga feldspathoidal syenites has a single highly exsolved feldspar with a K-feldspar host. Nepheline exhibits a little variation in composition with some deviation in the Na:K ratios from the ideal value of 3:1. The composition of the nepheline is mostly restricted to the Morozewicz - Buerger convergent field in the system Ne- Ks-Qz, which is a characteristic of subsolvus nepheline syenites. The crystallization process at lower temperatures might have given rise to subsolvus types from a single high temperature feldspar hypersolvus assemblage. The composition of all the feldspathoidal syenite suites suggest a pressure of >1 and < 5 kb except sodalite rich foyaites. Sodalite and cancrinite show constant composition with relatively high SiO_2 and Al_2O_3 whereas CaO is slightly low.*

INTRODUCTION

The Koga undersaturated alkalic igneous-carbonatite complex is the most interesting for the petrogenetic study of the alkaline rocks of N W Pakistan. This plutonic complex is one of the several intrusions of the alkaline igneous province which extends over 200 Km from the Loe-Shilman in the west and across eastern Afghanistan to Terbela Dam in the east. The Koga feldspathoidal complex occurs in the middle part of the Ambela-Utla granitic batholith and forms horse shoe shaped outcrop. It is well exposed near type locality of Koga (34^0.23N, 72^0.28E) in the Chamla valley Buner Swat at a distance of about 55 km northwest of Mardan district.

The Alkaline Igneous Province of NW Pakistan is emplaced within the thrust belts of Lesser and Higher Himalayas along the continental margin of the Indo-Pakistan plate. The occurrence of various alkaline complexes are believed to be related to the extensional or rifting episodes associated with alkaline and carbonatitic magmatism during the Late Paleozoic to the Tertiary (Kempe 1973, 1976; Zeitler 1982, 1988. Maluski & Matte 1984).

The detailed account of the geology and petrography of the Koga alkaline complex is given by several authors (Siddiqui et al. 1968, Chaudhry et al. 1981 and Baloch 1994). The complex exhibits a wide spectrum of feldspathoidal syenites, genetically related to ijolite - nepheline syenites - carbonatites - fenite associations. The predominant feldspathoidal rocks are essentially pyroxene nepheline syenites, foyaites, sodalite - concrinite bearing foyaitic pegmatites, garnet - bearing nepheline syenites, pulaskites and alkali syenites.

The first detailed account of mineralogy of the Koga feldspathoidal syenites was undertaken by Baloch, (1994).

This paper presents the electron microprobe investigations of feldspathoids minerals. There is a little doubt that nepheline is a late-stage crystallizing primary phase. However, the inter-relationships between the contemporaneous crystallizing phases of plagioclase, nepheline and alkali feldspar is of considerable significance in understanding the felsic mineral crystallisation trends in the highly evolved alkaline magmas.

PETROGRAPHY

More than 80 samples were collected from the various feldspathoidal rock units for this study.

The mineralogy was determined first by optical microscopy, X-ray diffraction and then electron microprobe was used to know the composition of different phases in the rock suites. Based on chemical characteristics and the modal mineralogy of feldspars, feldspathoids and mafic minerals, the Koga feldspathoidal complex is grouped into the following rock types :

Foyaites, sodalite-cancrinite foyaites, feldspathoidal syenites, pulaskites, garnet-bearing nepheline syenites and alkali synites.

Detailed petrographic description of the Koga feldspathoidal syenites is given by Siddiqui et al. 1968, Chaudhary et al. 1981 and Baloch 1994. Only a brief account will be presented here for the samples studied.

The feldspathoidal rocks are essentially pyroxene nepheline syenites containing minor and accessory biotite, magnetite, garnet, sphene, apatite and zircon. The rocks occur commonly as coarse and medium grained with hypidiomorphic heterogranular texture. Aplitic varieties show saccharoidal to hypidiomorphic growth and at places exhibit flow structure. The feldspathoidal syenites have a single exsolved feldspar with a K-feldspar host. Plagioclase is scare or absent. The feldspars are unzoned, almost pure albite and K-feldspar. The microcline microperthites are very well developed due to slow cooling of the magma. In a few rocks there is also a separated Na-feldspar hosted perthite. Nepheline occurs as subhedral to anhedral grains exhibiting two generations. The fresh grains are subhedral, unaltered and occasionally forming clusters. The granular texture of coarse grained varieties indicates that nepheline tends to approach cotectic crystallization with alkali feldspars and pyroxene. The anhedral nepheline shows replacement by cancrinite. Sodalite and cancrinite are present in the pegmatites of the Koga complex. The mafic minerals occur as aggregates and clots as well as subhedral to anhedral grains. Pyroxene and biotites are generally fresh and of primiary crystalline phase, coexisting in most of the rocks. Pyroxene is more abdundant minor phase, fine to medium grained and yellowish green in colour. Na-rich clinopyroxenes are typical aegirine. Biotites occur as red-brown to yellowish brown pleochroic patches, mostly unzoned. The amphiboles are absent or rare, reported only in one sample (S-1). Garnet and sphene are present in few samples. Garnet bearing feldspathoidal syenites are typically exposed at Bibi Dherai and near Sura where garnet is invariably associated mainly with pyroxenes.

Major minerals in the paragenesis mineralogy consist of nepheline (5-35%) , microcline (20-70%) albite (traces to few percent), cancrinite and sodalite (up to 12-15% respectively in some sections), Aegirine (2-3%) biotite (1-4%), iron ore (mainly magnetite up to 3%) and sphene and garnet (up to 1 and 4% respectively in some sections). Apatite and zircon are ubiquitous accessory minerals.

FELDSPATHOIDS MINERAL CHEMISTRY

Representative samples from various feldspathoidal rock suites were chosen for detailed electron microprobe studies. Mineral analyses were performed at the Department of Geology, University of Leicester, U.K. on a Jeol Superprobe JXA 8600 with an online computer for ZAF correction and utilizing appropriate natural and synthetic standards for calibration. Quantitative results were obtained on the wavelength dispersive system using the operating conditions of 15 k V acceleration voltage and 0.03 micro ampere sample current.

Nepheline

Analyses of the nephelines from the Koga complex are given in Tables 1 calculated on the basis of 4 oxygens. Nepheline is present in significant amount as major mineral phase, other feldspathoids such as sodalite and cancrinite are present in many parts of the complex.

The nepheline analyses are plotted in the Ne - Ks - Qz system at P_{H2O} 1000 Kg/cm^2 after Hamilton and MacKenzie (1965) in Fig. 1, showing the composition of analysed nephelines in the feldspathoidal syenite. There is a little variation in nepheline composition from the Koga feldspathoidal syenite complex, although they show some variation in the Na:K ratio. This does not show ideal ratio of 3:1 due to the excess of ions such as SiO_2 and K_2O. The contents of FeO and CaO are significantly low.

The nephelines show an excess of Si and a deficiency of Al. The greater excesses of silica over that required by stoichiometry indicate temperatures in the general range of 750^0 C to 950^0 C (Hamiltion, 1961), but the nephelines from Koga do not show much excess of Si, and these were not formed at such high temperatures but probably at temperature lower than 750^0 C.

The composition of nepheline from the Koga complex (Ne_{80} Ks_{20} Qz_0 to Ne_{80} Ks_{15} Qz_5) lie inside the Morozewics - Buerger convergence field of plutonic

nephelines (Tilley, 1954) and shows a limited range of solid solution as defined by Hamiltion (1961), indicating that the Koga nephelines crystallized or recrystallized over a narrow range of temperature. The nephelines equilibration temperatures are consistent with the slow cooling annealing at lower temperature. This must be followed by the relatively slow equilibration of nepheline to compositions within Morozewicz - Buerger field as found in other nepheline syenite complexes (Tilley, 1954). Thus the Koga feldspathoidal rocks are characterized by subsolvus nepheline syenites. The nephelines have been crystallized under plutonic environment.

The compositions of nephelines from different complexes of the world plot more or less in the same field as those from the Koga feldspathoidal syenite, only the nepheline from Blue Mountain and Bigwood complexes are plotted in Fig. 1.

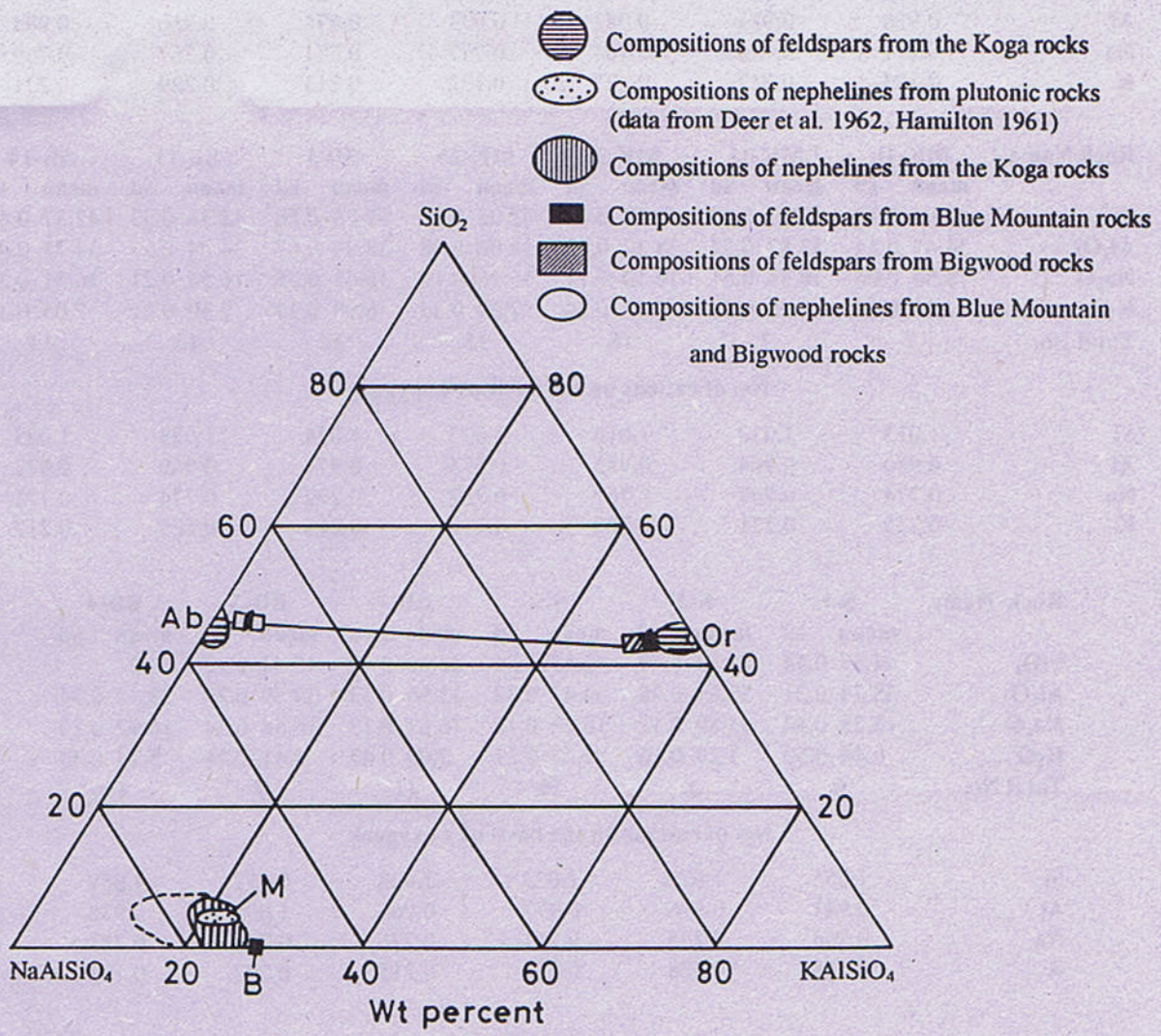

Fig. 1 Compositions of nephelines and feldspars from the Koga feldspathoidal syenites, Blue Mountain and Bigwood complexes plotted on the system $NaAlSiO_4$-$KalSiO_4$-SiO_2 M and B are Morozewics and Buerger compositions .

Table 1
Microprobe analyses of nephelines from the Koga Complex

Rock Name	K-2		K-6		K-8		K-9		MK-2		MK-5		MK-6	
	mean	sd	mean	sd	mean	sd	mean	sd	mean	sd	mean	sd	mean	sd
SiO_2	43.34	0.55	42.17	0.50	41.89	0.45	42.50	0.36	41.13	0.87	42.05	0.37	41.25	0.29
Al_2O_3	33.79	0.43	32.73	0.35	34.33	0.34	34.10	0.72	33.21	0.82	34.39	0.67	34.19	0.17
Na_2O	16.70	0.59	16.53	0.27	16.18	0.21	16.56	0.38	15.99	0.37	16.36	0.10	16.17	0.15
K_2O	6.31	0.36	7.04	0.35	7.33	0.16	6.21	0.52	6.72	0.65	7.43	0.26	7.08	0.22
Total No.	10		29		11		18		7		5		18	
No. of cations on the basis of 4 oxygens														
Si	1.040		1.017		1.016		1.028		1.023		1.016		1.011	
Al	0.956		0.981		0.982		0.973		0.974		0.980		0.988	
Na	0.777		0.773		0.761		0.777		0.771		0.767		0.769	
K	0.193		0.217		0.227		0.192		0.213		0.229		0.221	

Rock Name	MK-16		MK-18		MK-24		MK-25		SB-1		SB-11		SB-14	
	mean	sd	mean	sd	mean	sd	mean	sd	mean	sd	mean	sd	mean	sd
SiO_2	42.04	0.10	42.67	0.49	41.64	0.24	42.08	0.92	42.26	0.56	42.38	0.32	42.37	0.49
Al_2O_3	34.47	0.14	33.87	0.73	34.17	0.12	34.02	0.48	33.99	0.67	34.04	0.53	34.13	0.45
Na_2O	16.54	0.06	16.38	0.61	16.10	0.11	16.16	0.16	16.43	0.25	16.54	0.21	16.51	0.24
K_2O	7.31	0.07	7.18	0.67	7.32	0.24	7.04	0.34	6.99	0.34	7.30	0.21	7.05	0.37
Total No.	7		7		18		15		12		13		14	
No. of cations on the basis of 4 oxygens														
Si	1.015		1.030		1.016		1.023		1.024		1.023		1.023	
Al	0.980		0.964		0.983		0.975		0.971		0.969		0.972	
Na	0.774		0.767		0.761		0.762		0.772		0.774		0.773	
K	0.225		0.221		0.228		0.218		0.216		0.225		0.217	

Rock Name	S-1		S-3		S-6		BD-1		BD-3		BD-4	
	mean	sd	mean	sd	mean	sd	mean	sd	mean	sd	mean	sd
SiO_2	44.59	0.54	41.73	0.49	42.53	0.40	42.66	0.42	40.44	0.22	0.52	
Al_2O_3	33.74	0.21	33.81	0.38	34.47	0.32	33.96	0.53	34.59	0.29	33.34	0.34
Na_2O	16.38	0.14	15.89	0.11	16.10	0.15	16.61	0.13	16.66	0.24	16.92	0.20
K_2O	6.49	0.58	7.29	0.16	7.47	0.21	7.00	0.47	6.41	0.24	5.74	0.43
Total No.	6		4		19		11		7		19	
No. of cations on the basis of 4 oxygens												
Si	1.055		1.022		1.023		1.028		0.997		1.057	
Al	0.941		0.976		0.977		0.965		1.005		0.938	
Na	0.760		0.755		0.751		0.776		0.796		0.783	
K	0.198		0.228		0.228		0.215		0.202		0.175	

Cancrinite

Cancrinite is present in the Koga feldspathoidal syenite complex principally in the pegmatites, which have larger quantities compared to other units of the complex. Analysis are given in the Table 2, calculated on the basis of 12 oxygens. These concrinites lack FeO and K_2O. The SiO_2 and Al_2O_3 are present in excess as compared to the analyses shown by Phoenix and Nuffield (1949), Takla and Griffin (1980) and Flohr and Ross (1990). The CaO contents are less in the Koga complex from those of Takla and Griffin (1980) and Flohr and Ross (1990).

Table 2
Microprobe analyses of cancrinite from the Koga Complex

Rock Name	K-2		K-3		K-4		K-6		K-9		MK-1		MK-3	
	mean	sd	mean	sd	mean	sd	mean	sd	mean	sd	mean	sd	mean	sd
SiO_2	41.45	0.58	38.14	0.62	38.60	1.38	39.80	1.66	40.52	0.20	40.21	0.21	40.61	0.19
Al_2O_3	33.81	0.44	31.10	0.38	31.36	1.46	32.73	1.78	33.45	0.27	33.32	0.21	33.18	0.37
CaO	4.99	0.27	4.82	0.09	4.65	0.61	7.21	0.45	6.58	0.82	7.10	0.15	6.77	0.08
Na_2O	17.72	1.24	19.72	0.19	18.17	1.21	17.78	0.78	17.74	0.78	16.19	0.31	16.63	0.25
Total No.	23		4		25		7		16		33		10	
No. of cations on the basis of 12 oxygens														
Si	3.011		2.942		2.987		2.940		2.957		2.967		2.785	
Al	2.895		2.828		2.855		2.850		2.878		2.898		2.874	
Ca	0.338		0.398		0.385		0.571		0.515		0.561		0.533	
Na	2.496		2.950		2.720		2.547		2.510		2.316		2.370	

Rock Name	MK-5		MK-6		MK-10		MK-14		MK-16		MK-18		SB-1	
	Mean	sd	mean	sd	mean	sd	mean	sd	mean	sd	mean	sd	mean	sd
SiO_2	39.85	1.62	40.26	0.37	40.01	0.49	40.71	0.37	40.82	1.07	39.43	0.77	41.15	1.13
Al_2O_3	32.92	1.17	33.	0.34	33.01	0.52	33.82	0.59	33.44	0.65	32.33	0.99	33.59	0.54
CaO	5.09	0.17	5.56	0.36	5.41	0.27	4.68	1.18	4.19	0.34	5.13	0.45	5.13	1.28
Na_2O	17.40	1.04	17.30	0.45	17.69	0.51	17.84	0.67	18.74	0.66	18.63	1.08	17.58	0.98
Total No.	5		21		5		18		27		19		9	
No. of cations on the basis of 12 oxygens														
Si	2.984		2.972		2.976		2.987		2.997		2.965		3.007	
Al	2.906		2.918		2.894		2.926		2.895		2.866		2.893	
Ca	0.408		0.440		0.431		0.368		0.330		0.413		0.402	
Na	2.527		2.476		2.551		2.538		2.668		2.716		2.490	

Rock Name	SB-5		SB-11		S-1		S-3		BD-3	
	mean	sd	mean	sd	mean	sd	mean	sd	mean	sd
SiO2	40.55	0.50	41.10	0.47	40.59	0.27	39.66	0.99	40.10	1.99
Al2O3	33.45	0.34	33.77	0.43	33.74	0.21	32.31	1.40	32.44	1.69
CaO	5.86	0.57	4.63	0.36	9.17	0.23	4.42	0.51	3.36	0.39
Na2O	16.6	0.24	18.04	0.76	14.43	0.28	18.88	0.65	19.68	0.92
Total No.	6		13		12		10		7	
No. of cations on the basis of 12 oxygens										
Si	2.991		3.001		2.958		2.984		3.003	
Al	2.909		2.907		2.899		2.866		2.864	
Ca	0.463		0.362		0.716		0.356		0.270	
Na	2.383		2.554		2.039		2.754		2.857	

Sodalite

Sodalite is present in the sodalite rich feldspathoidal syenite. Analyses are presented in Table 3 calcuated on the basis of 25 oxygens. Sodalites are higher in SiO_2, Al_2O_3 and Na_2O as compared to those by Taylor, (1967), whereas they are similar to sodalite from the Coldwell alkaline complex N W Ontario by Roger et al. (1982).

Cancrinite and sodalite show more or less constant composition in different units of the Koga complex.

Table 3
Microprobe analyses of sodalite from the Koga Complex

Rock Name	K-9		MK-1		MK-6		MK-10		SB-1		SB-5		SB-11	
	mean	sd	mean	sd	mean	sd	mean	sd	mean	sd	mean	sd	mean	sd
SiO_2	39.93	0.47	39.45	0.31	39.32	0.37	39.51	0.60	39.91	0.32	39.81	0.22	39.75	0.28
Al_2O_3	33.12	0.65	32.72	0.21	33.27	0.37	33.21	0.70	32.85	0.40	32.37	0.48	33.04	0.26
Na_2O	25.65	0.55	25.68	0.12	25.28	0.38	25.51	0.29	25.67	0.42	25.47	0.40	25.88	0.18
Total No.	6		13		9		3		7		3		3	
No. of cations on the basis of 25 oxygens														
Si	6.113		6.101		6.069		5.782		6.129		6.160		6.096	
Al	5.978		5.965		6.054		6.304		5.947		5.905		5.974	
Na	7.614		7.700		7.565		7.963		7.643		7.642		7.695	

DISCUSSION

The features of the Koga feldspathoidal syenites are quite typical of the similar undersaturated alkaline rocks found in the world. The textural relationships, mineral assemblages and compositional trends, in general coincide with those of the well studied nepheline syenite rocks from Gardar Province, Greenland (Upton 1974, Upton et al. 1985), Kola Peninsula, USSR (Gerasimovsky et al. 1974) Monchique complex Portugal (1978), Coldwell complex, Ontario (Mitchell and Platt 1982), Chilwa Province, Malawi (Woolley and Platt 1986), Mont Saint Hilaire complex, Quebec (Currie et al. 1986). Magnet Cove complex, Arkansas (Flohr and Ross 1990) and Red Hill complex, New Hampshire (Dismal Victoria Lan, Antarctica (Worly and Cooper 1995) Dorias and Floss 1992)

The Koga feldspathoidal syenite constitutes most important rock units of the Koga-Ambela alkali complex that is an integral part of so called Alkaline Igneous Province of northwest Pakistan. Current geochemical studies have delineated at least three major rock asociations in the Koga-Ambela alkali complex (Mateen et al. in preparation). The magmatic suites are:

1. Postassic mafic dykes and K-rich syenites granites Lamprophyres-K-rich syenites-granite
2. Ijolite feldspathoidal syenites -carbonate-fenites.
3. Alkali gabbro/dolerite-syenite-quartz syenite-granite.

The Koga complex is believed to be polygenetic intrusions of distinct suites emplaced relatively at shallow depth. The feldspathoidal rocks appear to have generated from the common parental magmas under the different conditions of oxygen fugacity, silica and alkali activity, volatile fluids and metasomatism. The nature of magma and conditions under which it crystallized are difficult to assess. Nevertheless, the mineral assembages and compositions provide some indication of the formation of feldspathoidal rocks.

The composition of nephelines are restricted within the narrow Morozewic and Buerger convergence field under plutonic conditions of nepheline crystallization which is a characteristic of subsolvus feldspathoidal syenites as found in the nepheline syenite complexes (Tilley, 1954). Nephelines do not show much excess of Si and exhibit a limited range of solid solutions indicating that the nephelines were crystallized or recrystallized at relatively lower temperature with slow cooling under plutonic environment, probably at temperatures below 750^{O}C. Textural relationships with alkali feldspar indicate that nepheline is a primary phase for most of the feldspathoidal syenites except sodalite-cancrinite foyaites.

The chemical analyses of all the rocks units of the Koga complex when plotted as CIPW normative mineralogy in the nepheline-kalsilite-silica system, indicated a pressure > 1 and < 5 Kb except sodalite rich foyaites (Baloch, 1994). Similarly, majority of the rock groups fall almost on the minima of Ne-Ab-Or system showing feldspar crystallization at 1-2 Kb PH_2O. The final stage of crystallization represented by cancrinite and sodalite-rick foyaites.

The development of sodalite in the Koga rocks, particularly the pegmatitic foyaites, as primiary phases associated with nepheline and alkali feldspars, indicates late-stage crystallization of Na-rich liquid phase. The sodalite at the magmatic stage crystallizes over a wide range of temperatures and pressure (400^{O}C to 800^{O}C at 1 Kbar) in the SiO_2 - undersaturated silicate melts (Dear et al. 1992). It is observed that the sodalite preceded nepheline in the crystallization of highly differentiated phonolitic magma of Tenerife, Canary Island, at an estimated temperatures greater than 680^{O}C and fluid pressure less that 1.6 K bar (Wolff, 1987).

REFERENCES

Baloch, I. H., 1994. The Koga feldspathoidal syenite complex, Northwestern Pakistan: Mineralogy and industrial applications. Unpublished PhD thesis, Univ. of Leicester.

Bose, M. K., 1970. Petrology of the intrusive alkalic suite of Karaput, Orissa. *Jour. Geol. Soc.* India. **11**, 99 - 126.

Bowen, N. L. and Ellestad, R. B., 1936. Leucite and pseudoleucite. *Am. Mineral.* **21**, 363 - 368.

Chaudhry, M. N., Ashraf, M. and Hussain, S. S., 1981. Petrology of Koga nepheline syenite and pegmatite of Swat District. *Geol. Bull.* Punjab Univ. **16**, 83 - 97.

Currie, K. L., Eby, G, N. and Gittins, J., 1986. The petrology of the Mont Saint Hilaire complex, southern Quebec: An alkaline gabbro - peralkaline syenite association. *Lithos.* **19**, 65 - 81.

Deer, W. A., Howie, R. A. and Zussman, J., 1992. An introduction to the rock-forming minerals. 2nd ed. Loodon: Longman.

Dorias, M. J. and Floss, C., 1992. An ion and electron microprobe study of the mineralogy of enclaves and host syenites of Red Hill Complex, New Hampshire, USA. *Jour. Petrol.* **33**, 1193 - 1218.

Flohr, M. J. K. and Ross, M., 1990. Alkaline igneous rocks of Magnet Cove, Arkansas; Mineralogy and geochemistry of syenites. *Lithos.* **26**, 67 - 98.

Gerasimovsky, V. I., 1974. Trace elements in selected groups of alkaline rocks. In H. Sorensen (Editor). The alkaline rocks. John Wiley, New York. 402 - 412.

Hamilton, D. L. and MacKenzie, W. S., 1965. Phase-equilibrium studies in the system $NaAlSiO_4$ (nepheline) - $KalSiO_4$ (kalsilite) - SiO_2 - H_2O. *Min. Mag.*, (Tilley Volume), **55**, 214 - 231.

Hamilton, D. L., 1961. Nepheline as crystallization temperature indicators. *Jour. Geol.* **69**, 321 - 329.

Kempe, D. R. C., 1973. The petrology of the Warsak alkaline granites, Pakistan and their relationship to other alkaline rocks of the region. *Geol. Mag.* **110**, 385 - 404.

Maluski, H. and Matte, P., 1984. Ages of alpine tectometamorphic events in the Northwestern Himalaya (North pakistan) by 39Ar/40Ar, *Tectonics*. **3**, 1 - 18.

Mitchell, R. H. and Platt, R. G., 1982. Mineralogy and petrology of nepheline syenites from the Coldwell alkaline complex, Ontario, Canada. *Jour. Petrol.* **23**, 186 - 214.

Miyashiro, A., 1951. The ranges of chemical composition in nepheline and their petrogenetic significance. *Geochim. Cosmochim. Acta.* **1**, 278 - 283.

Morozewicz, J., 1928. Uber die chemische Zusammensetzung de gesteinsbildenden nephelines. *Fennia.* **22**, 1 - 16.

Phoenix, R. and Nuffield, E. W., 1949. Cancrinite, Ontario, Canada. *Am. Mineral.* **34**, 452 - 455.

Roger, H., Mitchell. and Platt, R. G., 1982. Mineralogy and petrology of nepheline syenite from the Coldwell Alkaline Complex, Ontiro, Canada. *Jour. Petrol.* **23**, 186 - 214.

Siddiqui, S. F. A., Chaudhry, M. N. and Shakoor, A., 1968. Geology and petrology of the feldspa-thoidal syenite and associated rocks of the Koga area, Chamla valley, Swat, West Pakistan. *Geol. Bull.* Punjab Univ. **7**, 1 - 30.

Takla, M. A. and Griffin, W. L., 1980. Cancrinite (microsommite), metabasalt, St John's Island, Red Sea, Egypt. *Neues Jahrb. Min. Monat.* 345 - 352.

Taylor, D., 1967. Blue sodalite, sodalite bearing nepheline syenite pegmatite, Laven, Langesundsfjord, Norway. *Contrib. Min. Petrol.* **16**, 172-88

Tilley, C. E., 1954. Nepheline alkali feldspar paragenesis. *Am. J. Sci.* **252**, 65 - 75.

Upton, B. G. J., 1974. The alkaline province of South-West Greenland. In: H. Sorensen (editor). The Alkaline Rocks. John Wiley. New York. 221 - 238 pp.

Upton, B. G. J., Stephenson, D. and Martin, A. R., 1985. The Tugtutq older giant dyke complex: mineralogy and geochemistry of an alkali gabbro - augite - foyaite association in the Garder Province of South Greenland. *Min. Mag.* **49**, 623 - 642.

Wolf, J. A., 1987. Crystallization of nepheline syenite in a subvolcanic system: Tenerife, Canary Island. *Lithos*. **20**, 207 - 223.

Woolley, A. R. and Platt, R. G., 1986. The mineralogy of nepheline syenite complexes from the northern part of the Chilwa Province, Malawi. *Min. Mag.* **50**, 597 - 610.

Worley, B. A., Cooper, A. F. and Hall, C. E., 1995. Petrogenesis of carbonate-bearing nepheline syenites and carbonatites from Southern Victoria Land, Antractica: orgin of carbon and the effects of calcite-graphite equilbrium. *Lithos* **35**, 183-199.

Zeitler, P. K., 1982. Uproofing history of a suture zone in Himalaya of Pakistan by means of fission-track annealing ages. *Earth Planet. Sc. Lett.* **57**, 227 - 240.